THE UNIVERSITY OF QUEENSLAND

AUSTRALIA

Lattice Boltzmann modelling of supercritical shallow water flows

Amir Hossein Hedjripour

Master's Degree in Civil Engineering-Hydraulic Structures

A thesis submitted for the degree of Doctor of Philosophy at

The University of Queensland in 2018

School of Civil Engineering

Abstract

The Lattice Boltzmann Method (LBM) is a promising tool to model fluid flows. This thesis presents a summary of the investigations carried out to apply the LBM to study run-up of waves induced by bores on beaches. The thesis starts with a critical review of the common numerical models used in fluid mechanics with a specific focus on the origin and historical advances in the LBM. This indicated that at the outset of this study it was accepted that LBM application was limited to flows with subcritical regime. Hence, modelling supercritical run-up flow did not appear possible with LBM. The major achievement of current work is a one-dimensional Lattice Boltzmann Model which is developed to solve the shallow water equations for steady and unsteady flows within both the subcritical and supercritical regimes. The asymmetric LBM proposed by Chopard et al. (2013) is extended through a generalised Galilean transformation applied to the standard LBM scheme. The transformation yields a general asymmetric Lattice Boltzmann Model scheme which can successfully model a wide range of subcritical and supercritical flows, and enables implementation of the asymmetric model for practical purposes.

In the current work a new set of the Equilibrium Distribution Functions, boundary conditions and the external force weights are derived for the generalised transformed scheme. A new stability region is also defined, allowing selection of a lattice speed that maintains numerical stability for a wider range of sub- and supercritical flows and combinations of those flow conditions, compared to the previous scheme with fixed asymmetry. The model is validated against a range of benchmark cases in open-channel hydraulics that demonstrate the applicability of the new model. The applicability of the model to solve nearshore problems, such as wave run-up, is studied further by a critical review of existing shoreline treatment techniques and developing a new wetting-drying boundary condition.

A wetting-drying boundary condition is developed using LBM fundamentals, which is a modified version of the technique proposed by Liu and Zhou (2014), to accommodate the transformation. The modified algorithm is successfully implemented in the transformed scheme. However, due to very shallow depths that inevitably occur in nearshore zone, the flow conditions in that area fall outside the numerical stability zone defined for the transformed scheme, resulting in instability. It is concluded that while the transformed scheme can successfully be applied to both subcritical and supercritical regimes, in its current form it has limited applicability to problems involving very shallow flows where the Froude and lattice Froude numbers will not be encompassed by the stable zone.

Declaration by author

This thesis is composed of my original work, and contains no material previously published or written by another person except where due reference has been made in the text. I have clearly stated the contribution by others to jointly-authored works that I have included in my thesis.

I have clearly stated the contribution of others to my thesis as a whole, including statistical assistance, survey design, data analysis, significant technical procedures, professional editorial advice, and any other original research work used or reported in my thesis. The content of my thesis is the result of work I have carried out since the commencement of my research higher degree candidature and does not include a substantial part of work that has been submitted to qualify for the award of any other degree or diploma in any university or other tertiary institution. I have clearly stated which parts of my thesis, if any, have been submitted to qualify for another award.

I acknowledge that an electronic copy of my thesis must be lodged with the University Library and, subject to the policy and procedures of The University of Queensland, the thesis be made available for research and study in accordance with the Copyright Act 1968 unless a period of embargo has been approved by the Dean of the Graduate School.

I acknowledge that copyright of all material contained in my thesis resides with the copyright holder(s) of that material. Where appropriate I have obtained copyright permission from the copyright holder to reproduce material in this thesis.

Publications during candidature

Hedjripour, A.H., Callaghan, D.P. & Baldock, T.E., 2016. Generalized transformation of the lattice Boltzmann method for shallow water flows. Journal of Hydraulic Research, pp.1–18.

Hedjripour, Amir; Callaghan, David; Baldock, Tom., 2014. Steady and unsteady supercritical shallow water modelling using a transformed lattice Boltzmann scheme. 3rd IAHR Europe Congress, Porto, Portugal.

Publications included in this thesis

No publications included.

Contributions by others to the thesis

No contributions by others.

Statement of parts of the thesis submitted to qualify for the award of another degree

None.

Acknowledgements

I would like to express my sincere gratitude to my principal advisor Professor Tom Baldock for his continuous support, patience and immense knowledge. With all my work and family commitments during the course of current research work, I would not have been able to complete my PhD study without his extraordinary serenity and flexibility. I would also like to thank Doctor David Callaghan for his indisputable computer programming skills which have been very helpful to me and his valuable comments on the structure and contents of this document.

Keywords

Galilean Transformation, Lattice Boltzmann Method, Shallow water equations, Supercritical flow, Asymmetric scheme, Wave run up, Wet-dry interface

Australian and New Zealand Standard Research Classifications (ANZSRC)

ANZSRC code: 090509, Water Resources Engineering, 70%
ANZSRC code: 960903, Coastal and Estuarine Water Management, 30%

Fields of Research (FoR) Classification

FoR code: 0905, Civil Engineering, 80%
FoR code: 020304, Thermodynamics and Statistical Physics, 20%

Table of Contents

1. Introduction 13
2. Governing Equations on Fluid Flow 17
2.1. Continuity Equation 17
2.2. Momentum Equation 17
2.3. Stress-Strain Rate Relationships 18
2.4. The Navier-Stokes Equations 18
2.5. Summary 20
3. Literature Review 21
3.1. Traditional Numerical Methods in Computational Fluid Dynamics 21
3.2. Recent Techniques in Computational Fluid Dynamics 31
3.3. Summary 48
4. Lattice Boltzmann Modelling of Shallow Water Flows 50
4.1. Equilibrium Distribution functions 50
4.2. The force term 52
4.3. Lattice Isotropy 53
4.4. The D2Q9 Scheme 54
4.5. Numerical Diffusivity in LBM 57
4.6. Treatment of units in LBM 58
4.7. Standard LBM Test Cases 61
4.8. Froude Number Limitation in LBM 63
4.9. Asymmetric LBM for Supercritical Flow 65
4.10. Summary 79
5. Generalized transformation of D1Q3 scheme 80
5.1. Equilibrium Distribution Functions 80
5.2. Chapman-Enskog Expansion 82
5.3. Stability Criteria 84

5.4. Boundary Conditions 87
5.5. Lattice isotropy....88
5.6. Generalised transformation of D2Q9 scheme....90
5.7. Summary 91
6. Validation of the transformed D1Q3 model....92
6.1. Steady flow test cases....94
6.2. Unsteady flow test cases....108
6.3. Summary 114
7. Shoreline Boundary Conditions 115
7.1. Review of Moving Shoreline Treatment Techniques....115
7.2. Shoreline Boundary Condition for the Transformed Scheme....119
7.3. Limitations at very shallow depths 122
7.4. Low-amplitude wave run up....129
7.5. Summary 135
8. Conclusions and recommendations....137
Appendix A- Derivation of the equilibrium functions for the standard D2Q9 Shallow Water LBM 146
Appendix B- Specific transformation of D2Q9 LBM 159

List of Figures

Figure 3-1 Finite Element Method- The exact solution (solid curve) is approximated by dashed lines.....24

Figure 3-2 Graphical representation of the interpolant in the SPH method.....31

Figure 3-3 Collison-streaming steps in LBM. The left figure shows the particles on adjacent lattices colliding and the right figure shows the new equilibrium functions after the streaming step. 36

Figure 3-4 The D2Q9 scheme used by Salmon (1999). The numbered arrows show the directions that any particle is allowed to move in the collision-streaming process. 42

Figure 3-5 The D1Q3 and D2Q5 LBM schemes. 47

Figure 4-1 Slip and No-slip boundary conditions at solid walls for D2Q9 scheme. 55

Figure 4-2 Velocity profiles in Slip and No-slip boundary conditions.....55

Figure 4-3 – LBM output of velocity profile in Poiseuille flow 61

Figure 4-4 The M2 profile generated by the model compared with analytical solution.....62

Figure 4-5 Subcritical flow modelling in an open channel with a bump. 63

Figure 4-6 The standard (symmetric) and asymmetric D1Q3 schemes. 66

Figure 4-7 The stability region of the asymmetric D1Q3 LBM (Chopard et al. 2013). Fr denotes Froude number and ψ is the Lattice Froude number $\psi = e/gh$ 68

Figure 4-8 The broad-crested weir case in supercritical flow. 70

Figure 4-9 The S2 curve generated by the model compared with analytical solution. 71

Figure 4-10 The S3 curve generated by the model compared with analytical solution. 72

Figure 4-11 The M3 curve generated by the model compared with analytical solution.....73

Figure 4-12 modelling of critical flow occurring over a broad-crested weir.....74

Figure 4-13 Lattice Boltzmann simulation of hydraulic jump in an open channel. 75

Figure 4-14 Stability region for Chopard et al. (2013) D1Q3 scheme. 77

Figure 4-15 Variation of Fr-y for the critical flow over a weir test case. 78

Figure 4-16 supercritical flow case over local bed rise, solid line: Fr-Ψ data, dashed lines and shaded area: Chopard et al. (2013) numerical stability zone. 79

Figure 5-1 Lattice configuration in the transformed scheme. 80

Figure 5-2 Enlarged numerical stability zone. solid bold line, transformed scheme; dotted line, Chopard et al. (2013). Top: stability envelope for $\alpha = 1, \beta = 3$. Below: stability envelope for $\alpha = 2, \beta = 5$. 86

Figure 5-3 the EDFs for the transformed D1Q3 scheme.....87

Figure 5-4 directional force term weight functions in the transformed scheme. 90

Figure 6-1a. Stability zone and Fr-Ψ for the M2 flow profile, case 1. Solid lines, boundaries of the present stability zone; dashed lines, boundaries of the Chopard et al. (2013) stability zone. 95

Figure 6-2a. Stability zone and Fr-Ψ for the M3-M2 flow profile, case 2. Solid lines, boundaries of the present stability zone; dashed lines, boundaries of the Chopard et al. (2013) stability zone.....97

Figure 6-3a. Stability zone and Fr-Ψ for the S2 flow profile, case 3. Solid lines, boundaries of the present stability zone; dashed lines, boundaries of the Chopard et al. (2013) stability zone. 98

Figure 6-4a. Stability zone and Fr-Ψ for the S3 flow profile, case 4. Solid lines, boundaries of the present stability zone; dashed lines, boundaries of the Chopard et al. (2013) stability zone. 100

Figure 6-5a. Stability zone and Fr-Ψ for subcritical flow over a hump, case 5. Solid lines, boundaries of the present stability zone; dashed lines, boundaries of the Chopard et al. (2013) stability zone.....102

Figure 6-6a. Stability zone and Fr-Ψ for supercritical flow over a hump, case 6. Solid lines, boundaries of the present stability zone; dashed lines; boundaries of the Chopard et al. (2013) stability zone.....103

Figure 6-7a. Stability zone and Fr-Ψ for critical flow over a weir, case 7. Solid lines, boundaries of the present stability zone; dashed lines, boundaries of the Chopard et al. (2013) stability zone.....105

Figure 6-8a. Stability zone and Fr-Ψ for the M2-S2 flow profile, case 8. Solid lines, boundaries of the present stability zone; dashed lines, boundaries of the Chopard et al. (2013) stability zone. 106

Figure 6-9a. Velocity profile for the tidal flow case in Bermudez et al. (1994), reproduced with the asymmetric scheme. Solid line, analytical solution; dotted line, LBM. 109

Figure 6-10 Location of the arbitrary points in the dam-break case for comparison with ANUGA. 111

Fig.6-11. Comparison of flow depth time series at selected locations (STA.1 to STA.5) for the transformed LBM and ANUGA model for the dam-break flow case on smooth bed, case 10. Solid line, ANUGA; dotted line, LBM. 111

Fig.6-12. Comparison of longitudinal water surface profiles by the transformed LBM and ANUGA models at 1 second intervals for the dam-break case on smooth bed, case 10. Solid line, LBM; data points, ANUGA. 112

Figure 6-13. Stability zone and Fr-*Ψ* for the dam break case on smooth bed, case 10. Solid lines, boundaries of the present stability zone; dashed lines, boundaries of the Chopard et al. (2013) stability zone. 113

Fig.6-14. Comparison of flow depth time series at selected locations for the transformed LBM and ANUGA model for the dam-break flow case on rough bed, case 11. Solid line, ANUGA; dotted line, LBM. 114

Figure 7-1 Indicative wet and dry lattices at the shore by Liu and Zhou (2014). 118

Figure 7-2 Variation of Froude number in the wave run up case using the standard LBM scheme at 1 second intervals between 7s and 12s. 123

Figure 7-3a. Stationary water in a tank with end depth 1.0m. 124

Figure 7-4a. Stationary water in a tank with end depth 0.001m-water level plotted at 1s intervals. 125

Figure 7-5. Dam break test case on dry bed, transformed scheme, water surface profile plotted at 1s intervals. 127

Figure 7-6 values of Fr-Ψ for the dam break case on dry bed, transformed scheme with *e*=1m/s, plotted at 1s intervals. 127

Figure 7-7a. Solitary wave run up test case- transformed scheme; water surface plotted at 0.5s intervals.....128

Figure 7-8a. Low-amplitude wave run up- standard LBM scheme, water surface profile plotted at 0.4s intervals.....130

Figure 7-9a. Low-amplitude wave run-up- transformed LBM scheme.....131

Figure 7-10 Shoreline location in low amplitude wave run-up case – standard LBM. 132

Figure 7-11 Shoreline location in low amplitude wave run-up case – asymmetric LBM...133

Figure 7-12 Water surface profiles-standard vs. transformed scheme for the low-amplitude wave run-up case at 9s. standard LBM (solid line); asymmetric LBM (dashed line). 133

Figure 7-13 Water surface profiles-standard vs. transformed scheme for the low-amplitude wave run-up case at 10s. standard LBM (solid line); asymmetric LBM (dashed line). 134

Figure 7-14 Water surface profiles-standard vs. transformed scheme for the low-amplitude wave run-up case at 11s. standard LBM (solid line); asymmetric LBM (dashed line). 134

Figure 7-15 Water surface profiles-standard vs. transformed scheme for the low-amplitude wave run-up case at 12s. standard LBM (solid line); asymmetric LBM (dashed line). 135

List of Tables

Table 6.1 Physical and lattice data for each test case. 92

1. Introduction

This research aims at applying Lattice Boltzmann Modelling techniques to study flow field patterns and flow characteristics (depth, velocity, etc.) with a focus on shallow water problems in supercritical flow regimes. The Lattice Boltzmann Methods (LBM) have recently attracted widespread global attraction as alternative modelling approach to fluid problems, including solutions of the Shallow Water Equations (SWE).

Unlike to standard 'top-down' approaches to solve fluid problems which treat the fluid as a continuum and involve solution of differential equations developed to represent flow behaviour, the LBM is a distinctive approach to fluid simulations in the sense of its 'bottom-up' particle-based approach, which unlike the traditional 'top-down' approaches does not need simplifying assumptions on the physics of the problem such as mathematical treatment of governing equations, elimination of the insignificant parameters and characteristics and simplified representation of changes in physical properties of the domain.

At a microscopic level, the behaviour of fluid particles may be defined by equations of molecular dynamics and the position and velocity of each particle can be determined from Newton's equations of motion. While this can easily be programmed for a computer, the large number of particles involved in an even small domain makes it impractical for use in modelling macroscopic dynamics of the systems usually involved in engineering problems. To overcome this limitation, the LBM utilises a 'mesoscopic' approach which uses ensembles of particles instead of individual particles. While the particles are assumed to be located on arrays at discrete points on a lattice, their behaviour is expressed through a set of 'Equilibrium Distribution Functions'. Particles are allowed to move to other locations on the lattice network according to simple kinetic rules which preserve mass, energy and momentum. The macroscopic characteristics of the fluid such as depth and velocity are determined from the mesoscopic properties based on the continuum equations they are required to obey.

In addition to the robust underlying physics used in the LBM, it has certain strengths in parallelisation of computations (because in each time step the same calculations are performed at each lattice) and implementation of complex boundary conditions (because they are applied locally regardless of the complexity). It is also a faster model to run compared to its standard 'top-down' counterparts. These advantages place LBM as a

versatile candidate for improved representation of the model physics where complex boundary conditions are involved or flow behaviour in a local context is the focus.

Some potential areas of application are:

1. wave kinematics in the swash zone, particularly the rotational tip identified by Barnes & Baldock (2010) where LBM could potentially offer a more localised investigation of the wave tip.
2. investigation of wave run-up and run-down involving supercritical flow regimes, as will be discussed further in Chapters 5 and 7.
3. The LBM representation of bore propagation into shallow waters
4. dam-break flows
5. implementation of improved tools to simulate multi-phase fluid interfaces
6. an alternative approach to model complex geometries and boundary conditions
7. sediment transport in the swash zone using a particle-based approach.

In the current context, shallow water is defined as an area where surface waves are noticeably affected by bottom topography. Typically, this implies a water depth equivalent to less than half the wavelength (Sorensen 2006). The current research seeks to propose and apply an alternative LBM scheme and apply it to supercritical shallow water flows, particularly in the swash zone, where supercritical regimes are present. Through detailed investigation of flow fields and velocities, it is hoped that the proposed model will bridge the gap in the existing LBM schemes in modelling supercritical flow regimes and assist in improved understanding of flow hydrodynamics in this area.

The thesis is organised as follows:

Chapter 2 provides a brief overview of the equations governing fluid flow, including continuity (conservation of mass), momentum, stress-strain rate relationships and the Navier-Stokes Equations, including the Shallow Water Equations.

Chapter 3 presents a critical review of the most common numerical schemes used in fluid dynamics; including the Finite Difference Method, the Finite Element Method, the Finite Volume Method, Smooth Particle Hydrodynamics and the Lattice Boltzmann Method. A summary of the background, formulation and the methodology adopted in each approach is presented with the advantages and drawbacks of the approach discussed. In this chapter, the strength of LBM over other numerical schemes, as well as its potential advantages in

investigation of specific problems, are highlighted. The Lattice Boltzmann Method is discussed in more detail with a focus on fluid flow and recent advances in the LBM representation of shallow water flows.

Chapter 4 outlines the standard LBM for shallow water flows and discusses its underlying properties including the Equilibrium Distribution Functions (both 1D and 2D schemes), isotropy requirements, numerical diffusivity, implementation of external forces and the stability requirements. Implementation of units in LBM is discussed in this chapter, with an example presenting values in both dimensionless and physical unit form, which yield identical results. A few examples are presented in this section to demonstrate how a standard LBM would be applied to benchmark open-channel flow cases such as flow over a weir or spatially-varied flows such as an M2 backwater curve. The asymmetric LBM scheme proposed by Chopard et al. (2013) which was a breakthrough, enabling LBM to be applied to both subcritical and supercritical regimes is also presented with some test cases. The limitations associated with the stability requirements of the asymmetric scheme is also discussed.
The current research work, which was carried out on a part-time basis, commenced in 2009 and at a time when LBM application was limited to supercritical flows. The asymmetric scheme concept was proposed by Chopard et al. (2013) and was selected for further investigation and improvement to expand its applicability to practical problems.

In Chapter 5 a generalised transformation of the 1D LBM scheme is presented as an extension of the asymmetric scheme proposed by Chopard et al. (2013). The Equilibrium Distribution Functions, force term weight factors, stability requirements and boundary conditions are all derived in parametric form to align with the geometric and displacement configurations of the proposed scheme. A Chapman-Enskog Expansion is also performed on the proposed scheme to show it solves the Shallow Water Equations. The proposed scheme has the advantage of being applicable to both subcritical and supercritical regimes, while applicability of other LBM schemes is limited to subcritical flows only.

A number of test cases are presented in Chapter 6 to validate the proposed scheme. The test cases comprise standard spatially-varied flow cases from open-channel hydraulics and covered both subcritical and supercritical flow regimes. In these test cases, model results are compared with analytic solutions from the energy and momentum equations and close agreement was found between the modelled and analytic results. A supercritical dam-break case into a downstream tailwater is also included in the test cases to demonstrate

applicability of the proposed model to unsteady flows where the flow regime is supercritical. Model results were compared against the results from the ANUGA finite volume model and excellent agreement was observed in the water profiles and water level time series.

In Chapter 7 application of the proposed scheme to swash zone problems are investigated. A review of the commonly used numerical techniques for shoreline treatment are presented, including the technique proposed by Liu and Zhou (2014), which was selected for implementation. An adjustment was performed on the technique proposed by Liu and Zhou (2014) to accommodate the transformed scheme and it was used to simulate a number of cases involving wet-dry interfaces. While the modified wet-dry boundary condition appeared to successfully allow water progress into the dry zone, the inevitable adjustments applied to the boundary conditions to cater for the scheme asymmetry did not appear to correctly represent the physics. The modelled wave run-up profiles did not match those produced using the standard scheme, more importantly, it was evident that the transformed scheme cannot be used for very shallow flows where the lattice Froude number is greater than one (Chapter 5) because the solution will fall outside the stability zone. Such a condition would occur in stationary water with a bore approaching a beach.

Conclusions and recommendations for further research and possible extension of the transformed scheme are included in Chapter 8.

In Appendix A detailed derivation of the equilibrium functions are presented for the standard D2Q9 LBM scheme for shallow water flows. These do not appear in complete and detailed form in the literature to the author's knowledge.

In Appendix B, a detailed derivation of the equilibrium functions in D2Q9 LBM scheme for a specific transformation case of framework speed $U = {}^{e}/_{3}$ in the transverse lattice direction is presented. Projected lattice speeds are calculated for each of the 9 directions and the Equilibrium Distribution Functions are derived for the moving framework. However, these equilibrium functions have not been used further and remain to be applied in further work.

2. Governing Equations on Fluid Flow

This chapter reviews the model representations of fluid dynamics in the mathematical form. It is important to emphasize that these mathematical equations are merely approximations to the actual behaviour of fluid; therefore, understanding the assumptions and limitations in deriving these equations in essential in their proper use.

2.1. Continuity Equation

The Law of Conservation of Mass for a control volume of fluid yields, in the integral form:

$$\oint_{C.S.} \rho v \mathrm{d}A + \frac{\partial}{\partial t} \int_{C.V.} \rho \mathrm{d}V = 0. \tag{2.1}$$

in which ρ is fluid density, v denotes velocity and $\mathrm{d}A$ and $\mathrm{d}V$ represent differential surface area and volume. If the Divergence theorem,

$$\iiint_{C.V.} (\nabla . F) \mathrm{d}V = \oiint_{C.S.} (F . n) \mathrm{d}A. \tag{2.2}$$

is applied to this integral equation, we obtain (Hughes and Brighton 1999):

$$\frac{\partial \rho}{\partial t} + \frac{\partial}{\partial x}(\rho u) + \frac{\partial}{\partial y}(\rho v) + \frac{\partial}{\partial z}(\rho w) = 0. \tag{2.3}$$

where u, v and w represent velocity components. Using the tensor notation and neglecting changes in density this equation reduces to:

$$\frac{\partial}{\partial x_i}(\rho u_i) = 0. \tag{2.4}$$

2.2. Momentum Equation

Applying the momentum principle to an elemental cube of fluid with negligible variation in density in Cartesian coordinates yields the Euler equation (Holthuijsen 2007), which may be written in the vector form:

$$\frac{\partial u}{\partial t} + \frac{\partial (uu)}{\partial x} + \frac{\partial (vu)}{\partial y} + \frac{\partial (wu)}{\partial z} = -\frac{1}{\rho}\frac{\partial p}{\partial x}. \quad \text{(momentum in x – direction)}$$
$$\frac{\partial v}{\partial t} + \frac{\partial (uv)}{\partial x} + \frac{\partial (vv)}{\partial y} + \frac{\partial (wv)}{\partial z} = -\frac{1}{\rho}\frac{\partial p}{\partial y}. \quad \text{(momentum in y – direction)} \qquad (2.5)$$
$$\frac{\partial w}{\partial t} + \frac{\partial (uw)}{\partial x} + \frac{\partial (vw)}{\partial y} + \frac{\partial (ww)}{\partial z} = -\frac{1}{\rho}\frac{\partial p}{\partial z}. \quad \text{(momentum in z – direction)}$$

which can be expressed in the brief tensor form:

$$\frac{\partial u_i}{\partial t} + u_j \frac{\partial u_i}{\partial x_j} = -\frac{1}{\rho}\frac{\partial p}{\partial x_i}. \qquad (2.6)$$

2.3. Stress-Strain Rate Relationships

Using the tensor notation, stress-strain relationship in a fluid may be expressed as:

$$s_{ij} = -p d_{ij} + m\left(\frac{\partial u_i}{\partial x_i} + \frac{\partial u_j}{\partial x_i} - \frac{2}{3} d_{ij} \frac{\partial u_k}{\partial x_k}\right) + z d_{ij} \frac{\partial u_k}{\partial x_k}. \qquad (2.7)$$

z is the coefficient of viscosity defined as $z = l + \frac{2}{3}m$ where $m$is the dynamic viscosity of fluid, l (used in the coefficient of viscosity) is a second coefficient of viscosity (Hughes and Brighton 1999) and δ_{ij} is the Kronecker Delta defined as:

$$d_{ij} = \begin{cases} 1 & i = j \\ 0 & i \neq j \end{cases}$$

2.4. The Navier-Stokes Equations

The Navier-Stokes equations are the complete equations of motion for a viscous Newtonian fluid. Using Equations (2.6) and (2.7):

$$r\left(\frac{\partial u_i}{\partial t} + u_i \frac{\partial u_i}{\partial x_j}\right) = -\frac{\partial p}{\partial x_i} + F_i + \frac{\partial}{\partial x_j}\left[m\left(\frac{\partial u_i}{\partial x_i} + \frac{\partial u_j}{\partial x_i} - \frac{2}{3} d_{ij} \frac{\partial u_k}{\partial x_k}\right)\right] + \frac{\partial}{\partial x_i}\left(z \frac{\partial u_k}{\partial x_k}\right). \qquad (2.8)$$

Changes in viscosity are usually negligible and can be removed from the derivatives. Using the vector notation these equations reduce to:

$$r\frac{DV}{Dt} = r\left[\frac{\partial V}{\partial t} + (V \cdot \nabla)V\right] = -\nabla p + F + m\nabla^2 V. \qquad (2.9)$$

or

$$\rho\left[\frac{\partial V}{\partial t} + \nabla\left(\frac{V^2}{2}\right) - \vec{V} \times \left(\nabla \times \vec{V}\right)\right] = -\nabla p + F + \mu\nabla^2 V \,. \tag{2.10}$$

In which $\nabla^2 V = \nabla\left(\nabla \cdot \vec{V}\right) - \nabla \times \left(\nabla \times \vec{V}\right)$ where $\vec{V} \bullet \vec{V}$ and $\vec{V} \times \vec{V}$ are divergence and curl operators applied to velocity vector V, respectively as defined for any vector $\vec{V} = V_x\vec{\imath} + V_y\vec{\jmath} + V_z\vec{k}$ as below:

$$\text{div}\left(\vec{V}\right) = \nabla.\vec{V} = \frac{\partial V_i}{\partial x} + \frac{\partial V_j}{\partial y} + \frac{\partial V_k}{\partial z} \tag{2.11}$$

$$\text{curl}\left(\vec{V}\right) = \nabla \times \vec{V} = \frac{\partial V}{\partial x}\vec{\imath} + \frac{\partial V}{\partial y}\vec{\jmath} + \frac{\partial V}{\partial z}\vec{k} \tag{2.12}$$

This is equivalent to the full form:

$$\begin{aligned}
&\rho\left(\frac{\partial u}{\partial t} + u\frac{\partial u}{\partial x} + v\frac{\partial u}{\partial y} + w\frac{\partial u}{\partial z}\right) = -\frac{\partial P}{\partial x} + F_x + \mu\left(\frac{\partial^2 u}{\partial x^2} + \frac{\partial^2 u}{\partial y^2} + \frac{\partial^2 u}{\partial z^2}\right).\\
&\rho\left(\frac{\partial v}{\partial t} + u\frac{\partial v}{\partial x} + v\frac{\partial v}{\partial y} + w\frac{\partial v}{\partial z}\right) = -\frac{\partial P}{\partial y} + F_y + \mu\left(\frac{\partial^2 v}{\partial x^2} + \frac{\partial^2 v}{\partial y^2} + \frac{\partial^2 v}{\partial z^2}\right)\\
&\rho\left(\frac{\partial w}{\partial t} + u\frac{\partial w}{\partial x} + v\frac{\partial w}{\partial y} + w\frac{\partial w}{\partial z}\right) = -\frac{\partial P}{\partial z} + F_z + \mu\left(\frac{\partial^2 w}{\partial x^2} + \frac{\partial^2 w}{\partial y^2} + \frac{\partial^2 w}{\partial z^2}\right)
\end{aligned} \tag{2.13}$$

which can be written in brief tensor notation (Hughes and Brighton 1999):

$$\rho\left[\frac{\partial w_i}{\partial t} + w_j\frac{\partial w_i}{\partial x_j}\right] = -\frac{\partial p}{\partial x_i} + F_i + \mu\frac{\partial^2 w_i}{\partial x_j \partial x_j} \tag{2.14}$$

The Shallow Water Equations (SWE), also called *Saint Venant* equations in their one-dimensional form, are a set of hyperbolic partial differential equations derived from depth-integrating the Navier-Stokes equations with the assumption of hydrostatic pressure distribution over the depth. This is the case where the horizontal length scale is much greater than the vertical length scale.

The key limitations of the SWE are as follows:

- they are derived for shallow water in which the wavelength is much larger than the wave height.
- they neglect vertical velocity and assume that the horizontal velocities do not vary with depth.
- they are derived for an incompressible fluid.
- they approximate the pressure variation with depth with a hydrostatic distribution.
- they do not consider the effect of wind, Coriolis forces and any tangential stress at water/air interface such as those introduced by wind. It is however possible to incorporate the above forces into the SWE with additional terms.

2.5. Summary

An overview of the physical equations governing fluid flow was provided in this chapter, including continuity, momentum equation, stress-strain equation and the Navier-Stokes equation with the shallow water equations which are a special form of the Navier-Stokes equations. These equations will be recovered in the following chapters to demonstrate applicability of the numerical schemes in fluid flow simulations.

3. Literature Review

This chapter includes an overview of the most commonly used numerical schemes in fluid problems. There have been numerous approximations, modifications and formulations applied to each of the numerical methods discussed in this chapter by many researchers to represent the physics of fluid flow. These, however, have been excluded from this chapter for brevity as they are not directly related to the current work. A concise review of the Finite Difference Method, the Finite Element Method, the Finite Volume Method, Smoothed Particle Hydrodynamics and the Lattice Boltzmann Method is provided and the numerical stability, advantages and shortfalls of each method are discussed. Review of the Lattice Boltzmann Method is carried out in more details with a focus on its limitations and advancements by various researchers. Further critical review of the existing shallow water LBM and shoreline treatment techniques will be provided in Chapters 4 and 7.

3.1. Traditional Numerical Methods in Computational Fluid Dynamics

Fluid flow is modelled by equations from physics that conserve mass and satisfy Newton's second law on momentum; these basic equations are in the form of Partial Differential Equations (PDE). To have an appropriate understanding of flow parameters and their interactions with surrounding environment, these PDEs must be solved by some means. An ideal solution to the governing equation of any physical problem is the one that would provide an exact and closed-form answer. Nevertheless, analytic solution of real world problems is generally impossible or extremely difficult due to complexities and uncertainties associated with geometry, properties of materials and environmental elements and typical boundary conditions in the real world. Instead of such an approach which would be impossible to implement, the usual approach is to estimate those unknown parameters and approximate the governing differential equations to algebraic equations which can be assessed using mathematical and numerical tools. This is the subject of Computational Fluid Dynamics (CFD), which at the beginning was an area of interest for engineers and scientists but now has become an independent branch of mathematics itself.

In brief, CFD is the process of approximating these partial differential equations to simplified algebraic equations that can be solved systematically using computers. It consists of three main steps:

1. representation of the physical process in form of PDEs (fluid mechanics)

2. development of a mathematical model for the physical process including identification of an appropriate numerical technique, boundary values and discretisation methods
3. pre-processing the problem to provide inputs to the mathematical model (and computer)
4. post-processing and physical interpretation of the mathematical model outputs in form of tabulated data and visual graphs

This chapter concentrates on step 2, and gives a summary and comparative study between some of the most widely used mathematical models for approximation of the differential equations in fluid dynamics.

3.1.1. Finite Difference Method

The Finite Difference Method (FDM) is one of the oldest numerical methods used to solve differential equations and is as old as differential calculus itself (Šoln 1996). In this method, derivatives of a function are replaced by one of the following approximations that are called forward differences, central differences and backward differences, respectively (Kuzmin 2007):

$$\frac{\partial f}{\partial x} = \lim_{\Delta x \to 0} \frac{f(x+\Delta x) - f(x)}{\Delta x} = \lim_{\Delta x \to 0} \frac{f(x+\Delta x) - f(x-\Delta x)}{2\Delta x} = \lim_{\Delta x \to 0} \frac{f(x) - f(x-\Delta x)}{\Delta x} = \tag{3.1}$$

If we discretise the domain $x \in [0,X]$ into N elements and denote values of x and $f(x)$ at nodal points by pair x_i and f_i where $i=0,1,2,\ldots,N$, from a Taylor expansion, we have:

$$f(x) = \sum_{n=0}^{\infty} \frac{(x - x_i)^n}{n!} \left(\frac{\partial^n f}{\partial x^n} \right)_i \tag{3.2}$$

where n is the derivative order of function $f(x)$.

For the forward difference method:

$$\begin{aligned} f_{i+1} &= f_i + (\Delta x)\frac{\partial f}{\partial x} + \frac{(\Delta x)^2}{2}\frac{\partial^2 f}{\partial x^2} + \frac{(\Delta x)^3}{6}\frac{\partial^3 f}{\partial x^3} + \ldots \\ \left(\frac{\partial f}{\partial x}\right)_i &= \frac{f_{i+1} - f_i}{\Delta x} - \frac{\Delta x}{2}\left(\frac{\partial^2 f}{\partial x^2}\right)_i - \frac{(\Delta x)^2}{6}\left(\frac{\partial^3 f}{\partial x^3}\right)_i - \ldots = \frac{f_{i+1} - f_i}{\Delta x} + O(\Delta x) \end{aligned} \tag{3.3}$$

For the central difference method:

$$f_{i+1} = f_{i-1} + (2\Delta x)\frac{\partial f}{\partial x} + \frac{(2\Delta x)^2}{2}\frac{\partial^2 f}{\partial x^2} - \frac{(2\Delta x)^2}{2}\frac{\partial^2 f}{\partial x^2} - \frac{(2\Delta x)^3}{6}\frac{\partial^3 f}{\partial x^3} + \ldots$$
$$\left(\frac{\partial f}{\partial x}\right)_i = \frac{f_{i+1} - f_{i-1}}{2\Delta x} - \frac{(\Delta x)^2}{6}\left(\frac{\partial^3 f}{\partial x^3}\right)_i - \ldots = \frac{f_{i+1} - f_i}{\Delta x} + O(\Delta x)^2 \quad (3.4)$$

and for the backward difference method:

$$f_{i-1} = f_i - (\Delta x)\frac{\partial f}{\partial x} + \frac{(\Delta x)^2}{2}\frac{\partial^2 f}{\partial x^2} - \frac{(\Delta x)^3}{6}\frac{\partial^3 f}{\partial x^3} + \ldots$$
$$\left(\frac{\partial f}{\partial x}\right)_i = \frac{f_{i+1} - f_i}{\Delta x} + \frac{\Delta x}{2}\left(\frac{\partial^2 f}{\partial x^2}\right)_i - \frac{(\Delta x)^2}{6}\left(\frac{\partial^3 f}{\partial x^3}\right)_i - \ldots = \frac{f_{i+1} - f_i}{\Delta x} + O(\Delta x) \quad (3.5)$$

where *O(Dx)* and $O(Dx)^2$ denote order of truncation errors.

From a mathematical perspective, the truncation errors of even orders $\frac{\partial^2}{\partial x^2}, \frac{\partial^4}{\partial x^4}, \ldots$ represent numerical diffusion while the odd orders $\frac{\partial^3}{\partial x^3}, \frac{\partial^5}{\partial x^5}, \ldots$ create numerical dispersion (Andersson et al. 2011).

The FDM had been in use well before computers became available (Thomée 2001). Even now and with the use of computers its algorithm can easily be coded by programming languages or spreadsheet programs and this simplicity makes it as a preferred method of numerical analysis that is still widely used when there is less concern about the accuracy of results.

The three sources of error in the Finite Difference Method are round-off error, truncation error and the convergence error. Round-off error is the loss of precision due to computer rounding of decimal quantities.

Truncation error (or discretisation error), indicated by *O(Dx)*, $O(Dx)^2$ and above, is caused by truncating the infinite Taylor expansion series and using a finite part of it. So, truncation error does not depend on the number of calculation segments in the domain and would still exist even if we use infinite number of elements to represent the problem domain.

The convergence error is related to the stability of the scheme implemented. Convergence means that by decreasing the increments Δx and Δt to zero, the approximated solution will approach the true solution of the differential equation being solved. A solution is called stable if the error caused by perturbations in the numerical solution (which is called the convergence error) remains bound.

While the FDM can produce good approximations to derivatives in relatively small sizes, the division of small quantities in its formulae can produce large numerical errors resulted from rounding off. This is particularly the case if one tries reducing the calculation step size to achieve higher precision.

3.1.2. Finite Element Method

Finite element analysis involves finding a function that approximates the exact solution for one or a set of Partial Differential Equations (PDE).

In other words, rather than finding an analytical solution to the set of PDEs or integral equations (which, in most cases is impossible), the Finite Element Method (FEM) attempts to find another function that approximates the exact solution and satisfies the initial values and all boundary conditions of the problem (Figure 3-1). Then the complex set of equations is replaced by an approximate set of ordinary differential or integral equations that can be evaluated using standard approaches. This means that the FEM approximates the solution of the differential equations but the FDM approximates the differential equation itself.

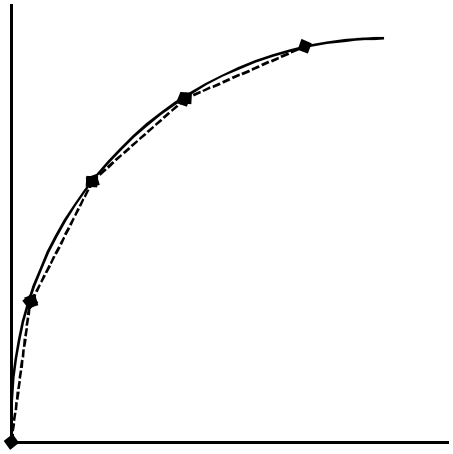

Figure 3-1 Finite Element Method- The exact solution (solid curve) is approximated by dashed lines.

The simplest form of approximation is using polynomial functions. Nevertheless, it is important to make sure that the selected set of equations is numerically stable; i.e. that they do not allow accumulation of errors during the solution convergence process and cause the results to be meaningless.

The error function in the Finite Element Method (FEM) is defined as follows, where $f(x)$ and $f_{ex}(x)$ denote approximation and exact solutions, respectively (Šoln 1996):

$$e(x)=f(x)-f_{ex}(x) \tag{3.6}$$

This error function is forced to be zero at "*n*" points in the domain where the values of exact function $f_{ex}(x)$ are either known from the physical boundary conditions or can be determined by another method (Šoln 1996).

$f(x)$ is selected as function of x and other unknown parameters: $f(x)=f(x,a_1,a_2,\ldots,a_n)$. Although $f(x)$ can be selected from a wide range of functions, it is often preferred to choose it as a linear function of the unknown parameters. So, for each nodal value x:

$$f(x)=\sum_{i=1}^{n} a_i P_i(x) \quad \text{or} \quad f(x)=\begin{bmatrix} P_1(x) & P_2(x) & \ldots & P_n(x) \end{bmatrix}' \begin{bmatrix} a_1 \\ a_2 \\ \ldots \\ a_n \end{bmatrix} \tag{3.7}$$

where $P_i(x)$ i=1,2,…,n is a set of linearly independent functions (usually selected as polynomial functions) and $a_1, a_2, \ldots, a_n$ are general approximation coefficients. "*n*" is the number of parameters used for the approximation function.

If we discretise the domain into "*m*" nodal points (or Degrees of Freedom) and show the nodal points by j=1, 2,…,m the error function must be forced to be zero at these nodal points, thus:

$$f(x_j)=f_{ex}(x_j)=f_j \qquad \text{where } j=1, 2,\ldots,m \tag{3.8}$$

$$f(x)=\sum_{j=1}^{m} f_j Q_j(x) \quad \text{or} \quad f(x)=\begin{bmatrix} Q_1(x) & Q_2(x) & \ldots & Q_m(x) \end{bmatrix}' \begin{bmatrix} f_1 \\ f_2 \\ \ldots \\ f_m \end{bmatrix} \tag{3.9}$$

where f_i denote nodal parameters and $Q_i(x)$ are interpolation functions that take a value of 1 at the corresponding node and diminish to zero at other nodes (this is necessary to force the error function to zero at the nodal points):

$$Q_i(x_i)=\delta_{ij} \tag{3.10}$$

where δ_{ij} is the Kronecker delta.

Because a_i values in Eq.(3.7) do not always have a certain physical meaning, they are conveniently replaced by f_i values which are the exact values of the function at m points.

Eq. (3.7) applies to each node and if we generalize it to the whole domain, for each node j=1,2,…,m we will have a similar equation as we have in Eq. (3.7). This ends up in a matrix form for the whole domain:

$$\begin{bmatrix} f_1 \\ f_2 \\ \dots \\ f_m \end{bmatrix} = \begin{bmatrix} P_1(x_1) & P_2(x_1) & \dots & P_n(x_1) \\ P_1(x_2) & P_2(x_2) & \dots & P_n(x_2) \\ \dots & \dots & \dots & \dots \\ P_1(x_m) & P_2(x_m) & \dots & P_n(x_m) \end{bmatrix} \begin{bmatrix} a_1 \\ a_2 \\ \dots \\ a_n \end{bmatrix} \tag{3.11}$$

This is not necessarily a square matrix (in general $n \le m$); however, we may choose the same number of nodal points and $P_i(x)$ functions (m=n) which in that case Equations (7), (9) and (11) yield:

$$\begin{bmatrix} P_1(x) & P_2(x) & \dots & P_n(x) \end{bmatrix} = \begin{bmatrix} Q_1(x) & Q_2(x) & \dots & Q_n(x) \end{bmatrix} \begin{bmatrix} P_1(x_1) & P_2(x_1) & \dots & P_n(x_1) \\ P_1(x_2) & P_2(x_2) & \dots & P_n(x_2) \\ \dots & \dots & \dots & \dots \\ P_1(x_n) & P_2(x_n) & \dots & P_n(x_n) \end{bmatrix} \tag{3.12}$$

or in short notations:

$$[P]_{1\times n} = [Q]_{1\times n} \times [P]_{n\times n} \tag{3.13}$$

which means:

$$[Q]_{1\times n} = [P]_{1\times n} \times [P]^{-1}_{n\times n}. \tag{3.14}$$

As we can select P functions from simple polynomial functions, Eq.(3.14) is the key to evaluate the interpolation functions Q that lead to developing the approximate function $f(x)$ from Eq. (3.9). Precision of the finite element analysis can be improved by simply increasing the number of nodes (n) which means making the computational mesh finer (Šoln 1996).

The FEM have been successfully applied by many people to solve fluid dynamics problems, including benchmark problems of the diffusion equation and the dispersion/Advection equation (Reddy 2005).

The following summarized description of the FEM reveals its mathematical advantages over the FDM in terms of (Reddy 2005):

- strong and rigorous mathematical foundation which makes the quality of the FEM approximations often higher than FDM approximations.

- flexibility in definition of number and location of nodal points makes it easier to handle complex geometries, complex boundary conditions and initial values or study localized effects by refining the mesh at points of interest. This is the most attractive feature of the FEM.
- flexibility of defining non-homogeneous bodies.
- dealing with nonlinearities in the problem.
- effectively addressing boundary conditions.

Disadvantage of this method are:

- relatively more complex approach in developing approximate functions and problem domain.
- experience and judgment are needed to construct a good finite element model.
- a powerful computer and reliable FEM software are essential.
- input and output data may be large and tedious to prepare and interpret.
- a specific numerical result is obtained for a specific problem. A general closed-form solution, which would permit one to examine system response to changes in various parameters, is not produced.
- the FEM is applied to an *approximation* of the mathematical model of a system (the source of so-called inherited errors).

The three main sources of error in the FEM are discretisation errors, formulation errors and numerical errors.

Discretisation error results from transforming the physical system (for example geometry of the system) into a finite element model. While the finite element model should reasonably be an accurate approximation of the physical problem, in most cases it does not represent the actual boundaries of the physical system.

Formulation error results from the use of formulas and elements that don't precisely describe the behaviour of the physical problem. For example, the rate of change or variation for a specific parameter may be assumed linear over the domain and this will produce a formulation error if it is used to formulate a more complex (i.e. quadratic, cubic, exponential, etc.) rate of change (Bokil and Gibson 2007). Numerical (truncation and round-off) errors occur as in the FDM because of numerical calculation procedures.

There are certain stability conditions that a finite element model must meet. These conditions ensure that the solution approximated in FEM has the same unique properties of the solution that would have been obtained from the analytic solution. The stability conditions include 'rank sufficiency' and 'Jacobian positiveness' which are determined from the matrices discussed above.

3.1.3. Finite Volume Method

The Finite Volume Method (FVM) is one of the most attractive and popular discretisation models used in CFD. It has some aspects of the FDM in the general approach of developing the approximating equations while the discretisation of the domain is more like the FEM; i.e. calculating the values on discrete points on a mesh. Discrete approximations of gradient, divergence and curl terms in integral equations are also evaluated using Gauss' theorem.

This method is essentially based on the integral form of the mass conservation law by setting the incoming flux into a control volume equal to the flux leaving the reference volume; this gives FVM a strong physical foundation. The idea in the FVM is to discretise the domain into control volumes (or cells) and approximate the mass conservation integral in each of those cells.

The conservation law of mass may be expressed as:

$$\frac{\mathrm{d}}{\mathrm{d}t}\int_{C.V.}\rho \mathrm{d}V = \oint_{C.S.}\vec{j}.\mathrm{d}\vec{\sigma} \tag{3.15}$$

where r is fluid density, $\mathrm{d}\vec{\sigma}$ is the surface element normal vector pointing outward to the reference volume, $\vec{j}$ is the flux passing through the control volume and *C.V.* and *C.S.* denote control volume and control surface, respectively.

Using the Divergence (Gauss) theorem, Eq. (3.15) may be re-arranged as:

$$\int_{C.V.}\left(\frac{\partial \rho}{\partial t} + \nabla.\vec{j}\right)\mathrm{d}V = 0 \tag{3.16}$$

If we want Eq. (3.16) to hold for any values in the control volume and assume that this integrand is continuous, it necessitates:

$$\frac{\partial \rho}{\partial t} + \nabla.\vec{j} = 0 \tag{3.17}$$

where $\nabla.\vec{j}$ denotes the divergence of vector $\vec{j}$.

For a 1-D model, if *u* denotes fluid velocity Eq. (3.17) is as simple as:

$$\frac{\partial \rho}{\partial t} + \frac{\partial (\rho u)}{\partial x} = 0 \tag{3.18}$$

And if we simplify this further by assuming a constant average velocity $\bar{u} = u(x,t)$, Eq. (3.18) reduces to the Advection equation:

$$\frac{\partial \rho}{\partial t} + \bar{u}\frac{\partial (\rho)}{\partial x} = 0 \tag{3.19}$$

An interesting property of the Advection equation is that the solution remains the same throughout the calculation. However, it moves with a constant speed $x - \bar{u}t$ = constant in the positive *x* direction, making a set of “characteristic” lines.

If the assumed 1-D domain is discretised into *N* cells (control volumes) and we assume an average density $\bar{\rho}_i$ (*i*=1, 2,…,*N*) for each control volume, Eq.(3.16) may be written as:

$$\frac{d}{dt}\int_{x_i}^{x_{i+1}} \rho(x,t)dx = -\bar{u}\rho(x_{i+1},t) + \bar{u}\rho(x_i,t) \tag{3.20}$$

which can be approximated to:

$$\frac{\left(\bar{\rho}_i^{n+1} - \bar{\rho}_i^{n}\right)dx}{dt} = -\bar{u}\rho(x_{i+1},t) + \bar{u}\rho(x_i,t). \tag{3.21}$$

in which the time axis has been divided into sections of length d*t* and the *i*th cell average at time *n*.d*t* is represented by:

$$\bar{\rho}_i^{n} \approx \int_{x_i}^{x_{i+1}} \rho(x, t = n\mathrm{d}t)dx\,. \tag{3.22}$$

The discrete values of density at the end points of each element will be obtained from the average element density Eq. (3.22) and the concept of characteristic lines. Rearranging Eq. (3.21) yields:

$$\bar{r}_i^{n+1} = \left(1 - \bar{u}\frac{\mathrm{d}t}{\mathrm{d}x}\right)\bar{r}_{i+1}^{n} + \left(\bar{u}\frac{\mathrm{d}t}{\mathrm{d}x}\right)\bar{r}_i^{n} \quad \Rightarrow \quad \bar{r}_i^{n+1} = (1-l)\bar{r}_{i+1}^{n} + l\,\bar{r}_i^{n} \qquad \left(l = \bar{u}\frac{\mathrm{d}t}{\mathrm{d}x}\right). \tag{3.23}$$

This is a straight solver algorithm for the Advection equation using FVM provided that at each time step the value of $\bar{r}_0^n$ is supplied to initiate the calculations. Sources of error in the FVM are the same round-off error, discretisation error and truncation error. If the d*t*/d*x* value is constant, the truncation error will be in order of *O(Dx)* and if the solution is smooth enough, this error converges to zero by reducing the size of *Dx*.

The attractiveness of the FVM lies in several aspects: the FVM conserves the variables on a coarse mesh (which is an important feature for fluid problems), it can be easily applied to irregular and unstructured meshes and handles heterogenous material very well, as each cell can be assigned different properties. Moreover, using Gauss' theorem in this method effectively reduces the number of computational dimensions from the volume to the surface bordering the control volume and this is a remarkable advantage especially when a large domain in being studied (Warburton 2005).

Convergence and stability of a FVM depend on the approximation method used to estimate the flux values at cell interfaces. The most commonly interpolation methods used are:

- Upwind Differencing Scheme (UDS): this method approximates flux at each node based on the value at its upstream node. It first order accurate and unconditionally stable, although highly diffusive.
- Central differencing Scheme (CDS): this method uses linear interpolation between adjacent nodes. It is second order accurate and its solutions may be associated with oscillations. To improve the stability of this scheme usually variation limits are set to suppress the oscillations. This scheme is widely used due to its combined accuracy and stability.
- Quadratic Upwind Interpolation (QUICK): in this method, the interpolation is made by a quadratic equation (parabola) and is third order accurate. Although this is a highly accurate scheme, it may have stability issues at high gradients.

To assist in stabilising FV models it is common to start the model with a low order scheme (such as UDS) to determine the approximate range of the interface values and switch to the higher order schemes to fine-tune the results.

3.2. Recent Techniques in Computational Fluid Dynamics

3.2.1. Smoothed Particle Hydrodynamics

The Smoothed Particle Hydrodynamics (SPH) method is a Lagrangian and relatively newer approach to calculate PDEs. It was originally developed by astrophysicists to study complex physics of moving space particles in three dimensions. Unlike the three previous methods, SPH focuses on particles instead of the whole domain and so it is a mesh-free method; i.e. does not need a grid to evaluate the differential equations (Monaghan 1992).

As the term 'smoothed' suggests, in SPH some particle properties are determined by averaging over neighboring particles. As such, the effect of neighbouring particles on the average is more than those distantly parsed. The core solver of SPH is based on an interpolation function that allows definition of a function in terms of its values at some disordered points. This *interpolant* may be defined as:

$$A_I(r) = \int A(r')\times\delta(r - r', h)\,dr' \tag{3.24}$$

where A is any arbitrary variable (material property) and δ is the Kronecker delta. The integration takes place over the entire space and W is a weight function (interpolating kernel) to calculate the averages discussed above. As expected from a weighting function, it has the following properties as graphically shown in Figure 3-2 (Monaghan 1992):

$$\int W(r - r', h)\,dr' = 1 \tag{3.25}$$

and

$$\lim_{h \to 0} W(r - r', h) = \delta(r - r') \tag{3.26}$$

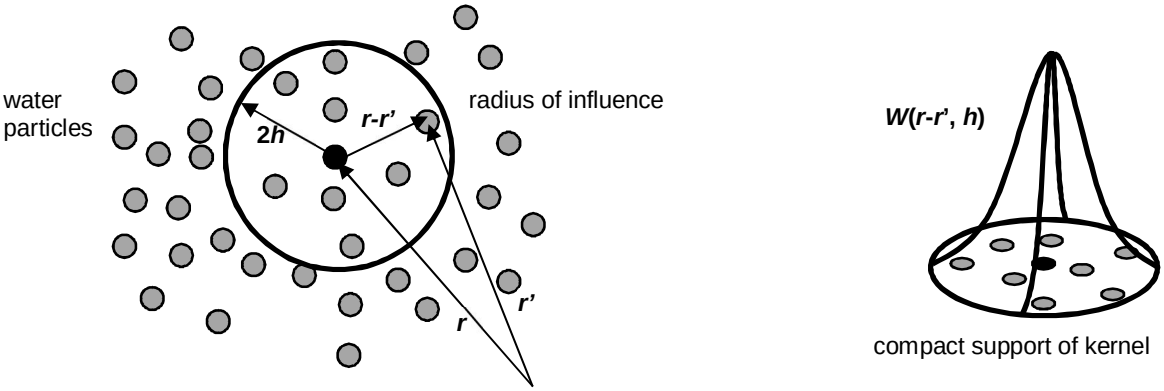

Figure 3-2 Graphical representation of the interpolant in the SPH method.

The integrand in Eq.(3.24) can be approximated by a summation interpolant to assist with the numerical calculations:

$$A_s(r) = \sum_b m_b \frac{A_b}{r_b} W(r - r_b, h). \tag{3.27}$$

where *b* denotes a particle label, thus particle *b* has mass m_b, velocity v_b, density r_b and is located at position r_b. A_b is the value of an arbitrary quantity at r_b.

The key point in this method is that if the selected kernel is differentiable, a differentiable interpolant of a function from its values at the interpolation points would be developed and its derivatives evaluated using ordinary differentiation rules without any need for a Finite Difference Method or other approximations. For example, ∇A from Eq. (3.27) is simply expressed as:

$$\nabla A_s(r) = \sum_b m_b \frac{A_b}{r_b} \nabla W(r - r_b, h). \tag{3.28}$$

Using a Taylor expansion of A_b around r_b it is concluded that the interpolation is associated with no error for constant functions.

If it is desired to find a physical interpretation for the SPH solution, it is always preferred to use a Gaussian kernel. Gaussian functions appear as the density function of the Normal distribution, with a characteristic symmetric “bell shape” curves as shown in Figure 3-2. They are widely used in problems dealing with fluids; for example, where the diffusion equation is adopted to describe the time evolution of a mass-density under diffusion. For this reason, Gingold and Monaghan (1977) recommended using a Gaussian kernel for the SPH equation. For 1-D problems the kernel would be:

$$W(x,h) = \frac{1}{h\sqrt{p}} e^{-\left(x^2/h^2\right)} \tag{3.29}$$

The error introduced into the solution by approximating Eq. (3.24) to Eq. (3.27) depends on how the particles (interpolation points) are disordered and is usually $O(h^2)$ or better. It is important to note that although the integration (and summation) is specified to be taken over the entire space, it is possible to reduce the number of contributing particles by choosing a *W* that diminishes for all $|r - r_b| \geq h$.

A computationally effective kernel is the kernel introduced by Lattanzio et al. (1985) based on spline functions:

$$W = \frac{s}{h^n}\begin{cases} 1 - \frac{3}{2}q^2 + \frac{3}{4}q^3 & \text{if } 0 \le \frac{r}{h} \le 1 \\ \frac{1}{4}(2-q)^3 & \text{if } 1 \le \frac{r}{r} \le 2 \\ 0 & \text{otherwise} \end{cases} \tag{3.30}$$

where n denotes the number of dimensions and s is normalization constant which takes the following values for 1D, 2D and 3D problems:

$$\frac{2}{3} \qquad \frac{10}{7p} \qquad \frac{1}{p}$$

The benefits of implementing this kernel are:

- the second derivative of this kernel is continuous and thus it is not sensitive to the disorders and errors of approximating Eq. (3.24) to Eq. (3.27)
- for all points with $r > 2h$ the second derivative diminishes to zero
- the dominant error term in the integral interpolant has order $O(x^2)$

The most outstanding feature of SPH is that it inherently conserves mass, momentum and energy. The flexibility of replacing kernels in SPH is its other great advantage. Depending on the problem being investigated, the following smoothing kernel types may be used (Rosswog 2015):

- kernels with vanishing central derivatives: these kernels are widely used and are good for density estimations for they are insensitive to the location of the particles. Examples of these kernels are: B-spline functions (Schoenberg 1946), parametrised family of kernels (Cabezón et al. 2008) and Wendland kernels (Wendland 1995).
- kernels with non-vanishing central derivatives; in these kernels the derivatives remain finite in the centre, meaning that the repulsive force between the particles will never vanish. These kernels were originally developed to achieve very regular distribution of particles and avoid pairing instabilities between the particles. Examples of this group are the linear quartic kernels (Valcke et al. 2010) and quartic core kernel (Rosswog 2015).

SPH is being increasingly used in CFD areas, including coastal engineering problems; certain advantages over the grid-based methods are (Cercos-Pita et al. 2016, Monaghan 2012, Wei et al. 2017):

- due to the nature of SPH modelling, it honours the conservation of mass principle because the particles are mass representatives and therefore there is no need to have additional formulations to make the model mass-conservative.
- resolution of the model can be locally adjusted by defining the number of particles (that represent density).
- instead of solving a set of linear system of equations, pressure is calculated based on weighted contributions of pressure in neighbouring particles and therefore pressure can be traced on a real-time basis.
- for problems when two phases of fluids are present, unlike mesh-based methods that track and verify each fluid boundaries at each time step, SPH creates a free surface for the fluids with particles representing the denser fluid (for example water) and the voids between the particles representing lighter fluid (usually air).

A disadvantage of SPH models over the grid-based methods in that a large number of particles need to be simulated to yield the same resolution of results as a mesh-based approach; although many of these particles that “fill” the fluid volume may not be rendered during the simulations.

3.2.2. Lattice-Boltzmann Method

The Lattice Boltzmann Method (LBM) is another relatively new particle-based technique used in fluid problems. This method is an improved version of Lattice Gas Automata (LGA).

Cellular automaton consists of a set of cells on a grid whose status evolves over discrete time steps according to the pre-defined rules that determine the state of each cell in new time step based on the states of its neighbouring cells (Rothman and Zaleski 1997). In the simplest case that can be easily programmed for a computer, each cell takes a value of 0 or 1, which can be interpreted as “existence” or “non-existence” of particles on a domain which is presented by a lattice mesh (Sukop and Thorne 2007).

In the original LGA method, rather than solving the Navier-Stokes equations, fluid particles were allowed to displace on a discrete lattice mesh and each lattice node was connected to its neighbouring nodes via predefined links. While mass and momentum were precisely conserved in LGA through the collision rules, it had critical deficiencies, including lack

of Galilean relativity (especially for the modern physics problems), statistical noise (unexplained variation) which was intrinsic to this method, explicit dependence of pressure to velocity, which was obviously unphysical and exponential complexity for three-dimensional lattices. Galilean relativity/invariance is a principle of relativity stating that the fundamental laws of physics are the same in all inertial frames. It is a basic requirement demanded by any physical model and LGA could not satisfy this requirement due to density-dependence of a so-called $g(\rho)$ factor (Frisch et al. 1987).

Later and to remove the statistical noise of this method, the Boolean particle number in LGA was replaced by its ensemble in form of a density distribution (McNamara and Zanetti 1988) and the discrete collision rule was replaced by a continuous collision operator (Qian et al. 1992). Following these improvements, Galilean invariance was easily achieved for advection terms[1] (Krüger et al. 2017).

Although not related directly to the scope of current research, it is worthwhile to mention that a prominent advantage of the LBM is its relative simplicity in problems dealing with multi-phase fluid systems. The LBM is founded on particle interactions (which may represent molecules) and hence it is more convenient if the LBM is used to define a system of particles with different momentum (which will represent different fluid viscosities in the macroscopic scale), their boundaries and interactions. Despite the rising attractiveness of the LBM (especially in modelling complex fluid systems), it has certain shortcomings. These include limitations in modelling high Mach numbers, which is analogous to supercritical shallow water flows, and a thermo-hydrodynamic pattern, because the modelled interface of multiphase fluids is usually thick and the ratio of fluid densities at the interface is smaller than the real fluids (Succi 2001).

Based on the principles of Boolean algebra, if the presence or absence of a particle with density distribution $f_i(x,t)$ at any lattice node and each time step is indicated by 0 or 1, which can move via certain links to its neighbouring locations at speed e, the whole process of collision and steaming can be explained as below:

[1] In fact, LBM is not strictly Galilean invariant due to the $O(u^3)$ error that exists in the standard LBM resulting from the minimal discretisation of velocity space. However, it is seldom an issue unless very large velocity gradients are being simulated.

When a particle moves to an adjacent location there are two possibilities:

a) the adjacent location is empty: In this case the particle with density distribution $f_i(x,t)$ moves to the new location without any interaction with other particles
b) if two or more particles with $f_i(x,t)$ occur at the same site at the same time, there will be a total density distribution of particles entering the site with density distribution $f_i^{in}(x,t)$. Once the particles collide there will be a new distribution $f_i^{out}(x,t)$ resulting from the collision. In the next time step $(t+\Delta t)$ particles will leave the location towards neighbouring sites with their new speeds resulting from the collision. A collision operator is needed to define the collision process and new velocities.

This process can be summarized as:

$$f_i^{out}(x,t) = f_i^{in}(x,t) + \Psi_i\left(f^{in}\right) \qquad \text{(Collision)} \tag{3.31}$$

$$f_i^{in}(x + e_i\Delta t, t + \Delta t) = f_i^{out}(x,t) \qquad \text{(Streaming)} \tag{3.32}$$

in which $e_i = \Delta x/\Delta t$ is the lattice speed and is constant across the domain, f^{in} is the resultant density distribution from all occurring particles and Ψ_i represents the collision operator. The collision-streaming process is shown in Figure 3-3.

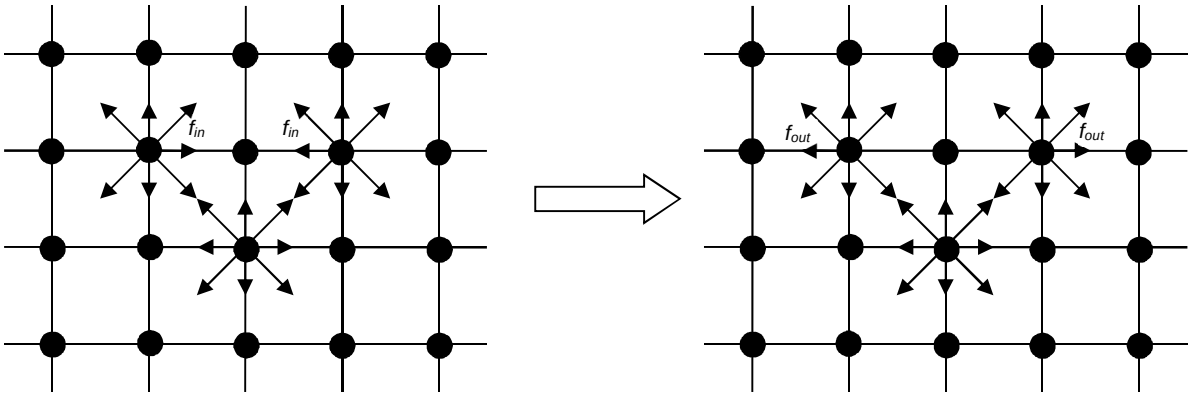

Figure 3-3 Collison-streaming steps in LBM. The left figure shows the particles on adjacent lattices colliding and the right figure shows the new equilibrium functions after the streaming step.

A widely used and computationally-efficient collision operator was developed by Bhatnagar, Gross and Krook (BGK) using the concepts of relaxation time (τ) and an Equilibrium Distribution Function (f_{eq}) (Bhatnagar et al. 1954):

$$\Psi_i(f^{in}) = \frac{1}{\tau}(f_i^{eq} - f_i^{in}) \tag{3.33}$$

Equations (3.32)and (3.33) are often expressed in a single form as:

$$f_i(x + e_i\Delta t, t + \Delta t) = f_i(x,t) + \frac{1}{t}(f_i^{eq} - f_i). \tag{3.34}$$

The relaxation time is a dimensionless parameter reflecting the speed of the equilibration and depends on transport coefficients such as diffusivity and viscosity (Krüger et al. 2017).

A fluid can generally be described and studied at three levels (Frisch et al. 1986) :

1. Molecular: At this level particle motion is reversible and governed by the laws of Hamiltonian mechanics.
2. Kinetic: At this level fluid behaves according to an irreversible low-density Boltzmann approximation.
3. Macroscopic: At this level, fluid can be studied using a continuum approximation.

Maxwell was the first to realise that the macroscopic behaviour of a fluid can be expressed by putting together the thermodynamic equilibrium variables (local density, momentum, temperature, etc.) that vary in space and time; such variables would be approximated from the molecular and kinetic study of fluid particles (Maxwell 1890). Maxwell's idea was later developed and finalised by Chapman and Cowling (1960) and Uhlenbeck &Ford (1963).

In 1972, a mathematical presentation of a model that satisfies these criteria was proposed for the first time (Hardy and Pomeau 1972) and a year after that the very first microscopic model, which in the continuum limit reproduced the main fluid characteristics, was developed by Hardy, de Pazzis and Pomeau (the famous HPP model) in a benchmark paper (Hardy et al. 1973). This model comprised square, two-dimensional lattices with unit spacing, unit discrete microscopic velocities and discrete time steps (and hence was viewed as a form of a "Boolean" model) which was demonstrated to lead to precise thermodynamical laws at the macroscopic level. This model consisted of lattices with four particles of equal mass, which were only allowed to move in one of the defined links to a vacant neighbouring site. The incoming particles from different sites to the same site were allowed to collide head-to-head and get replaced by a resultant particle moving at right angle to the direction of original particles. In another work, the equilibrium state of particles was investigated and the Navier-

Stokes equations were mathematically derived from this model using a transport coefficient (Hardy and Pazzis 1976).

A decade later, Frisch, Hasslacher and Pomeau studied a hexagonal lattice system (FHP model) and demonstrated that cellular automata can be used as an efficient tool to simulate the 2D nonlinear Navier-Stokes equations and called it a lattice gas model (Frisch et al. 1986). If N_i are the average population at a vertex with velocities in the direction i, then the macroscopic density and momentum would be defined as:

$$\rho = \sum_i N_i \tag{3.35}$$

$$\rho u = \sum_i N_i c_i \tag{3.36}$$

where u is the macroscopic velocity and c_i is the unit velocity vector in direction i. They suggested that the N_i values were computed using the Fermi-Dirac distribution in the general form of:

$$N_i = \frac{1}{1+e^{(\alpha+\beta c_i.u)}} \tag{3.37}$$

It was still not known how to address the 3D version of the Navier-Stokes equations using this method, because no regular 3D lattices were found to meet the required symmetry conditions. However, the FHP model suggested that splitting the time evolution could assist in overcoming this problem.

Later on the same year, the results of an important work proposing two strategies for approaching the 3D Navier-Stokes equations on lattices were published (D'Humières and Lallemand 1986):

1. a pseudo 3D model in which a fourth dimension was introduced to give the model an effective 3D symmetric structure.
2. a multi-speed model on a cubic lattice where particle velocities were 0, 1 or $\sqrt{2}$.

This was the first lattice gas model that could effectively solve the 3D version of the Navier-Stokes equations.

A comprehensive description of the physics and underlying mathematics of this model with detailed explanation of the 2D and 3D case of the Navier-Stokes equation was published a year later (Frisch et al. 1987). That publication was followed by a brief description of the lattice gas hydrodynamics (Frisch 1989).

The lattice gas model was still suffering from two main shortcomings:

1. a non-Galilean invariance caused by a density-dependent coefficient in the convection term.
2. a velocity-dependent equation of state; which made a relatively poor representation of the true hydrodynamic equations

McNamara and Zanetti (1988) proposed using the mean population of particles instead of the Boolean variables of lattice gases. This allowed the population density function to take any real number between 0 and 1. This suggestion resulted in significant reduction of statistical noise in the lattice gas models (McNamara and Zanetti 1988). The resulting model was more effective than the LGA models and was named the Lattice Boltzmann Model (LBM).

In 1992 a collision operator was proposed as an alternative to the collision rules adopted in lattice gas and lattice Boltzmann models (Qian et al. 1992). This collision operator was taken from an earlier work by Bhatnagar, Gross and Krook, famous as the BGK collision operator, and resulted in a numerical scheme to solve the Navier-Stokes equations with second-order accuracy. This method was efficient, noise-free, had Galilean invariance and a velocity-independent pressure, provided that proper equilibrium function and relaxation parameters were chosen (Bhatnagar et al. 1954). The work by Qian et al. was a major milestone in applying lattice gas models for fluid problems; the LBM had now been recognized as an alternative method to the traditional numerical schemes for fluid flow and started to attract the attention of scientists and researchers around the world.

In a paper released in the same year (Chen et al. 1992) it was demonstrated how the problems of traditional lattice gas automaton models can be eliminated by using a single-time relaxation approximation and a particular Maxwell-type distribution. They. helped to solve the complete set of Navier-Stokes equations using an efficient parallelised computational scheme. Later in the same year, the FHP model was applied to simulate non-Newtonian fluids by using the extensional viscosity of a lattice gas (Ahner and Dooher 1992).

In 1996, results of investigations on stability issues that LBM users were encountering with BGK relaxation times were published (Sterling and Chen 1996). Based on these investigations, it was concluded that the linear stability for the system depends on the distribution of mass at a site, the relaxation time, the average velocity and the wave number of perturbations. In this work, stability results for a 7-velocity square lattice and a 15-velocity cubic lattice were reported and it was shown that the results common to all cases were (Sterling and Chen 1996):

1. the BGK relaxation time must not be less than 1/2.
2. there is a maximum stable mean velocity for fixed values of the other parameters.
3. as the relaxation time increases, the maximum stable velocity increases monotonically until a fixed speed is reached, which does not change further. This maximum speed, expressed in lattice units, varied for the hexagonal, square and cubic lattices studied in that work.

Two important papers about LBM applications in fluid flow were published in 1997 almost at the same time: The first one described the work on LBM with BGK relaxation terms using a two-dimensional 9-bit square lattice (D2Q9) scheme (Figure 3-4) by He and Luo (1997). Because of the density fluctuations in incompressible LBM models, it was suggested that pressure (p) is used instead of the mass density (ρ). The incompressible Navier-Stokes equations were derived from the model using the Chapman-Enskog procedure (a procedure in which the Navier-Stokes equation and its transport coefficients are derived from the Boltzmann equation). It was also shown that the results of the LBM model were in excellent agreement with theory for two cases studies: a plane Poiseuille flow and the 2D Womersley (1955) flow[2] (He and Luo 1997).

The second paper discussed the velocity and pressure boundary conditions for 2D and 3D lattice Boltzmann BGK models, with details on modelling slip and no-slip walls and inflow/outflow conditions. It was shown that the numerical results are 2nd order accurate and the bounce-back boundary condition had a more stable behaviour compared to the other published boundary conditions (Zou and He 1997).

[2] Womersley flow is the fluid flowing in a conduit where the pressures at the ends of the conduit are time-dependent and vary periodically. Womersley was the first to study and propose a method for calculation of velocity, rate of flow and viscous drag in arteries when the pressure gradient is known (Womersley 1955).

An overview of the LBM findings with a focus on case studies of cavity flows, flow over a backward-facing step and flow around a circular cylinder was published by Chen and Doolen in 1997. In this work, the advantages of LBM in modelling complicated boundary conditions, multi-phase and multi-component interfaces, fluid turbulence and reaction diffusion systems to traditional numerical methods were discussed (Chen and Doolen 1997).

Buick and Greated (1998) used the LBM to simulate the gravitational interaction of waves between two immiscible, viscous fluids of different densities and the results including wave speeds, oscillation frequency and damping rate were found to be in close agreement with theory (Buick and Greated 1998).

Salmon (1999) applied the LBM to model ocean circulations with shallow water and no-slip boundary conditions. He derived Equilibrium Distribution Functions that satisfied the Shallow Water Equations based on the general form that was previously presented in a work by Rothman and Zaleski (1997) and used them in his D2Q9 scheme (Figure 3-4). To maximise entropy and for a D2Q9 lattice it is required that:

$$h(x,t) = \sum_{i=0}^{8} h_i(x,t) \tag{3.38}$$

$$hu(x,t) = \sum_{i=0}^{8} c_i h_i(x,t) \tag{3.39}$$

which through the Chapman-Enskog expansion are shown to correspond to conservation of mass and momentum, respectively. A third condition is also required to make the momentum flux of LB particles equal to the momentum flux:

$$\sum_i c_{i\alpha} c_{i\beta} h_i^{eq} = \frac{1}{2} g h^2 \delta_{\alpha\beta} + u_\alpha u_\beta h \tag{3.40}$$

where $\delta_{\alpha\beta}$ is the Kronecker delta function:

$$\delta_{ij} = \begin{cases} 0, & if\ \ i \neq j \\ 1, & if\ \ i = j \end{cases} \tag{3.41}$$

and *h* and *u* are flow depth (pressure) and velocity, respectively.

Based on the lattice symmetry, Rothman and Zaleski (1997) assumed that the solution of these equations is in the general form of:

$$h_i^{eq}(h,u,v) = A(h) + B(h)c_{i\alpha}u_\alpha + C(h)c_{i\alpha}c_{i\beta}u_\alpha u_\beta + D(h)\delta_{\alpha\beta}u_\alpha u_\beta + O(u^3) \quad (3.42)$$

After determination of A, B, C and D coefficients, which are functions of *h* and independent of *u*, Salmon (1999) obtained the following solutions for the equations:

$$h_0^{eq} = h - \frac{5gh^2}{6e^2} - \frac{2h}{3e^2}\mathbf{u_i}\mathbf{u_i}$$

$$h_i^{eq} = \frac{gh^2}{6e^2} + \frac{h}{3e^2}e_{\alpha i}\mathbf{u_i} + \frac{h}{2e^4}e_{\alpha i}e_{\alpha j}\mathbf{u_i}\mathbf{u_j} - \frac{h}{6e^2}\mathbf{u_i}\mathbf{u_i} \quad \text{(odd i)} \quad (3.43)$$

$$h_i^{eq} = \frac{gh^2}{24e^2} + \frac{h}{12e^2}e_{\alpha i}\mathbf{u_i} + \frac{h}{8e^4}e_{\alpha i}e_{\alpha j}\mathbf{u_i}\mathbf{u_j} - \frac{h}{24e^2}\mathbf{u_i}\mathbf{u_i} \quad \text{(even i)}$$

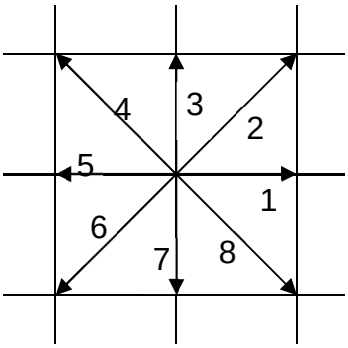

Figure 3-4 The D2Q9 scheme used by Salmon (1999). The numbered arrows show the directions that any particle is allowed to move in the collision-streaming process.

Detailed derivation of Equations (3.43) is provided in Appendix A and a high-level derivation was previously given in Zhou (2004).

In a paper by Dellar (2002), the isothermal Navier-Stokes equations were obtained from a truncated moment expansion of the equilibrium function and then applied to the Shallow Water Equations. In the appendix of this paper he demonstrated that the Equilibrium Distribution Functions (EDF) are of indefinite sign, and except for the rest state (u=0), that all equilibrium functions are positive (Dellar 2002). From the physical perspective, EDFs represent mass in a system and naturally are expected to take positive values. For the standard D1Q3 scheme it can easily be proved that all EDFs will remain positive provided that the local Mach number remains low (Yang et al. 2012) but in a D2Q9 scheme they could

take negative quantities. While negativity of EDFs has the potential of producing numerical instability, this is not always the case as long as the summation of those is a positive number.

Zhou (2002) presented a D2Q9 lattice Boltzmann method for the shallow water equations (LABSWE) using the EDFs proposed earlier (Salmon 1999) and claimed that it solved steady and unsteady flow problems using source terms such as bed slope and friction to incorporate external forces imposed to the model. Zhou used the inflow and outflow boundary condition schemes proposed earlier (Zou and He 1997) and demonstrated that the precision of the results depend on the size of the lattice selected until convergence occurs. The results of Zhou's model were in excellent agreement with the analytical solutions for some benchmark problems such as subcritical steady flow over a bump, tidal wave flow, flow around a cylinder and flow in a channel with sudden expansion (Zhou 2002).

Zhou defined certain stability conditions for the lattice Boltzmann method (Zhou 2004):

1. the kinematic viscosity υ should be positive:

$$\upsilon = \frac{e^2 \Delta t}{6}(2\tau - 1) > 0 \Rightarrow \tau > \frac{1}{2} \tag{3.44}$$

2. the magnitude of the resultant velocity must be smaller than the speed calculated with the lattice size divided by the time step. Using $u = \sqrt{gh}$ for wave speed:

$$\frac{u_j u_j}{e^2} < 1 \Rightarrow \frac{gh}{e^2} < 1 \tag{3.45}$$

3. since the lattice Boltzmann is limited to low speed flows, it was suggested to be applied to subcritical flows only:

$$\frac{u_j u_j}{gh} < 1 \tag{3.46}$$

The failure of LBM to model high velocity flows is due to one of its intrinsic limitations. The EDFs in LBM are derived from Taylor series expansion of Maxwell function in terms of Mach number. This inevitably limits the range of Mach number (analogous to Froude number) that can be used in the lattice, because the particle velocities have to remain finite (Guo and Shu 2013, Jenssen et al. 2001). Lattice Boltzmann models solve the compressible, isothermal Navier-Stokes equations. As such, it is required that the Mach number (the ratio of the fluid speed to the speed of sound) remains small to mimic an approximately isothermal and

incompressible state of flow (Dellar 2001). In open-channel hydraulics, Froude number is used more often, which is conceptually analogous to Mach number.

Zhou (2007) used the model he had introduced earlier (LABSWE) to simulate discontinuous flows. In this work, Zhou treated curved boundaries using an elastic-collision scheme for slip or semi-slip boundary condition or the bounce-back scheme for no-slip boundary condition (Zhou 2007). Later Zhou and Liu provided an update to LABSWE in regards to treatment of external forces (Zhou and Liu 2013). In different papers, Zhou and others applied LABSWE in various applications such as:

1. small perturbation of the free surface in a quasi-stationary case: From hydrodynamics, the initial water pulse on the surface splits into two waves and starts travelling to upstream and downstream at a characteristic speed $\sqrt{gh}$ and the results from his model showed good agreement with theoretical results (Zhou 2007).
2. 2D dam break case: In this case study Liu et al. (2009) considered a square reservoir with a constant tail water depth downstream. Flow regime through this simulation remained subcritical at all lattice locations. From theory, in the moment of dam failure a bore wave is expected to propagate downstream and a depression wave upstream. The results of his model demonstrated very good agreement with existing solutions (Liu et al. 2009).
3. interaction between a surge and a cylinder: In this case, Zhou used a no-slip boundary condition at the solid boundaries of the cylinders and again, he showed that his model closely reproduces the results proposed by other literature.
4. a LBM with an added algorithm that allowed simulating wet-dry interface in shallow water flows (Liu and Zhou 2014).
5. a shallow water LBM used in morphodynamics and sediment transport (Zhou 2014).
6. an axisymmetric LBM for rotational flows with added sink and source terms (Zhou 2011).
7. a shallow water LBM with Multi-Relaxation Time (MRT) to allow more efficient solution of flow problems where due to complexity of flow physical characteristics of flow are dominant in one direction (Zhou 2012).
8. a Multi-block lattice Boltzmann simulations of solute transport in shallow water flows (Liu et al. 2009)

Thömmes et al. (2007) applied the LBM to solve the Shallow water Equations with bed slope and bed friction as the source terms and validated it for standard test cases of a tidal wave flow and steady flow over a hump. In their D2Q9 model they adopted the same EDFs by Salmon (1999) and the boundary conditions suggested by Zou and He (1997). They verified their model for mean flow conditions using data from the Strait of Gibraltar (Thömmes et al. 2007).

Klar et al. (2008) applied a BGK lattice Boltzmann model with the shallow water equilibrium functions proposed by Salmon (1999) and the boundary conditions by Zou and He (1997) to simulate dispersion of pollutants. They considered the effects of bed slope, bed friction, Coriolis forces and wind stresses in their investigations and defined the relaxation time τ_f in terms of the physical viscosity and simulation time steps:

$$\tau_f = \frac{3\nu_H}{c^2} + \frac{\Delta t}{2} \tag{3.47}$$

and for the transport equation they defined the relaxation time as a function of the diffusion coefficient and the time step:

$$\tau_g = \frac{3\nu_C}{c^2} + \frac{\Delta t}{2} \tag{3.48}$$

They demonstrated that the results of their model have good agreement with a few benchmark problems and Strait of Gibraltar pollutant transport data (Klar et al. 2008).

In a publication by Frandsen (2008a), the application of LBM in modelling fluid flow with a focus on waves and coastal problems was discussed. Frandsen investigated the suitability of a 1-D LBM with a BGK scheme to simulate the behaviour of free-surface non-linear waves in shallow water with the assumption that the waves did not overturn (Frandsen 2008a). Frandsen had interest in time evolutions of the free-surface elevation and velocities as indicators of the numerical scheme performance and used the single relaxation time similar to Eq. (3.48) and maintained the solution within the range $\tau > {}^{\Delta t}/_{2}$ to ensure numerical stability. A new set of Equilibrium Distribution Functions were derived for the proposed 1D model (Frandsen 2008a) as shown in (3.49).

$$f_0^{eq} = h - \frac{gh^2}{2c^2} - \frac{hu^2}{c^2} \tag{3.49}$$

$$f_1^{eq} = \frac{gh^2}{4c^2} + \frac{hu}{2c} + \frac{hu^2}{2c^2}$$

$$f_2^{eq} = \frac{gh^2}{4c^2} - \frac{hu}{2c} + \frac{hu^2}{2c^2}$$

Frandsen applied this model to study run-up of a long non-breaking shallow water wave on a sloping beach. To avoid reflection at the open end of the domain (ocean end), a damping numerical scheme at that end was adopted. For the wet-dry interface two methods were used:

- Thin film layer on the beach.
- The shoreline algorithm of Lynett et al (2002).

Frandsen demonstrated that the results of this model have very good agreements with the semi-analytical predictions of Carrier et al. (2003) for tsunami wave run-up and run-down on a beach. It was also noted that although the inundation lengths yielded by this model agreed with other studies, the thin film approach generated highly inaccurate velocities during the run-down. It was then suggested to adopt higher-order schemes with at least second-order accuracy, improve the BGK collision operator by using Multi-Relaxation Time (MRT) schemes, undertake further work in treatment of boundaries (including bed friction, sediment transport effects and open-end boundary) and the effect of breaking waves. In the Frandsen model, which was the state-of-the-art LBM for shallow water and coastal applications, the flow regime remained subcritical throughout the simulation. This was a significant shortcoming that limited the applicability of LBM to non-breaking waves. There was a need to extend the limits of LBM applicability to critical and supercritical regimes so it could be applied to a range of practical problems such as swash zone hydrodynamics in coastal engineering.

In another paper published on the same year, Frandsen compared the same approach with a second-order accurate finite difference LBM in which the force terms and the collision operator are approximated with second-order accuracy and concluded that the new scheme is more efficient (Frandsen 2008b).

Frandsen summarized those findings and investigations and described the results of applying LBM to some case studies in single-phase highly viscous fluid bores in fixed tanks, water-based bores in moving tanks and dam break simulations (Frandsen 2008c). The Froude number in these studies always remained below one.

Some other related works include studies of Caiazzo (2008) who proposed a simple algorithm to initialize nodes located on moving boundaries of a LBM and compared it to some benchmark problems and studies of Banda, Seäid and Thömmes (2009) of LBM application to modelling dispersion problem in shallow waters and pollutant transport.

Servan-Camas and Tsai (2009) investigated the numerical stability of LBM with the BGK collision operator and its relation to non-negativity of the equilibrium distribution functions (EDFs). In their study, they identified the domains in which the EDFs remain positive and therefore obtained linear stability and non-negativity domains for three different lattices (D2Q9, D1Q3 and D2Q5) with linear and second-order EDFs. They studied variations of the Courant parameter Cr = u/c < 1 (u and c are flow and lattice speed, respectively) versus different relaxation times and presented numerically stable zones for each lattice scheme. They also found that the second-order EDFs have larger stability and positive domains than the linear ones. As a result of their studies, non-negativity of the EDFs was concluded as a sufficient condition for linear stability and becomes a necessary condition if relaxation time is selected close to 0.5.

Liu et al. (2009) applied the LABSWE model (by Zhou) to simulate subcritical flow channel junctions. In this model, they considered the turbulence caused by the combination of the main channel and the tributary flows. Their model utilised a multi-block lattice scheme at the junction location. In addition to verifying the model for the 90º junction, they used it to study variation of flow depth, velocity and occurrence of flow separation at the junction (Liu et al. 2009).

A D2Q5 LBM (Figure 3-5) with higher order of accuracy was implemented by Zhang et al. (2009) to simulate the wave equation.

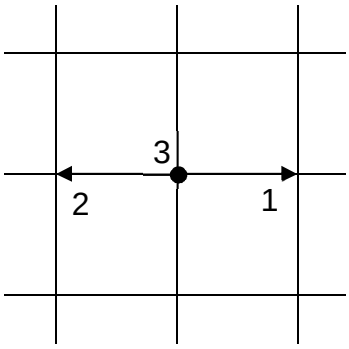

The D1Q3 LBM scheme

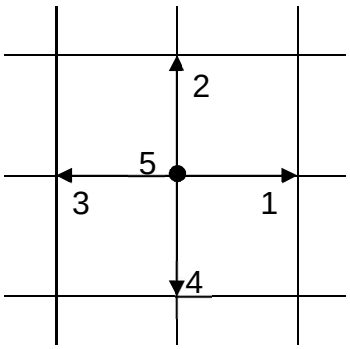

The D2Q5 LBM scheme

Figure 3-5 The D1Q3 and D2Q5 LBM schemes.

Liu, Zhou, Burrows and Peng studied partial dam-break and circular dam break problems using the LABSWE model developed by Zhou earlier (Liu et al. 2009). Eddy simulation was also included in their model to accommodate for the effects of flow turbulence. Tubbs and Tsai presented the summary of their works on applying a 3D LBM and solving multi-layer shallow water equations using high performance computing (Tubbs and Tsai 2009).

Maier and Bernard (2010) adopted a second-order accurate technique to their LBGK model to improve accuracy and reduce required grid resolution for fluid flow about solid boundaries (like pore-scale simulations). They tested the model for different cases including uniform flow past an isolated sphere, quadratic flow past a sphere near a wall, flow through an array of spheres (Maier and Bernard 2010). Some other related research in this area include the works by Jafari et al. (2010) who used a D2Q9 LBGK model with the Salmon equilibrium distribution functions to investigate particle dispersion and deposition in a channel with a square cylinder obstruction and the critical review of the force term in LBM by Mohamad and Kuzmin (2010). This discussed the three most commonly used algorithms for adding force term to LBM with BGK method and the results were validated and compared by using a natural convection problem as a test platform. The results showed that adding the force term to the collision-streaming equation is a more accurate representation of the external force. However, for more viscous flows adding the extra force term to the collision term improved predictions.

Yojina et al. (2010) used LBM to study subcritical flow patterns around square obstacles in a 2D channel. In their study, the original form of EDFs was used, without special treatment for the shallow water equations:

$$f_\alpha^{eq} = w_\alpha \rho \left(1 + 3\frac{\vec{e}_\alpha . \vec{u}}{e^2} + \frac{9}{2}\frac{(\vec{e}_\alpha . \vec{u})^2}{e^4} - \frac{3}{2}\frac{u^2}{e^2}\right) \tag{3.50}$$

where the weighting factor w_α was defined as:

$$w_\alpha = \begin{cases} 4/9, & \alpha = 0 \\ 1/9, & \alpha = 1,2,3,4 \\ 1/36, & \alpha = 5,6,7,8 \end{cases} \tag{3.51}$$

3.3. Summary

A critical review of the most common numerical methods used to solve fluid problems including the Finite Difference Method, the Finite Element Method, the Finite Volume

Method, the Smoothed Particle Hydrodynamics Method and the Lattice Boltzmann Method has been presented. The Lattice Boltzmann Method (LBM) was selected for extension of its applicability to supercritical flow problems and so was further investigated by providing a review on its evolution, applications and limitations. The first LBM using the Shallow Water Equations was a D2Q9 scheme developed by Salmon in 1999.

While the conventional LBM provides a robust and efficient tool for simulation of fluid flow problems, they lack the ability to model high-speed flows, which drastically limits their applicability to engineering problems.

The main aim of current research is to use LBM as an alternative modelling tool to study flows with supercritical flow regime, such as those occurring in the swash zone, with a focus on run-up wave tip and bore propagation. LBM was selected due to its unique features that facilitate definition of particles and tracking their displacement at each time step. For the low depth and relatively high flow velocities in the swash zone, the flow regime in this region is almost always supercritical and so improvement of LBM was required to apply it to supercritical flows. Although there have been previous studies for the subcritical non-breaking waves (Frandsen 2008), no record of applying LBM for simulation of supercritical breaking waves was found.

4. Lattice Boltzmann Modelling of Shallow Water Flows

In this chapter, a detailed review of the features and properties of the standard 1D and 2D LBM schemes are presented. The application of standard LBM and its limitation is simulating supercritical flow regimes is highlighted. The asymmetric scheme by Chopard et al. (2013) to model a limited range of supercritical flows is also presented and its performance validated via a number of test cases. The limitations of the asymmetric scheme are discussed which will lead to the main subject of current research work in the next chapter.

4.1. Equilibrium Distribution functions

To fully understand the basis of the standard D1Q3 scheme, derivation of the Equilibrium Distribution Functions for the standard D1Q3 scheme are provided below. To the author's knowledge these derivations have not been provided in this level of detail in the literature.

We assume that the Equilibrium Distribution Functions for the standard Lattice Boltzmann Model can be expressed as a power series in macroscopic velocity as proposed by Rothman & Zaleski (1997):

$$f_\alpha^{eq} = A_\alpha + B_\alpha e_{\alpha i} u_i + C_\alpha e_{\alpha i} e_{\alpha j} u_i u_j + D_\alpha u_i u_i \tag{4.1}$$

and this will be applied to the standard one-dimensional scheme shown in Figure 4-6a.
Due to symmetry of the lattice, the coefficients A, B, C and D will have the same symmetric properties, so Eq.(4.1) may be written as:

$$f_0^{eq} = A_0 + D_0 u_i u_i \qquad \text{(rest state)} \tag{4.2}$$

$$f_\alpha^{eq} = A + B e_{\alpha i} u_i + C e_{\alpha i} e_{\alpha j} u_i u_j + D u_i u_i \qquad (\alpha = 1,2). \tag{4.3}$$

The Equilibrium Distribution Functions must preserve mass and momentum in the system. For shallow water flows these are expressed by the following equations:

$$\sum_\alpha f_\alpha^{eq}(x,t) = h(x,t) \tag{4.4}$$

$$\sum_\alpha e_{\alpha i} f_\alpha^{eq}(x,t) = h(x,t) u_i(x,t) \tag{4.5}$$

$$\sum_{\alpha} e_{\alpha i} e_{\alpha j} f_{\alpha}^{eq}(x,t) = \frac{1}{2} g h^2(x,t)\delta_{ij} + h(x,t) u_i(x,t) u_j(x,t). \tag{4.6}$$

Substituting Eq.(4.2) and Eq.(4.3) into Eq.(4.4) yields ($i = j = 1$):

$$A_0 + D_0 u_i u_i + 2A + \sum_{\alpha=1,2} B e_{\alpha i} u_i + \sum_{\alpha=1,2} C\, e_{\alpha i} e_{\alpha j} u_i u_j + 2D u_i u_i = h$$

$$\Rightarrow A_0 + D_0 u_i u_i + 2A + (B e_{1i} u_i + B e_{2i} u_i) + (C e_{1i} e_{1i} u_i u_i + C e_{2i} e_{2i} u_i u_i) + 4D u_i u_i = h$$

$$\Rightarrow A_0 + D_0 u_i u_i + 2A + (B e u_i - B e u_i) + (C e^2 u_i u_i + C e^2 u_i u_i) + 4D u_i u_i = h$$

$$\Rightarrow (D_0 + 2Ce^2 + 4D) u_i u_i + (A_0 + 2A) = h.$$

After equating the coefficients of identical terms:

$$D_0 + 2Ce^2 + 2D = 0 \tag{4.7}$$

$$A_0 + 2A = h. \tag{4.8}$$

Substituting Eq.(4.2) and Eq.(4.3) into Eq. (4.5) yields:

$$A_0 e_{0i} + D_0 e_{0i} u_i u_i + \sum_{\alpha=1,2} \left(A e_{\alpha i} + B e_{\alpha i} e_{\alpha j} u_j + C e_{\alpha i} e_{\alpha j} e_{\alpha k} u_j u_k + D e_{\alpha i} u_j u_j \right) = h u_i$$

$$\Rightarrow A_0(0) + D_0(0) + A e_{1i} + A e_{2i} + B e_{1i} e_{1i} u_i + B e_{2i} e_{2i} u_i + C e_{1i} e_{1i} e_{1i} u_i u_i +$$

$$C e_{2i} e_{2i} e_{2i} u_i u_i + D e_{1i} u_i u_i + D e_{2i} u_i u_i = h u_i$$

$$\Rightarrow Ae - Ae + Be^2 u_i + Be^2 u_i + Ce^3 u_i u_i - Ce^3 u_i u_i + De u_i u_i - De u_i u_i = h u_i$$

$$2Be^2 = h. \tag{4.9}$$

Substituting Eq.(4.2)and Eq.(4.3) into Eq.(4.6) yields:

$$\sum_{\alpha=1,2} \left(A e_{\alpha i} e_{\alpha j} + B e_{\alpha i} e_{\alpha j} e_{\alpha k} u_k + C e_{\alpha i} e_{\alpha j} e_{\alpha k} e_{\alpha l} u_k u_l + D e_{\alpha i} e_{\alpha j} u_k u_k \right) = \frac{1}{2} g h^2 \delta_{ij} + h u_i u_j$$

$$A e_{1i} e_{1i} + A e_{2i} e_{2i} + B e_{1i} e_{1j} e_{1k} u_k + B e_{2i} e_{2j} e_{2k} u_k + C e_{1i} e_{1j} e_{1k} e_{1l} u_k u \quad +$$

$$C e_{2i} e_{2j} e_{2k} e_{2l} u_k u_l + D e_{1i} e_{1j} u_k u_k + D e_{2i} e_{2j} u_k u_k = \frac{1}{2} g h^2 \delta_{ij} + h u_i u_j$$

$$Ae^2 + Ae^2 + Be^3 u_i - Be^3 u_i + Ce^4 u_i u_j + Ce^4 u_i u_j + De^2 u_i u_i + De^2 u_i u_i$$

$$= \frac{1}{2} g h^2 \delta_{ij} + h u_i u_j.$$

Equating the coefficients of identical terms gives:

$$Ce^4 + 2De^2 = 0 \tag{4.10}$$

$$2Ae^2 = \frac{1}{2}gh^2 \tag{4.11}$$

$$Ce^4 = h. \tag{4.12}$$

The six unknown coefficients are determined by simultaneous solution of Equations (4.10) to (4.12):

$$A_0 = h - \frac{gh^2}{2e^2} \qquad D_0 = \frac{-h}{e^2} \qquad A = \frac{gh^2}{4e^2} \qquad B = \frac{h}{2e^2} \qquad C = \frac{h}{e^4} \qquad D = \frac{-h}{2e^2}$$

and the equilibrium functions will take the form:

$$f_0^{eq} = h - \frac{gh^2}{2e^2} - \frac{hu^2}{e^2}$$

$$f_1^{eq} = \frac{gh^2}{4e^2} + \frac{hu}{2e} + \frac{hu^2}{2e^2} \tag{4.13}$$

$$f_1^{eq} = \frac{gh^2}{4e^2} - \frac{hu}{2e} + \frac{hu^2}{2e^2}$$

The same approach may be adopted to derive the EDFs for the D2Q9 scheme as presented in Salmon (1999) and Zhou (2004) in high level. In appendix A, a full detailed derivation of the EDFs for the standard D2Q9 scheme is presented.

4.2. The force term

There are several techniques to incorporate the external force in LBM.
Guo et al. (2002) suggested that the force term is introduced into the collision term of LBM:

$$f_i(\mathbf{x} + \mathbf{e}_i\Delta t, t + \Delta t) - f_i(\mathbf{x}, t) = -\frac{1}{\tau}\left[f_i(\mathbf{x}, t) - f_i^{eq}(\mathbf{x}, t)\right] + \Delta t F_i \tag{4.14}$$

in the general form of:

$$F_i = w_i\left[A + \frac{\mathbf{B}.\mathbf{e}_i}{c_S^2} + \frac{\mathbf{C}:(\mathbf{e}_i\mathbf{e}_i - c_S^2\mathbf{I})}{2C_S^4}\right] \tag{4.15}$$

where C_S^2 is the square of sound speed and w_i are directional weights determined to satisfy lattice isotropy conditions as will be discussed in the next section. A, $\mathbf{B}$ and $\mathbf{C}$ are functions of F and can be determined by letting the moments of F_i satisfy the hydrodynamic equations. Guo et al. (2002) determined these coefficients and suggested that the following form of Eq. (4.15) is implemented:

$$F_i = \left(1 - \frac{1}{2\tau}\right) w_i \left[\frac{\mathbf{e}_i - \mathbf{v}}{C_S^2} + \frac{(\mathbf{e}_i . \mathbf{v})}{C_S^4} \mathbf{e}_i\right] . \mathbf{F} \tag{4.16}$$

and the fluid velocity is determined by:

$$\mathbf{v} = \frac{1}{h}\left(\sum_i \mathbf{e}_i f_i + \frac{\Delta t}{2}\mathbf{F}\right) \tag{4.17}$$

Many LBM researchers have been adopting various forms of Equation (4.15) in their work among which He and Luo (1997) presented a simplified version of Equations (4.16) and (4.17) in form of:

$$F_i = \frac{w_i \mathbf{e}_i}{C_S^2} \mathbf{F} \tag{4.18}$$

$$\mathbf{v} = \frac{1}{h} \sum_i \mathbf{e}_i f_i \tag{4.19}$$

which has been largely used in the LBM users' community and implemented in the current research. The point forces calculated from this equation have been incorporated into the model in form of a centred scheme, which means at each lattice point the force terms is calculated based on the average values of force at its adjacent lattices. This implementation is shown to provide a more accurate representative of the external forces (Zhou 2004).

4.3. Lattice Isotropy

Consider a lattice gas automata or any arbitrary *DmQn* lattice Boltzmann system where *m* is number of dimensions in space and *n* denotes lattice vector directions. If such a system is expected to be used in isothermal fluid modelling and recover the Navier-Stokes equations, it is a requirement for this system to show isotropic behaviour. Certain criteria are needed to be in place to consider the fact that for any particle that moves to its neighbouring locations, there will be different lengths that need to be travelled by the particle. For example, in the D2Q9 scheme shown in Figure 3-4, the odd-numbered links have shorter lengths compared to the even links, whose lengths are $\sqrt{2}$ times the other ones.

The following criteria will guarantee an isotropic response of the system (Frisch et al. 1987, Wolfram 1986). In these equations c is lattice speed, w_i are directional weights, C_S is the sound speed in lattice system and $\delta_{\alpha\beta}$ is the Kronecker Delta (the speed of sound enters these equations from the ideal gas equations used in the BGK collision model).

$$\sum_i w_i = 0 \tag{4.20}$$

$$\sum_i w_i c_{i\alpha} = 0 \tag{4.21}$$

$$\sum_i w_i c_{i\alpha} c_{i\beta} c_{i\gamma} = 0 \tag{4.22}$$

$$\sum_i w_i c_{i\alpha} c_{i\beta} c_{i\gamma} c_{i\xi} c_{i\eta} = 0 \tag{4.23}$$

$$\sum_i w_i c_{i\alpha} c_{i\beta} = C_S^2 \delta_{\alpha\beta} \tag{4.24}$$

$$\sum_i w_i c_{i\alpha} c_{i\beta} c_{i\gamma} c_{i\xi} = C_S^4 (\delta_{\alpha\beta}\,\delta_{\gamma\xi} + \delta_{\alpha\gamma}\delta_{\beta\xi} + \delta_{\alpha\xi}\delta_{\beta\gamma}) \tag{4.25}$$

4.4. The D2Q9 Scheme

To develop a computer program that allows further study of the lattice Boltzmann method in shallow water flows, the general framework of the code snippets provided in Appendix B of Zhou (2004) was used as a base for further development. These snippets were set up based on a collision operator for the simplest case of D2Q9 scheme with unit lattice speed and time steps applied to a rectangular channel. The EDFs were those in Equation (3.43) derived by Salmon (1999) for the depth-averaged Shallow Water Equations. The code snippets were further improved by adding variables for lattice speed (e) and time step (Δt) and subroutines for the no-slip (bounce-back) and slip boundary conditions and inflow and outflow conditions.

For the D2Q9 scheme in Figure 4-1a, a no-slip boundary condition (at the boundary, the fluid will have zero velocity relative to the boundary) can be expressed as (Figure 4-1b):

$$f_2=f_6 \qquad f_3=f_7 \qquad f_4=f_8 \tag{4.26}$$

while for a slip boundary condition (fluid particles next to the solid boundary are allowed to move with other particles) the following is used (Figure 4-1c):

$$f_2=f_8 \qquad f_3=f_7 \qquad f_4=f_6 \tag{4.27}$$

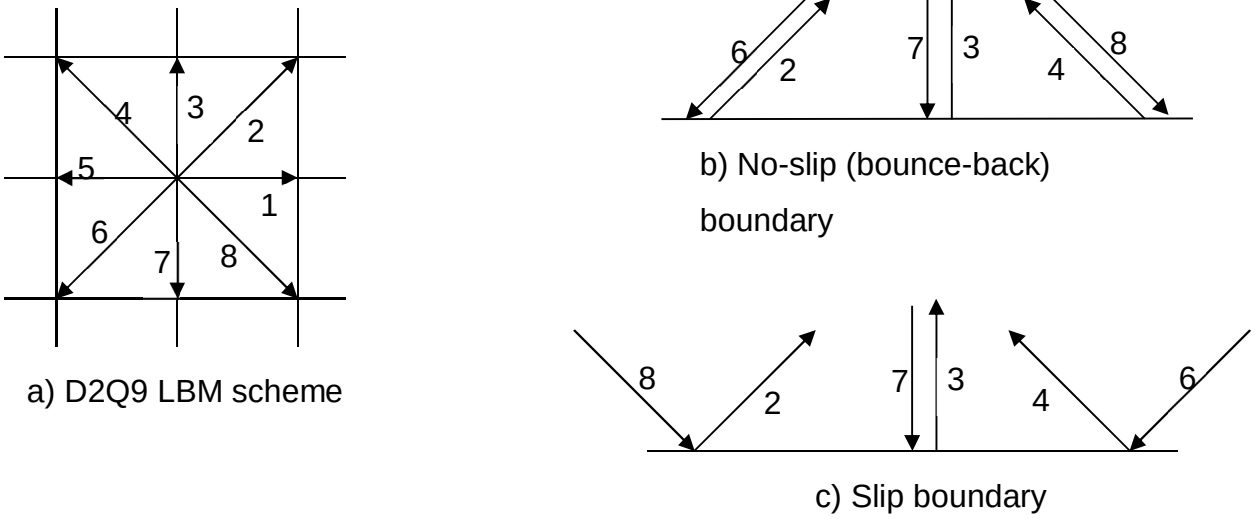

a) D2Q9 LBM scheme

b) No-slip (bounce-back) boundary

c) Slip boundary

Figure 4-1 Slip and No-slip boundary conditions at solid walls for D2Q9 scheme.

The suitability of this approach was verified by comparing model results for both conditions. The slip boundary conditions leaded to a uniform velocity distribution across the channel width and the no-slip boundary condition produced the parabolic profile of a laminar flow with zero velocity at the walls and maximum velocity at the channel centreline (Figure 4-2).

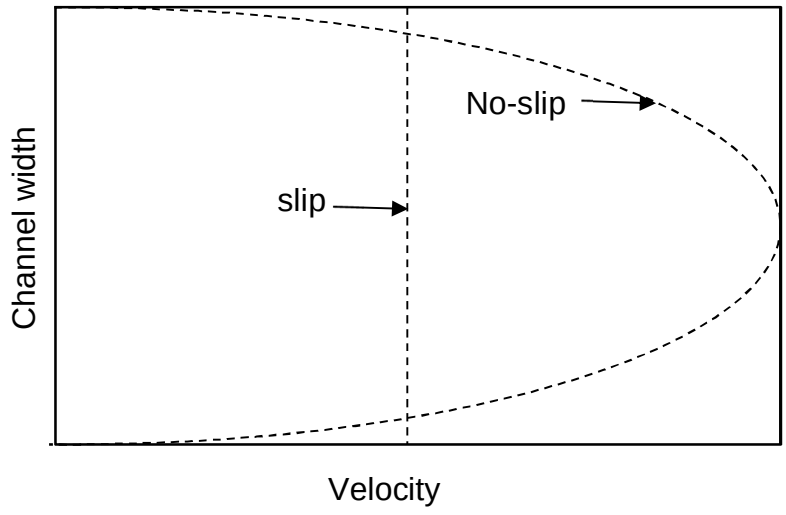

Figure 4-2 Velocity profiles in Slip and No-slip boundary conditions.

The code was also amended to cater for Inflow and outflow boundary conditions based on the approach recommended by Zou and He (1997). Based on this approach, if flow depth (*h*) and velocity components (*u,v*) are known at the inlet, the conditions required are:

$$\begin{cases} f_1 + f_2 + f_3 + f_4 + f_5 + f_6 + f_7 + f_8 + f_9 = h \\ e(f_1 + f_2 + f_8) - e(f_4 + f_5 + f_6) = hu \\ e(f_2 + f_3 + f_4) - e(f_6 + f_7 + f_8) = hv \end{cases} \quad (4.28)$$

By assuming v = 0 (for 1D flow case) and that the bounce-back rule is still correct for the non-equilibrium part of the particle distribution normal to the boundary ($f_3 - f_3^{eq} = f_7 - f_7^{eq}$), the unknown values of f_1, f_2 and f_8 at the inlet can be determined:

$$f_1 = f_5 + \frac{2hu}{3e} \quad (4.29)$$

$$f_2 = \frac{hu}{6e} + f_6 + \frac{f_7 - f_3}{2} \quad (4.30)$$

$$f_8 = \frac{hu}{6e} + f_4 + \frac{f_3 - f_7}{2} \quad (4.31)$$

Following the same procedure for the outlet will yield:

$$f_5 = f_1 - \frac{2hu}{3e} \quad (4.32)$$

$$f_4 = -\frac{hu}{6e} + f_8 + \frac{f_7 - f_3}{2} \quad (4.33)$$

$$f_6 = -\frac{hu}{6e} + f_2 + \frac{f_3 - f_7}{2} \quad (4.34)$$

4.5. Numerical Diffusivity in LBM

The kinetic equation for particle density is expressed by the advection equation:

$$\frac{\partial f_i(x,t)}{\partial t} + e\frac{\partial f_i(x,t)}{\partial x} = \Omega_i \tag{4.35}$$

where in LBM, *e* is the lattice speed:

$$\boldsymbol{e} = \frac{\Delta x}{\Delta t} \tag{4.36}$$

and Ω_i in the right-hand side represents the BGK collision operator:

$$\Omega_i = -\frac{1}{\tilde{\tau}}\left[f_i(x,t) - f_i^{eq}(x,t)\right]. \tag{4.37}$$

A Taylor expansion of the time and space derivatives yields:

$$\frac{\partial f_i(x,t)}{\partial t} = \frac{f_i(x,t+\Delta t) - \partial f_i(x,t)}{\Delta t} + \left(\frac{\Delta t}{2!}\frac{\partial^2 f_i}{\partial t^2} + \frac{\Delta t^3}{3!}\frac{\partial^3 f_i}{\partial t^3} + \cdots\right) \tag{4.38}$$

$$\frac{\partial f_i(x,t)}{\partial x} = \frac{f_i(x+\Delta x,t) - \partial f_i(x,t)}{\Delta x} + \left(\frac{\Delta x}{2!}\frac{\partial^2 f_i}{\partial x^2} + \frac{\Delta x^3}{3!}\frac{\partial^3 f_i}{\partial x^3} + \cdots\right). \tag{4.39}$$

Eliminating the 2nd and higher order terms and substituting into equation (4.37) yields:

$$\frac{f_i(x,t+\Delta t) - \partial f_i(x,t)}{\Delta t} + \boldsymbol{e}\frac{f_i(x+\Delta x,t+\Delta t) - f_i(x,t+\Delta t)}{\partial x} = -\frac{1}{\tilde{\tau}}\left[f_i(x,t) - f_i^{eq}(x,t)\right] \tag{4.40}$$

which can be re-arranged as:

$$f_i(x+\Delta x,t+\Delta t) = f_i(x,t)(1-\omega) + \omega f_i^{eq}(x,t) \tag{4.41}$$

where

$$\omega = \frac{\Delta t}{\tilde{\tau}} \tag{4.42}$$

Eq.(4.41) resembles Eq.(3.34) and shows that the current scheme is a first-order approximation of the kinetic equation at the macroscopic scale as it neglects the second and higher derivatives. By eliminating the second and higher derivatives, the standard LBM

schemes effectively solve Eq. (4.35) with those omitted terms appearing on the right-hand side; i.e., the numerical solution incorporates unwanted diffusive effects of the eliminated terms in the solution.

It is therefore expected that while the LBM yields satisfactory results for gradually varying flow cases, there will be instances where the omitted derivatives are more significant, their diffusive effects will be greater and the accuracy of the LBM scheme will reduce. Examples of these cases are Rapidly Varied Flows (RVF) in which the gradient of flow depth varies significantly over a short distance. For standard LBM, techniques to address numerical diffusivity have been discussed by La Rocca et al. (2012), amongst others.

4.6. Treatment of units in LBM

Lattice Boltzmann methods have been developed to assist in simulation of the physics of a real system. It is imperative that the lattice model is set up in a way that it represents the actual physics occurring in the real system. One of the major aspects required to achieve this is the scaling and units selected for the lattice.

Where a microscopic model (such as LBM) is used to simulate a macroscopic problem, there are two major constraints that drive the choice of units: First, the simulation should be equivalent, in a well-defined sense, to the physical system. Second, the parameters should be fine-tuned in order to reach the required accuracy, i.e. the grid should be sufficiently resolved, the discrete time step has to be sufficiently small, etc. (Latt 2008).

The unit conversion process for a lattice Boltzmann model is performed based on dimensional analysis and hydraulic similitude principles. For the incompressible Navier-Stokes equations, the consistency between the model and prototype is maintained through the Reynolds number (Re) or Froude number (Fr). Thus, the three systems need to be defined so that they have the same Reynolds numbers.

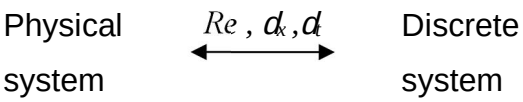

If l and t represent the real physical system parameters, the dimensionless time and positions are defined as:

$$l_{lb} = \frac{l_P}{\delta x} \text{ and } t_{lb} = \frac{t_P}{\delta t} \quad (4.43)$$

where p and lb subscripts denote the "Physical" and LBM systems, respectively. The same rule can be applied to convert other physical parameters such as velocity, acceleration or viscosity to lattice units:

$$V_{lb} = V_P . \frac{\delta t}{\delta x} \text{ (velocity)} \quad (4.44)$$

$$\upsilon_{lb} = \upsilon_P . \frac{\delta t}{\delta x^2} \text{ (viscosity)} \quad (4.45)$$

$$a_{lb} = a_P . \frac{\delta t^2}{\delta x} \text{ (acceleration)} \quad (4.46)$$

By replacing these values into the incompressible form of the Navier-Stokes equation, the Reynolds number and Froude number are defined as:

$$Re = (\frac{V . D}{\nu})_P = \frac{V_{lb} l_{lb}}{\nu_{lb}} \quad (4.47)$$

$$Fr = (\frac{V}{\sqrt{gD}})_P = \frac{V_{lb}}{\sqrt{g_{lb} l_{lb}}} \quad (4.48)$$

To define the proper discrete space interval δx, the reference length is divided by the number of lattice cells. The same is applicable to the total simulation time based on the selected time step.

If single-relaxation time BGK collision operator is used, the relaxation time can be calculated from:

$$\upsilon_{lb} = \frac{1}{c_s^2}(\tau - \frac{1}{2}) \quad (4.49)$$

where τ is the relaxation time ($\tau > \frac{1}{2}$) and $c_s^2 = \frac{1}{3}$ is the speed of sound in lattice units.

The process will be shown in an example:

Lattice Boltzmann is used to model Poiseuille flow driven by gravity between two vertical plates. Periodic boundaries are used in the flow direction and system is assumed infinite to

avoid any entry/exit effects. If a fluid with kinematic viscosity ν = 1×10-4 m²/s is used with a slit opening 2a = 1 mm, then the analytical solution suggests a parabolic velocity profile:

$$u(x) = \frac{g}{2\upsilon}(a^2 - x^2) \tag{4.50}$$

Maximum velocity occurs at the middle where x = 0. Substituting $a = 0.5mm$, $\nu = 1\times10^{-4}m^2/s$ and $g = 9.81m^2/s$ in Eq. (4.50) yields $u_{max} = 0.0123m/s$.

From geometry of parabola, we know that the average velocity occurs at 2/3 of the maximum velocity, therefore $u_{ave} = {}^2/_3 u_{max} = 0.008m/s$.

Reynolds number may be calculated using:

$Re = \frac{u.d}{\upsilon} = \frac{(0.008)(0.001)}{(0.0001)} = 0.08175$

Choosing a value of τ = 1.0 in Eq. (4.57) yields $\upsilon_{lb} = \frac{1}{6}$.

If we decide to use 10 lattices along the slit width: $\delta_x = \frac{0.001}{10} = 0.0001m$

To maintain dimensional consistency (4.53):

$$\upsilon_{lb} = \upsilon_P \frac{\delta t}{\delta x^2} \Rightarrow \delta t = \frac{\upsilon_{lb}}{\upsilon_P}\delta x^2 = \frac{\left(\frac{1}{6}\right)}{1\times10^{-4}}(1\times10^{-4})^2 = 2\times10^{-5}\ \text{s}$$

This means that each lattice time step is 2×10^{-5} seconds or $\frac{1}{2\times10^{-5}}$ = 60,000 iterations of lattice system would be required to simulate 1 second.

The gravitational acceleration in the lattice system will be calculated from Eq. (4.46):

$$g_{lb} = g_P.\frac{\delta t^2}{\delta x} = 9.81\times\frac{(2\times10^{-5})^2}{1\times10^{-4}} = 2.725\times10^{-5}\ lu/lt^2$$

Alternatively, this may also be obtained from Eq. (4.44) using the value of maximum velocity in lattice units:

$$V_{lb} = V_P.\frac{\delta t}{\delta x} = 0.008\times\frac{2\times10^{-5}}{1\times10^{-4}} = 0.002\ lu/lt$$

At x=0:

$$g = \frac{2\upsilon V_{max}}{a^2} = \frac{2\left(\frac{1}{6}\right)(0.002)}{(0.0001)^2} = 2.725\times10^{-5}\ lu/lt^2$$

The lattice Boltzmann modelling of the problem is compared to the theoretical solution in Figure 4-3.

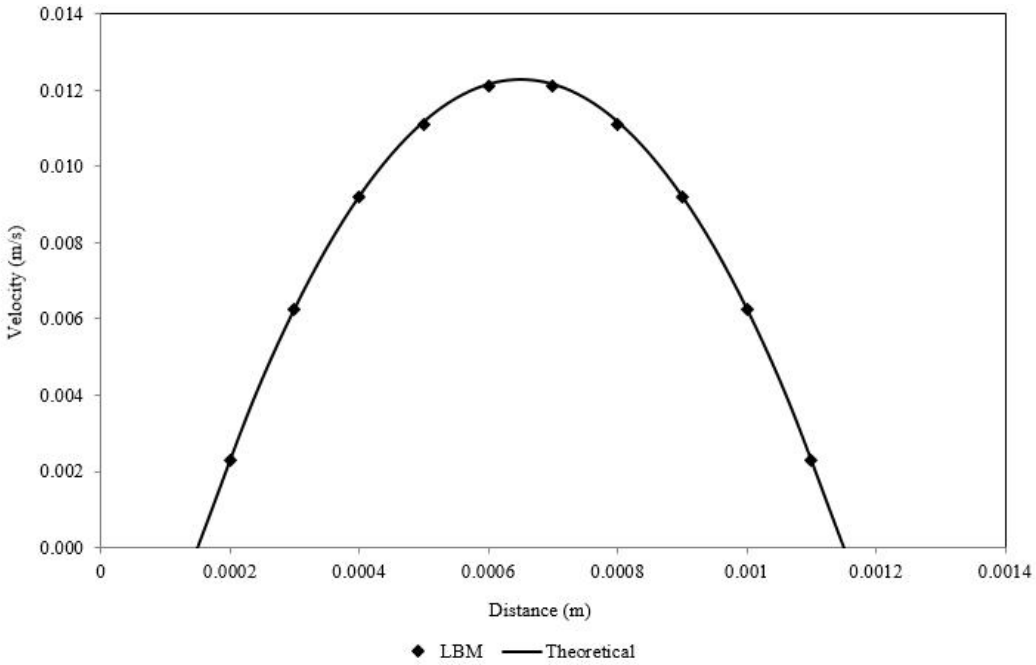

Figure 4-3 – LBM output of velocity profile in Poiseuille flow

4.7. Standard LBM Test Cases

A standard D2Q9 model was developed and verified for some open channel flow cases. As the simplest case, if external force to the fluid, F, was set to zero, flow depth and velocity were checked to remain unchanged throughout the iterations. If F was set as a constant, the flow kept accelerating (or decelerating depending on the sign of the force), which was expected from the theory as the total force term $F = F_{gravity} - F_{friction}$ would never come to a balance. The latter case would be interpreted as a Gradually Varied Flow (GVF) in which the channel bed has a grade milder than the critical slope and water surface profile has a negative slope (M profile), decreasing depth and increasing velocity.

The model was also verified for other benchmark open channel flow profiles. Figure 4-4 shows the M2 profile produced by the model for subcritical flow in a 400m long rectangular open channel with flow rate q=6m²/s, bed slope S=0.001 and Manning's coefficient n=0.013sm$^{-1/3}$ with the downstream depth set to critical depth (the M2 profile is the water surface profile in a channel with mild slope where critical depth occurs at the downstream end. In such case the upstream water surface eventually asymptotes to normal depth). Slip boundary conditions was used at the walls. The results have excellent agreement with those calculated from the Standard Step Method (Chanson 2004). The term 'difference' in Figure

4-4 and other figures refers to the departure of LBM results from the results of the selected analytical approach (which would still be associated with simplifications and inaccuracies).

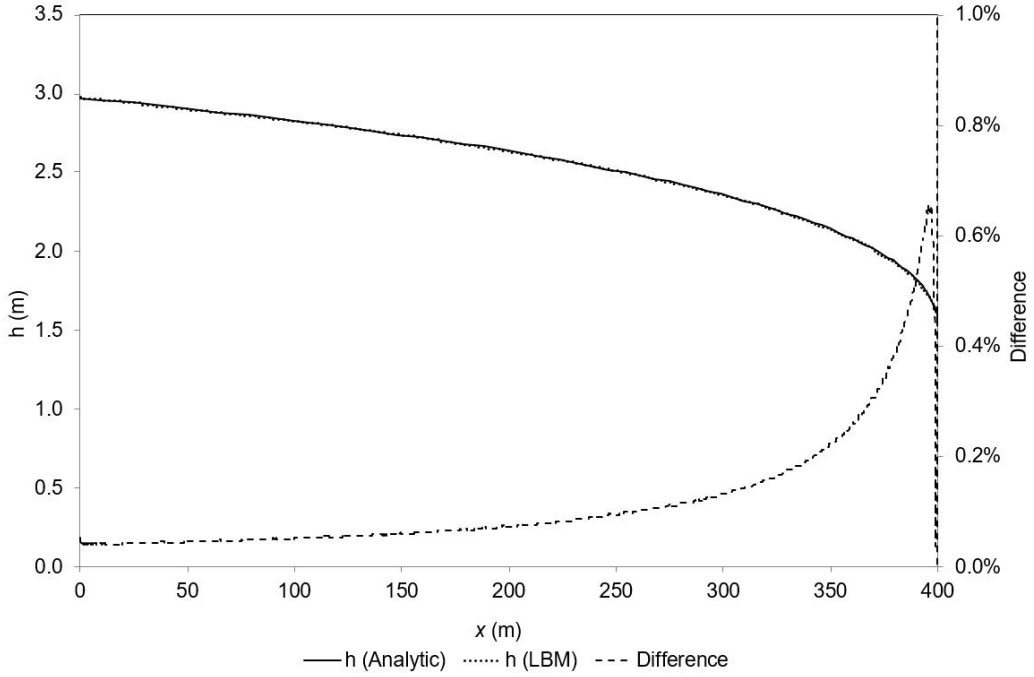

Figure 4-4 The M2 profile generated by the model compared with analytical solution.

Another test case was flow over a bump in a channel with subcritical flow. A 20m long rectangular channel was defined with Q= 4.42 m³/s and known subcritical downstream depth h=2.0 m. A hump was introduced in the middle of the channel with a maximum rise of 0.2m.

The results demonstrated that there is excellent agreement between model outputs and the analytical solution of this case from the Energy equation. The model predicted a drop in water depth over the bump, which only deviated by less than 1% from the theoretical solution using the energy equation. Figure 4-5 shows the comparison of the two approaches.

The following inflow/outflow boundary conditions were used in the model:

$$f_1^{eq}(1) = f_2^{eq}(1) + \frac{Q}{e}$$

$$f_2^{eq}(L) = f_1^{eq}(L) - \frac{Q}{e}$$

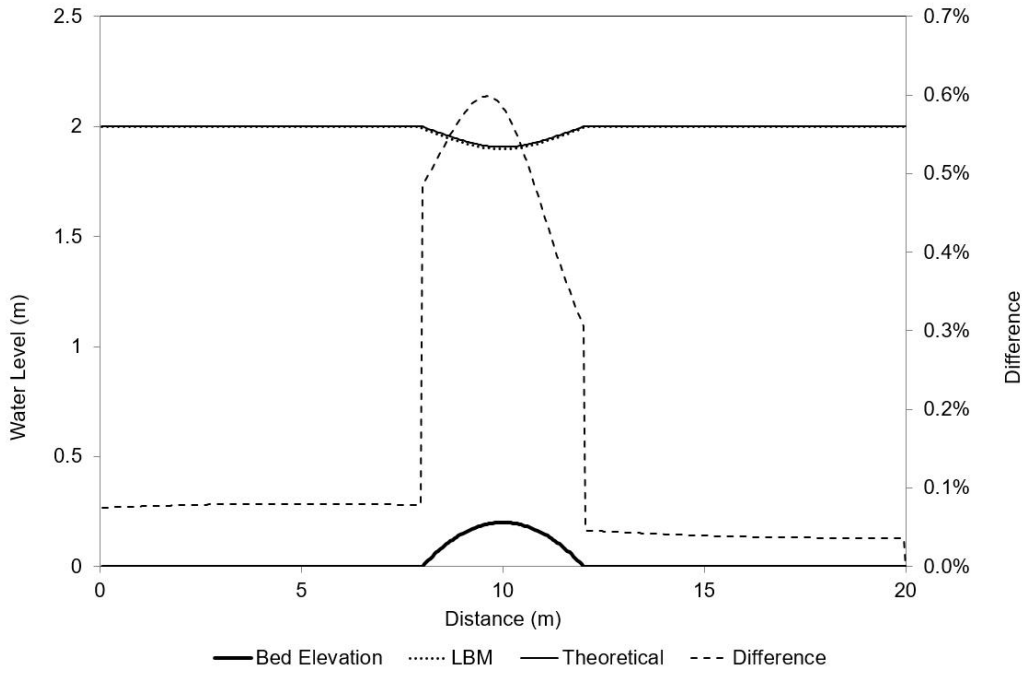

Figure 4-5 Subcritical flow modelling in an open channel with a bump.

4.8. Froude Number Limitation in LBM

In all previous LBM literature on fluid flow modelling by Zhou and others, it was clearly stated that LBM applications in fluid flow modelling (including SWE) are limited to subcritical flow. To verify this limitation, the bump height in the earlier subcritical flow case was increased until a critical depth was formed on top of the bump.

For that specific problem, critical depth for this flow was calculated $h_c = \sqrt[3]{\frac{q^2}{g}}$ = 1.26 m and the minimum specific energy $E = \frac{3}{2} y_c$ = 1.89 m. If the Energy equation holds between a cross section immediately upstream of the rising bump and the section with critical depth, it is required that the bump height is 0.362 m to have critical flow occurring.

In all attempts to run this scenario and higher bump heights, the model failed to yield an answer due to numerical instability. The GVF case also did not run when supercritical conditions were simulated. Further investigations on the values taken by model parameters revealed that the Equilibrium Distribution Functions (EDF) take extremely high or low values after a few iterations and this was the cause for the instability.

It was also noted that some of the EDFs take negative values during the iterations, adding up to negative values which raised a concern. EDFs are discrete single particle distribution functions/direction-specific densities (Sukop and Thorne 2007) and as such, their

summation should not take non-positive values. Indeed, the negative summation appeared to violate the fundamental assumptions of a particle-based model.

Step-by-step tracking of the EDF values made it evident that f_4, f_5 and f_6 take negative values during the simulations, causing the negative summation. Indeed, the negative values were introduced to the model by introduction of outflow boundary conditions Eq. (4.32)-(4.34), even before the iterations start.

The sign of EDSs for SWE have been discussed by Salmon (1999) and Dellar (2002) and both of them were contacted and consulted to provide a view on negativity of the EDFs. Dellar (pers. comm., 2011) clarified that the choice of the remaining free parameter in the EDFs for shallow water has the effect of making the distributions most prone to variation in sign due to a nonzero fluid velocity, since the sign-definite term becomes related to $O(Ma^2)$ while the sign-indefinite term is O(Ma) (Ma is the Mach number). Therefore, it was concluded that negativity of the EDFs is not necessarily the cause of model instability of the solution.

Since in the test cases referred to in literature, different lattice speeds (e) were used, the effect of the selected lattice speed on stability and convergence of the solution was also investigated.

By definition, lattice speed (e), lattice spacing (Δx) and time step (Δt) are related by $e = \Delta x/\Delta t$ and therefore specifying two of them would be sufficient in any problem. By trying different values of e and Δt it was revealed that each flow problem with subcritical regime worked only for a certain range of e values. Reducing Δx generally leaded to the improvement of solution accuracy, but it was not clear if e needed to be increased when a smaller lattice was selected. This was consistent with the recent findings published by van Thang et al (2010) who showed that the LBM surface wave speed must be slower than the lattice speed to have a stable scheme. They suggested to make this verification through two parameters: the fluid Froude number and a so-called lattice Froude number, defined as $\psi = {}^{e}/_{\sqrt{gh}}$ where e is the lattice speed and h is the flow depth. This will be discussed in more detail in the next section.

4.9. Asymmetric LBM for Supercritical Flow

As discussed earlier, a main limitation of all lattice Boltzmann models was that they only worked if Froude number was below 1. In other words, it was clearly stated by many researchers that LBM cannot be applied to supercritical regimes, where flow velocity exceeds surface wave speed (Chopard et al. 2013, Geveler et al. 2010, Liang et al. 2006, Mason 2002, van Thang et al. 2010, Zhou 2004).

To investigate the LBM issues with supercritical flow regimes, van Thang et al. (2010) published a paper for a D1Q3 lattice Boltzmann shallow water equation using the equilibrium functions previously derived by Frandsen (Frandsen 2008, van Thang et al. 2010). They provided a critical review of the force term centred-scheme proposed by Zhou in his paper (Zhou 2002) and in his book, which was a collection of his findings in LBM application in shallow water flows (Zhou 2004). Van Thang et al. (2010) showed that their numerical scheme is stable as long as the Froude number is not approaching or exceeding 1. They linearized the Shallow Water Equations in form of Eq.(4.51):

$$\delta_t \begin{pmatrix} \Delta h \\ \Delta u \end{pmatrix} = \begin{pmatrix} -u_0 & -h_0 \\ -g & -u_0 \end{pmatrix} \delta_x \begin{pmatrix} \Delta h \\ \Delta u \end{pmatrix} + \nu_0 \begin{pmatrix} 0 & 0 \\ r\dfrac{u_0}{h_0} & s \end{pmatrix} \delta_x^2 \begin{pmatrix} \Delta h \\ \Delta u \end{pmatrix} \tag{4.51}$$

where

$$\nu_0 = \Delta t v^2 \left(\tau - \frac{1}{2}\right) \tag{4.52}$$

and

$$\begin{aligned} r &= 1 - 3\Phi^2 - \Phi^2 \mathrm{Fr}^2 \\ s &= 1 - \Phi^2 - 3\Phi^2 \mathrm{Fr}^2 \end{aligned} \tag{4.53}$$

where Fr denotes the Froude number defined as:$\mathrm{Fr} = \frac{u}{\sqrt{gh}}$

and ϕ was defined as the ratio of wave speed to the lattice speed:

$$\phi = \frac{\sqrt{gh}}{e}.$$

Van Thang et al. (2010) defined an unconditional stable region for their numerical scheme in terms of the above two parameters and concluded that the value of relaxation time (τ) plays no role in the stability of the model as long as it is larger than or equal than 1/2. They also added that modelling flow with Froude number Fr = 1 is possible if ϕ is small enough so that the wave propagates slower than the lattice speed (*e*), which is the velocity at which information travels through the lattice network. In other words, the following two conditions should be satisfied which are akin to Courant conditions:

$u > \sqrt{gh} - e$ or $u < e - \sqrt{gh}$

These conditions can be expressed as:

$$1 - \frac{1}{\phi} < \mathrm{Fr} < \frac{1}{\phi} - 1 \qquad (4.54)$$

This model was applied to a network of open irrigation channels and showed that the results compare well with existing solution methods (van Thang et al. 2010).

Like other LBM schemes that were proposed to that date, this model had the limitation that it became numerically unstable for supercritical flow regimes where Fr > 1; however, the authors indicated that they had modified their model to obtain a new scheme that worked for both subcritical and supercritical flows and that the model would be released in a future publication.

The new scheme they suggested to overcome the difficulty of working with supercritical flow was presented in a subsequent publication by Chopard et al. (2013), which was the first shallow-water LBM to be applied to supercritical flows.

Chopard et al. (2013) proposed to use a Galilean transformation and make the scheme asymmetric before it can be applied to flows with Froude number greater than unity. In the new reference frame that was moving at a constant speed, the velocity vectors were asymmetric and therefore a new set of EDFs needed to be derived by consideration of the new reference framework.

a) The standard LBM scheme b) The asymmetric LBM scheme

Figure 4-6 The standard (symmetric) and asymmetric D1Q3 schemes.

Considering the D1Q3 scheme in Figure 4-6, if the reference frame is moving at a constant speed $U=e/2$, particle velocities in the new system (uppercase letters) are expressed as:

$$\begin{aligned} E_0 &= 0 + U = 0 + \frac{e}{2} = \frac{e}{2} \\ E_1 &= e + U = e + \frac{e}{2} = \frac{3e}{2} \\ E_2 &= -e + U = -e + \frac{e}{2} = -\frac{e}{2} \end{aligned} \tag{4.55}$$

If the new flow velocity $u = u - U = u - \frac{e}{2}$ is substituted in Eq.(4.13), the EDFs in the new moving reference frame will be:

$$\begin{aligned} f_0^{eq} &= \frac{3}{4}h - \frac{1}{e^2}\left(\frac{1}{2}gh^2 + hu^2\right) + \frac{1}{e}hu \\ f_1^{eq} &= -\frac{1}{8}h + \frac{1}{2e^2}\left(\frac{1}{2}gh^2 + hu^2\right) \\ f_2^{eq} &= \frac{3}{8}h + \frac{1}{2e^2}\left(\frac{1}{2}gh^2 + hu^2\right) - \frac{1}{e}hu \end{aligned} \tag{4.56}$$

To avoid particles falling on the half-integer sites on the lattice system, e is replaced by $2e$ in Equation (4.56) which gives the final form of equilibrium functions:

$$\begin{aligned} f_0^{eq} &= \frac{3}{4}h - \frac{1}{4e^2}(\frac{1}{2}gh^2 + hu^2) + \frac{1}{2e}hu \\ f_1^{eq} &= -\frac{1}{8}h + \frac{1}{8e^2}(\frac{1}{2}gh^2 + hu^2) \\ f_2^{eq} &= \frac{3}{8}h + \frac{1}{8e^2}\left(\frac{1}{2}gh^2 + hu^2\right) - \frac{1}{2e}hu \end{aligned} \tag{4.57}$$

Chopard et al. (2013) found that in the new scheme there is no absolute maximum value of Fr that guarantees solution stability. However, a new stability region was proposed by introducing a new parameter called lattice Froude number $\Psi = e/\sqrt{gh}$.

Fr < 1: $\quad -e < u - \sqrt{gh}$ and $e < u + \sqrt{gh} < 3e$

Fr > 1: $\quad u - \sqrt{gh} < e < u + \sqrt{gh} < 3e$

which, in terms of Fr and ψ can be expressed as:

$$\begin{aligned} &\Psi+1 < Fr < 3\Psi-1 \qquad (Fr < 1) \\ &\Psi-1 < Fr < \min(\Psi+1 , 3\Psi-1) \qquad (Fr > 1) \end{aligned} \tag{4.58}$$

Figure 4-7 shows the recommended stable region for the asymmetric D1Q3 shallow water LBM.

The stability criteria defined in Eq. (4.58) for flows with Fr>1 are only applicable to the D1Q3 LBM schemes based on the Equilibrium Functions derived from the SWE. It is noted that this region is too narrow to accommodate a wide range of flow conditions and so has limited practicality.

Although the non-SWE LBMs do not have to comply with Eq. (4.58), as a general rule, the LBM is only capable of representing the Navier-Stokes equations if fluid velocities are low. In other words, the LBM applicability to fluid flows is limited to flows with small Mach number *u*/*Cs*, where *Cs* is the speed of sound (Chen and Doolen 1997), analogous to subcritical shallow water flow.

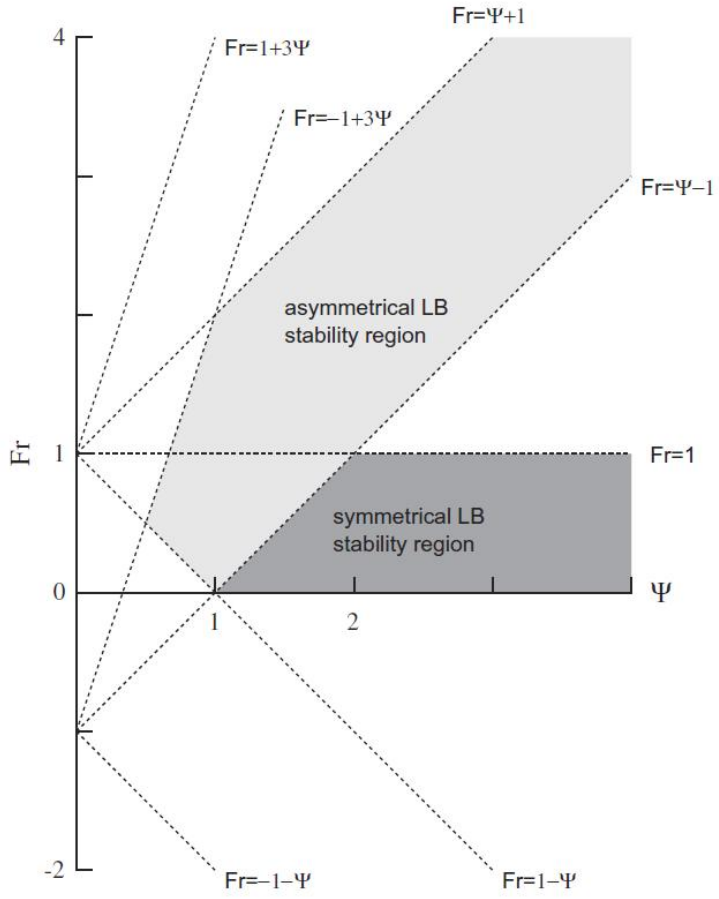

Figure 4-7 The stability region of the asymmetric D1Q3 LBM (Chopard et al. 2013). Fr denotes Froude number and ψ is the Lattice Froude number $\psi = e/\sqrt{gh}$.

A D1Q3 asymmetric LBM was developed based on the modifications proposed by Chopard et al. (2013) . To check the new asymmetric 1D model, the D1Q3 model was temporarily

made symmetric and the velocity components in the earlier D2Q9 model were set to zero in y-direction and its results were compared to the D1Q3 model. It was evident that the results were identical in both models so it was concluded that the D1Q3 model was set up properly. Nevertheless, this was predictable in advance because $f_1+f_2+f_8$ values in the 2D model added up to f_1 in the 1D code and $f_4+f_5+f_6$ added up to f_2 in the 1D code, which leads to identical results of both schemes.

The asymmetric D1Q3 model was applied to a range of open channel supercritical flow cases as discussed below.

4.9.1. Supercritical flow over a local bed level rise

The first test case used a 0.4m high bump with 10m upstream depth to induce a supercritical flow (Fr = 2.5):

q = 125 m²/s e = 13 m/s

y_1 = 0.4 m Δx = 0.01 m

With the selected e value, the stability criteria in Equation (4.58) were satisfied. The modelled and analytical was levels for this case are presented in Figure 4-8 where excellent agreement is evident between the two approaches.

The inflow/outflow used in the model for this case were as follows:

Inflow:

$$f_1^{eq}(1) = \frac{Q}{2e} - \frac{h(1)}{2} + f_2^{eq}(1)$$

$$f_3^{eq}(1) = \frac{3h(1)}{2} - \frac{Q}{2e} - 2f_2^{eq}(1)$$

$$f_1^{eq}(2) = f_1^{eq}(1)$$

$$f_1^{eq}(3) = f_1^{eq}(1)$$

Outflow:

$$f_2^{eq}(L) = 3f_1^{eq}(L) + f_3^{eq}(L) - \frac{Q}{e}$$

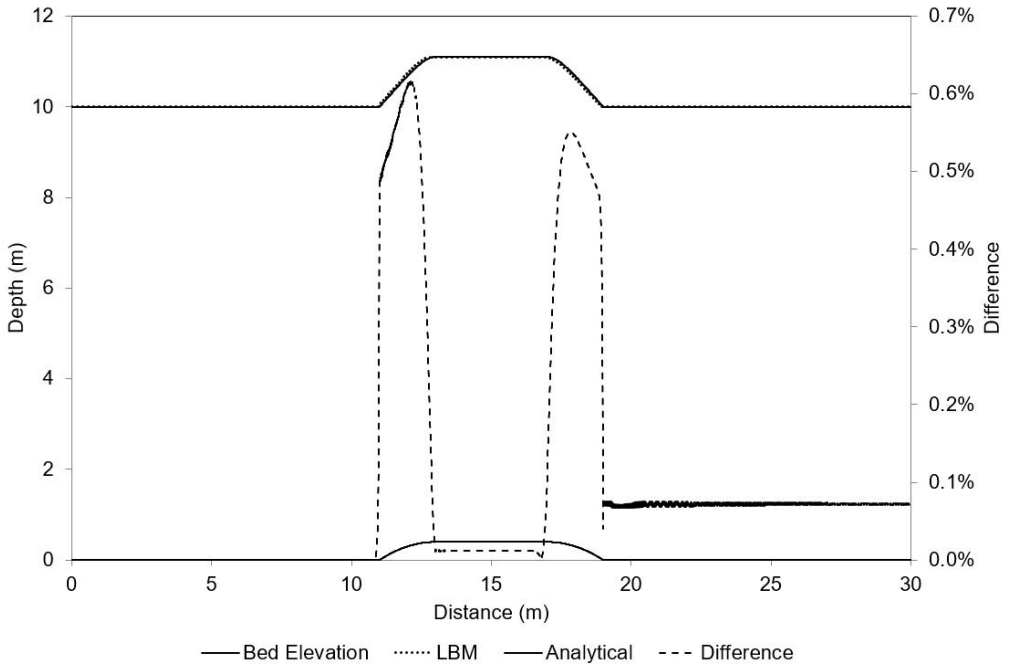

Figure 4-8 The broad-crested weir case in supercritical flow.

4.9.2. Supercritical flow in a channel with steep slope

As another test case, the asymmetric D1Q3 model was used to predict the S2 water surface profile in a 250m long rectangular open channel on a steep slope. The data for this case were:

Bed Slope: 2%
Flow Rate: 6 m^3/s
Upstream Depth: 1.4 m
Manning's n: 0.013 $sm^{-1/3}$
Lattice size (dx): 0.05 m

A zero-gradient boundary condition was defined at the downstream end.

$$f_2^{eq}(L) = f_2^{eq}(L-1)$$

Figure 4-9 compares model output against the analytical results for the standard step method showing excellent agreement.

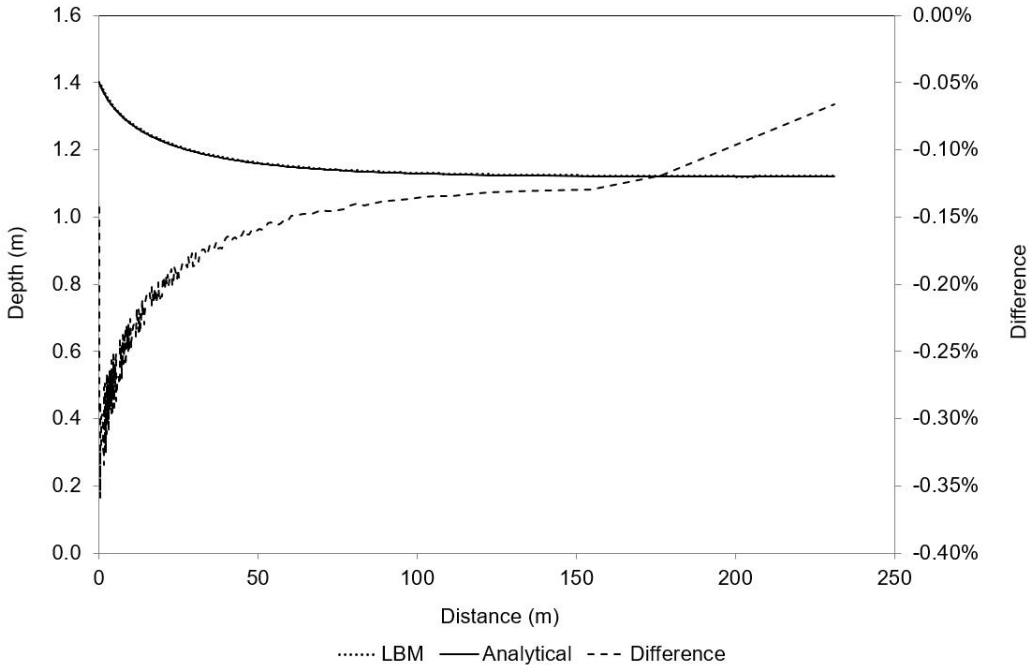

Figure 4-9 The S2 curve generated by the model compared with analytical solution.

Figure 4-10 shows LBM modelling of an S3 curve using the asymmetric scheme compared to the analytical solution for the following case:

Bed Slope: 0.02
Flow Rate: 6 m^3/s
Upstream Depth: 0.8 m
Manning's n: 0.013 $sm^{-1/3}$
Lattice size (dx): 0.1 m

Boundary conditions:

Upstream:

$$f_1^{eq}(1) = \frac{Q}{2e} - \frac{h(1)}{2} + f_2^{eq}(1)$$

$$f_3^{eq}(1) = \frac{3h(1)}{2} - \frac{Q}{2e} - 2f_2^{eq}(1)$$

$$f_1^{eq}(2) = f_1^{eq}(1)$$

$$f_1^{eq}(3) = f_1^{eq}(1)$$

Downstream:

$$f_2^{eq}(L) = 3f_1^{eq}(L) + f_3^{eq}(L) - \frac{Q}{e}$$

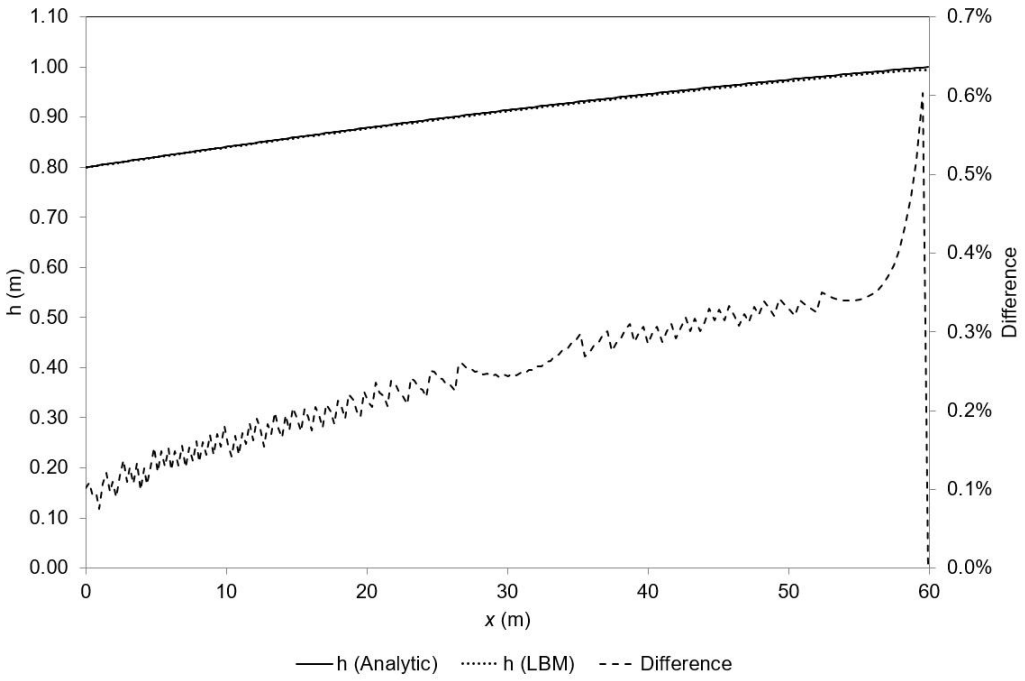

Figure 4-10 The S3 curve generated by the model compared with analytical solution.

4.9.3. Supercritical flow in a channel with mild slope

The asymmetric D1Q3 model was also tested for supercritical flow in a channel with mild slope. Figure 4-11 compares the LBM model results to the theoretical predictions for the following M3 flow profile:

Bed Slope: 0.001
Flow Rate: 6 m^3/s
Upstream Depth: 1.0 m
Manning's n: 0.013 $sm^{-1/3}$
Lattice size (dx): 0.01 m

The upstream/downstream boundary conditions:

Upstream:

$$f_1^{eq}(1) = \frac{Q}{2e} - \frac{h(1)}{2} + f_2^{eq}(1)$$

$$f_3^{eq}(1) = \frac{3h(1)}{2} - \frac{Q}{2e} - 2f_2^{eq}(1)$$

$$f_1^{eq}(2) = f_1^{eq}(1)$$

$$f_1^{eq}(3) = f_1^{eq}(1)$$

Downstream:

$$f_2^{eq}(L) = 3f_1^{eq}(L) + f_3^{eq}(L) - \frac{Q}{e}$$

It is noticed that very good agreement exists between the two curves.

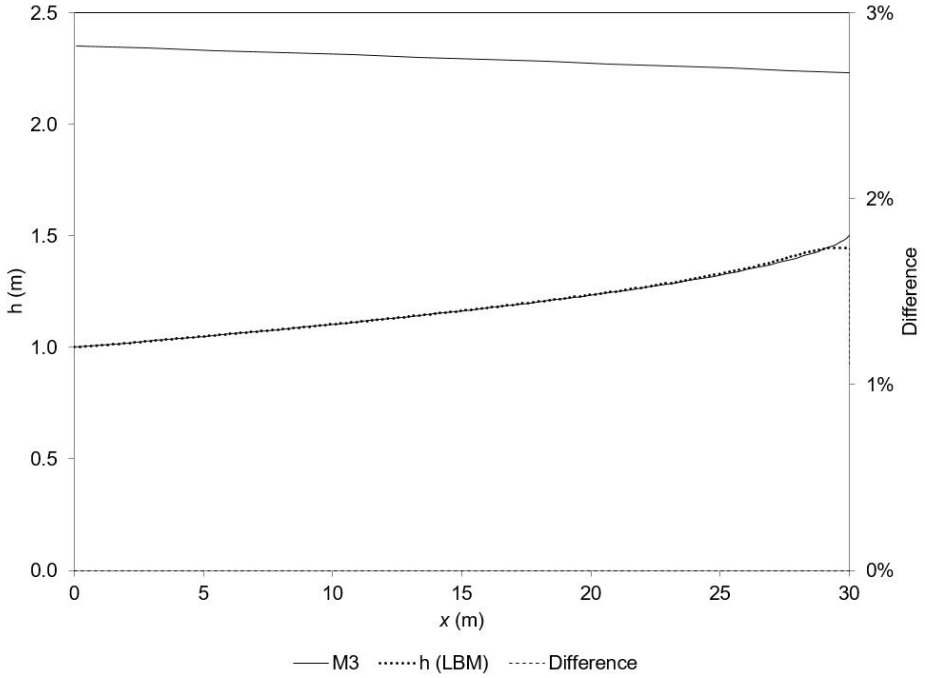

Figure 4-11 The M3 curve generated by the model compared with analytical solution.

4.9.4. Weir flow in a channel

Figure 4-12 shows the asymmetric D1Q3 scheme can successfully model a transitional case from subcritical to supercritical by introducing a bed rise of sufficient height in the domain. The problem data for this case are:

Flow Rate: 3.68 m^2/s
Upstream Depth: 1.6 m
Downstream Depth: 0.81 m
Manning's n: 0.013
Bump Height: 0.20 m
Lattice size (dx): 0.01 m

Boundary conditions:

Upstream:

$$f_1^{eq}(1) = \frac{Q}{2e} - \frac{h(2)}{2} + f_2^{eq}(1)$$

$f_3^{eq}(1) = \frac{3h(2)}{2} - \frac{Q}{2e} - 2f_2^{eq}(1)$

$f_1^{eq}(2) = f_1^{eq}(4)$

$f_1^{eq}(3) = f_1^{eq}(4)$

Downstream:

$f_2^{eq}(L) = 3f_1^{eq}(L) + f_3^{eq}(L) - \frac{Q}{e}$

As the Figure suggests, the difference between Energy Equation predictions and LBM can be as high as 4.9% on the weir.

If the supercritical depth downstream of the depth is defined and a subcritical tail water depth at the end of the channel is also specified, this model can simulate a hydraulic jump a shown in Figure 4-13. This shows the capability of LBM in simulating Rapidly Varied Flows, such as the hydraulic jump.

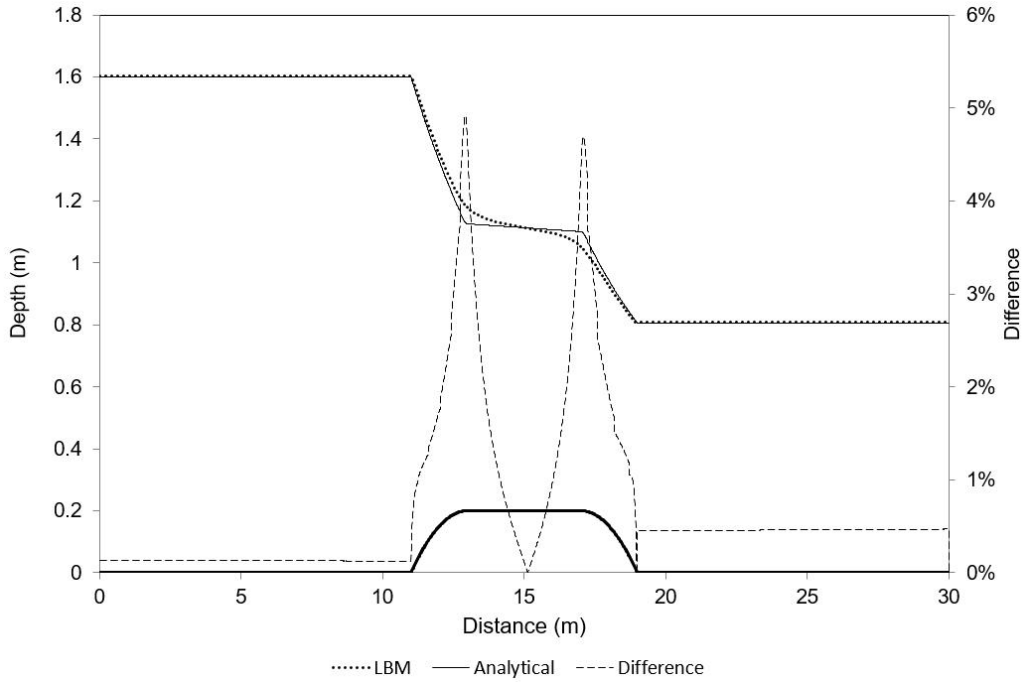

Figure 4-12 modelling of critical flow occurring over a broad-crested weir.

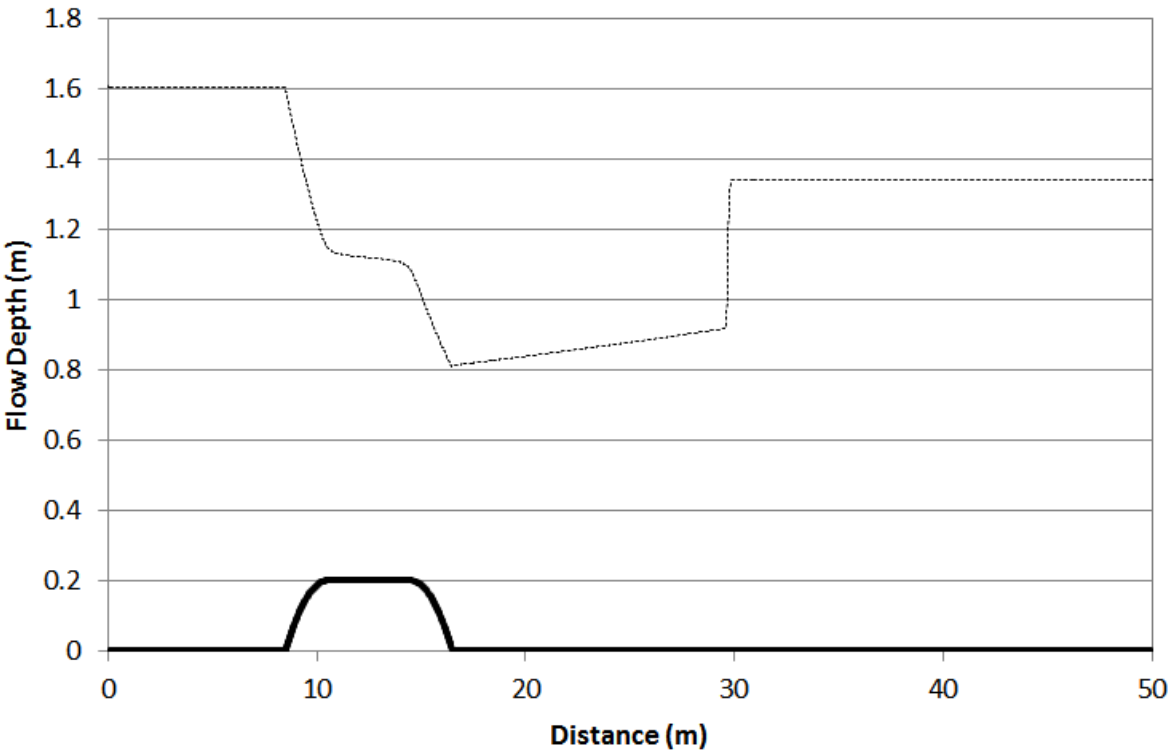

Figure 4-13 Lattice Boltzmann simulation of hydraulic jump in an open channel.

Although the above test cases show successful application of the asymmetric scheme to supercritical regime, it could not be applied to any arbitrary supercritical flow case. As will be discussed in the next section, a specific set of conditions had to be met to maintain the asymmetric numerically stable and that limited the applicability of the transformed scheme to a very specific set of problems.

4.9.5. Stability of the asymmetric D1Q3 scheme

The asymmetric D1Q3 scheme was only stable within a specific stability zone, which was given by Chopard et al. (2013). The stability zone was rather a narrow region and could only accommodate a very specific set of practical problems. It is essential that the underlying basis of the stability region is completely understood before any attempt is made to expand the scheme to accommodate other Froude numbers.

As a general rule, in all numerical schemes, the speed at which the calculations are performed (in the case of LBM, lattice speed) must be larger than wave speed to enable timely transmit of information. In a symmetric D1Q3 model this can be expressed by the following equations:

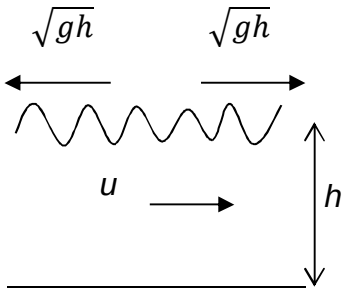

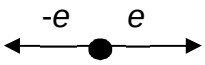

Subcritical Flow:

$e > \sqrt{gh} + u$ (Forward link)

$Fr < 1 \Rightarrow \frac{u}{\sqrt{gh}} < 1 \Rightarrow u < \sqrt{gh} \Rightarrow e > \sqrt{gh} - u$ (Backward link)

Supercritical Flow:

$e > \sqrt{gh} + u$ (Forward link)

$Fr > 1 \Rightarrow \frac{u}{\sqrt{gh}} > 1 \Rightarrow u > \sqrt{gh} \Rightarrow e > u - \sqrt{gh}$ (Backward link)

For the asymmetric scheme proposed by Chopard et al. (2013) these equations will be in the following form:

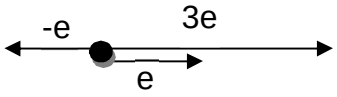

Subcritical Flow:

$3e > \sqrt{gh} + u \Rightarrow Fr < 3\psi - 1$ (Forward Link)

$Fr < 1 \Rightarrow \frac{u}{\sqrt{gh}} < 1 \Rightarrow u < \sqrt{gh} \Rightarrow e > \sqrt{gh} - u \Rightarrow Fr > 1 - \psi$ (Backward Link) (4.59)

Supercritical Flow:

$3e > \sqrt{gh} + u \Rightarrow Fr < 3\psi - 1$ (Forward Link)

$Fr > 1 \Rightarrow \frac{u}{\sqrt{gh}} > 1 \Rightarrow u > \sqrt{gh} \Rightarrow e > u - \sqrt{gh} \Rightarrow Fr < \psi + 1$ (Backward Link) (4.60)

where $\psi = {}^{e}/_{\sqrt{gh}}$ is the Lattice Froude number.

In addition to these criteria, there is another condition which also needs to be met and that is the CFL condition. CFL (named after its developers Courant-Friedrichs-Lewy) is a necessary condition for convergence in explicit time-marching numerical schemes (Courant et al. 1959). According to the CFL condition, the time step selected in solution has to be less than a certain time otherwise the simulation will become unstable or produces incorrect results. If a wave is moving across a discrete spatial grid and we are to compute its amplitude at discrete equal time intervals, these time intervals must be less than the time that takes for the wave to travel to adjacent grid points:

$$\frac{\Delta x}{\Delta t} < \sqrt{gh} + u \tag{4.61}$$

Chopard et al. (2013) identified another condition that needed to be met which was related to upper limit of, the selected lattice speed (*e*) being bound by the surface wave speed. The underlying basis for this requirement was not provided but it was evident that this condition needed to be satisfied to keep the model stable. The lattice speed must always satisfy the following equation, regardless of the physics of the problem:

$$e < u + \sqrt{gh} \Rightarrow Fr > \psi - 1 \tag{4.62}$$

For the D1Q3 scheme proposed by Chopard et al., the numerically stable zone is shown with shaded areas in Figure 4-14.

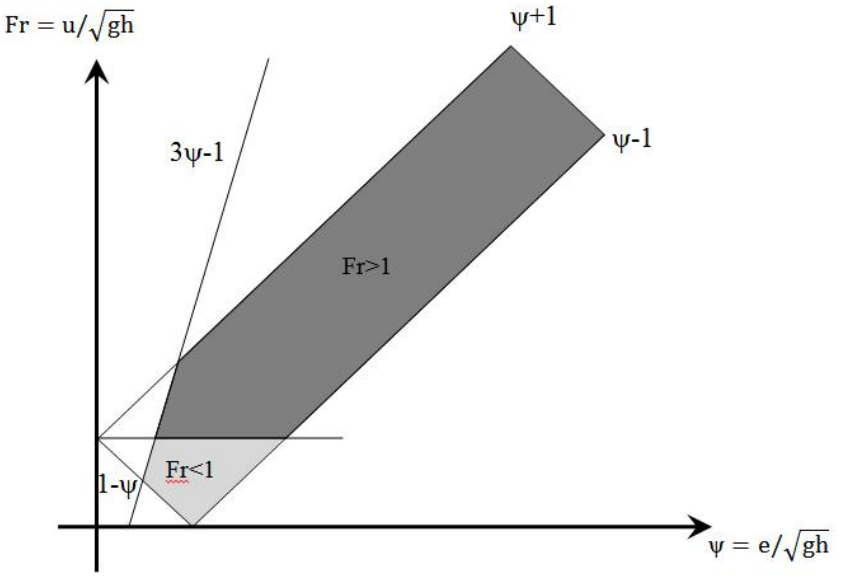

Figure 4-14 Stability region for Chopard et al. (2013) D1Q3 scheme.

The dark shaded area in Figure 4-14 relates to the supercritical regime and the light shaded area represents the subcritical regime. The range of subcritical flows encompassed by this zone is very small; i.e. it cannot cater for flow cases where the Froude number is small (such as stationary water case in which the Froude number is zero). The range of the Froude numbers covered in the supercritical zone is not extensive either, which limits the applicability of this scheme.

For the test case of critical flow over the bump shown in Figure 4-12, the values of Fr and ψ were plotted along the channel to track the transition of flow regime from subcritical to supercritical (Figure 4-15). As it can be seen these values remain in the stable zone during the simulation.

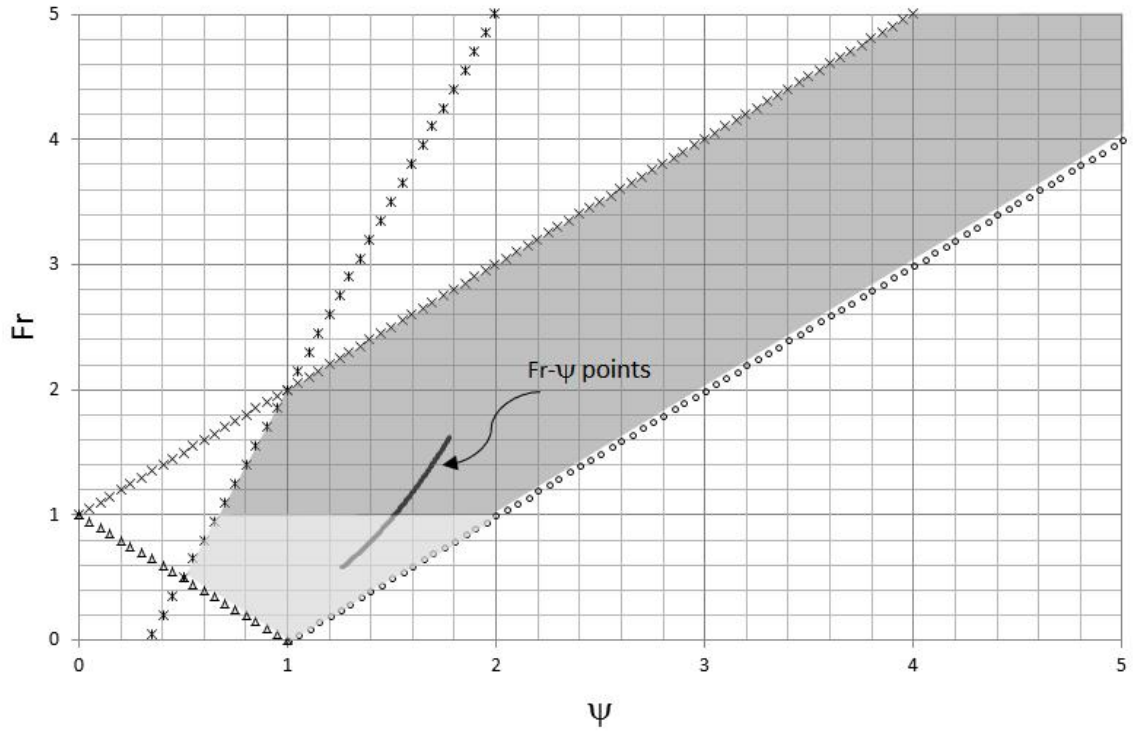

Figure 4-15 Variation of Fr-y for the critical flow over a weir test case.

The asymmetric model was tested for a particular case of supercritical flow over a local bed level rise. The flow rate per unit width was set to 3m²/s, upstream depth set to 2m and the maximum bed level rise was set to 0.5m. It was noticed that the asymmetric scheme became quickly unstable and did not converge to a solution. The reason was that the correct solution fell outside the stability zone by Chopard et al. (2013). This is graphically shown in Figure 4-16.

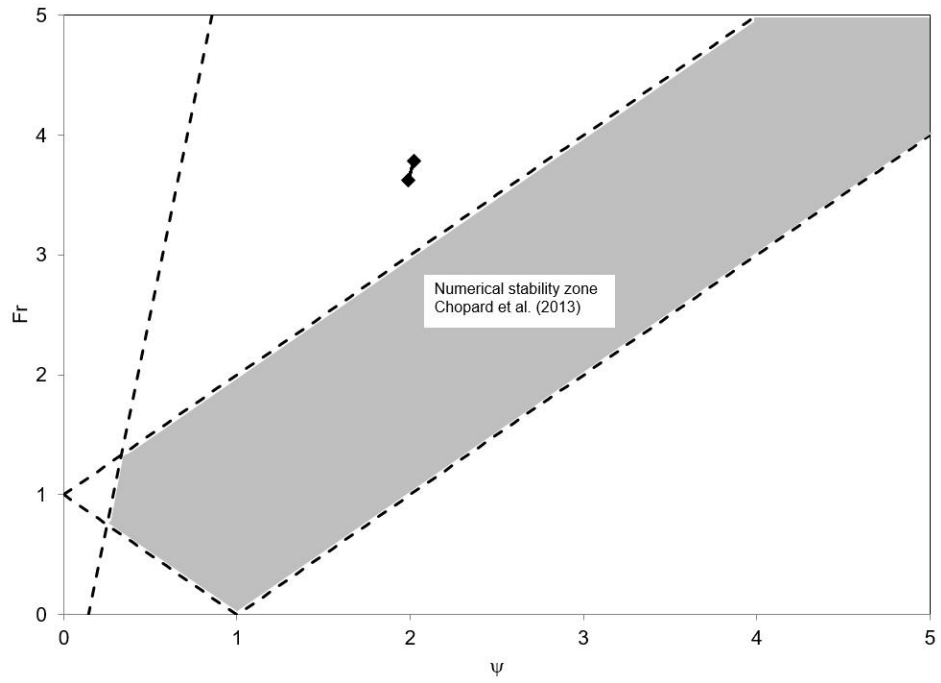

Figure 4-16 supercritical flow case over local bed rise, solid line: Fr – Ψ data, dashed lines and shaded area: Chopard et al. (2013) numerical stability zone.

A number of approaches could be considered to resolve this issue, including introduction of a variable grid size for the domain, implementation of variable lattice speeds in different zones of the domain and a modified asymmetry of the scheme to broaden the stable zone. Following unsuccessful attempts in implementing non-uniform lattice grid and variable lattice speed it was decided to use the asymmetry idea proposed by Chopard et al. (2013) and develop a generalised form of the asymmetric scheme to expand the stability zone.

4.10. Summary

This chapter provided a detailed overview of the standard LBM including Equilibrium Distribution Functions, the isotropic properties, numerical diffusivity and limitations associated with the flow regime. The standard D1Q3 model (Frandsen 2008) and D2Q9 model (Zhou 2002) were introduced and examined through a number of simple test cases where modelled results were compared with the analytic solutions. The asymmetric scheme proposed by Chopard et al. (2013) was introduced as the breakthrough to successful application of LBM to supercritical regimes. Although the asymmetric LBM proposed by Chopard et al. (2013) remained stable in supercritical regimes, its numerical stability requirements were too narrow to accommodate the wide range of flow regimes encountered in practical applications. This called for extension of the proposed scheme to encompass a wider set of data.

5. Generalized transformation of D1Q3 scheme

In this chapter a generalised Galilean transformation is proposed for the standard D1Q3 scheme based on the idea of a moving framework and Galilean transformation proposed by Chopard et al. (2013). The general transformation allows selection of the asymmetry parameters and lattice configurations to match the requirements of the physical system being modelled. A proper set of model parameters yields a wider stability zone, compared to the zone proposed by Chopard et al. (2013) and can cater a wider range of Froude numbers. Re-derivation of the entire 1D LBM framework for a general transformation, including new Equilibrium Distribution Functions, force term weight factors, inflow and outflow boundary conditions and stability criteria are discussed.

The contents of this chapter are largely based on a published paper by Hedjripour et al. (2016).

5.1. Equilibrium Distribution Functions

We decide to adopt a generic approach in the Galilean transformation using an arbitrary parameter λ:

$$\lambda = \frac{\alpha}{\beta} \qquad (\alpha < \beta \quad , \quad \alpha, \beta \in \mathbb{N} \quad , \quad \alpha \not\equiv \beta) \tag{5.1}$$

where α and β are natural numbers called the asymmetry parameters. The physical interpretation of the asymmetry parameters may be better understood by referring to Figure 5-1 in which $(\lambda + 1)$ represents the factor for the forward motion each particle, $(\lambda - 1)$ represents the backward speeds and the ratio λe is the speed at which the whole lattice framework moves.

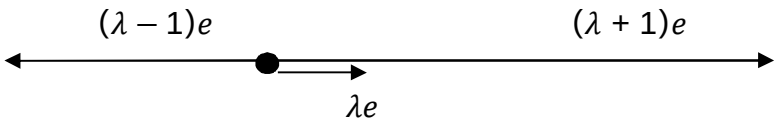

Figure 5-1 Lattice configuration in the transformed scheme.

Assuming that the system travels at speed λe, the lattice velocities in the new framework will be:

$$\begin{aligned} E_0 &= 0 + \lambda e = \lambda e \\ E_1 &= e + \lambda e = (\lambda + 1)e \\ E_2 &= -e + \lambda e = (\lambda - 1)e \end{aligned} \tag{5.2}$$

Substituting the new velocity $(u - \lambda e)$ in the D1Q3 Equilibrium Distribution Functions in Eq. (4.13) yields:

$$\begin{aligned} f_0^{eq} &= (1-\lambda^2)h + \frac{2\lambda}{e}hu - \frac{1}{e^2}\left(\frac{gh^2}{2} + hu^2\right) \\ f_1^{eq} &= \frac{1}{2}(\lambda^2 - \lambda)h + \frac{1}{e}\left(\frac{1}{2} - \lambda\right)hu + \frac{1}{2e^2}\left(\frac{gh^2}{2} + hu^2\right) \\ f_2^{eq} &= \frac{1}{2}(\lambda^2 + \lambda)h - \frac{1}{e}\left(\frac{1}{2} + \lambda\right)hu + \frac{1}{2e^2}\left(\frac{gh^2}{2} + hu^2\right) \end{aligned} \tag{5.3}$$

It can be shown that these functions meet the mass conservation and momentum criteria.

$$\begin{aligned} \sum f_i^{eq} = &\left[(1-\lambda^2)h + \frac{2\lambda}{e}hu - \frac{1}{e^2}\left(\frac{gh^2}{2} + hu^2\right)\right] \\ &+ \left[\frac{1}{2}(\lambda^2 - \lambda)h + \frac{1}{e}\left(\frac{1}{2} - \lambda\right)hu + \frac{1}{2e^2}\left(\frac{gh^2}{2} + hu^2\right)\right] \\ &+ \left[\frac{1}{2}(\lambda^2 + \lambda)h - \frac{1}{e}\left(\frac{1}{2} + \lambda\right)hu + \frac{1}{2e^2}\left(\frac{gh^2}{2} + hu^2\right)\right] = h \end{aligned} \tag{5.4}$$

$$\begin{aligned} \sum E_i f_i^{eq} = &(\lambda e)\left[(1-\lambda^2)h + \frac{2\lambda}{e}hu - \frac{1}{e^2}\left(\frac{gh^2}{2} + hu^2\right)\right] \\ &+ [(\lambda+1)e]\left[\frac{1}{2}(\lambda^2 - \lambda)h + \frac{1}{e}\left(\frac{1}{2} - \lambda\right)hu + \frac{1}{2e^2}\left(\frac{gh^2}{2} + hu^2\right)\right] \\ &+ [\,(\lambda-1)e]\left[\frac{1}{2}(\lambda^2 + \lambda)h - \frac{1}{e}\left(\frac{1}{2} + \lambda\right)hu + \frac{1}{2e^2}\left(\frac{gh^2}{2} + hu^2\right)\right] = hu \end{aligned} \tag{5.5}$$

$$\begin{aligned} \sum {E_i}^2 f_i^{eq} = &(\lambda e)^2\left[(1-\lambda^2)h + \frac{2\lambda}{e}hu - \frac{1}{e^2}\left(\frac{gh^2}{2} + hu^2\right)\right] \\ &+ [(\lambda+1)e]^2\left[\frac{1}{2}(\lambda^2 - \lambda)h + \frac{1}{e}\left(\frac{1}{2} - \lambda\right)hu + \frac{1}{2e^2}\left(\frac{gh^2}{2} + hu^2\right)\right] \\ &+ [\,(\lambda-1)e]^2\left[\frac{1}{2}(\lambda^2 + \lambda)h - \frac{1}{e}\left(\frac{1}{2} + \lambda\right)hu + \frac{1}{2e^2}\left(\frac{gh^2}{2} + hu^2\right)\right] \\ &= \frac{1}{2}gh^2 + hu^2 \end{aligned} \tag{5.6}$$

Scaling up the new lattice velocities (*E*) by β to avoid falling on non-integer points:

$$E_0 = \beta\lambda e = \beta\left(\frac{\alpha}{\beta}e\right) = \alpha e$$
$$E_1 = \beta(\lambda + 1)e = \beta\left(\frac{\alpha + \beta}{\beta}\right)e = (\alpha + \beta)e \quad (5.7)$$
$$E_2 = \beta(\lambda + 1)e = \beta\left(\frac{\alpha - \beta}{\beta}\right)e = (\alpha - \beta)e$$

The Equilibrium Distribution Functions for the new physical system will take the following forms:

$$f_0^{eq} = (1 - \lambda^2)h + \frac{2\lambda}{\beta e}hu - \frac{1}{\beta^2 e^2}\left(\frac{gh^2}{2} + hu^2\right)$$
$$f_1^{eq} = \frac{1}{2}(\lambda^2 - \lambda)h + \frac{1}{\beta e}\left(\frac{1}{2} - \lambda\right)hu + \frac{1}{2\beta^2 e^2}\left(\frac{gh^2}{2} + hu^2\right) \quad (5.8)$$
$$f_2^{eq} = \frac{1}{2}(\lambda^2 + \lambda)h - \frac{1}{\beta e}\left(\frac{1}{2} + \lambda\right)hu + \frac{1}{2\beta^2 e^2}\left(\frac{gh^2}{2} + hu^2\right)$$

5.2. Chapman-Enskog Expansion

To ensure that the proposed transformed scheme solves the shallow water equations, a multi-scale Chapman-Enskog expansion up to second order is performed to recover the hydrodynamic Saint-Venant equations. The expansion involves the following steps as described in detail in in detail in van Thang et al. (2010):

(1) A Taylor expansion of f_i in Eq. (3.34) around (*x*,*t*) up to second order yields:

$$\Delta t\frac{\partial f_i}{\partial t} + e_i\Delta t\frac{\partial f_i}{\partial x} + \frac{1}{2}\Delta t^2\frac{\partial^2 f_i}{\partial t^2} + \frac{1}{2}{e_i}^2\Delta t^2\frac{\partial^2 f_i}{\partial x^2} + e_i\Delta t^2\frac{\partial f_i}{\partial x\partial t} = \frac{1}{\tau}\left(f_i^{eq} - f_i\right) \quad (5.9)$$

(2) Perturbing the particle distribution functions around f_i^{eq} in terms of Knudsen number $\boldsymbol{\varepsilon}$ gives (Abe 1997):

$$f_i = f_i^{eq} + \varepsilon f_i^{(1)} + \varepsilon^2 f_i^{(2)} + \cdots \quad (5.10)$$

(3) Taking the first two moments of Eq.(5.9) results in:

$$\frac{\partial h}{\partial t} + \frac{\partial (hu)}{\partial x} = 0 \tag{5.11}$$

$$\frac{\partial (hu)}{\partial t} + \frac{\partial (\Pi^{eq} - \Gamma)}{\partial x} = 0 \tag{5.12}$$

where the dissipative current (Γ) is defined as:

$$\Gamma = \Delta t \left(\tau - \frac{1}{2}\right)\left[-\frac{\partial \Pi^{eq}}{\partial h}\frac{\partial (hu)}{\partial x} - \frac{\partial \Pi^{eq}}{\partial (hu)}\frac{\partial \Pi^{eq}}{\partial x} + \frac{S^{eq}}{\partial x}\right] \tag{5.13}$$

and:

$$\Pi^{eq} = \sum_i {E_i}^2 f_i^{eq} \tag{5.14}$$

$$S^{eq} = \sum_i {E_i}^3 f_i^{eq} \tag{5.15}$$

The transformed EDFs yield the same second moment (Π^{eq}) as the standard LBM scheme:

$$\Pi^{eq} = \frac{1}{2} g h^2 + h u^2. \tag{5.16}$$

The S^{eq} expression, in which the last two terms are absent in the standard LBM scheme, is simplified to:

$$S^{eq} = (\beta^2 - 3\alpha^2) e^2 h u + 3\alpha e \left(\frac{1}{2} g h^2 + h u^2\right) + \alpha(\alpha^2 - \beta^2) h e^3 \tag{5.17}$$

Using the expressions:

$$\frac{\partial \Pi^{eq}}{\partial (hu)} = \frac{\partial}{\partial (hu)}\left[\frac{1}{2} g h^2 + \frac{1}{h}(hu)^2\right] = 2u \tag{5.18}$$

$$h\frac{\partial u}{\partial x} = \frac{\partial (hu)}{\partial x} - u\frac{\partial h}{\partial x} \tag{5.19}$$

$$\frac{\partial \Pi^{eq}}{\partial x} = \frac{\partial \Pi^{eq}}{\partial h}\frac{\partial h}{\partial x} + \frac{\partial \Pi^{eq}}{\partial u}\frac{\partial u}{\partial x} = (gh - u^2)\frac{\partial h}{\partial x} + 2u\frac{\partial (hu)}{\partial x} \tag{5.20}$$

the dissipative term for the generalised transformed scheme will reduce to:

$$\Gamma = \Delta t\left(\tau - \frac{1}{2}\right)\left\{[-gh - 5u^2 + 6\alpha eu + (\beta^2 - 3\alpha^2)]\frac{\partial(hu)}{\partial x} + [-2ghu + 3\alpha ghe + 2u^3 + \alpha(\alpha^2 - \beta^2)e^3 - 3\alpha eu^2]\frac{\partial h}{\partial x}\right\} \quad (5.21)$$

Substituting α=0 and β=1 makes Eq. (5.21) match the dissipation term for the standard 1D LBM scheme (van Thang et al. 2010) and for values of α=1 and β=2 it returns the calculated dissipation term for Chopard's asymmetric scheme (Chopard et al. 2013) except for the coefficient of u^2 which appears incorrectly calculated as (-3) in both of the above references.

For values of $\tau \approx {}^1/_2$, the dissipative term calculated by Eq. (5.21) becomes insignificant and the standard shallow water equations are recovered.

5.3. Stability Criteria

The stability zone boundaries for the transformed scheme will be determined from the numerical and physical restraints on the system. Like any other piecewise numerical approach, the CFL condition must be met to ensure information will be propagated at the required speed in the domain to capture the physical water velocity. This imposes conditions on the lattice speed which are derived for the subcritical and supercritical regimes:

For the subcritical regime:

$$(\alpha + \beta)e > \sqrt{gh} + u \Rightarrow Fr < (\alpha + \beta)\psi - 1 \text{ (Forward link)}$$
$$Fr < 1 \Rightarrow \frac{u}{\sqrt{gh}} < 1 \Rightarrow u < \sqrt{gh} \Rightarrow (\beta - \alpha)e > \sqrt{gh} - u \Rightarrow \quad (5.22)$$
$$Fr > 1 - (\beta - \alpha)\psi \text{ (Backward link)}$$

and for the supercritical regime:

$$(\alpha + \beta)e > \sqrt{gh} + u \Rightarrow Fr < (\alpha + \beta)\psi - 1 \text{ (Forward link)}$$
$$Fr > 1 \Rightarrow \frac{u}{\sqrt{gh}} > 1 \Rightarrow u > \sqrt{gh} \Rightarrow (\beta - \alpha)e > u - \sqrt{gh} \Rightarrow \quad (5.23)$$
$$Fr < 1 + (\beta - \alpha)\psi \text{ (Backward link)}$$

The other condition set by Chopard et al. (2013) must also be met to guarantee stability of the solution, regardless of the flow regime. This is to limit the speed at which information travels in the system (lattice speed) to the physical speed in the system:

$$e < u + \sqrt{gh} \Rightarrow Fr > \psi - 1 \tag{5.24}$$

The stability conditions for subcritical flows can be summarised as an envelope defined by the following boundaries:

$$\begin{aligned} Fr &< (\alpha + \beta)\psi - 1 \\ Fr &> 1 + (\alpha - \beta)\psi \\ Fr &> \psi - 1 \end{aligned} \tag{5.25}$$

The boundaries of the stability envelope for supercritical flow may be summarised as:

$$\begin{aligned} Fr &< (\alpha + \beta)\psi - 1 \\ Fr &< 1 + (\beta - \alpha)\psi \\ Fr &> \psi - 1 \end{aligned} \tag{5.26}$$

Equations (5.25) and (5.26) may be re-arranged to assist in selection of a proper lattice speed (*e*) for a problem:

For sub-critical flow:

$$\begin{aligned} e &> \frac{1}{\alpha + \beta}(\sqrt{gh} + u) \\ e &< \frac{1}{\alpha - \beta}(u - \sqrt{gh}) \\ e &< (u + \sqrt{gh}) \end{aligned} \tag{5.27}$$

For supercritical flow:

$$\begin{aligned} e &> \frac{1}{\alpha + \beta}(\sqrt{gh} + u) \\ e &> \frac{1}{\beta - \alpha}(u - \sqrt{gh}) \\ e &< (u + \sqrt{gh}) \end{aligned} \tag{5.28}$$

Adoption of Equations (5.27) and (5.28) allows definition of a more expanded stability envelope compared to that proposed by Chopard et al. (2013). The asymmetry parameters (α and β) and lattice speed (e) can be selected based on based on Equations (5.27) and (5.28) and the hydraulic characteristics of the problem being solved to yield a stability envelope that fully encompasses the solution. The expanded stability envelope for two sets of asymmetry parameters are shown as examples in Figure 5-2.

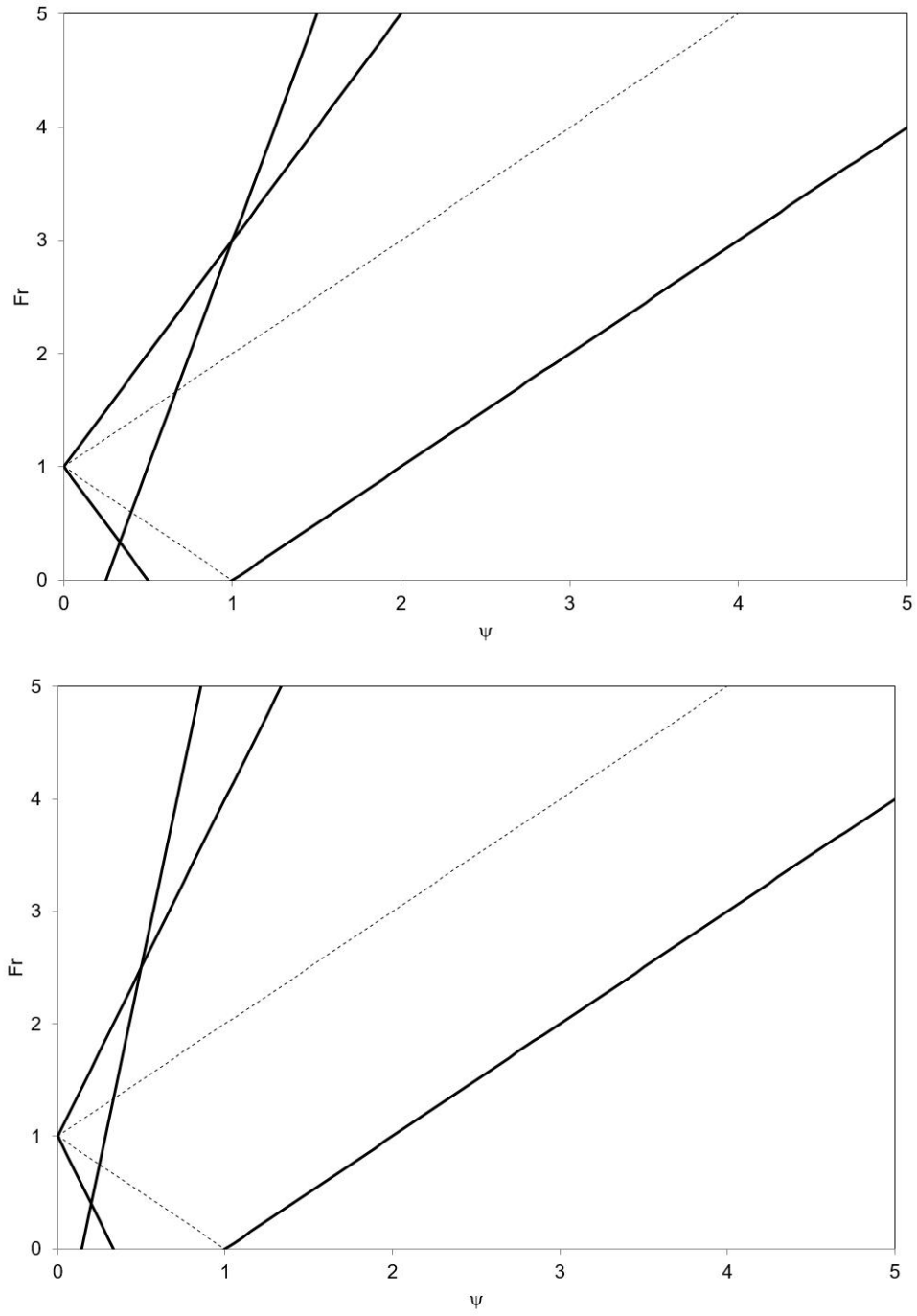

Figure 5-2 Enlarged numerical stability zone. solid bold line, transformed scheme; dotted line, Chopard et al. (2013). Top: stability envelope for $\alpha = 1, \beta = 3$. Below: stability envelope for $\alpha = 2, \beta = 5$.

It should be noted that while the new stability envelope encompasses a wider range of Froude numbers, notably larger Froude numbers, there are still some flow conditions that cannot be accommodated by the transformed scheme. As Figure 5-2 suggests, the lower bound of the stability envelope of the transformed scheme for values of $\Psi > 1$ remains identical to Chopard et al. (2013) and cannot accommodate very small Froude numbers (such as Fr=0). However, for values of $\Psi < 1$ the range of subcritical Froude numbers accommodated by the transformed scheme is larger than Chopard et al. (2013), which is limited to a singular point at Fr = 1. This shows the revised stability envelope can accommodate an extended range of flows, both in subcritical and supercritical regimes, compared to the asymmetric scheme by Chopard et al. (2013).

5.4. Boundary Conditions

The inflow and outflow boundary conditions at the two ends of the model were not discussed in Chopard et al. (2013). Here the method proposed by Zou and He (1997) will be applied to the transformed scheme to derive the inflow and outflow boundary conditions.

At domain inlet and for the first lattice, the values of f_1 and f_3 cannot be calculated from the inside lattices and must be determined from the inflow boundary conditions and the known value of f_2 at the first lattice (Figure 5-3):

$$f_1 + f_2 + f_3 = h \tag{5.29}$$

$$(\alpha + \beta)ef_1 + (\alpha - \beta)ef_2 + \alpha ef_3 = Q \tag{5.30}$$

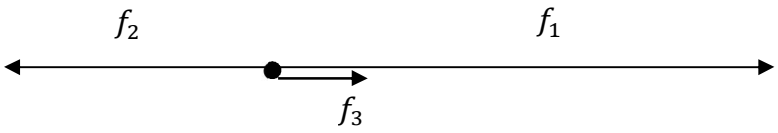

Figure 5-3 the EDFs for the transformed D1Q3 scheme.

Simultaneous solution of Equations (5.29) and (5.30) yields the following two equations which will be used to determine f_1 and f_3 at the very first lattice:

$$f_1 = \frac{Q}{\beta e} - \frac{\alpha}{\beta}h + f_2 \tag{5.31}$$

$$f_3 = \left(1 + \frac{\alpha}{\beta}\right) h - 2f_2 - \frac{Q}{\beta e} \tag{5.32}$$

The f_1 values for lattice numbers 2 to $\alpha + \beta$ also cannot be calculated from the inside lattices and need to be specified in the boundary conditions. These will be calculated assuming insignificant variation in the forward EDF at the first lattices in the domain, which is equivalent to a zero gradient in the value of f_1; i.e.

$$f_1(k) = f_1(\alpha + \beta + 1) \qquad (1 \leq k \leq \alpha + \beta) \tag{5.33}$$

If the selected α value is such that $\alpha > 1$, the values of f_3 for lattice numbers 2 to α also need to be specified by adopting a zero gradient for the f_3 function; i.e.:

$$f_3(m) = f_3(\alpha + 1) \qquad (\alpha > 1 \quad , \quad 1 \leq m \leq \alpha) \tag{5.34}$$

At domain outlet and for the very end lattice the unknown f_2 value will be determined using the known values of f_1 and f_3 and Equation (5.30):

$$f_2 = \frac{1}{\alpha - \beta}\left[\frac{Q}{e} - (\alpha + \beta) f_1 - \alpha f_3\right] \tag{5.35}$$

Similarly, the f_2 values for lattice numbers $N - (\beta - \alpha) + 1$ to N (the number of lattices) also need to be specified in the boundary conditions. These will be calculated assuming a zero gradient in the value of f_2; i.e.

$$f_2(n) = f_2\big(N - (\beta - \alpha)\big) \qquad [N - (\beta - \alpha) + 1] \leq n \leq N \tag{5.36}$$

5.5. Lattice isotropy

As discussed before, not every lattice system is appropriate for use in the LBM. To recover the Navier-Stokes equations, a lattice system must satisfy several symmetry conditions to ensure isotropic behaviour. These symmetry conditions, often viewed as *orthogonal* properties between lattice vectors, are summarised in Eq. (5.37) (Frisch et al. 1987, Wolfram 1986).

$$\sum_i w_i = 1$$
$$\sum_i w_i c_{i\alpha} = 0$$
$$\sum_i w_i c_{i\alpha} c_{i\beta} c_{i\gamma} = 0$$
$$\sum_i w_i c_{i\alpha} c_{i\beta} = C_S^2 \delta_{\alpha\beta} \qquad (5.37)$$
$$\sum_i c_{i\alpha} c_{i\beta} c_{i\gamma} c_{i\delta} = C_S^4 \left(\delta_{\alpha\beta}\delta_{\gamma\delta} + \delta_{\alpha\gamma}\delta_{\beta\delta} + \delta_{\alpha\delta}\delta_{\beta\gamma}\right)$$
$$\sum_i w_i c_{i\alpha} c_{i\beta} c_{i\gamma} c_{i\delta} c_{i\epsilon} = 0$$

These set of equations in (5.37) were used to determine the force term weighting factors for different lattice configurations (Figure 5-4). For example, in the standard one dimensional D1Q3 scheme these equations yield 4/6 for the rest state and 1/6 for the two directions as it will be shown below. The new weighting factors and the C_S value were derived for the generic transformed D1Q3 configuration from Eq. (5.37) as follows:

$$\sum_i w_i = 1 \Rightarrow w_0 + w_1 + w_2 = 1$$
$$\sum_i w_i c_{i\alpha} = 0 \Rightarrow \alpha\, w_0 + (\alpha + \beta)\, w_1 + (\alpha - \beta)\, w_2 = 0 \qquad (5.38)$$
$$\sum_i w_i c_{i\alpha} c_{i\beta} c_{i\gamma} = 0 \Rightarrow \alpha^3\, w_0 + (\alpha + \beta)^3\, w_1 + (\alpha + \beta)^3\, w_2 = 0$$
$$\sum_i w_i c_{i\alpha} c_{i\beta} = C_S^2 \delta_{\alpha\beta} \Rightarrow \alpha^2\, w_0 + (\alpha + \beta)^2\, w_1 + (\alpha + \beta)^2\, w_2 = C_S^2$$

Simultaneous solution of equations (5.38) yields:

$$w_0 = \frac{2}{3} - \frac{2\alpha^2}{3\beta^2} \qquad (5.39)$$

$$w_1 = \frac{2\alpha^2 - 3\alpha\beta + \beta^2}{6\beta^2} \qquad (5.40)$$

$$w_2 = \frac{2\alpha^2 + 3\alpha\beta + \beta^2}{6\beta^2} \qquad (5.41)$$

$$C_S^2 = \frac{(\beta^2 - \alpha^2)(2\alpha^3 - 2\alpha^2 + \beta^2)}{3\beta^2} \tag{5.42}$$

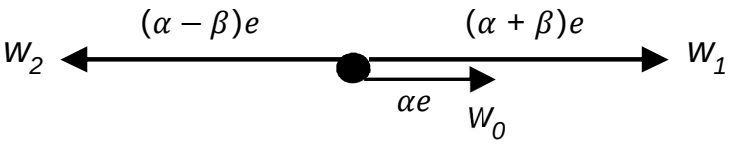

Figure 5-4 directional force term weight functions in the transformed scheme.

It can be verified that by substituting $\alpha = 0$ and $\beta = 1$ (standard D1Q3 scheme) in Equations (5.39) to (5.42) the calculated weighting factors are 4/6, 1/6 and 1/6 and C_S^2=1/3. Substituting α=1 and β=2 gives weighting factors 1/2, 0, 1/2 and C_S^2=1 as adopted by Chopard (2013). However, neither the derivation, nor the rationale behind this choice, was provided in the previous literature on LBM. Some researchers have also adopted uniform weights across the lattice. If for all directions it is assumed that $w_i = 1$ the fourth criteria in Equation (5.37) yields $C_S^2 = \frac{1}{2}$ which is the value used by Frandsen (2008a). However, this approach is only applicable if a normalised lattice velocity ($e = 1$) is been used.

5.6. Generalised transformation of D2Q9 scheme

Application of a generalised transformation to the D2Q9 scheme was expected to result in exhaustively complex calculations. Hence, a specific Galilean transformation was applied to the D2Q9 scheme with the lattice framework moving at speed $U = {}^{e}/_{3}$ in the transverse direction to derive the required EDFs (refer Appendix B).

Despite the simplicity of assuming a constant speed for the Galilean transformation, the calculations proved to result in a set of complex mathematical equations. A set of possible solutions were found for the equations that were derived for the specifically-transformed D2Q9 scheme. The force term weight factors were also determined for the new D2Q9 scheme. The detailed hand calculations for derivation of the EDFs and force term weight factors for the D2Q9 scheme are included in Appendix B.

The Galilean transformation of D2Q9 scheme was not pursued further in current study due to its complexities and the focus remined on expanding the applications of the transformed D1Q3 scheme.

5.7. Summary

Details of a new generalised Galilean transformation applied to the standard D1Q3 LBM was discussed in this chapter. Through selection of a proper set of asymmetry parameters, which would be selected in accordance of the properties of the physical system, the transformed LBM can be applied to a wide range of flow regimes, including subcritical, supercritical and the mix of both. The directional equilibrium functions were derived for the transformed scheme and Navier-Stokes equations were successfully recovered from the proposed Equilibrium Distribution Functions and lattice speeds through the Chapman-Enskog expansion. Detailed derivation of the adjusted the force term weight functions, inflow and outflow boundary conditions and the numerical stability criteria were also provided for the transformed scheme.

6. Validation of the transformed D1Q3 model

The new general asymmetric Lattice Boltzmann Model was validated by comparing the results to analytical and numerical solutions of benchmark cases in open-channel hydraulics. These include Gradually-Varied Flow (GVF) and Rapidly-Varied Flow (RVF) for both subcritical and supercritical flow regimes and both regimes simultaneously. For each scenario, the lattice asymmetry parameters α, β, and lattice speed, e, are selected so that the solution remains in the stability zone derived above. The model results are independent of the selected asymmetry parameters provided that the selected α and β place the solution fully within the stable solution zone. Boundary conditions are implemented as described above. Table 6.1 provides a summary of the geometry, the hydrodynamic conditions, and the lattice parameters for each case.

Table 6.1 Physical and lattice data for each test case.

	Case 1	Case 2	Case 3	Case 4	Case 5	Case 6	Case 7	Case 8	Case 9	Case 10	Case 11
Hydraulic condition	M2	M3	S2	S3	bump	bump	weir	critical	tidal flow	dam break	dam break
Unit flow rate, q (m²/s)	6.00	6.00	2.80	2.00	3.00	3.00	3.68	1.00	var.	var.	var.
Manning's n (s/m$^{1/3}$)	0.013	0.013	0.013	0.013	-	-	-	0.013	-	-	0.015
Channel length, L (m)	400	100	100	250	30	30	30	250	14000	200	200
Channel slope, S	0.001	0.001	0.070	0.020	0.000	0.000	0.000	0.001 0.050	var.	-	-
Critical depth, y_c (m)	1.542	1.542	0.928	0.742	0.972	0.972	1.114	0.467	var.	var.	var.
Normal depth y_n (m)	4.219	4.219	0.382	0.472	-	-	-	0.881 0.209	-	-	-
U/S* depth y_u (m)	2.975	0.695	0.500	0.230	2.000	0.400	1.600	0.757	var.	8.0	8.0
D/S* depth y_d (m)	1.542	1.542	0.382	0.472	1.370†	0.412†	0.806	0.209	var.	0.5	0.5
Weir height z (m)	-	-	-	-	0.500	0.150	0.199	-	-	-	-
Weir length L_w (m)	-	-	-	-	8	8	8	-	-	-	-
U/S* Froude	0.37	3.31	2.53	5.79	0.34	3.79	0.58	0.48	var.	var.	var.
D/S* Froude	1.00	0.63	3.79	1.97	0.60†	3.62†	1.63	3.35	var.	var.	var.
α	1	1	2	1	1	2	1	1	1	1	1
β	4	4	7	3	2	5	2	5	2	4	4

Table 6.1 (continued) Physical and lattice data for each test case.

	Case 1	Case 2	Case 3	Case 4	Case 5	Case 6	Case 7	Case 8	Case 9	Case 10	Case 11
C_s^2	5	5	$17\,4/9$	$2\,2/3$	1	$9\,1/4$	1	8	1	5	5
Lattice size Δx (m)	0.10	0.01	0.01	0.10	0.01	0.01	0.01	0.1	14	0.01	0.01
Lattice speed e (m/s)	3	5	4	5	5	4	5	3	4	3	3
U/S* Ψ	0.56	1.92	1.81	3.33	1.13	2.02	1.26	1.10	var.	var.	var.
D/S* Ψ	0.77	1.10	2.07	2.32	1.36†	1.99†	1.78	2.10	var.	var.	var.
Relaxation Parameter (τ)	1.0	2.0	2.0	2.0	1.0	1.0	1.5	2.0	0.6	1.0	1.0

*U/S: Upstream, D/S: Downstream †over the weir

The LBM model is compared to analytical solutions of the specific energy equation, or to the numerical solutions of the gradually varied flow equations using the standard step method (SSM) using a centred finite difference scheme with maximum step length of 0.02m. Numerical testing indicates that this step length is sufficient to ensure convergence of the SSM solutions such that a finer grid provided no increase in precision.

The shallow water equations represent an ideal fluid model and exclude fluid viscosity. Therefore, the relaxation parameter (τ) introduces numerical diffusion capable of suppressing unstable temporal updates which cross the stability zone. In some of the test cases with high Froude number a larger value of relaxation parameter was selected to maintain numerical stability.

The contents of this chapter are largely based on a published paper by Hedjripour et al. (2016).

6.1. Steady flow test cases

In this section details of the gradually-varied, steady flow cases simulated using the transformed scheme are presented and results compared to analytic results.

6.1.1. Case 1: Subcritical flow over a free overfall

Subcritical flow was modelled in a rectangular 400m long open channel with a drop at the downstream end, corresponding to a mild slope with depths between critical and normal and a M2 water surface profile. The upstream boundary conditions are flow rate (q) and zero-gradient of depth at the upstream end of the domain (Eq.(5.31)) and (5.32)). Bed friction was incorporated via the Manning's formula using a roughness coefficient of $n=0.013 sm^{-1/3}$. The downstream boundary condition is set using the known critical depth, flow rate and Eq. (5.35) to determine f_2 for the last lattice in the domain, and zero-gradient for other unknown f_2. The stability zone is illustrated in figure 6-1a; the values of $Fr - \Psi$ for all lattices in the domain are illustrated, with the boundary points marked by symbols. The solution is in the stable zone for the general scheme for all lattices along the channel, but outside the zone proposed by Chopard et al. (2013) at the upstream end of the channel. The water depths calculated by the model are compared to the numerical solution for an M2 profile from the standard step method (SSM) in figure 6-1b. There is excellent agreement between the two models and the maximum difference in the estimated depth is limited to 1.63% at the downstream boundary where the standard step model yields a vertical water surface.

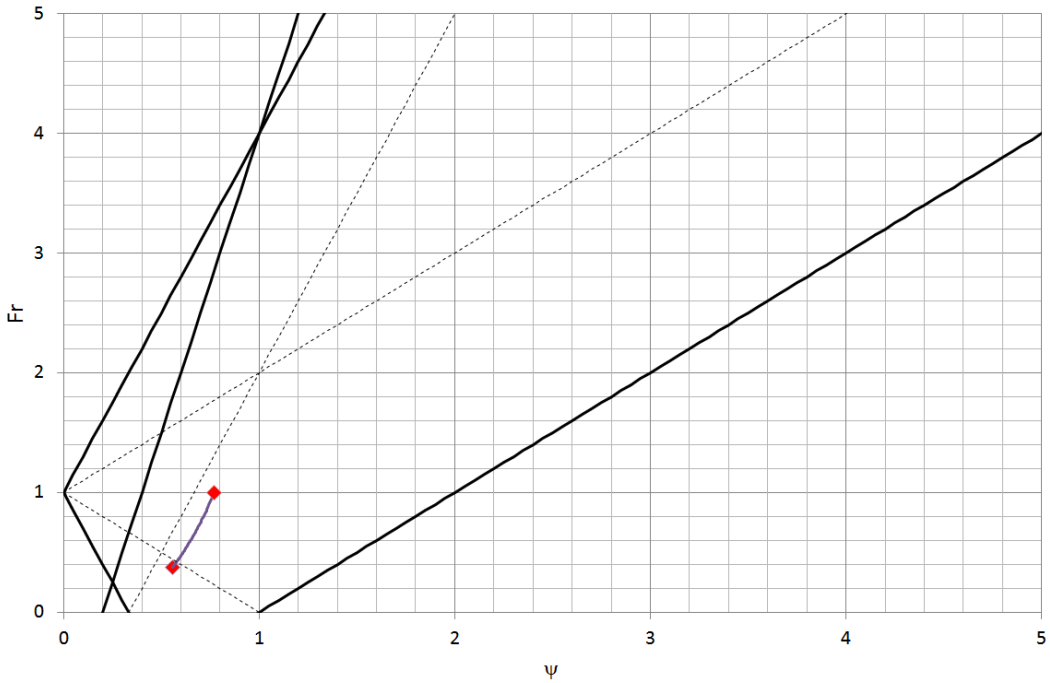

Figure 6-1a. Stability zone and Fr-Ψ for the M2 flow profile, case 1. Solid lines, boundaries of the present stability zone; dashed lines, boundaries of the Chopard et al. (2013) stability zone.

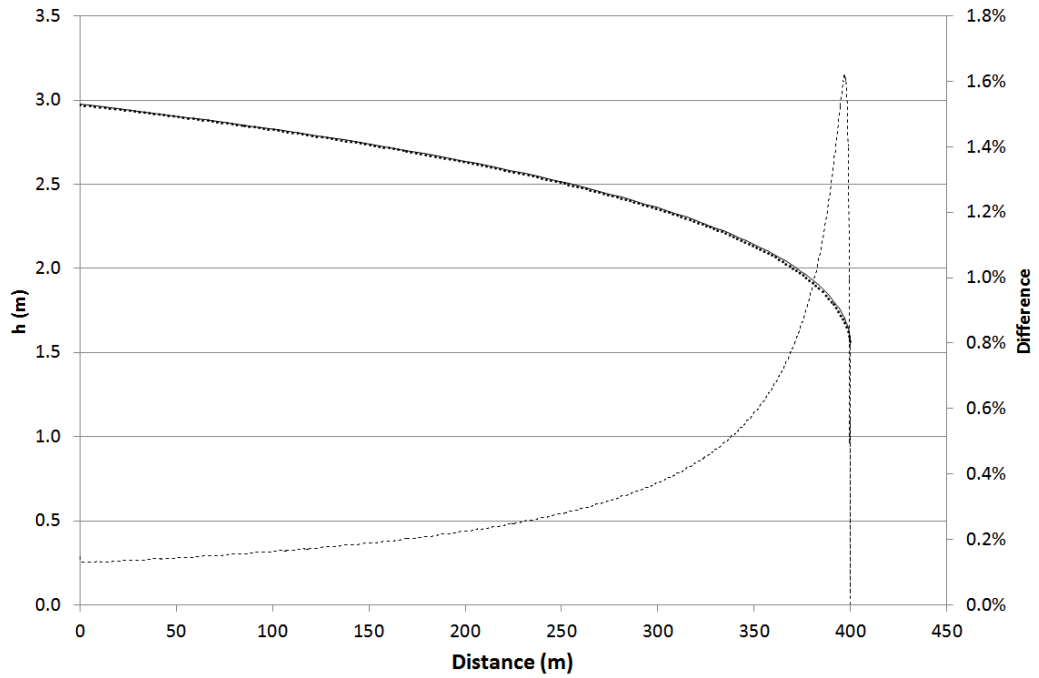

Figure 6-1b. Comparison of flow depth from the LBM model and the standard step model for the M2 profile, case 1. Solid line, SSM; dotted line, LBM; dashed line; difference.

6.1.2. Case 2: Supercritical flow downstream from a sluice gate

Supercritical flow released from a sluice gate at a Froude number of 3.3 and onto a long mild slope with a free overfall was simulated in a rectangular open channel for the same conditions as above. The initial depth (gate opening) was set to 0.695m (below the critical

depth) but no downstream depth was set to the model, again representing a free-fall condition. A supercritical flow with a M3 water surface profile (mild slope with depths less than critical) is expected, followed by a hydraulic jump and an M2 curve again to the free overfall. The upstream boundary conditions are again flow rate (q) and zero-gradient of depth at the upstream end of the domain; however, since supercritical flow is controlled from upstream, f_0 and f_1 for the first lattice were determined from the known h and q at the first lattice. A zero-gradient boundary condition was applied to f_2 at the downstream end of the channel and the last f_2 value was determined based on known flow rate at the outlet. The stability zone and water surface are illustrated in figure 6-2a and figure 6-2b, the latter again compared to the standard step method. The model automatically forms a hydraulic jump to transition between the two gradually varied flow profiles and the computed water depths closely satisfy the standard hydraulic jump equation, Equation (6.1), which excludes the influence of the bed slope and friction.

$$\frac{h_2}{h_1} = \frac{1}{2}\left(\sqrt{1 + 8\mathrm{Fr}_1^2} - 1\right) \tag{6.1}$$

There is a near perfect match between the two models in the supercritical flow region, with the maximum difference not exceeding 0.04%. However, the difference increases between the M2 curves, but this is largely because the conditions at the free overfall differ in the LBM model, with critical flow occurring upstream of the overfall. This is a well-known characteristic of real flows. Note that matching the two standard step solutions at the hydraulic jump compresses the jump to a discontinuity; again the LBM solution is more realistic.

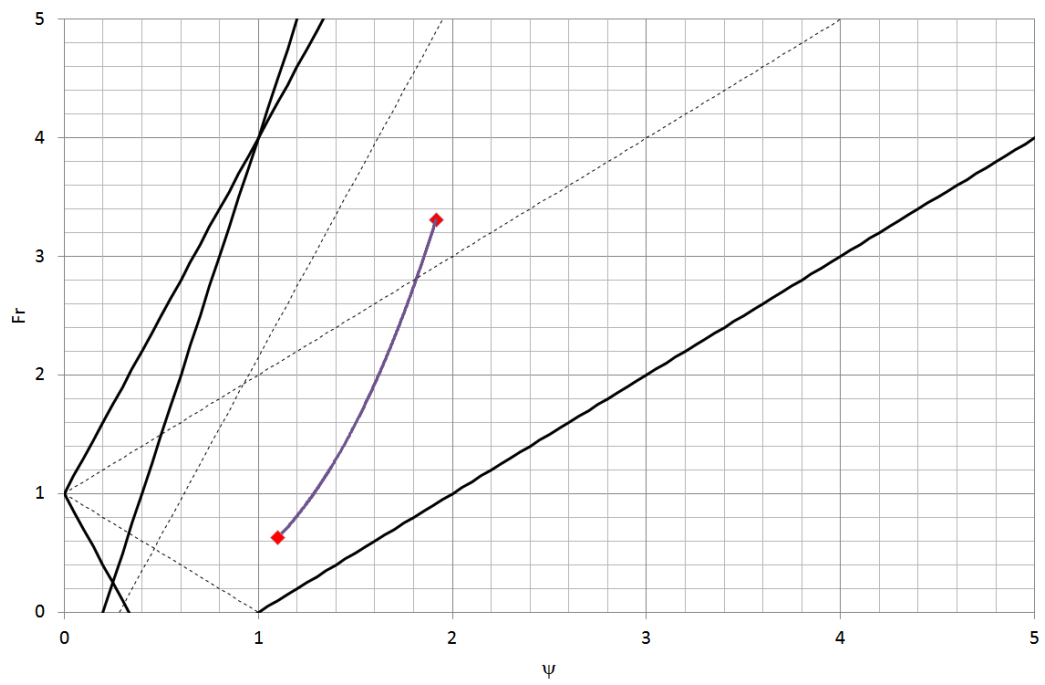

Figure 6-2a. Stability zone and Fr-Ψ for the M3-M2 flow profile, case 2. Solid lines, boundaries of the present stability zone; dashed lines, boundaries of the Chopard et al. (2013) stability zone.

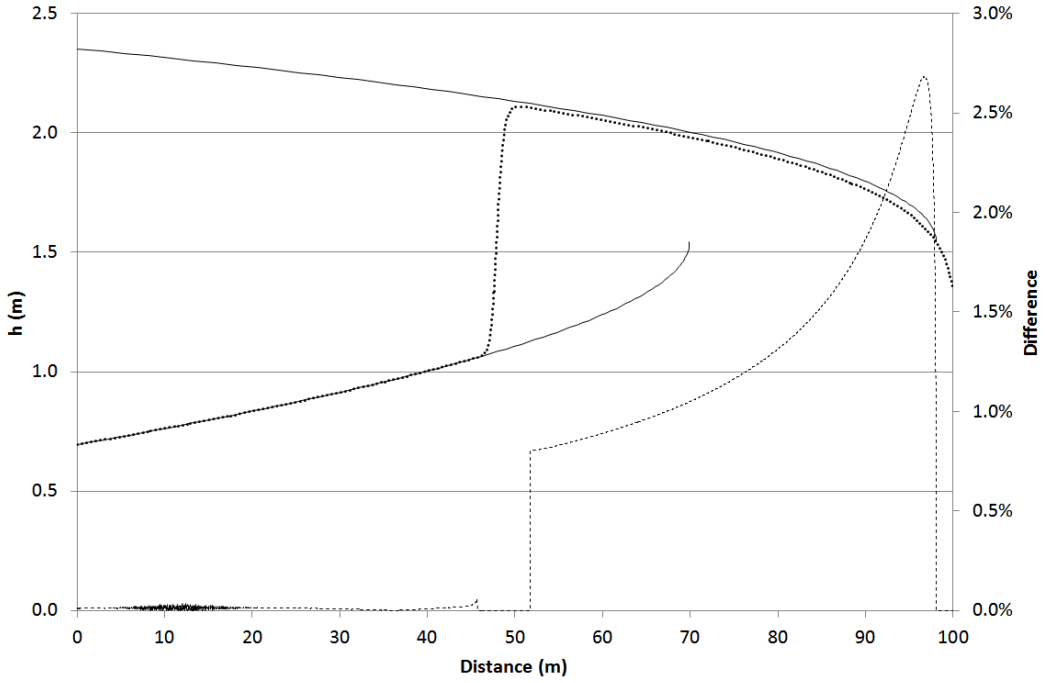

Figure 6-2b. Comparison of flow depth from the LBM model and the standard step model for the M3-M2 profile, case 2. Solid line, SSM; dotted line, LBM; dashed line; difference.

6.1.3. Case 3: Accelerating supercritical flow in a steep channel

Accelerating supercritical flow was modelled in a steep open channel, corresponding to a S2 profile (steep slope with depths greater than normal and less than critical) with the flow asymptotic to constant normal depth at the downstream end of the domain. Zero-gradient in

f was used to determine the unknown f_0 and f_1 at the upstream end and zero-gradient in depth was imposed at the downstream end to calculate the unknown f_2 values. The solution is again stable outside the zone proposed by Chopard et al. (2013). The upstream Froude number was 2.53 and the downstream Froude number was 3.79 as shown in Figure 6-3a. Figure 6-3b illustrates close agreement between the LBM model-generated S2 profile and the standard step method. The normal (supercritical) flow depth is correctly predicted by the LBM model.

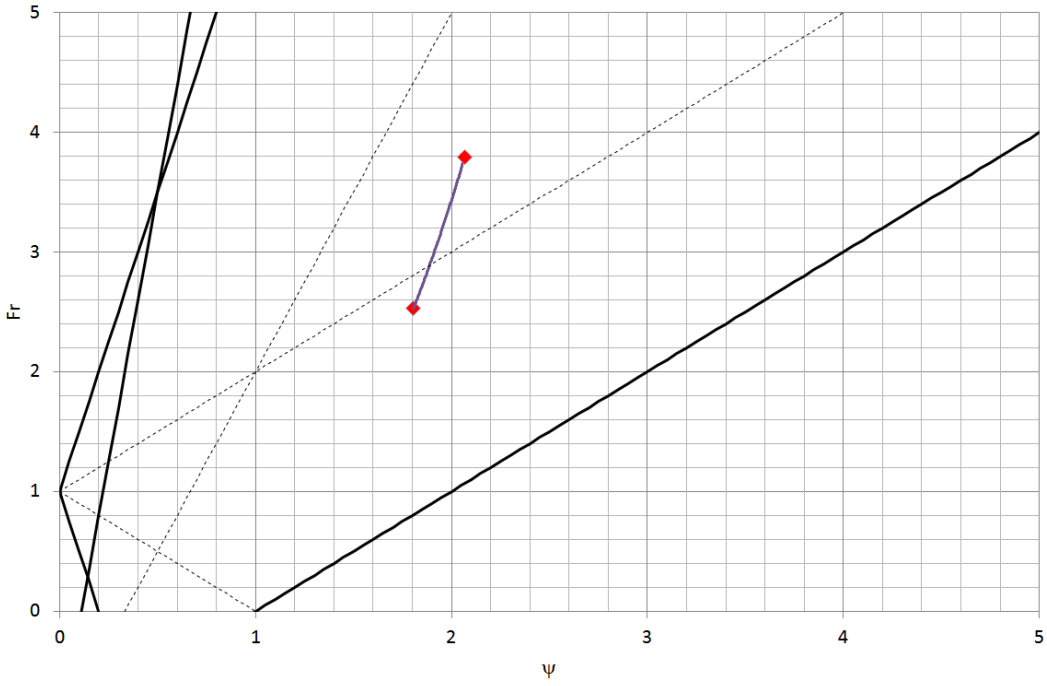

Figure 6-3a. Stability zone and Fr-Ψ for the S2 flow profile, case 3. Solid lines, boundaries of the present stability zone; dashed lines, boundaries of the Chopard et al. (2013) stability zone.

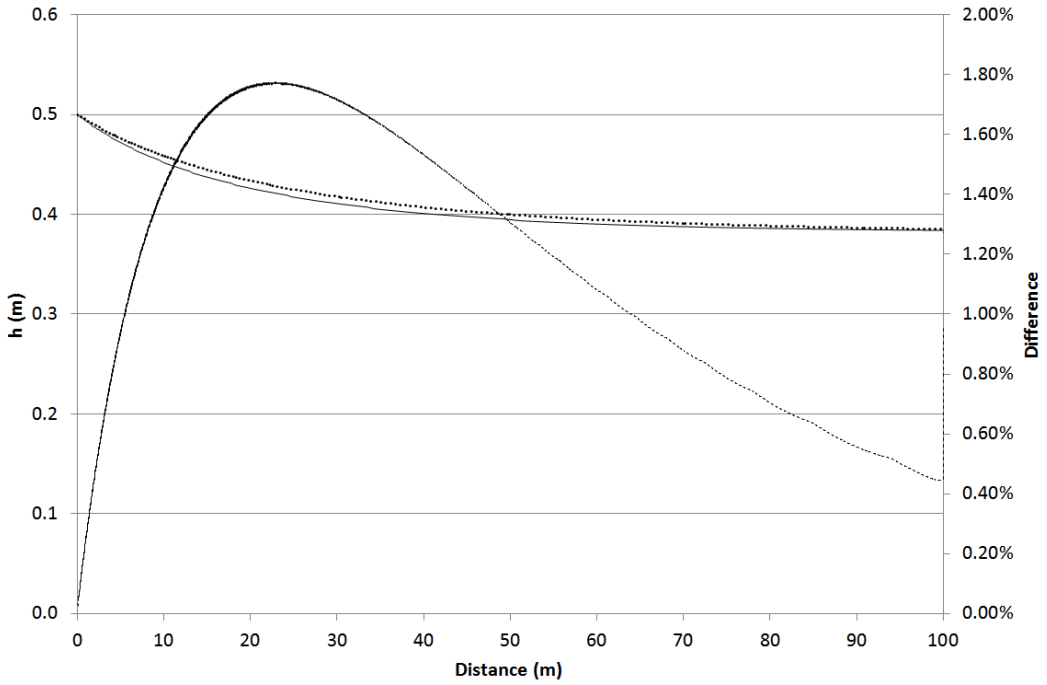

Figure 6-3b. Comparison of flow depth from the LBM model and the standard step model for the S2 profile, case 3. Solid line, SSM; dotted line, LBM; dashed line; difference.

6.1.4. Case 4: Decelerating supercritical flow in a long steep channel

Decelerating supercritical flow was modelled in a steep channel, corresponding to a S3 gradually varied flow profile, again asymptotic to normal depth. Equations (5.31) and (5.32) with known q and h at the upstream of the domain were used to determine f_0 and f_1 at the first lattice. For the downstream boundary condition, zero-gradient of depth was used to determine the unknown f_2. The upstream conditions correspond to a high Froude number of 5.79, with a downstream Froude number for the normal flow of 1.97 (figure 6-4a). This again corresponds to conditions outside the Chopard et al. (2013) stability zone. As illustrated in figure 6-4b, there is again excellent agreement between the LBM computed depth and those calculated from the standard step method.

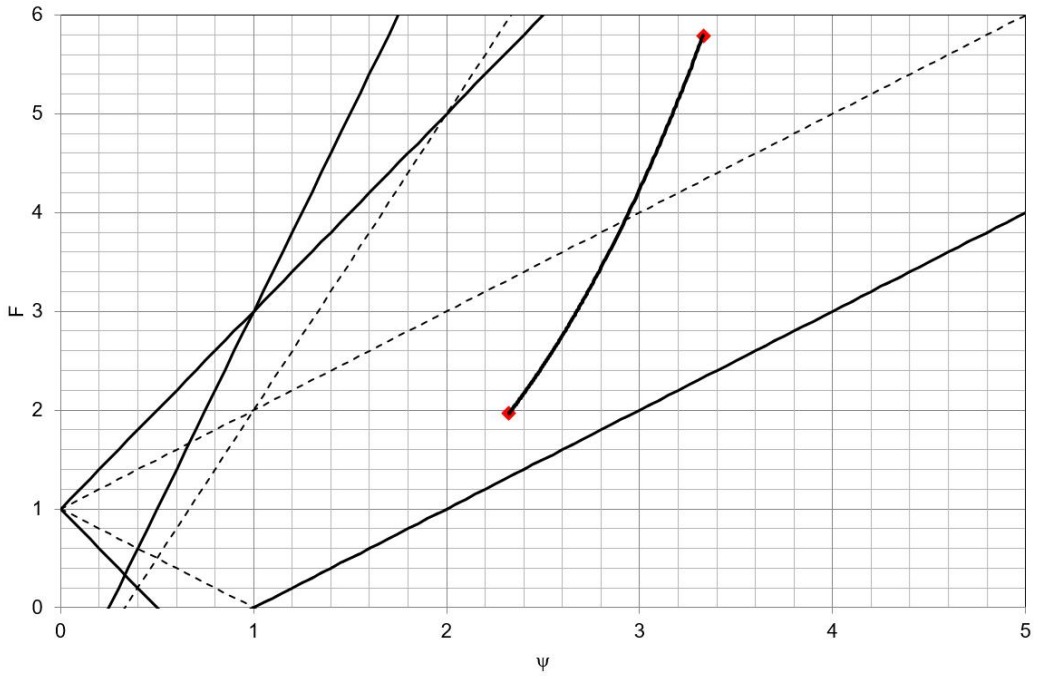

Figure 6-4a. Stability zone and Fr-Ψ for the S3 flow profile, case 4. Solid lines, boundaries of the present stability zone; dashed lines, boundaries of the Chopard et al. (2013) stability zone.

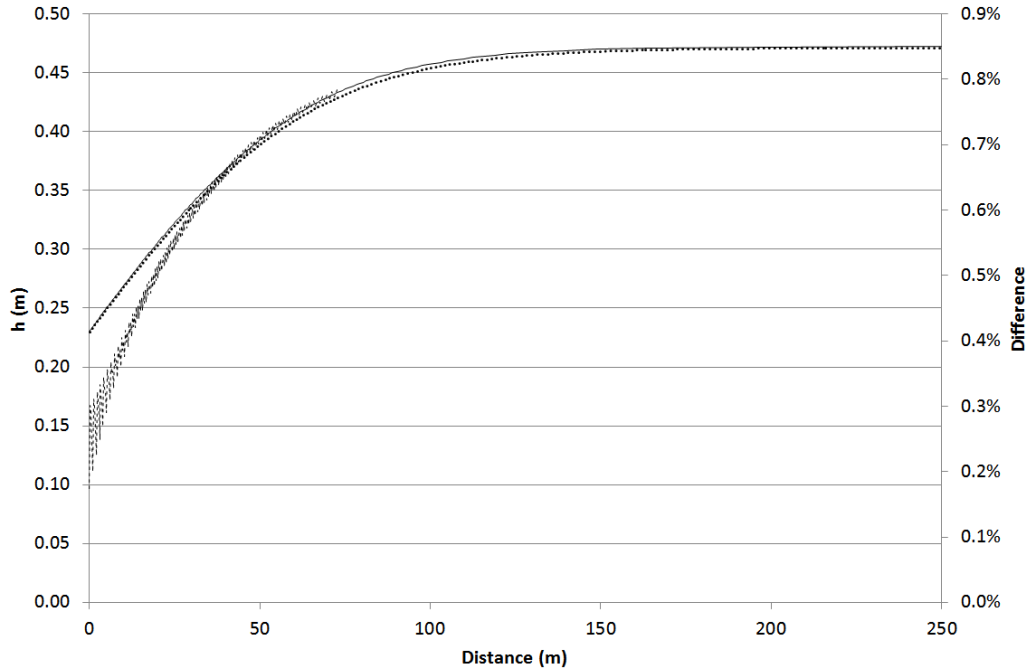

Figure 6-4b. Comparison of flow depth from the LBM model and the standard step model for the S3, case 4. Solid line, SSM; dotted line, LBM; dashed line; difference.

6.1.5. Cases 5 and 6: Flow over a local bump in a horizontal frictionless channel

The model was also validated for flow over a hump in a horizontal frictionless rectangular channel for both subcritical and supercritical regimes, with results compared to the analytical solution from the energy equation. The flow rate for the subcritical case was q = 3 m²/s and the bump height was set to 0.50 m, which does not induce a weir flow. For the upstream boundary conditions, f_0 and f_1 at the first lattice were determined assuming known flow rate (q) and zero-gradient in depth. The other unknown f_0 and f_1 were determined assuming zero-gradient in their respective values from the first known lattice. For the downstream boundary condition, the known flow rate was used to determine f_2 for the last lattice in the domain and zero-gradient in f_2 was used to determine the remaining f_2. Figure 6-5a shows the variation of Froude number and lattice Froude number in the domain, which is within the Chopard et al. (2013) stability zone. Figure 6-5b shows excellent agreement between the theoretical and modelled water surface profiles with maximum difference not exceeding 0.66% along the channel. Note that the LBM model contains some relaxation, whereas the analytical solution assumes changes in bed elevation are instantaneously reflected in the water surface profile. This leads to differences in the two solutions at locations of rapid change in gradient in the bed elevation. The same scenario was also modelled for a supercritical flow regime, with a set upstream depth and Fr = 3.79. Figure 6-6a shows the Fr and Ψ in the domain, outside the Chopard et al. (2013) stability zone and figure 6-6b again shows excellent agreement between modelled and analytical water surface profiles, with a local rise in the water surface (and depth) over the hump.

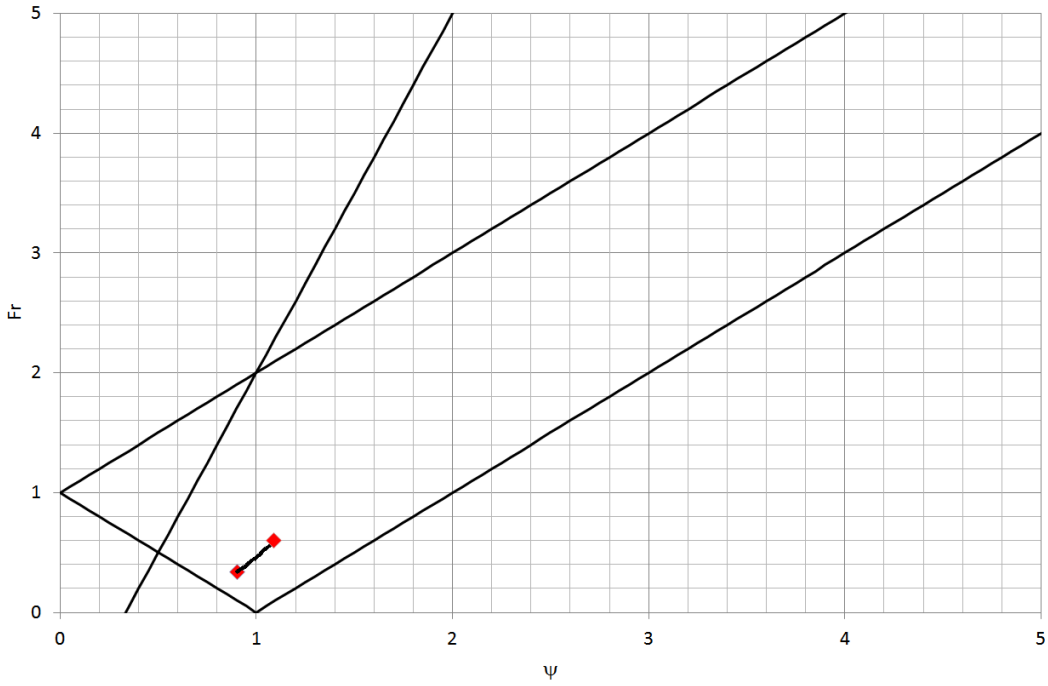

Figure 6-5a. Stability zone and Fr-Ψ for subcritical flow over a hump, case 5. Solid lines, boundaries of the present stability zone; dashed lines, boundaries of the Chopard et al. (2013) stability zone.

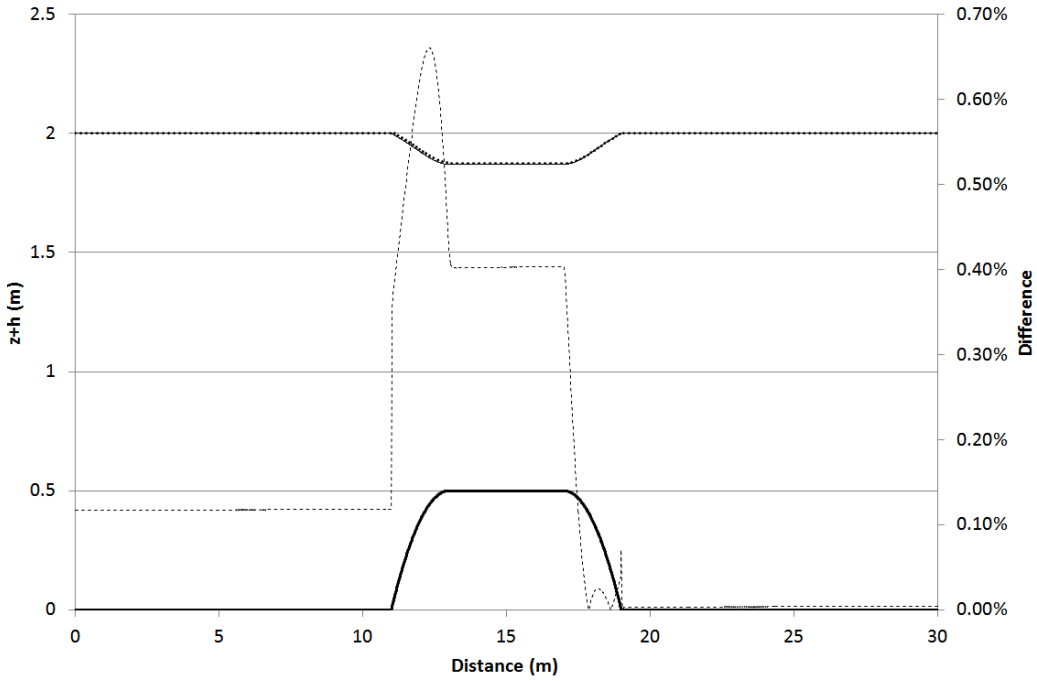

Figure 6-5b. Comparison of flow depth from the LBM model and the analytical solution of the energy equation for the subcritical flow over a hump, case 5. Solid line, analytical solution; dotted line, LBM; dashed line; difference.

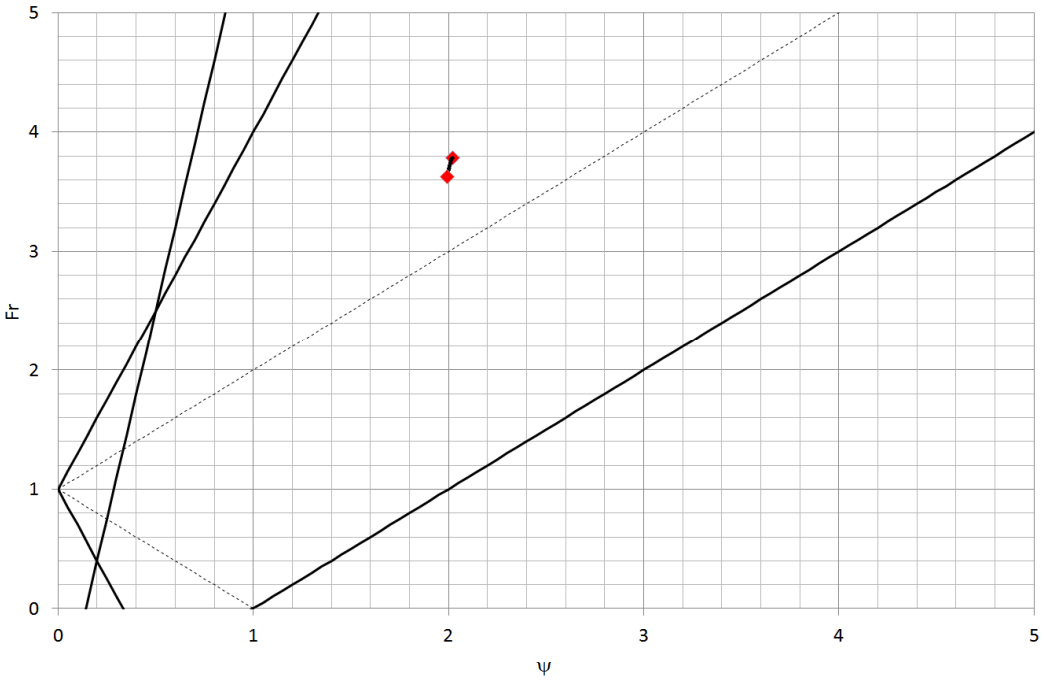

Figure 6-6a. Stability zone and Fr-Ψ for supercritical flow over a hump, case 6. Solid lines, boundaries of the present stability zone; dashed lines; boundaries of the Chopard et al. (2013) stability zone.

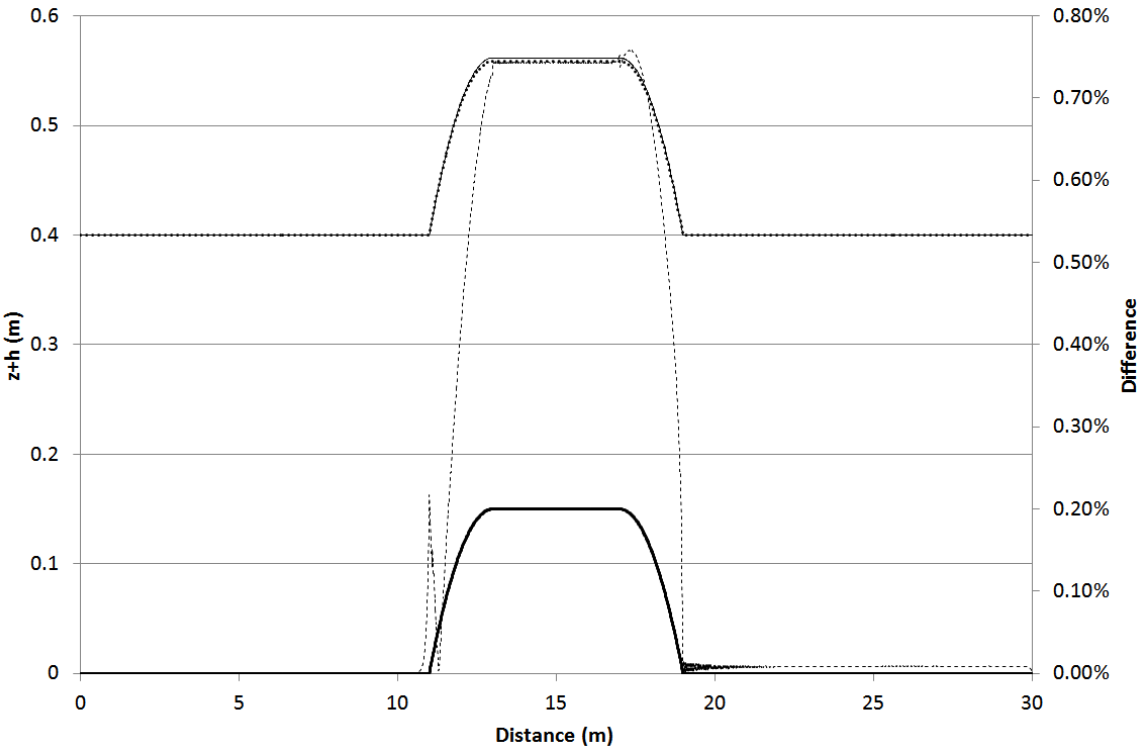

Figure 6-6b b. Comparison of flow depth from the LBM model and the analytical solution of the energy equation for the supercritical critical flow over a hump, case 6. Solid line, analytical solution; dotted line, LBM; dashed line; difference.

6.1.6. Case 7: Weir flow in a horizontal frictionless channel

The model was used to simulate a weir flow in a rectangular, horizontal frictionless channel with bump height z = 0.2 m, with upstream Froude number equal to 0.58 and a downstream Froude number of 1.63. Upstream boundary conditions were zero-gradient of f_0 and f_2, with f_0 and f_1 at the first lattice calculated from the model generated depth and flow rate at that point. At the downstream boundary, f_2 for the last lattice was calculated based on the known flow rate and the other f_2 values were calculated based on zero-gradient of f_2. None of the upstream or downstream depths were forced and critical flow conditions are not prescribed, such that the LBM model calculates the weir flow and afflux solely from the discharge and bed elevation. This case falls within the Chopard et al. (2013) stability zone (figure 6-7a). Figure 6-7b compares the modelled water surface profile against the calculated profile from the energy equation. Upstream and downstream of the weir there is excellent agreement the modelled and calculated water surface profiles. Again, differences reach about 6% at the upstream and downstream faces of the weir. The energy equation predicts a constant water depth (equal to critical depth) over the weir crest but the LBM model predicts a smooth curve that passes through critical depth at a single point and does not yield a curve that maintains critical depth over the weir crest. The LBM model results are more realistic; the analytical solution contains discontinuities in the gradient of the water surface, which are smoothed out in the LBM. Further, observations of critical flow over broad-crested weirs show a smooth transition in the water surface profile, not the constant depth predicted by the energy equation.

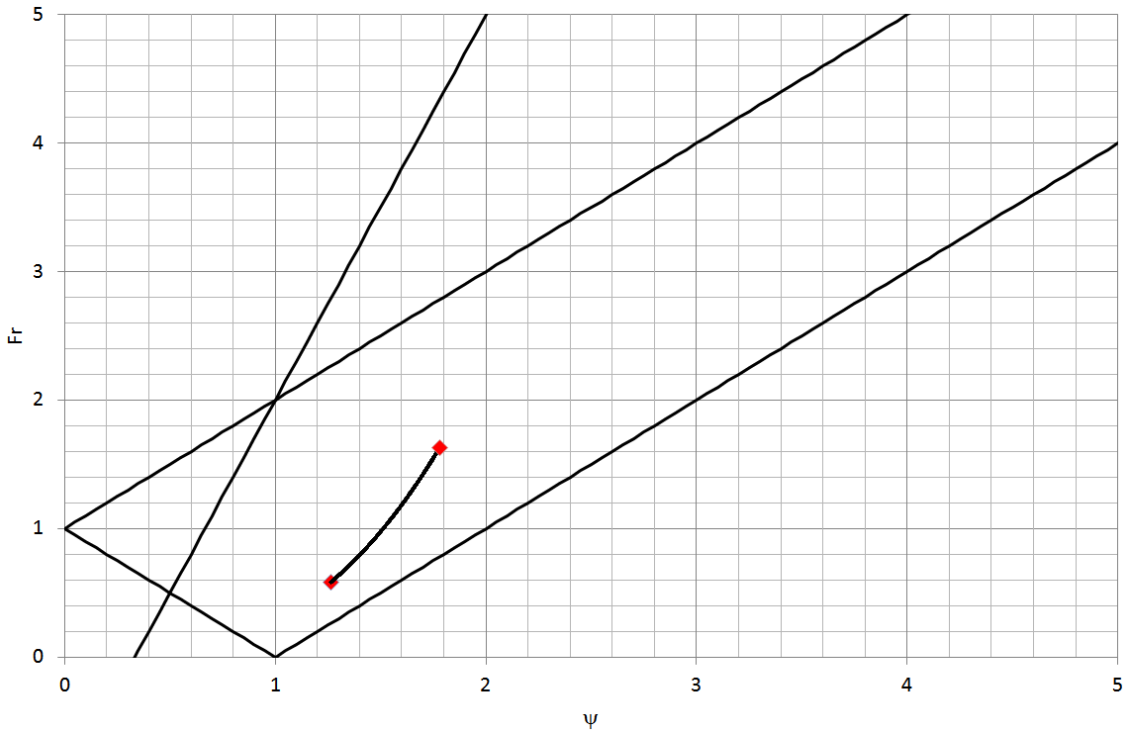

Figure 6-7a. Stability zone and Fr-Ψ for critical flow over a weir, case 7. Solid lines, boundaries of the present stability zone; dashed lines, boundaries of the Chopard et al. (2013) stability zone.

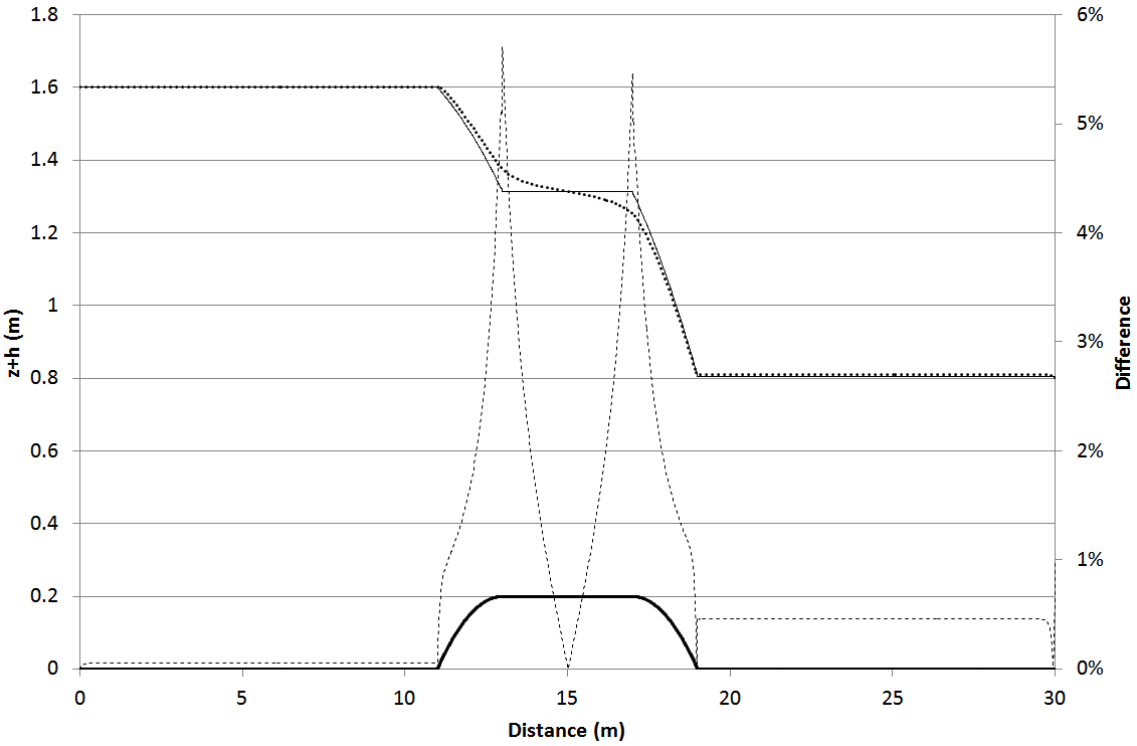

Figure 6-7b. Comparison of flow depth from the LBM model and the analytical solution of the energy equation for the critical flow over a weir, case 7. Solid line, analytical solution; dotted line, LBM; dashed line; difference.

6.1.7. Case 8 - Flow in a mild slope channel leading to a long steep channel

Flow over a channel transition from mild to steep was modelled to verify occurrence of critical flow depth and the automatic formation of a hydraulic control at the transition. The steep channel section was sufficiently long to allow the flow to asymptote to normal depth (i.e. a supercritical depth). With the normal flow regime being subcritical in the first channel it is expected that critical flow occurs around the transition to change flow regime from sub- to supercritical. No upstream or downstream depths were imposed, allowing the model to determine the depths based on the friction conditions and the flow rate. Figure 6-8a shows the variation of Fr and Ψ along the domain and Figure 6-8b compares the LBM model and the standard step model for the upstream and downstream gradually varied flow curves initiated at critical depth at the transition. The LBM profile is again likely to be more realistic as it predicts critical flow occurring slightly upstream of the transition and a smoother flow profile over the transition, while the standard-step method assumes critical depth to occur exactly at the transition and yields a vertical water surface at the transition from subcritical to supercritical flow. Neither condition occurs in practice.

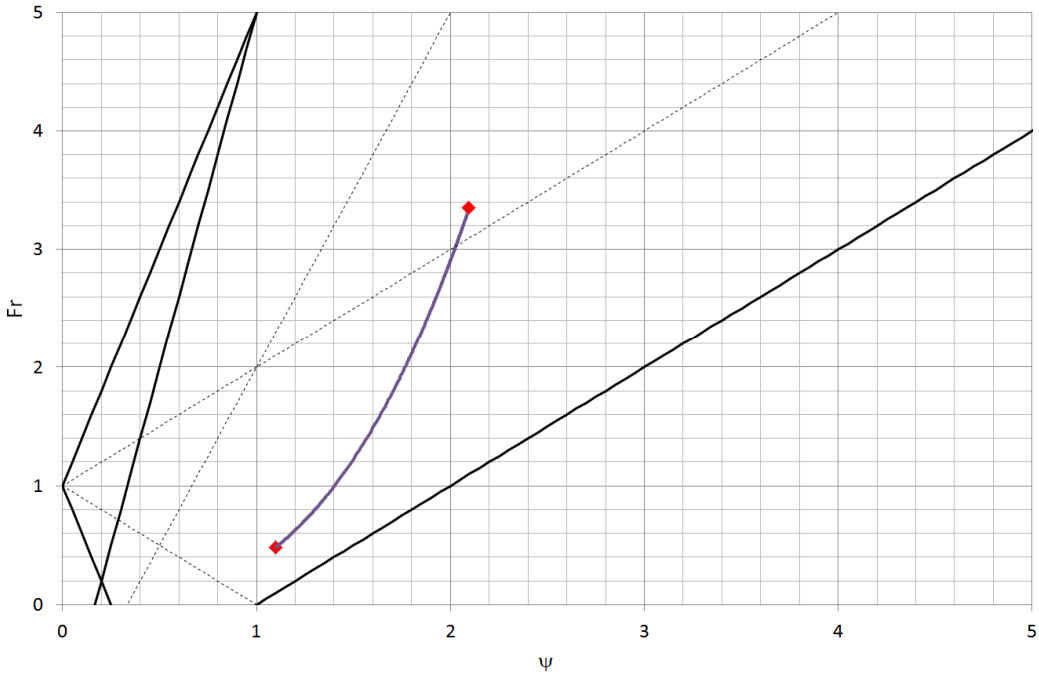

Figure 6-8a. Stability zone and Fr-Ψ for the M2-S2 flow profile, case 8. Solid lines, boundaries of the present stability zone; dashed lines, boundaries of the Chopard et al. (2013) stability zone.

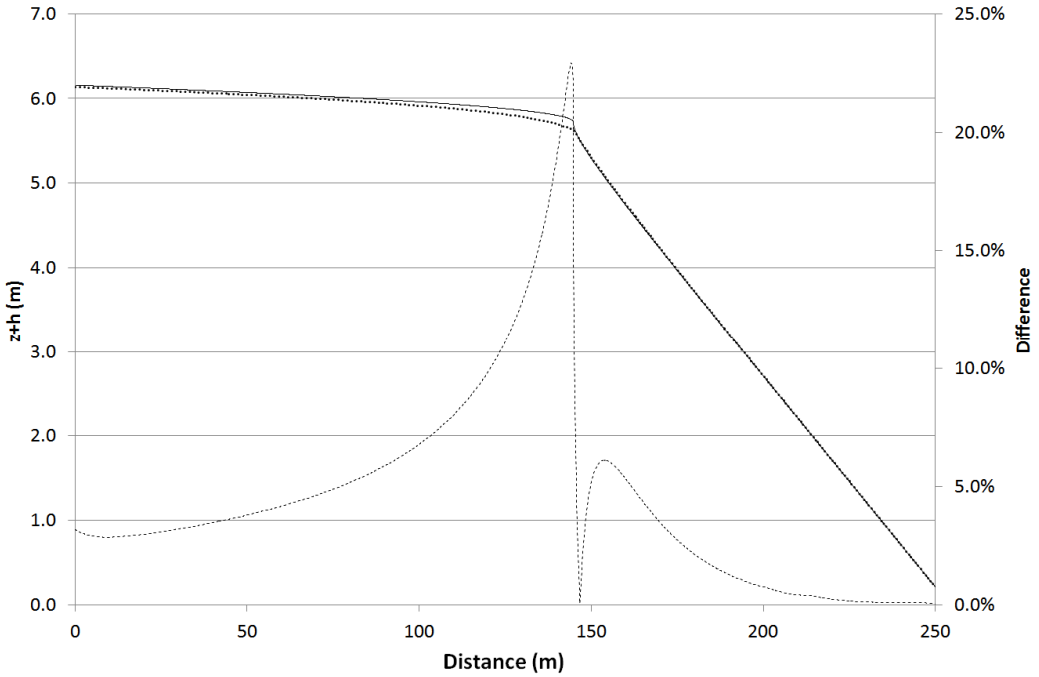

Figure 6-8b. Comparison of flow depth from the LBM model and the standard step model for the M2-S2 profile, case 8. Solid line, SSM; dotted line, LBM; dashed line; difference.

6.2. Unsteady flow test cases

The transformed scheme was used to model three unsteady test cases: a tidal wave flow case involving a fully subcritical regime and two dam-break cases on smooth and rough beds involving supercritical flows. The results of the tidal wave case were compared against analytic solutions and the results of the dam-break cases were compared with results of a finite volume model.

6.2.1. Case 9: Tidal Wave Flow

Here we have reproduced the results of a tidal wave propagation in a relatively short coastal region extending 14,000m from the shore with frictionless variable bed depth. Bermudez et al.(1994) have developed an analytical solution for a tidal wave case where the ocean floor elevation varies by Eq.(6.2):

$$Z(x) = 10 + \frac{40x}{L} + 10sin\left[\pi\left(\frac{4x}{L} - \frac{1}{2}\right)\right] \tag{6.2}$$

and the initial and boundary conditions are defined by Eqs. (6.3) to (6.6).

$$h(x,0) = 60.5 - Z(x) \tag{6.3}$$

$$\boldsymbol{u}(x,0) = 0 \tag{6.4}$$

$$\boldsymbol{u}(L,t) = 0 \tag{6.5}$$

$$h(0,t) = 64.5 - 4sin\left[\pi\left(\frac{4t}{86400} + \frac{1}{2}\right)\right] \tag{6.6}$$

The analytical solution for water depth and velocity are given by Eqs. (6.7) and (6.8).

$$h(x,t) = 64.5 - Z(x) - 4sin\left[\pi\left(\frac{4t}{86400} + \frac{1}{2}\right)\right] \tag{6.7}$$

$$\boldsymbol{u}(x,t) = \frac{(x-L)\pi}{5400h(x,t)}cos\left[\pi\left(\frac{4t}{86400} + \frac{1}{2}\right)\right] \tag{6.8}$$

Thömmes et al.(2007) also used this case to verify their sub-critical LBM shallow water model. Although the Froude number in this case stays well below unity throughout the domain, it is included here to demonstrate the ability of the transformed model in handling irregular bed geometry. Results of the asymmetric scheme are identical to the earlier solution, proving the correctness of the force terms and weight factors.

Figure 6-9a shows the analytical and modelled velocity profiles at time t = 9117.5s where very good agreement is seen between the two curves. The analytical and modelled water surface profiles are compared in Figure 6-9b from which an excellent agreement is evident between the two approaches.

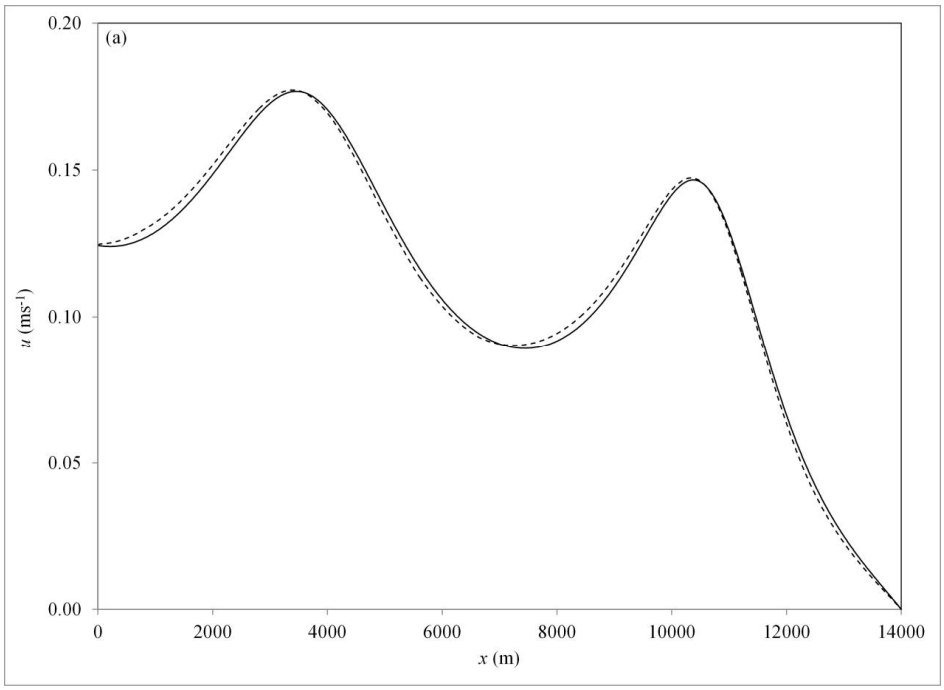

Figure 6-9a. Velocity profile for the tidal flow case in Bermudez et al. (1994), reproduced with the asymmetric scheme. Solid line, analytical solution; dotted line, LBM.

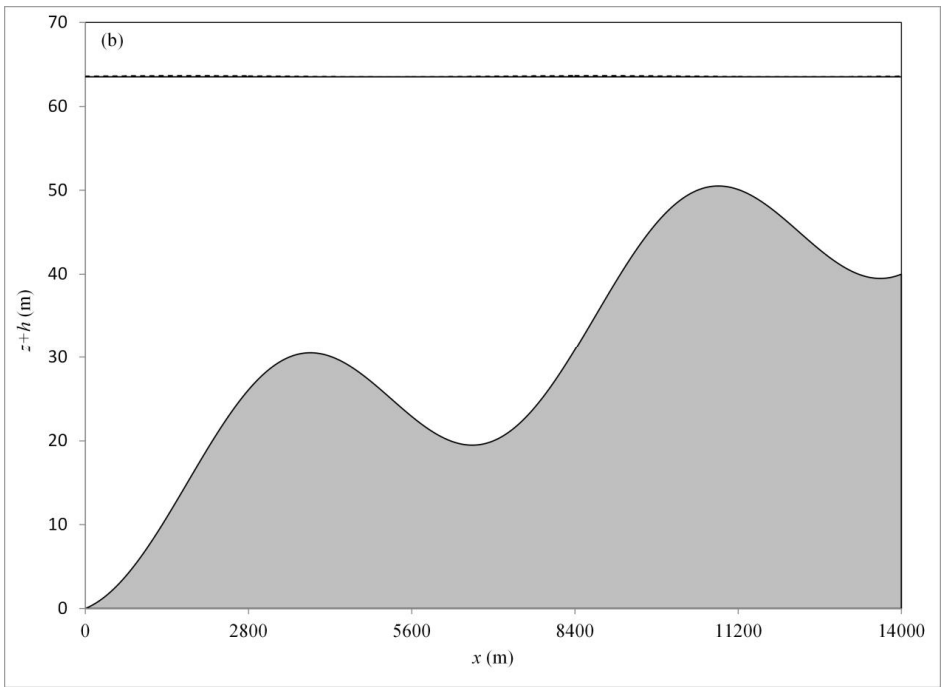

Figure 6-9b. Water surface profile for the tidal flow case in Bermudez et al.(1994), reproduced with the asymmetric scheme. Solid line, analytical solution; dotted line, LBM.

6.2.2. Case 10: Dam-break on a smooth bed

A dam-break flow case was modelled to verify applicability of the model for unsteady flow cases with Fr > 1. This was the time that the transformed scheme was applied to unsteady flow because no such test case was included in Chopard et al. (2013) This case pushes the limits of LBM further to cover unsteady supercritical flows.

The dam-break was released from a 40m long reservoir into a 200m long frictionless horizontal channel using asymmetry parameters α = 1, β = 4 and lattice speed e = $3m/s$. The upstream and tailwater depths were set to 8m and 0.5m, respectively and the water surface profile was plotted for a total 15 seconds at 0.2sec intervals. Five virtual gauges were defined along the channel at arbitrary points x=20m, 40m, 60m, 100m and 120m to track variation of the modelled water surface in each time step; these are shown by STA.1 to STA.5 in Figure 6-10.

The LBM-generated depth time series of arbitrary points on water surface at the location of the virtual gauges were compared to those from the ANUGA shallow-water model in Fig.6-11. ANUGA is a finite volume model two-dimensional shallow water equation solver, developed by the Australian National University (ANU) and Geoscience Australia (GA). It has been widely verified for a range of flow conditions (Nielsen et al. 2005), including dam-break flows (Barnes and Baldock 2010). The Froude number in this simulation reached 1.97, which is in the supercritical region. As illustrated there is excellent agreement between the LBM and ANUGA time series.

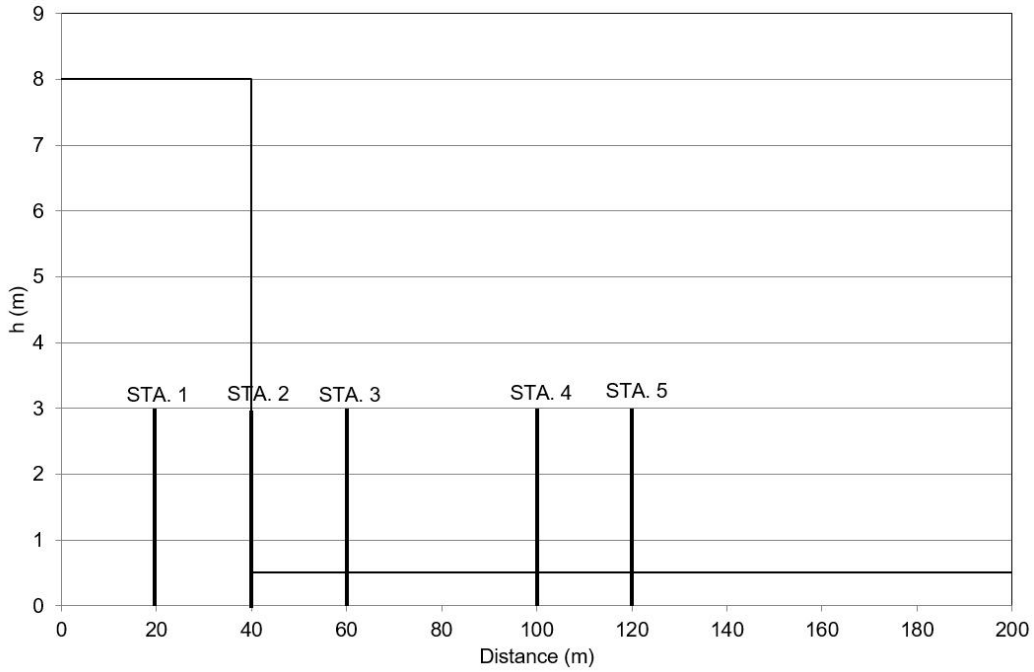

Figure 6-10 Location of the arbitrary points in the dam-break case for comparison with ANUGA.

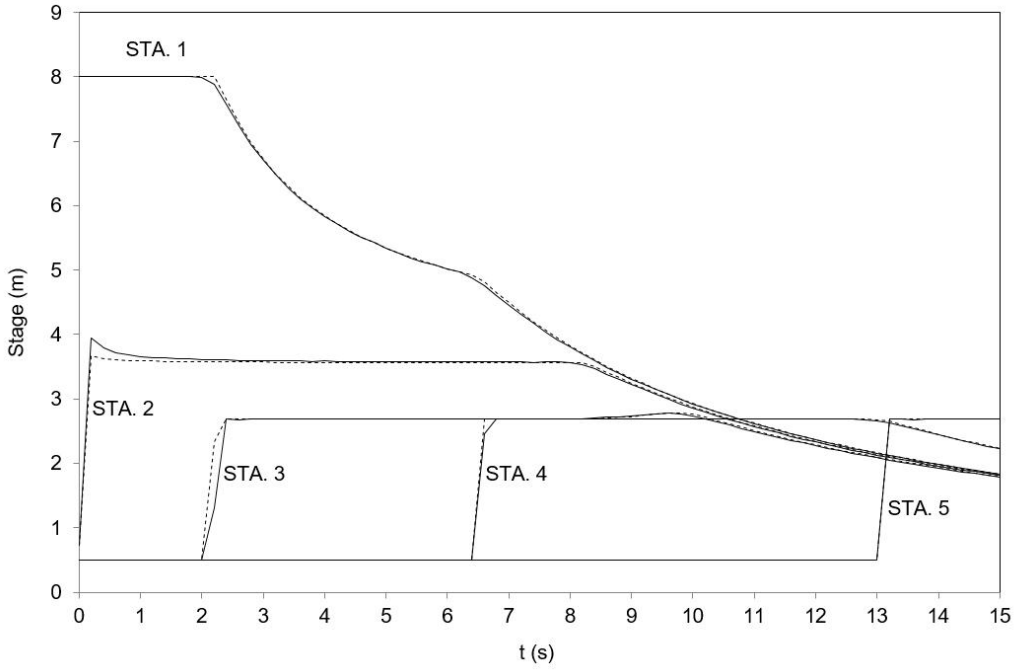

Fig.6-11. Comparison of flow depth time series at selected locations (STA.1 to STA.5) for the transformed LBM and ANUGA model for the dam-break flow case on smooth bed, case 10. Solid line, ANUGA; dotted line, LBM.

Water surface profiles generated by the transformed LBM scheme were also plotted at 1s intervals and compared with data points from ANUGA at the location of the virtual gauges. Excellent agreement was found as shown in Fig.6-12.

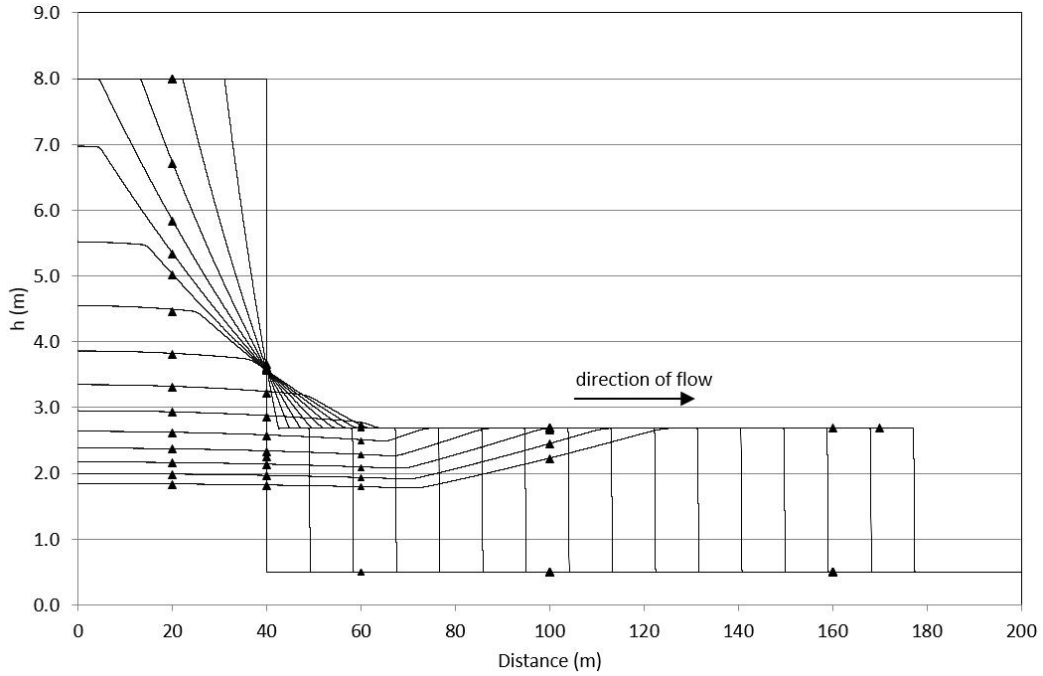

Fig.6-12. Comparison of longitudinal water surface profiles by the transformed LBM and ANUGA models at 1 second intervals for the dam-break case on smooth bed, case 10. Solid line, LBM; data points, ANUGA.

The fine dotted curves in Figure 6-13 show the values of Fr-ψ for the dam break case on smooth bed at 1s intervals. The start and end points of each curve indicate zero Froude numbers, which is resulting from the stationary water. As seen in Figure 6-13, utilising the transformed scheme with a proper set of asymmetry parameters provides a stability zone encompassing the entire solution. Otherwise, this solution would not have remained stable with the Chopard et al. (2013) scheme as both the lower bound and upper bound of the curves fall outside their proposed stability zone.

To the author's knowledge, this is the first time that the LBM can successfully be applied to a dam-break case involving supercritical flow regime. All previous dam-break studies with the LBM were limited to subcritical conditions including the paper by Liu et al. (2009).

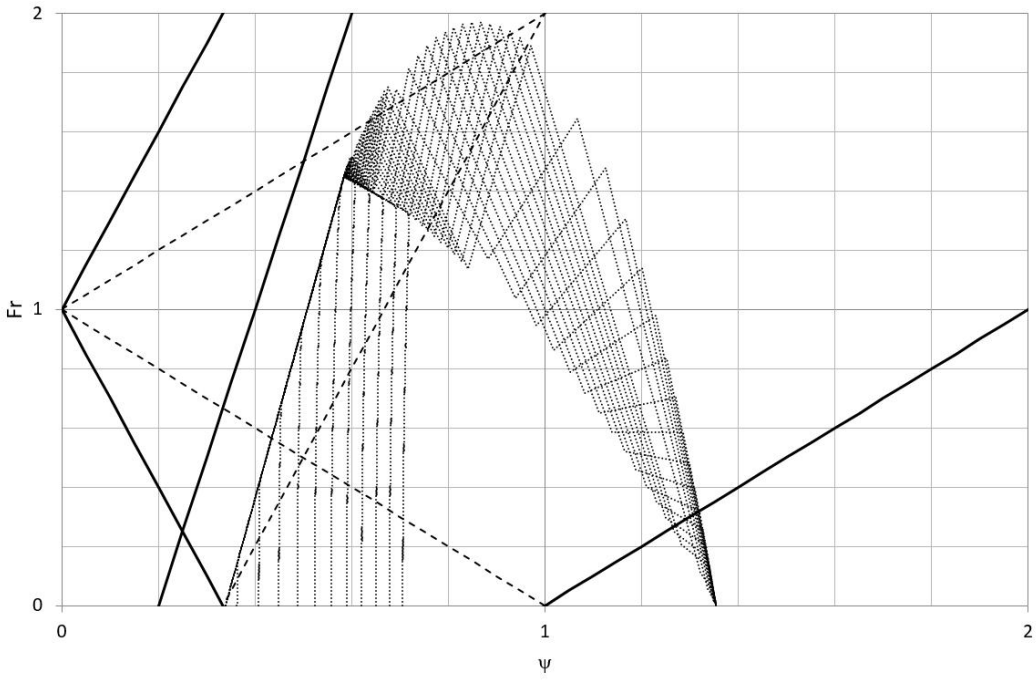

Figure 6-13. Stability zone and Fr-Ψ for the dam break case on smooth bed, case 10. Solid lines, boundaries of the present stability zone; dashed lines, boundaries of the Chopard et al. (2013) stability zone.

6.2.3. Case 11: Dam-break on a rough bed

A Manning's coefficient of n=0.015sm$^{-1/3}$ was introduced in the model to represent bed friction. The frictional resistance was modelled using Manning's formula as per Eq.(6.9) in which S_0 is the channel bed slope, n is Manning's roughness coefficient and R is the hydraulic radius. The ANUGA model also utilises Eq.(6.9) to calculate friction forces.

$$F_F = gh\left(S_0 - \frac{(nV)^2}{R^{4/3}}\right) \tag{6.9}$$

Following introduction of friction, more difference was observed between the LBM and ANUGA results as shown in Fig.6-14, although there is still reasonably good agreement between the two time series. The dotted lines in the figure show the values of Fr-ψ at different times at the location of the virtual gauges in Figure 6-10.

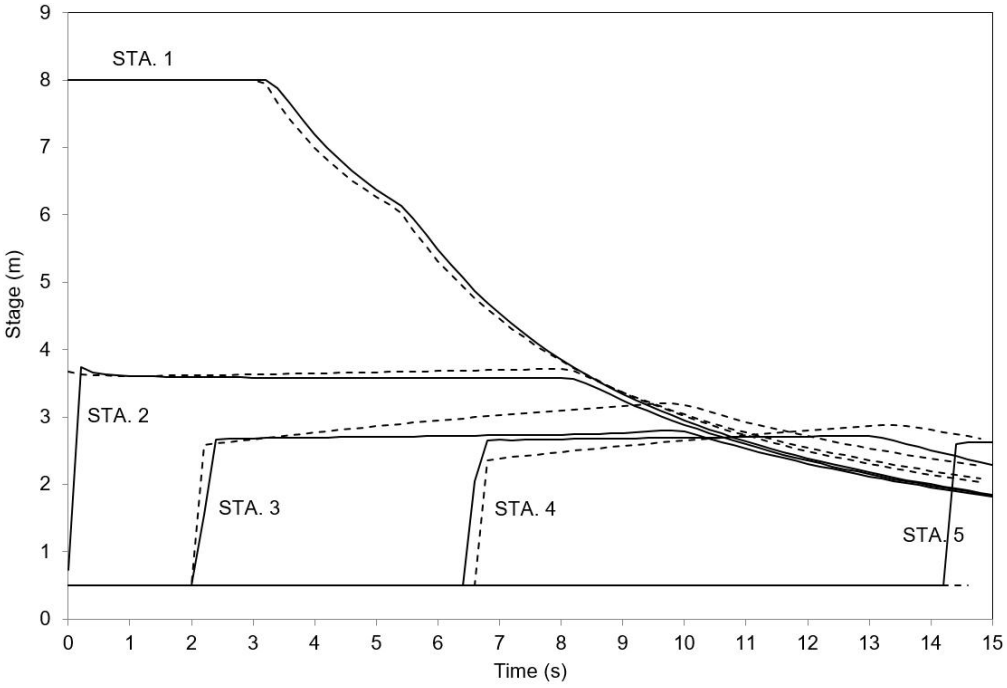

Fig.6-14. Comparison of flow depth time series at selected locations for the transformed LBM and ANUGA model for the dam-break flow case on rough bed, case 11. Solid line, ANUGA; dotted line, LBM.

6.3. Summary

A number of test cases have been presented to validate the proposed transformed LBM. The test cases were mostly selected from cases with supercritical regime to demonstrate the improved ability of the proposed scheme over standard LBM schemes and the asymmetric scheme (Chopard et al. 2013) in handling both sub- and supercritical flows. The transformed model results were compared with analytical solutions of some standard steady-state open-channel problems such as subcritical flow over a free overfall, supercritical flow downstream of a sluice gate and subsequent hydraulic jump, accelerating and decelerating supercritical flow cases in a steep channel and subcritical and supercritical flows over a weir. In all cases, very good to excellent agreement was observed between the modelled and analytical solutions. The transformed scheme was also tested for a tidal flow case and in which its results matched very closely with the analytical solutions. A dam-break case was also set up involving high differential head between the dam water level and tail water, resulting in supercritical flows. The water surface profiles generated by the transformed scheme were in excellent agreement with the predicted values from ANUGA finite volume model. It is shown that the transformed scheme extends the range of applicability of the LBM to both steady and unsteady flow.

7. Shoreline Boundary Conditions

In this chapter, the most commonly used techniques for implementation of boundary conditions at wet-dry interfaces are reviewed and a tailormade interface boundary condition is developed to be incorporated in the transformed LBM. Complementing the transformed scheme with a shoreline boundary condition will enable it to be applied to investigate swash zone problems such propagation of tidal bores, wave run-up and run-down.

It was expected that due to occurrence of very low Froude numbers near the shoreline where water is at rest state, the transformed scheme will not be a proper platform for simulating nearshore problems. However, as it will be discussed in this chapter, it was observed that the standard LBM was successfully applied to coastal problems (such as wave run-up), although Froude number at the wave of the tip instantaneously entered the supercritical regime. This made it worthwhile to test the transformed scheme for nearshore problems, hoping that the local instantaneous instabilities would vanish likewise and not prevent a solution.

7.1. Review of Moving Shoreline Treatment Techniques

Numerous studies have been undertaken on simulation of shoreline movement; i.e. the wetting-drying process associated with the moving shoreline. The first attempts made were by utilising the Priessmann Slot Method (PSM) which involved adopting a deep but narrow slot in all computational cells to ensure no cell will become completely dry. The Preissmann Slot Method was an idea originally developed by Preissmann and Cunge (1961) for the pressurised fluid conduits so they can be treated by the same set of partial differential equations governing open channel flows. In this method, the proper selection of the slot width is critical so that the waves in the resembled open channel system travel at the same speed as the acoustic surge in the original pressurised system. PSM has certain shortfalls, most importantly the inability to sustain the negative pressures in pressurised conduit systems and its numerical instabilities.

Sielecki and Wurtele (1970) proposed numerical integration of the shallow-water equation over a sloping bottom with a free lateral boundary condition so that the position of the free surface on the sloping boundary was systematically determined at each time step (Sielecki and Wurtele 1970). This method had the advantage that no additional lateral boundary condition needed to be applied to the solution.

Mahdavi and Talebbeydokhti (2009) modelled non-breaking and breaking solitary wave run-up using a finite volume model with an explicit centred scheme in conjunction with an upstream scheme of conservation laws to estimate interface fluxes along with the surface gradient. The proposed model was shown to be stable with a robust algorithm. For time integration of the equations they used an optimal third-order Runge-Kutta explicit scheme.

Titov et al. (1995) proposed a finite difference approximation of the characteristic form of the shallow water equations on a variable grid to model a one-dimensional long wave run-up. This model, however, did not provide the details of the wave at the time of breaking

Madsen et al. (1997) utilised a technique in which the solid beach was numerically replaced by a porous media with very fine porosity and then used a set of two-dimensional Boussinesque-type equations with improved dispersion characteristics to address wave run-up problems, including those with breaking waves. Their model produced a shift between the breaking point and the point where wave setup in the mean water level was initiated.

Bates and Hervouet (1999) used a fixed numerical grid for a two-dimensional finite-element framework to model partially-wet and dry grid elements. They proposed an algorithm for use in the finite element model and showed improvement of the accuracy of the results compared to other finite element models; however, they had no physical data to validate their results and the complex topography used in their simulations did not allow for analytic solution of their test cases. Hu et al. (2000) proposed a one-dimensional finite volume numerical model for simulation of wave run-up and overtopping and proposed a minimum friction depth to overcome the instabilities caused by the effect of minimum water depth. This model was shown to yield results closely agreeing with those from laboratory tests and analytic solutions. However, it was not tested for irregular waves.

One of the popular methods of wave run-up shoreline treatment is the moving boundary algorithm proposed by Lynett et al. (2002) which utilised a high-order finite difference scheme and extrapolation of water surface through the wet-dry boundary into the dry region. This model was shown to be sensitive to the definition of the bed friction but in general was in excellent agreement with analytical and experimental results from several test cases. The main advantages of this model were its easy implementation, numerical stability and independence from additional assumptions on dissipative mechanisms. They also developed an eddy viscosity model to address the breaking waves. In the extrapolation technique, the wet-dry boundary could sit between the nodal points. Later Fuhrman and

Madsen (2008) applied the same extrapolation technique to a more accurate version of the Boussinesq-type model originally developed by Madsen. In 2D test cases, their model had excellent agreement with analytical results but diverged significantly from the theoretical solution for longer times.

Another popular technique is the idea of adopting a thin-film, firstly developed by Dodd (1998) that solves the Shallow-Water Equations using an upwind finite-volume technique incorporating a Roe-type Riemann solver by taking into account bed shear stress. Despite other finite difference methods which assumed linear or quadratic elements between computational nodes, in the thin-film technique the same data are interpreted to be piecewise constant. In the thin film algorithm, each cell is assumed dry when the water depth in that cell falls below a minimum pre-defined water depth (h_{min}). This model, which was an upwind scheme, was shown to be in good agreement with results from previous experiments and studies by others and did not produce numerical oscillations at shock waves, such as bores (Dodd 1998). The Thin Film technique was later applied by Oey to the Princeton Ocean Model (Oey 2005) and more recently discussed by Sobey (2009). LeVeque and George (2008) proposed a wave-propagation algorithm in a high-resolution finite volume model to solve hyperbolic systems of conservation laws. In their work a Riemann solver was used to treat the bathymetry and dry states.

Most recently, Liu and Zhou (2014) proposed a new approach for shoreline treatment based on the theory of lattice Boltzmann dynamics and applied it to the standard LBM scheme. Due to the underlying physics used in this method, which is intrinsic to LBM fundamentals and lack of physical assumptions and approximations, it was selected for further modification for utilisation in the transformed LBM. Straight-forward integration of this boundary condition into the transformed model was another reason which made this the preferred technique for a shoreline boundary condition. This technique is explained in detail in the following paragraphs.

Liu and Zhou (2014) applied the Chapman-Enskog analysis and a Taylor expansion to set up a relationship between the last dry lattice in the domain and its adjacent wet node. These relationships were used to determine the unknown EDFs and therefore could easily be supplemented to any LBM in order to address wetting-drying boundary condition. In this method, the physical variables of a dry cell (water depth and velocity) are directly determined so when the dry cell becomes wet and the Equation (7.1) does not return a zero value.

$$h(x,t) = \sum_{i=0}^{8} h_i(x,t) \tag{7.1}$$

A second-order Taylor expansion of the streaming equation around $\Delta t=\varepsilon$ was done following a Chapman-Enskog expansion and neglecting the higher orders of ε. This yielded an equation to determine the backward EDF (f_2) of the first dry cell (d_1 in Figure 7-1) in time step $t+\Delta t$ for a case where the forward EDF (f_1) of the adjacent wet lattice (w_2 in Figure 7-1) is positive, i.e. the fluid where at the wet lattice has sufficient momentum to reach the neighbouring dry lattice. If the forward EDF (f_1) of the adjacent wet lattice (w_2) is negative, the backward EDF (f_2) of the dry cell (d_1) will be determined using the standard bounce-back scheme. The rest-state particle distribution function of the dry cell is determined by averaging the rest-state particle distribution functions of its neighbouring lattices:

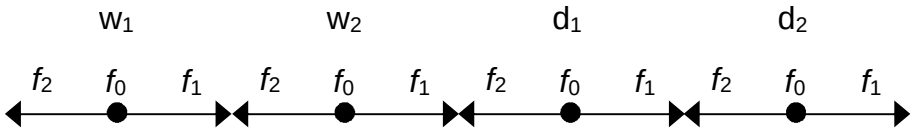

Figure 7-1 Indicative wet and dry lattices at the shore by Liu and Zhou (2014).

and of course the value of $f_1^t(d_1)$ is determined as usual from the internal lattices through the collision-streaming process.

By using the above EDFs at lattice d_1, the water depth at that cell can be calculated. If the calculated water depth $h \leq 0$ it means cell d_1 will be remain otherwise if $h > 0$ cell d_1 will be regarded as a wet cell.

if $f_1^t(d_1) > 0$

$$f_2^t(d_1) = \frac{-gh\tau}{2e^2}\left(z_b(x+e_2\Delta t) - z_b(x)\right) - \frac{\Delta t\tau}{2e^2}e_2 C_b u|u| - \tau\left(f_2^0(x+e_2\Delta t) - f_2^0(x)\right) \tag{7.2}$$

if $f_1^t(d_1) < 0$

$$f_2^t(d_1) = f_1^t(d_1) \tag{7.3}$$

$$f_0^t(d_1) = \frac{f_0^t(w_2) + f_0^t(d_2)}{2} \tag{7.4}$$

For the run-down it can be similarly determined whether cell w_2 will be dry or wet at each time step.

It is worth noting at the shoreline treatment technique proposed by Liu and Zhou (2014) was developed for the standard LBM and as such its application was limited to subcritical regimes. Future work may be required to consider shock-capturing techniques, in which case some of the simplicity proposed in this algorithm may be improved.

7.2. Shoreline Boundary Condition for the Transformed Scheme

The methodology adopted by Liu and Zhou was followed to derive the unknown Equilibrium Distribution Functions (EDFs) at the wet/dry interface for the transformed LBM.
From Equation (4.14):

$$f_\alpha(\mathbf{x} + \mathbf{e}_i\Delta t, t + \Delta t) - f_\alpha(\mathbf{x}, t) = -\frac{1}{\tau}\left[f_\alpha(\mathbf{x}, t) - f_\alpha^{eq}(\mathbf{x}, t)\right] + \frac{w_i e_{\alpha i}\Delta t F_i(x, t)}{C_S^2} \tag{7.5}$$

Performing a Taylor expansion and substituting $\Delta t = \varepsilon$:

$$\varepsilon\left(\frac{\partial}{\partial t} + e_i\frac{\partial}{\partial x}\right)f_\alpha + \frac{\varepsilon^2}{2}\left(\frac{\partial}{\partial t} + e_i\frac{\partial}{\partial x}\right)^2 f_\alpha + O(\varepsilon^3) = \frac{1}{\tau}\left(f_\alpha^{eq} - f_\alpha\right) + \frac{w_i e_{\alpha i}\Delta t F_i(x, t)}{C_S^2} \tag{7.6}$$

Similarly, f_α can be expanded in the following form:

$$f_\alpha = f_\alpha^{eq} + \varepsilon f_\alpha^{(1)} + O(\varepsilon^2) \sim f_\alpha = f_\alpha^{eq} + \varepsilon f_\alpha^{(1)} \tag{7.7}$$

Substituting f_α from Eq. (7.7) in Eq. (7.6) yields:

$$\begin{aligned}\varepsilon\left(\frac{\partial}{\partial t} + e_i\frac{\partial}{\partial x}\right)\left(f_\alpha^{eq} + \varepsilon f_\alpha^{(1)}\right) + \frac{\varepsilon^2}{2}\left(\frac{\partial}{\partial t} + e_i\frac{\partial}{\partial x}\right)^2\left(f_\alpha^{eq} + \varepsilon f_\alpha^{(1)}\right) + O(\varepsilon^3) \\ = -\frac{\varepsilon}{\tau}f_\alpha^{(1)} + \frac{w_i e_{\alpha i}\Delta t F_i(x, t)}{C_S^2}\end{aligned} \tag{7.8}$$

which after replacing $\Delta t = \varepsilon$ can be written as:

$$\left(\frac{\partial}{\partial t} + e_i\frac{\partial}{\partial x}\right)f_\alpha^{eq} = -\frac{1}{\tau}f_\alpha^{(1)} + \frac{w_i e_{\alpha i}F_i(x, t)}{C_S^2} \tag{7.9}$$

For a dry bed $f_\alpha^{eq} = 0$. Using the backward scheme:

$$\frac{\partial f_\alpha^{eq}}{\partial t} = \frac{f_\alpha^{eq}(t) - f_\alpha^{eq}(t-1)}{\Delta t} = 0 \tag{7.10}$$

Substituting Eq. (7.9) in Eq.(7.10) gives:

$$f_\alpha^{(1)} = \tau\left(\frac{w_i e_{\alpha i} F_i(x,t)}{C_S^2} - e_\alpha \frac{\partial f_\alpha^{eq}}{\partial x}\right) \tag{7.11}$$

which can be substituted in Eq.(7.7):

$$f_\alpha = f_\alpha^{eq} + \varepsilon\tau\left(\frac{w_i e_{\alpha i} F_i(x,t)}{C_S^2} - e_\alpha \frac{\partial f_\alpha^{eq}}{\partial x}\right) \tag{7.12}$$

because

$$\frac{\partial f_\alpha^{eq}}{\partial x} = \frac{f_\alpha^{eq}(x + e_\alpha \Delta t) - f_\alpha^{eq}(x)}{\Delta x} = 0 \tag{7.13}$$

we can conclude:

$$f_i = f_i^{eq} + \tau\left[\frac{\Delta t w_i e_{\alpha i} F_i(x,t)}{C_S^2} + f_i^{eq}(x) - f_i^{eq}(x + \Delta x)\right] \tag{7.14}$$

Equation (7.14) for $i = 2$ may be used to determine the unknown f_2 at the wet/dry interface in the transformed scheme. It can easily be shown that by substituting the external force terms resulting from varying bed elevation and friction for a standard LBM scheme Eq. (7.14) will return Eq.(7.2). An algorithm was added to the model to determine the location and depths of water at the shoreline.

The general set up of this algorithm was similar to Equations (7.2) to (7.4). However, due to the fundamental difference in configuration of the transformed scheme, those equations were adjusted to cater for the asymmetry associated with the transformed scheme.

In a standard LBM scheme, the value and sign of EDFs may directly be interpreted as the depth and directions of flow but in a transformed scheme this is not the case. In a transformed scheme, the EDFs can take different numerical values depending on physics of the problem and the asymmetry parameters.

To explain these differences better, we consider a simple stationary water case on a flat bed at depth *h*. In a standard LBM with any arbitrary lattice speed *C* we have:

$f_1 = 0, e_1 = C$

$f_2 = 0, e_2 = -C$

$f_3 = h, e_3 = 0$

which would yield still-state water depths and velocities as:

$$h = \sum f_i = 0 + 0 + h = h$$

$$u = \frac{1}{h}\sum e_i f_i = \frac{1}{h}(0 + 0 + 0) = 0$$

which perfectly represent the physical state of the problem.

However, if the transformed scheme is used to model the same case, the EDFs take totally different values which cannot be directly used to interpret the physical state of the system. For example, if the still water depth is 0.455m and we use α =1, β =4 with lattice speed 2*m/s*, the initial EDF and directional lattice velocities we be as follows:

$f_1 = -0.0347m, e_1 = (\alpha + \beta)C = 10m/s$

$f_2 = 0.0790m, e_2 = (\alpha - \beta)C = -6m/s$

$f_3 = 0.4107m, e_3 = \alpha C = 2m/s$

and the calculated depth and velocity:

$$h = \sum f_i = -0.0347 + 0.0790 + 0.4107 = 0.455m$$

$$u = \frac{1}{h}\sum e_i f_i = \frac{1}{0.455}[(-0.0347)(10) + (0.0790)(-6) + (0.4107)(2)] = 0.00088m/s$$

which is still sufficiently close to the initial depth and zero velocity values for practical applications, although the sign and magnitude of each EDF alone cannot be used to determine the physical depth and velocity.

Moreover, the sign of EDFs in the standard LBM has a specific physical meaning, which is the direction of flow. The conditional statements in Equations (7.2) to (7.4) are based on the fact that in the standard LBM the positive value of f_1 indicates flow in the forward direction. However, as shown in the above example, this is again not the case in the transformed scheme and a stationary water case may be represented by either negative or positive f_1 and f_2 values, depending on the problem set up.

In the view of the above fact, Equations (7.2) to (7.4) were replaced in the transformed scheme by conditions based on the magnitude of flow velocity compared to lattice speed as shown in Equation (7.15) to (7.17).

if $u[x-(\alpha+\beta)] \geq C$ (7.15)

$f_2^t(d_1)$ calculated from Eq.(7.14)

if $u[x-(\alpha+\beta)] < C$ (7.16)

$f_2^t(d_1) = f_1^t(d_1)$ (bounce-back)

$$f_0^t(d_1) = \frac{f_0^t(w_2) + f_0^t(d_2)}{2} \quad (7.17)$$

7.3. Limitations at very shallow depths

It was clearly known that the transformed scheme, in its current form, aims at simulating high-speed flows with large Froude numbers and may not be the ideal platform for flows with very low Froude number, such as stationary water in which Froude number is zero. Such low-Froude flows can easily be accommodated by the standard LBM schemes and would not need introduction of a transformation in the scheme geometry.

Although this limitation was known in advance, it was observed that the standard LBM can successfully be applied to a wave run-up case, although Froude number at the wave of the tip instantaneously entered the supercritical regime zone. This is shown in Figure 7-2 for a solitary wave run-up case in a 20m channel with the initial shoreline location at 16.7m. The dashed lines in Figure 7-2 represent the variation of Froude number for the wave run-up component using the standard (symmetric) LBM scheme. It is evident from the figure that the standard LBM can instantly handle supercritical flows at the wave tip and lattices immediately before that.

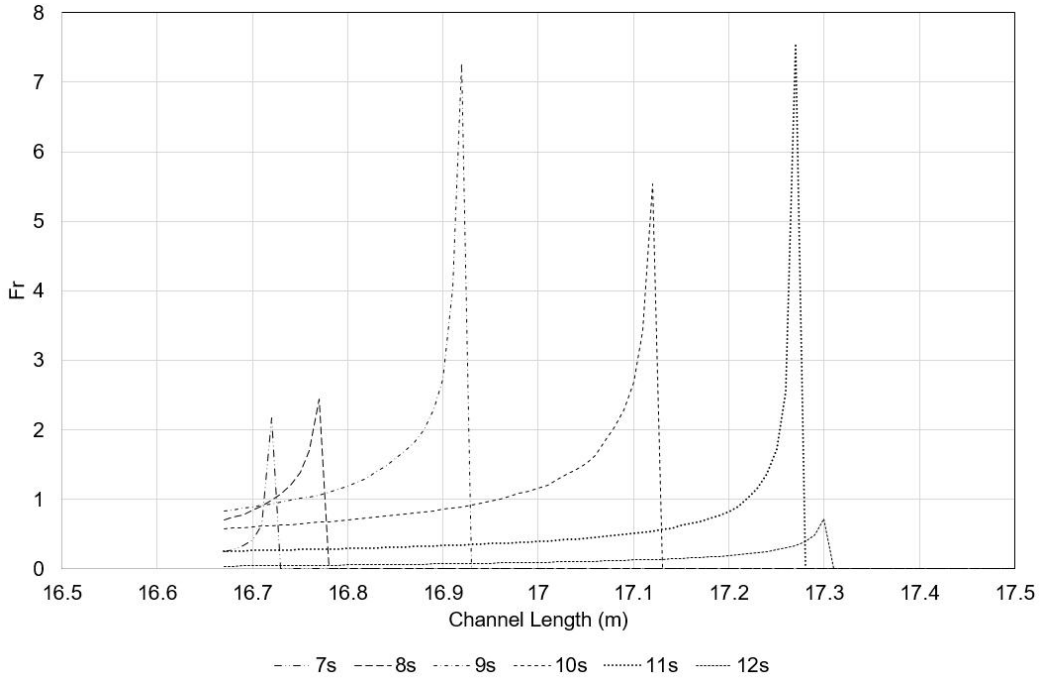

Figure 7-2 Variation of Froude number in the wave run up case using the standard LBM scheme at 1 second intervals between 7s and 12s.

This temporary and unexpected ability of standard LBM to accommodate supercritical flows is due to the unsteady nature of flow in those simulations which does not allow sufficient time for the instability to develop and propagate in the domain. This ability, however, made it worthwhile to test the transformed scheme for nearshore problems, hoping that a similar condition occurs, negating the local instantaneous instabilities. It should be noted that the nature of wave run-up problems requires both low and high Froude numbers.

The limitation of the transformed scheme is modelling very shallow flows is shown below in an example of stationary water on a sloped bed: Figure 7-3a shows a case with the shallow end depth of 1.0m modelled in the transformed scheme using lattice speed *e*=2m/s and asymmetry parameters α = 1 and β = 4. As the water surface plot and the stability data in Figure 7-3b suggest, with the selected lattice speed and asymmetry parameters the solution remains within the stable area of the transformed scheme, yielding a flat-water surface. It is highlighted that this solution resides outside the stability zone of the asymmetric scheme by Chopard et al. (2013).

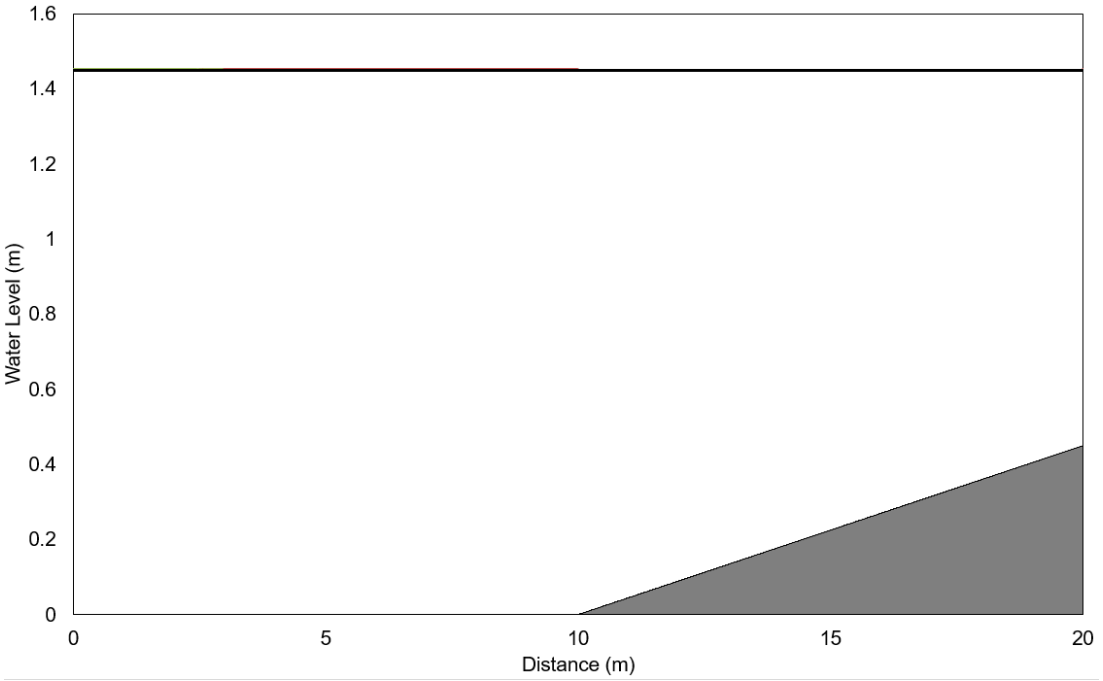

Figure 7-3a. Stationary water in a tank with end depth 1.0m.

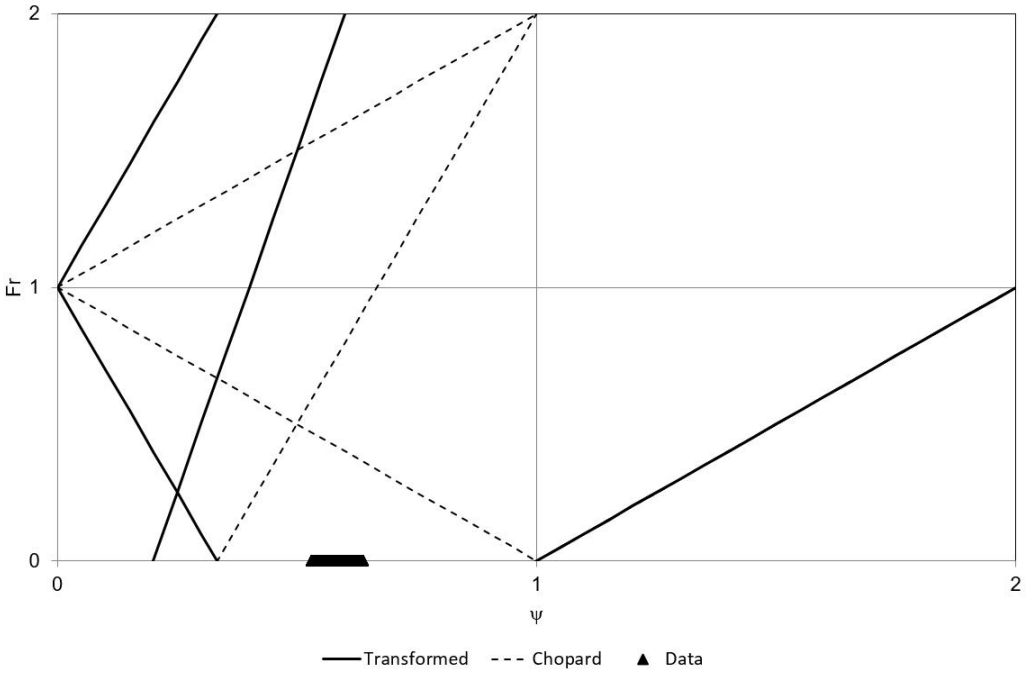

Figure 7-3b. Stability data for the stationary water in a tank with end depth 1.0m.

If the end depth in the above case is reduced to 0.001m (Figure 7-4a), even with using a smaller lattice speed *e*=1m/s the transformed scheme will become unstable at the shallow end just after 2 seconds, because the Fr and ψ values fall outside the stability zone (Figure 7-4b).

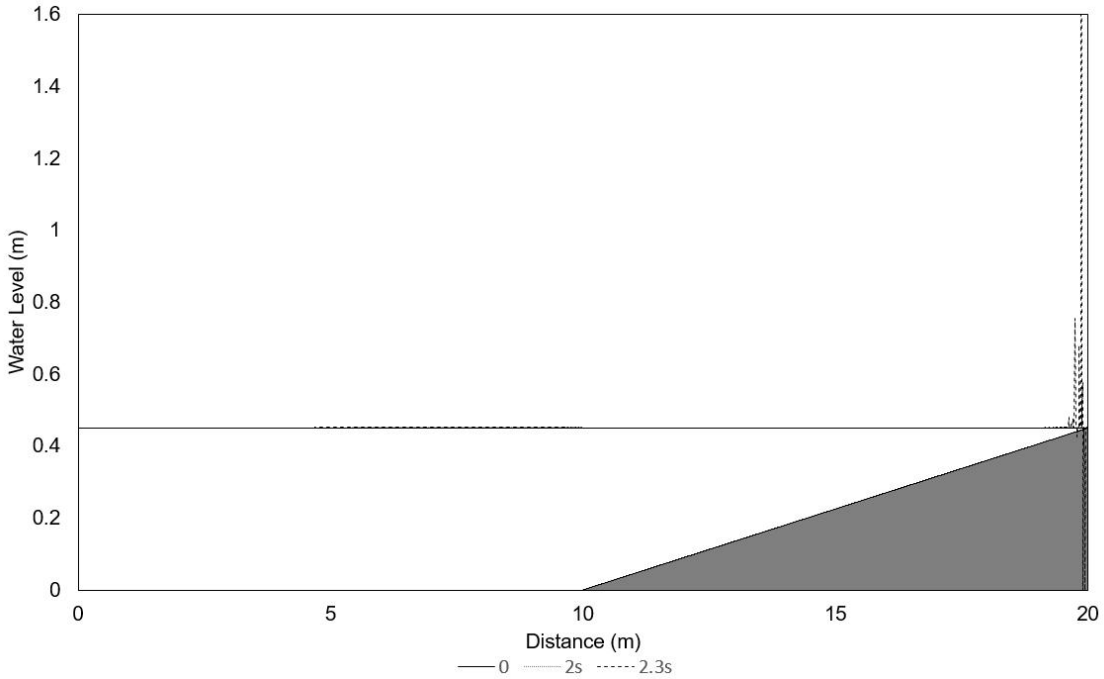

Figure 7-4a. Stationary water in a tank with end depth 0.001m-water level plotted at 1s intervals.

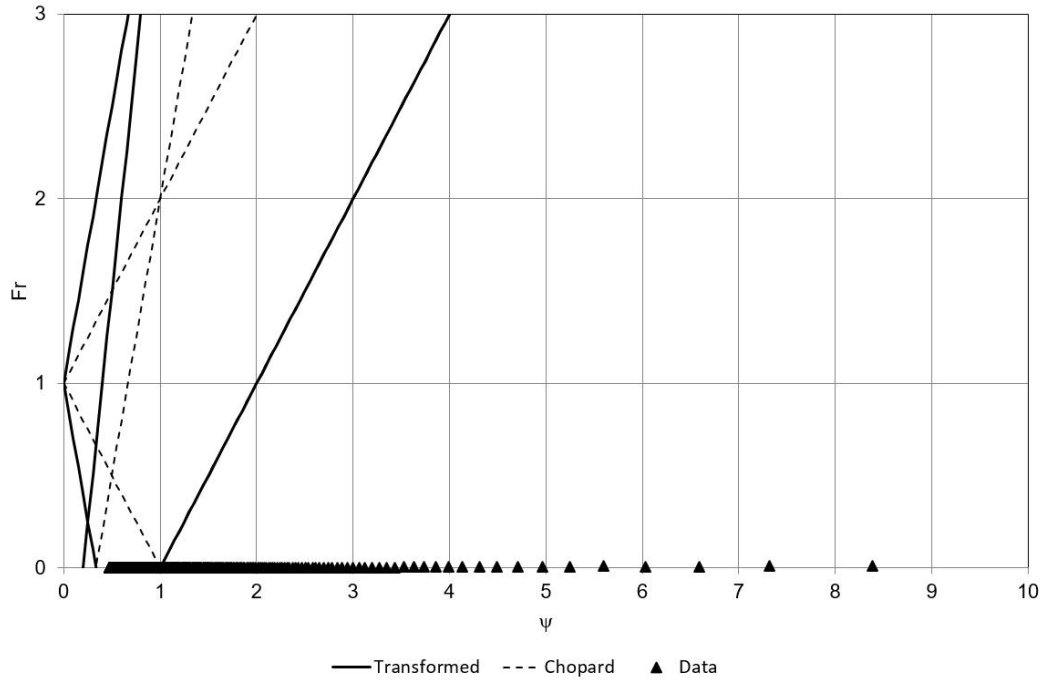

Figure 7-4b. Stationary water in a tank with end depth 0.45m-stability data.

Due to this limitation, the transformed scheme cannot practically be used to model cases involving a stationary shoreline because depths in the vicinity of the wet/dry interface generate very high lattice Froude numbers (ψ) which cannot be encompassed by the stability envelope.

In test case 1, the transformed scheme was used to model dam break on dry, smooth bed ending to a slope (an earlier dam break test case with tail water was carried out which gave valid results as presented in Fig.6-11).

The headwater depth in this case was set to 0.5m and the channel consisted of a 20m flat section ending to a 1(V):10(H) slope. The asymmetry parameters α = 1 and β = 5 with a lattice speed *e*=1m/s and τ = 1.5 were used.

The water surface profiles were plotted at 1s intervals as demonstrated in Figure 7-5. While the shoreline boundary condition successfully allows for progression of the wet domain into the dry zone, the selected lattice speed is not sufficiently high to allow the shoreline to move at the desired speed, limiting the shoreline speed to a constant speed equal to lattice speed (1m/s). This limiting effect forms a vertical wave front at the wet/dry interface as seen in the figure. The analytical solution for a dam-break case on frictionless bed yields a water surface asymptotic to bed at the front of the wave and obviously, the water surface profiles in Figure 7-5 are not correct. The modelled water surface, although incorrect, does not make the model unstable, although in the subcritical zone it often falls significantly outside the stability envelope, which is interesting (Figure 7-6).

The obvious solution to eliminate this problem would be using a higher lattice speed to allow the wave front move at its desired speed; however, a higher lattice speed increases the lattice Froude number (ψ) at the wet/dry interface, pushing the solution even more outside the stability zone and eventually making it unstable.

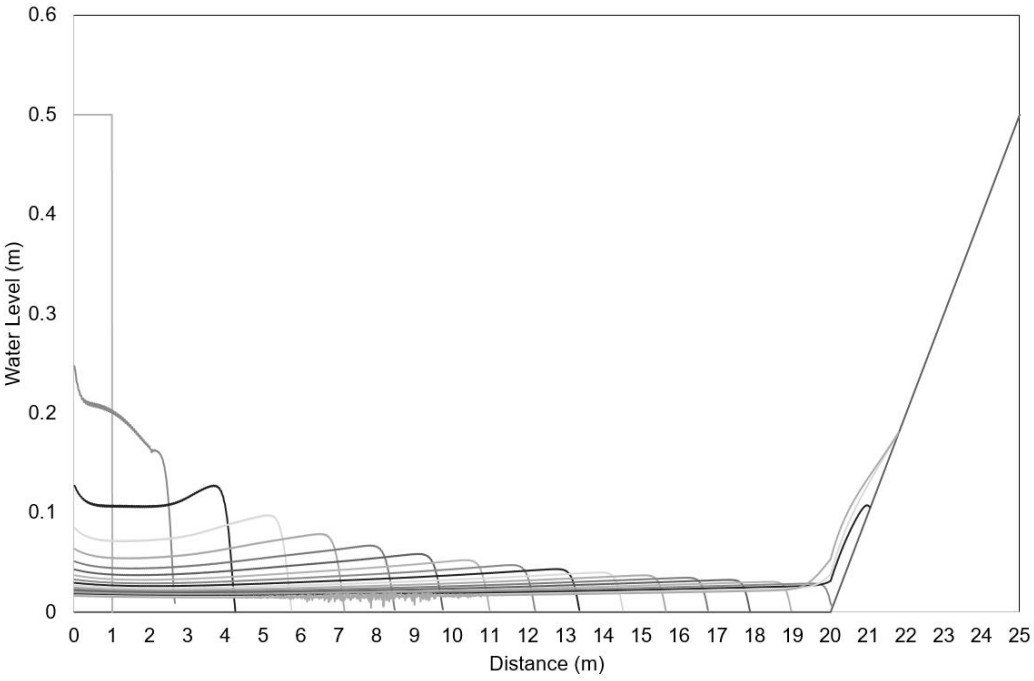

Figure 7-5. Dam break test case on dry bed, transformed scheme, water surface profile plotted at 1s intervals.

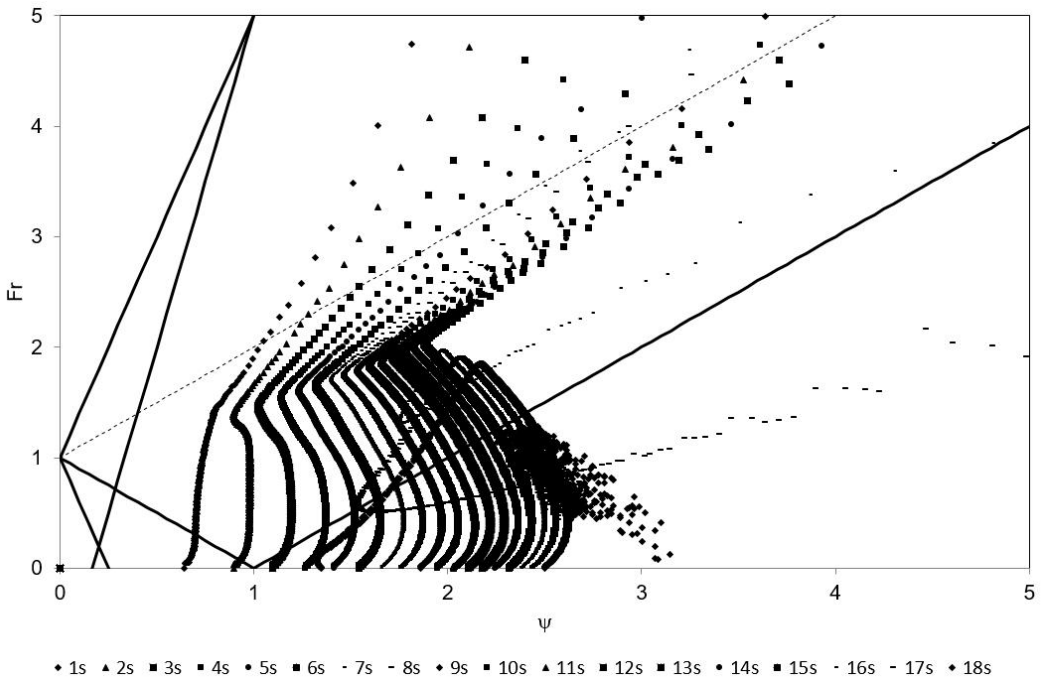

Figure 7-6 values of Fr-Ψ for the dam break case on dry bed, transformed scheme with *e*=1m/s, plotted at 1s intervals.

Another test case involving a solitary wave run up was set up to study the performance of the transformed scheme with the shoreline boundary condition. It should be made clear that the model is not able to model the run-down (back-wash) component of the flow.

In the solitary wave run up case, a solitary hyperbolic wave with amplitude η was set to propagate into a smooth channel with a constant adverse bed slope 1(V):15(H). Equation (7.18) with maximum water depth 1m at the deep end and *A*=0.35 and *B*=1 was used to set the initial wave conditions.

$$\eta = A.Sech^2(Bx) \tag{7.18}$$

The asymmetry parameters $\alpha = 1$ and $\beta = 4$ with a lattice speed $e = 1m/s$ and $\tau = 1.5$ were used to model this case.

The water surface profiles produced by the model are plotted at 0.5s intervals in Figure 7-7a and the run up profiles shown with greater detail in Figure 7-7b. Again, the movement of shoreline again occurs incorrectly at a constant speed equal to the set lattice speed (1m/s), which leaded to trimmed water surface profiles at the shoreline, similar to the vertical walls observed earlier. For the same reason mentioned earlier, using a larger lattice speed was not feasible as it made the solution unstable at the shallow end, prior to the wave arriving to the shore.

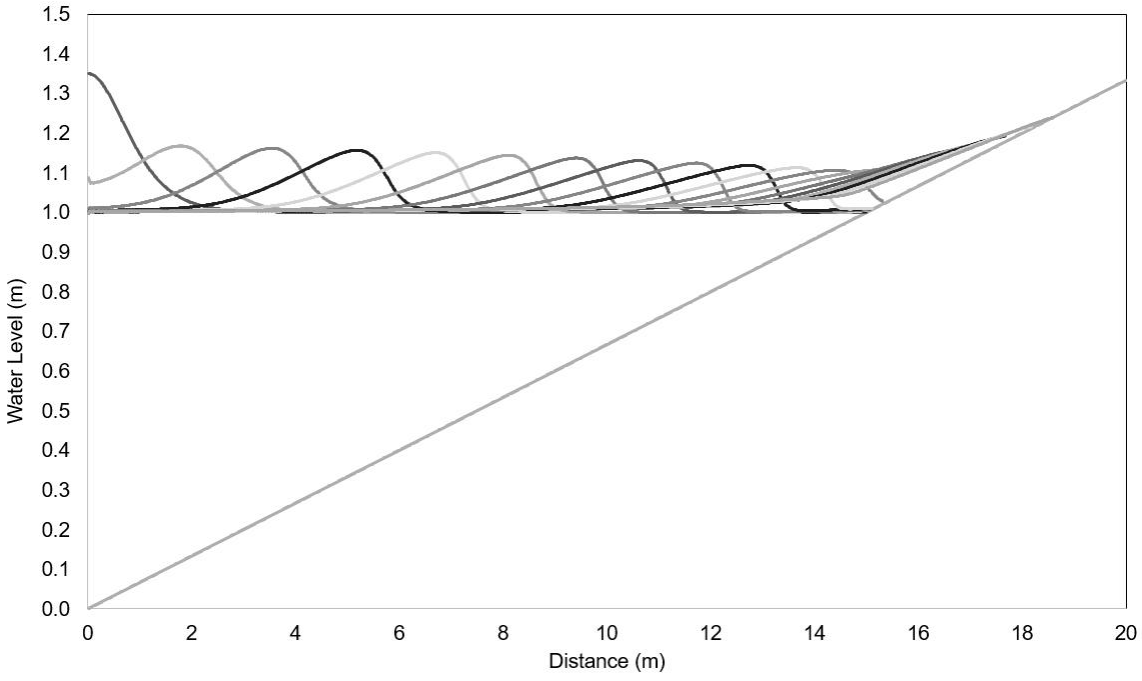

Figure 7-7a. Solitary wave run up test case- transformed scheme; water surface plotted at 0.5s intervals.

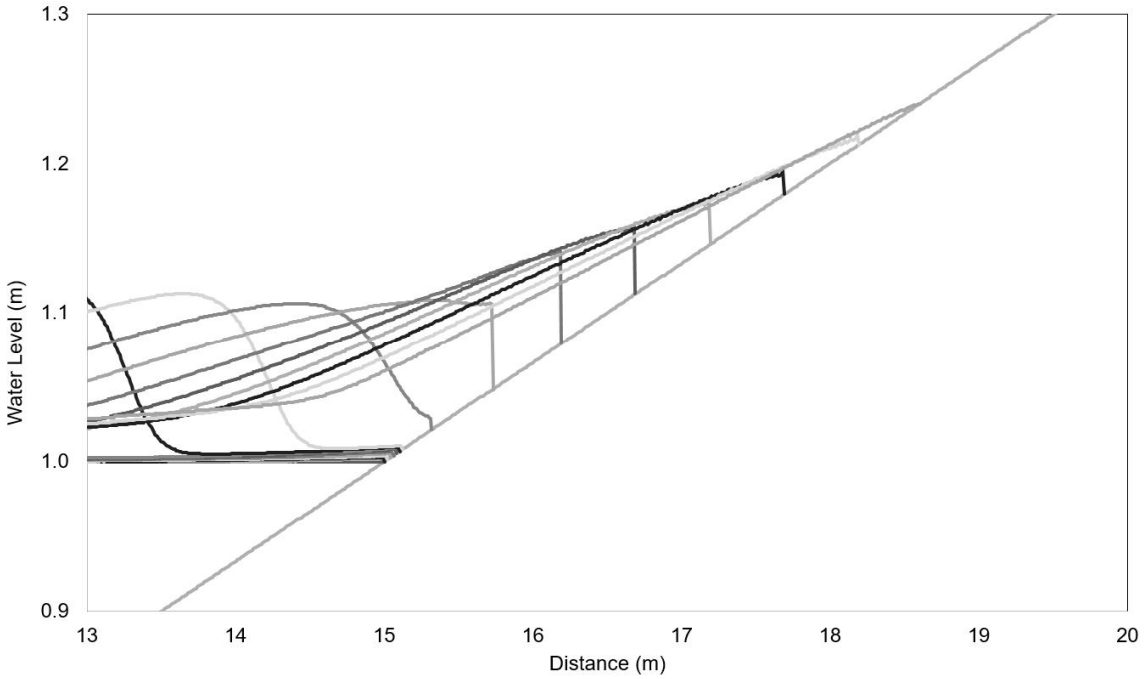

Figure 7-7b. Solitary wave run up test case- wave run up profiles- transformed scheme; water surface plotted at 0.5s intervals.

7.4. Low-amplitude wave run up

Since using high lattice speeds encourage instabilities at shallow depths, a low-amplitude solitary wave run up case was set up to investigate the transformed model capability in simulating flow velocities less than lattice speed.

A 10m long smooth horizontal channel ending to a 4.5% slope was modelled and water depth at the deep end was set to 0.3m with a solitary wave with y A=0.35 and B=1 in Eq. (7.18) at the upstream end. Both standard (symmetric) LBM (using α = 0 and β = 1 in the transformed scheme) and transformed (asymmetric) schemes were used to model this case and the run up profiles were compared. In the transformed scheme α = 1 and β = 4 with a lattice speed e=1m/s and τ = 1.5 were used. Figure 7-8a shows water surface profiles for the standard LBM scheme at 0.4s intervals and the run up profiles are shown with greater detail in Figure 7-8b. Figure 7-9a and Figure 7-9b show water surface profiles modelled using the transformed scheme.

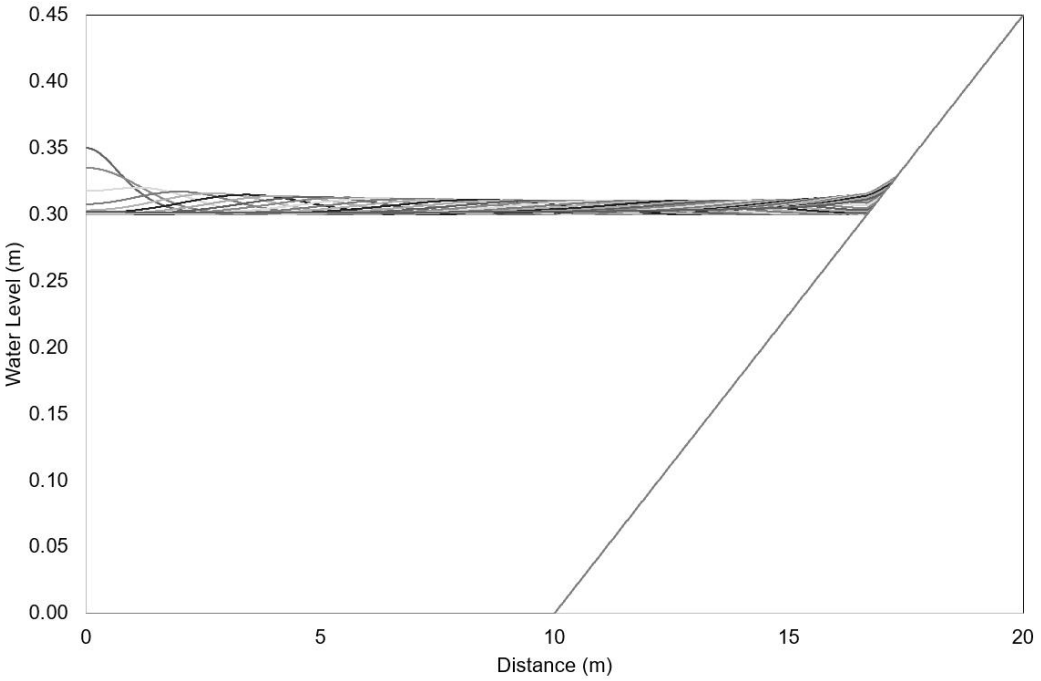

Figure 7-8a. Low-amplitude wave run up- standard LBM scheme, water surface profile plotted at 0.4s intervals.

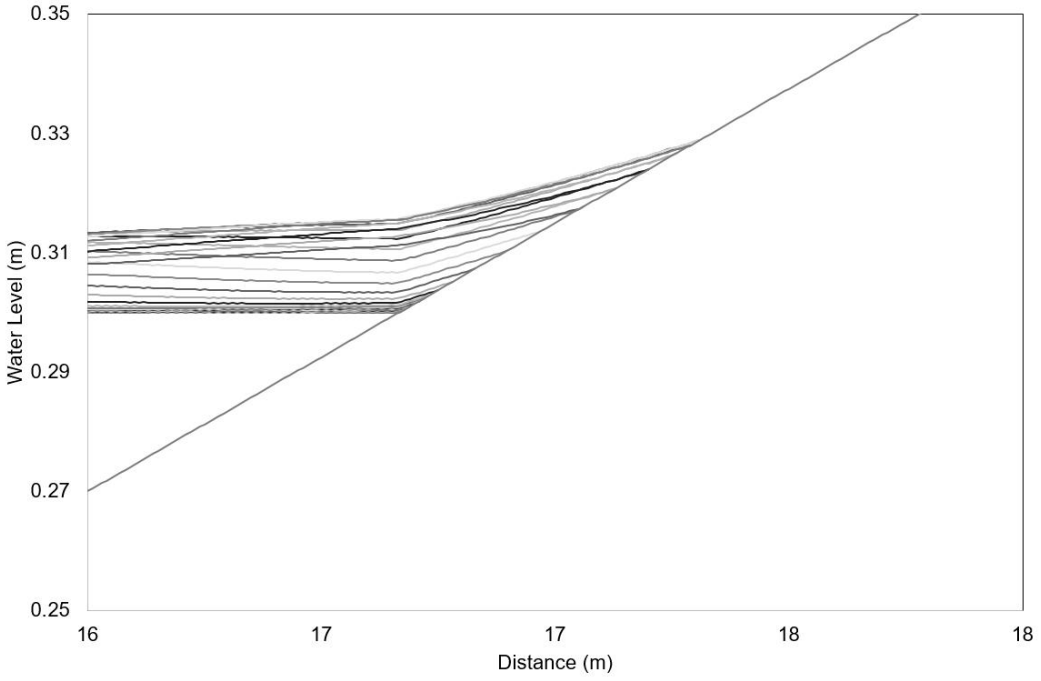

Figure 7-8b. Low-amplitude wave run-up- standard LBM scheme- run-up profiles.

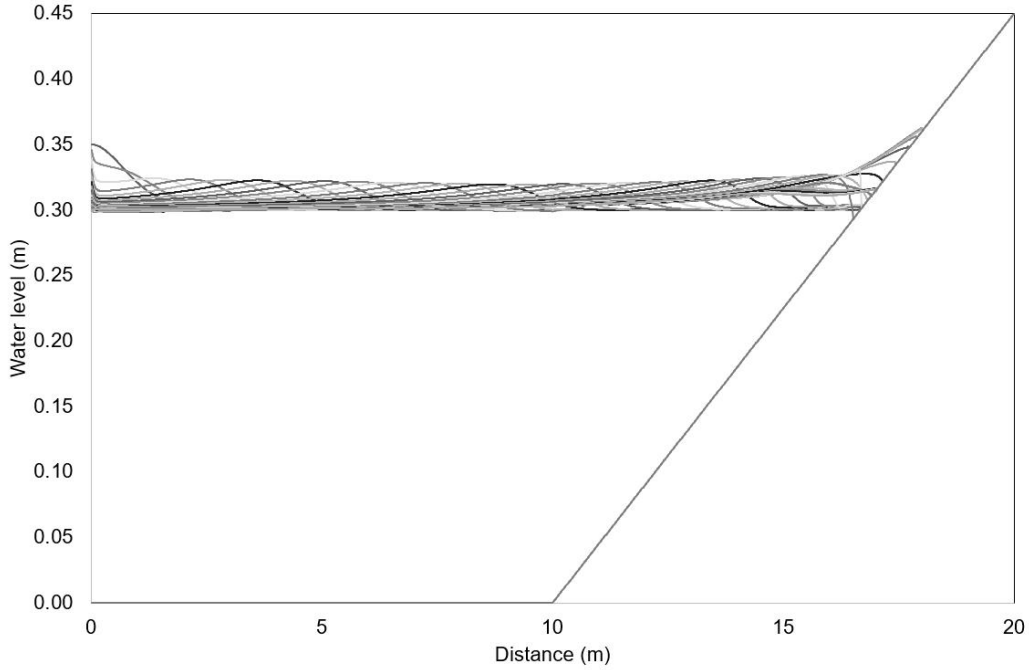

Figure 7-9a. Low-amplitude wave run-up- transformed LBM scheme.

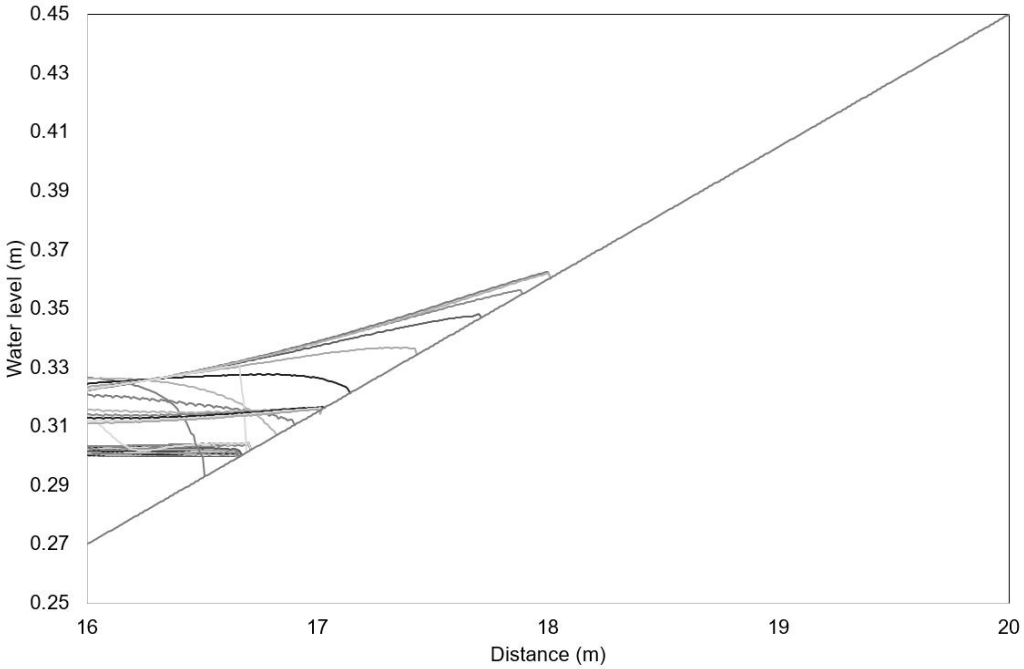

Figure 7-9b. Low-amplitude wave run up- transformed LBM scheme- run-up profiles.

The locations of shoreline versus time in both schemes are presented in Figure 7-10 and Figure 7-11 in 0.2s intervals. A slight amount of early run up was observed in both schemes and the transformed scheme showed instabilities at the lattices close to the shore. The standard scheme successfully ran both run-up and run-down of the wave, although it produced a kink at the initial location of the shoreline. However, the transformed scheme became unstable in the run-down component. As seen from Figure 7-10, the standard

scheme represents the decelerating flow in run up component better than the transformed scheme, which still appears to be limited by the lattice speed and moves at about the same constant rate of lattice speed, as the data points on the rising arm of the curve in Figure 7-11 suggest. It is worthy to note that the maximum run-up predicted by the two schemes are also significantly different.

There have been numerous research on analytical, numerical and experimental study of wave run-up on plane beaches, including Hibberd and Peregrine (1979) and Synolakis (1987). It is evident that the run-up profiles produced by the transformed scheme as shown in greater detail in Figure 7-12 to Figure 7-15 do not match any of those.

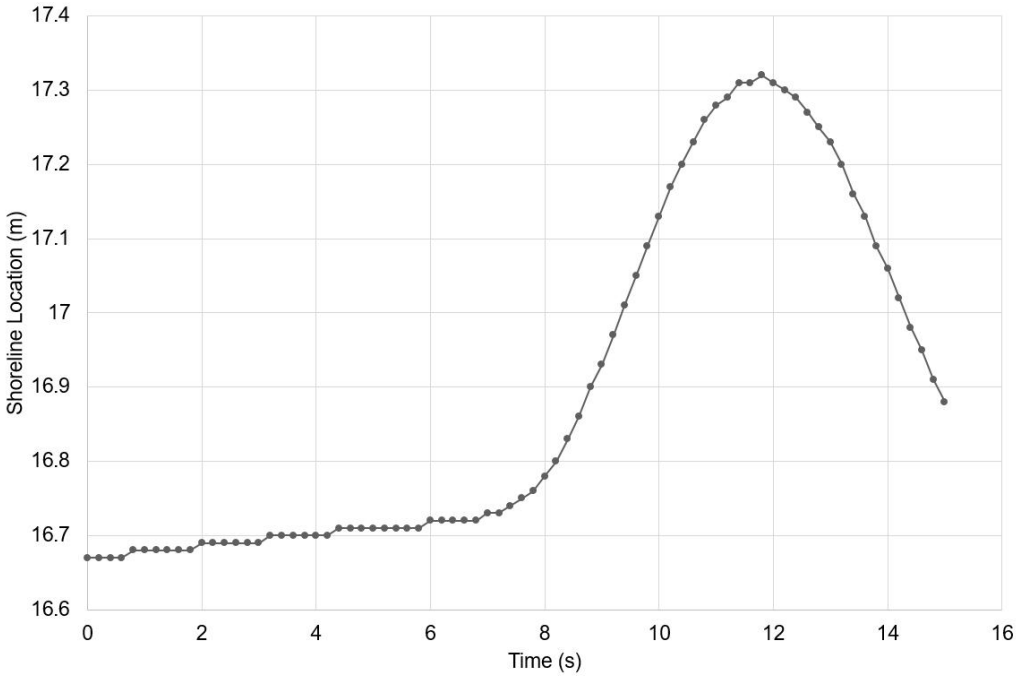

Figure 7-10 Shoreline location in low amplitude wave run-up case – standard LBM.

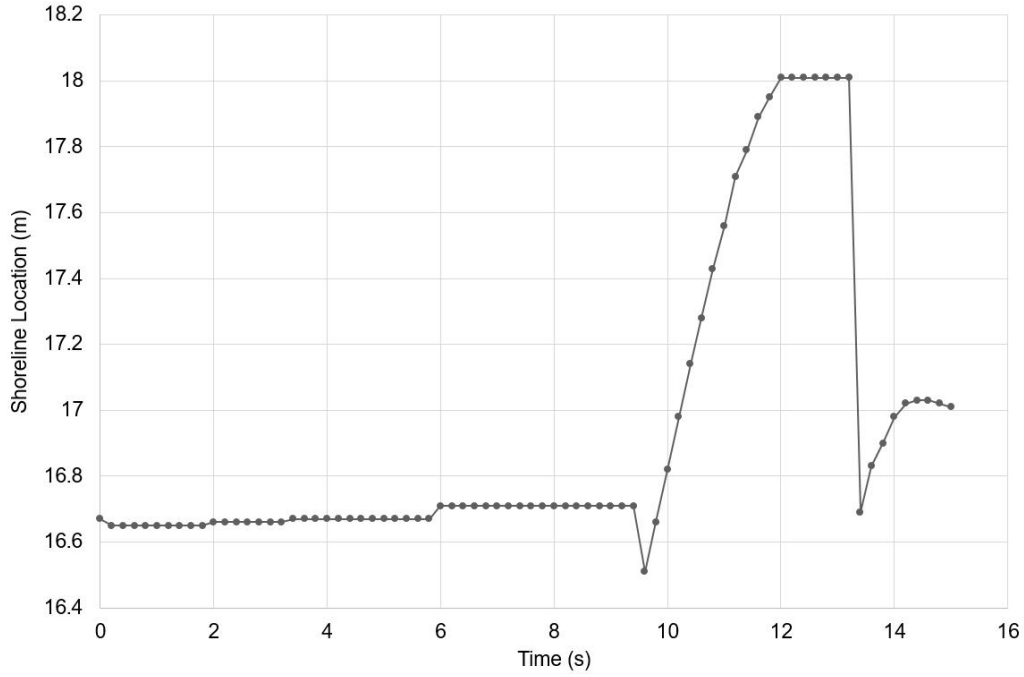

Figure 7-11 Shoreline location in low amplitude wave run-up case – asymmetric LBM.

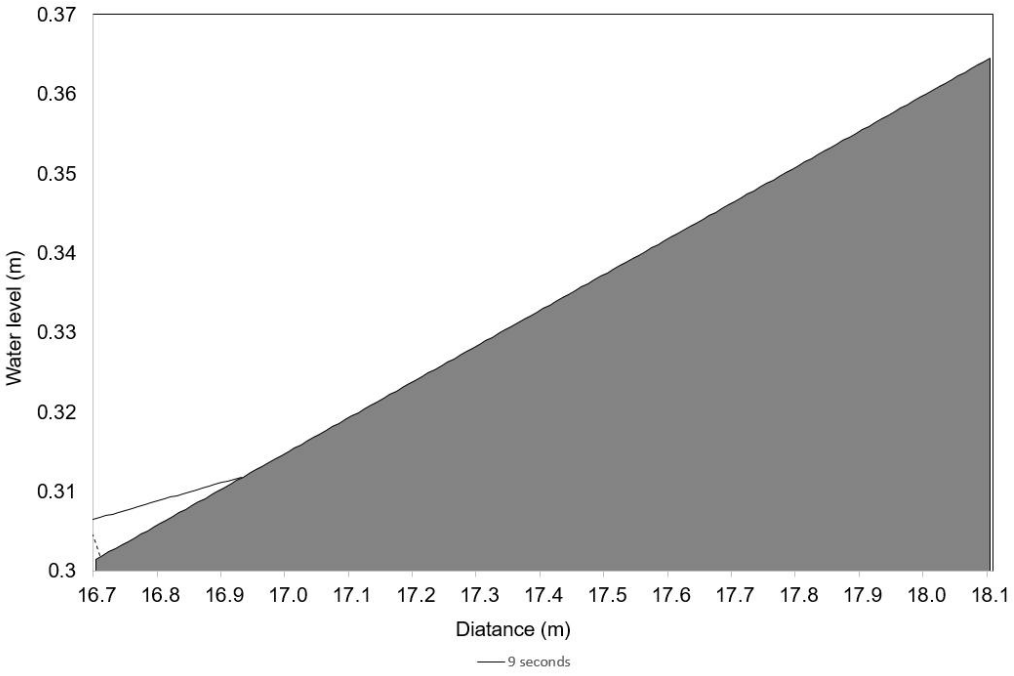

Figure 7-12 Water surface profiles-standard vs. transformed scheme for the low-amplitude wave run-up case at 9s. standard LBM (solid line); asymmetric LBM (dashed line).

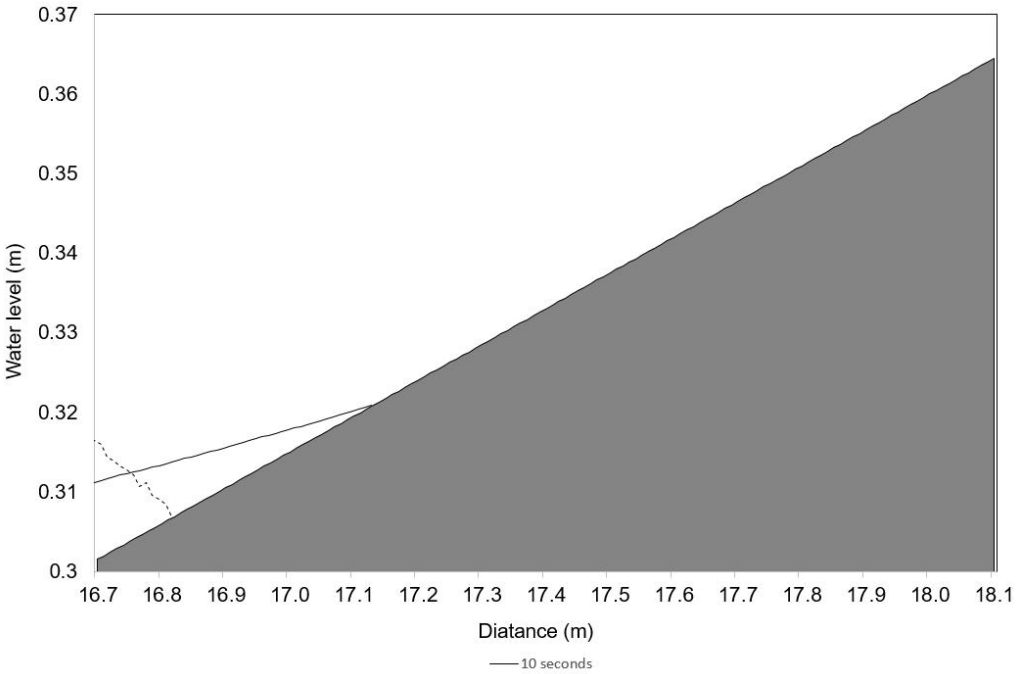

Figure 7-13 Water surface profiles-standard vs. transformed scheme for the low-amplitude wave run-up case at 10s. standard LBM (solid line); asymmetric LBM (dashed line).

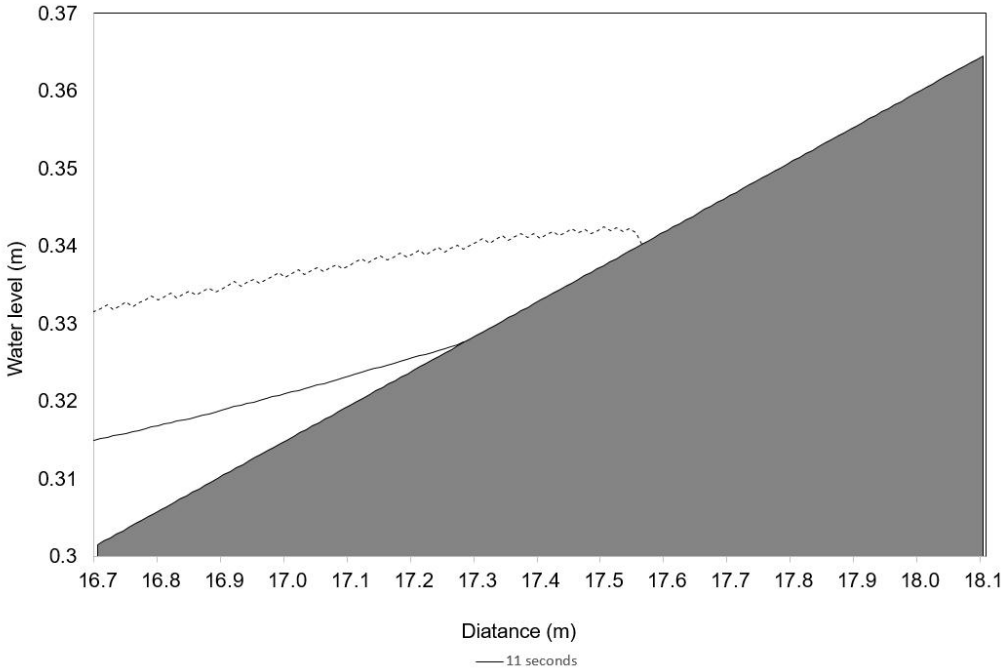

Figure 7-14 Water surface profiles-standard vs. transformed scheme for the low-amplitude wave run-up case at 11s. standard LBM (solid line); asymmetric LBM (dashed line).

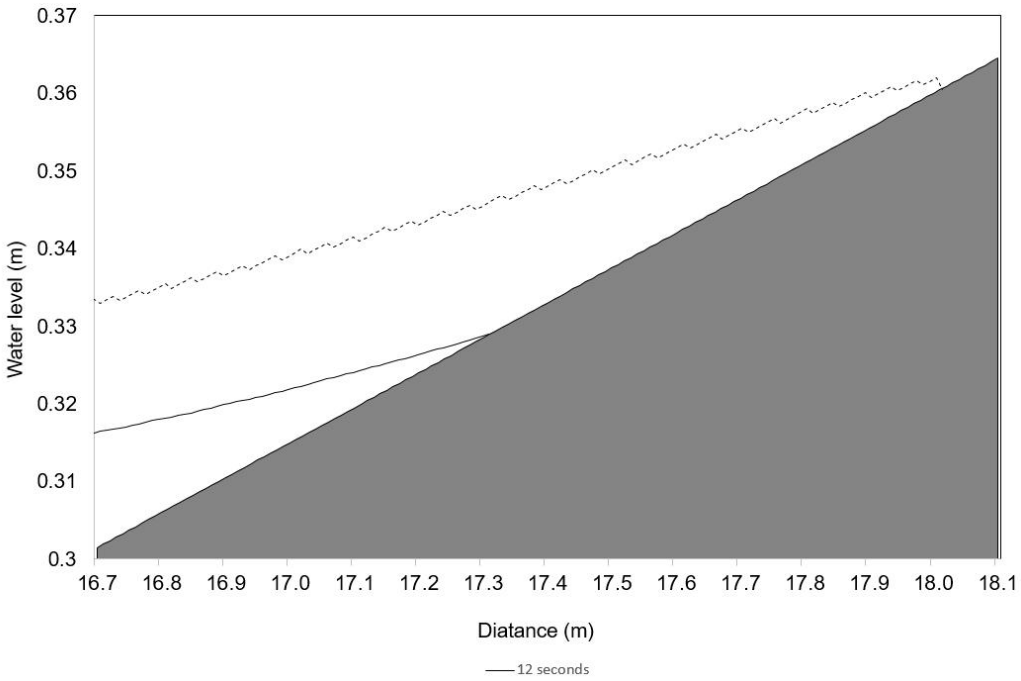

Figure 7-15 Water surface profiles-standard vs. transformed scheme for the low-amplitude wave run-up case at 12s. standard LBM (solid line); asymmetric LBM (dashed line).

It was concluded that the transformed scheme and the modified shoreline boundary condition in their current form could not be applied to problems with very shallow depths. This limitation inherently relates to the mathematical fundamentals on which the transformed scheme is based on and therefore trying different moving shoreline techniques would not help with resolving this issue. In addition to that, the modified shoreline treatment technique does not seem to use the correct conditions in applying the wet/dry interface algorithm.
As a conclusion, the transformed model in its current form cannot be applied to problems involving wave run-up and run-down.

7.5. Summary

Although the limitations of the transformed scheme in modelling very shallow flows was known, it was attempted to apply it to a number of problems involving very a shoreline where water depth in vicinity of the shore was very shallow. Specifically, stationary water with very shallow depths, dam-break on dry bed and solitary wave run-up cases were investigated. As discussed, it was observed that the standard LBM can instantaneously accommodate supercritical regimes occurring at the wave tip and this raised the hope that the transformed scheme may also be able to handle instantaneous instabilities.

In this chapter a review of various moving shoreline treatment techniques was provided with a focus on the algorithm proposed by Liu and Zhou (2014), which was specifically developed

for implementation in the standard LBM. Using the approach adopted by Liu and Zhou (2014), a wet-dry boundary condition was derived for the transformed scheme to enable determination of all EDFs at the shoreline interface. Modifications were also applied to the criteria used in the wet-dry boundary condition to accommodate the transformed scheme geometry.

The modified shoreline treatment technique was tested for a number of cases. It was evident that the very shallow water depths in nearshore areas often resulted in very large lattice Froude number (Ψ) values, falling outside the stability zone and leading to model instability. In wave run up cases and the dam break case on dry bed, it was observed that the shoreline moved at a constant speed equal to the lattice speed and this suggested that the selected lattice speed is not sufficiently large and limits movement of the shoreline at the desired speed. On the other hand, increasing lattice speed resulted in even higher lattice Froude numbers (Ψ), which accelerated model instability.

A low-amplitude wave run-up case was also investigated. This case was expected to require a lower lattice number but the location of shoreline for this case did not match those from a standard scheme. It was not clear if this mismatch was due to poor modification of the criteria governing wave run-up and run-down, or the intrinsic limitation of the transformed scheme.

The investigation on application of the transformed scheme to problems involving shorelines was concluded without success. Due to the inherent limitation of the proposed transformed scheme in simulating such flows, it is not expected that different shoreline treatment techniques will resolve this limitation.

8. Conclusions and recommendations

The purpose of this study was to apply Lattice Boltzmann Modelling (LBM) techniques to study shallow water flows with a focus on supercritical flow regimes.

An outline of the physical equations governing fluid flow including continuity, momentum equation, stress-strain and Navier-Stokes equations were provided to be used for validation of the derived LBM equations as discussed below. A critical review of the most-commonly numerical approaches to fluid flow problems was provided including the Finite Difference Method, the Finite Element Method, the Finite Volume Method, Smoothed Particle Hydrodynamics and the Lattice Boltzmann Methods. The strength of LBM over other numerical schemes, as well as its potential advantages in investigation of specific problems, was highlighted and the Lattice Boltzmann Method (LBM) was selected for extension of its applicability to supercritical flow problems and so was further investigated by providing a review on its evolution, applications and limitations. The main reason in selecting the Lattice Boltzmann Method was its unique features that facilitate definition of particles and tracking their displacement at each time step. Coastal engineering (such as swash zone problems) was a potential field to apply an improved LBM for supercritical flows, because the flow regime in this region is almost always supercritical and so out of the reach for the standard Lattice Boltzmann Models.

A detailed overview of the standard LBM was provided for both 1D and 2D standard shallow-water LBM schemes and their limitation is modelling supercritical flow regimes discussed with presentation of a number of test cases.

For the first time, Chopard et al. (2013) suggested a Galilean transformation of the 1D LBM scheme to overcome the limitation of modelling supercritical flow regimes. The proposed transformation resulted in an asymmetric scheme which had to meet a specific set of criteria to remain numerically stable. This asymmetric scheme was a breakthrough to successful application of LBM to supercritical regimes. However, it was associated with very specific numerical stability requirements which only allowed application of this model to a very narrow range of flow conditions encountered in practical applications. This called for extension of the proposed scheme to encompass a wider set of flow conditions.

In current research, a new transformed 1D LBM was presented, which is based on generalised transformation of the standard LBM. The proposed scheme allows proper selection of transformation parameters to accommodate a larger number of flow conditions

compared to the asymmetric scheme by Chopard et al. (2013), both in subcritical supercritical flow regimes. The full mathematical derivation of the Equilibrium Distribution Functions was provided in general form, which is absent from other literature. The force term weight factors were mathematically derived for the transformed scheme in general form, based on the isotropy requirements of the lattice, which its derivation and underlying fundamentals are completely absent from the existing literature. A modified form of the inflow-outflow boundary conditions was presented accommodate the asymmetry parameters and the stability criteria for the proposed scheme were derived in terms of the lattice asymmetry parameters to allow proper selection of the lattice geometry. Full details of the Chapman-Enskog expansion applied to the proposed scheme was provided. The Chapman-Enskog expansion was used to recover the Shallow Water Equations from the transformed lattice geometry and the new Equilibrium Distribution Functions to ascertain that the model will be solving the Shallow Water Equations. The proposed scheme was validated through several test cases and was proven to have the ability of handling both subcritical and supercritical regimes. This is a major improvement to the existing LBM, whose applicability is either limited to subcritical regime, or a narrow range of supercritical regimes.

The proposed model was applied to a number of steady-state and unsteady problems and very good to excellent agreement was observed between the modelled results and those from analytic solutions or other models. In each problem, the asymmetry parameters and lattice speeds were selected to define a stability envelope that encompassed the entire solution. To the authors knowledge, simulation of unsteady supercritical flows with LBM is currently absent from the literature. The range of Froude numbers in most of the test cases modelled with the proposed scheme were also outside of the reach of the existing Lattice Boltzmann Models, including the asymmetric scheme by Chopard et al. (2013).

The transformed scheme in its current form was developed with the aim of modelling high-speed flows and as such is associated with some limitations. Although the numerical stability envelope of the proposed scheme is larger than Chopard et al. (2013), it still has limited applicability to problems where combined low Froude numbers (Fr) and large lattice Froude numbers (Ψ) exist. This is due to the invariable nature of the stability envelope lower bound. This limitation was shown in the final chapter when the transformed scheme fails to model flow cases involving shorelines.

Despite its limitation in modelling low-Froude flow regimes, the transformed scheme is a breakthrough in LBM applications and allows it to be used as an efficient solution to a wide range of problems with both low and high Froude numbers.

While there is growing interest by the scientists and engineers in application of the LBM to fluid mechanics and hydraulics problems, a number of gaps were identified during the course of this study which may provide opportunities for further research. Some of the main ideas that would benefit from further investigations include:

- Galilean transformation of LBM schemes which solve the general form of Navier-Stokes equations, rather than the specific form of shallow water equations.
- Further work to extend the lower bound of the stability zone proposed in the current work to accommodate a larger number of flow cases.
- Complete application of the specific Galilean transformation to 2D LBM schemes and extend to a generalised form.
- Investigate using variable lattice speed or grid size in a simulation to satisfy the stability criteria on a local basis.
- Extension of the shoreline treatment technique by Liu and Zhou (2014) to the transformed LBM scheme through identification of the correct relationship between the algebraic values of the EDFs and physical movement of the shoreline.

Bibliography:

Abe, T. (1997). "Derivation of the Lattice Boltzmann Method by Means of the Discrete Ordinate Method for the Boltzmann Equation." *Journal of Computational Physics 131(1)*: 241-246 DOI: 10.1006/jcph.1996.5595.
Ahner, H. F. and J. Dooher (1992). "Application of Lattice-Gas Automata to Converging Flow and Non-Newtonian Fluids." *Physical Review A 45(10)*: 7632-7635.
Andersson, B., R. Andersson, L. Hakansson, M. Mortensen, R. Sudiyo and B. van Wachem (2011). Computational Fluid Dynamics for Engineers. Cambridge, Cambridge : Cambridge University Press.
Banda, M. K., M. Seaïd and G. Thömmes (2009). "Lattice Boltzmann simulation of dispersion in two-dimensional tidal flows." *International Journal for Numerical Methods in Engineering 77(6)*: 878-900 DOI: 10.1002/nme.2435.
Barnes, M. P. and T. E. Baldock (2010). "A Lagrangian model for boundary layer growth and bed shear stress in the swash zone." *Coastal Engineering 57(4)*: 385-396 DOI: 10.1016/j.coastaleng.2009.11.009.
Bates, P. D. and J. Hervouet (1999). "A new method for movingboundary hydrodynamic problems in shallow water." *Proceedings of the Royal Society A: Mathematical, Physical and Engineering Sciences 455(1988)*: 3107-3128 DOI: 10.1098/rspa.1999.0442.
Bermudez, A. and M. E. Vazquez (1994). "Upwind methods for hyperbolic conservation laws with source terms." *Computers and Fluids 23(8)*: 1049-1071 DOI: 10.1016/0045-7930(94)90004-3.
Bhatnagar, P. L., E. P. Gross and M. Krook (1954). "A Model for Collision Processes in Gases. I. Small Amplitude Processes and Charged and Neutral One-Component Systems " *Physical Review 94(3)*: 511-525 DOI: 10.1103/PhysRev.94.511.
Bokil, V. A. and N. L. Gibson (2007). Finite Difference, Finite Element and Finite Volume Methods for the Numerical Solution of PDEs. DOE Multiscale Summer School. Department of Mathematics, Oregon State University, Corvallis, OR.
Buick, J. M. and C. A. Greated (1998). "Lattice Boltzmann Modeling of Interfacial Gravity Waves." *Physics of Fluids 10(6)*: 1490-1511.
Cabezón, R. M., D. García-Senz and A. Relaño (2008). "A one-parameter family of interpolating kernels for smoothed particle hydrodynamics studies." *Journal of Computational Physics 227(19)*: 8523-8540 DOI: http://dx.doi.org/10.1016/j.jcp.2008.06.014.
Caiazzo, C. (2008). "Analysis of Lattice Boltzmann Nodes Initialization in Moving Boundary Problems." *Progress in Computational Fluid Dynamics 8(1-4)*: 3-10, <Go to ISI>://000256163500022.
Carrier, G. F., T. T. Wu and H. Yeh (2003). "Tsunami run-up and draw-down on a plane beach." *Journal of Fluid Mechanics 475*: 79-99.
Cercos-Pita, J. L., R. A. Dalrymple and A. Herault (2016). "Diffusive terms for the conservation of mass equation in SPH." *Applied Mathematical Modelling 40(19-20)*: 8722-8736 DOI: 10.1016/j.apm.2016.05.016.
Chanson, H. (2004). Hydraulics of Open Channel Flow, Elsevier Science.
Chapman, S. and T. G. Cowling (1960). "The mathematical theory of nonuniform gases." *Cambridge University Press*.
Chen, H., S. Chen and W. Matthaeus (1992). "Recovery of the Navier-Stokes Equations Using a Lattice-Gas Boltzmann Method." *Physical Review A 45(8)*: 5339-5342.
Chen, S. and G. Doolen (1997). "Lattice Boltzmann Method for Fluid Flows." *Annual Review of Fluid Mechanics 30*: 329-364.

Chopard, B., V. T. Pham and L. Lefèvre (2013). "Asymmetric lattice Boltzmann model for shallow water flows." *Computers & Fluids 88(0)*: 225-231 DOI: 10.1016/j.compfluid.2013.09.014.
Courant, R., K. Friedrichs and H. Lewy (1959). ON THE PARTIAL DIFFERENCE EQUATIONS OF MATHEMATICAL PHYSICS. A. California Univ Los.
D'Humières, D. and P. Lallemand (1986). "Lattice Gas Models for 3D Hydrodynamics." *Europhysics Letters 2(4)*: 291-297.
Dellar, P. (2001). "Bulk and shear viscosities in lattice Boltzmann equations." *Physical Review E 64(3)*: 031203, http://link.aps.org/doi/10.1103/PhysRevE.64.031203.
Dellar, P. (2002). "Nonhydrodynamic modes and a priori construction of shallow water lattice Boltzmann equations." *Physical Review 65(3)*.
Dodd, N. (1998). "Numerical model of wave run-up, overtopping, and regeneration." *Journal of Waterway, Port, Coastal and Ocean Engineering 124(2)*: 73.
Frandsen, J. B. (2008). "A 1-D Lattice Boltzmann Model Applied to Tsunami Runup Onto a Plane Beach." *Progress in Computational Fluid Dynamics 8(1-4)*: 283-309.
Frandsen, J. B. (2008). "Free-Surface Lattice Boltzmann Modeling in Single Phase Flows." *Progress in Computational Fluid Dynamics 8(1-4)*: 163-219.
Frandsen, J. B. (2008). "A simple LBE wave runup model." *Progress in Computational Fluid Dynamics 8(1-4)*: 222-232 DOI: 10.1504/PCFD.2008.018093.
Frisch, U. (1989). "Lattice Gas Automata for the Navier-Stokes Equations. A New Approach to Hydrodynamics and Turbulence." *Physica Scripta 40(423)*.
Frisch, U., D. d'Humières, B. Hasslacher, P. Lallemand, Y. Pomeau and J.-P. Rivet (1987). "Lattice Gas Hydrodynamics in Two and Three Dimensions." *Journal of Complex Systems 1*: 649-707, https://www-n.oca.eu/rivet/00pdf/1987_FHHLPR87a_ComplexSys_LGH.pdf.
Frisch, U., B. Hasslacher and Y. Pomeau (1986). "Lattice-Gas Automata for the Navier-Stokes Equation." *Physical Review Letters 56(14)*: 1505-1508, http://link.aps.org/doi/10.1103/PhysRevLett.56.1505.
Fuhrman, D. R. and P. A. Madsen (2008). "Simulation of nonlinear wave run-up with a high-order Boussinesq model." *Coastal Engineering 55(2)*: 139-154 DOI: 10.1016/j.coastaleng.2007.09.006.
Geveler, M., D. Ribbrock, D. Göddeke and S. Turek (2010). Lattice-Boltzmann Simulation of the Shallow-Water Equations with Fluid-Structure Interaction on Multi- and Manycore Processors. *Facing the Multicore-Challenge*. R. Keller, D. Kramer and J.-P. Weiss, Springer Berlin Heidelberg. 6310: 92-104.
Gingold, R. A. and J. J. Monaghan (1977). "Smoothed particle hydrodynamics: theory and application to non- spherical stars." *Monthly Notices of the Royal Astronomical Society 181(3)*: 375-389 DOI: 10.1093/mnras/181.3.375.
Guo, Z. and C. Shu (2013). Lattice Boltzmann method and its applications in engineering Zhaoli Guo, Chang Shu. Singapore ; Hackensack, N.J., Singapore ; Hackensack, N.J. : World Scientific Pub. Co.
Guo, Z., C. Zheng and B. Shi (2002). "Discrete lattice effects on the forcing term in the lattice Boltzmann method." *Physical Review E 65(4)*: 046308, http://link.aps.org/doi/10.1103/PhysRevE.65.046308.
Hardy, J. and O. d. Pazzis (1976). "Molecular dynamics of a classical lattice gas: Transport properties and time correlation functions." *Physical Review A 13(5)*: 1949-1961.
Hardy, J. and Y. Pomeau (1972). "Thermodynamics and Hydrodynamics for a Modeled Fluid." *Journal of Mathematical Physics 13(7)*: 1042-1051.
Hardy, J., Y. Pomeau and O. d. Pazzis (1973). "Time evolution of a two-dimensional model system. I. Invariant statesand time correlation functions." *Journal of Mathematical Physics 14(12)*: 1746-1759 DOI: 10.1063/1.1666248.

He, X. and L.-S. Luo (1997). "Lattice Boltzmann Model for the Incompressible Navier-Stokes Equation." *Journal of Statistical Physics 88(3/4)*: 927-944.
He, X., Q. Zou, L.-S. Luo and M. Dembo (1997). "Analytic solutions of simple flows and analysis of nonslip boundary conditions for the lattice Boltzmann BGK model." *Journal of Statistical Physics 87(1-2)*: 115-136 DOI: 10.1007/BF02181482.
Hedjripour, A. H., D. P. Callaghan and T. E. Baldock (2016). "Generalized transformation of the lattice Boltzmann method for shallow water flows." *Journal of Hydraulic Research 54(4)*: 371-388 DOI: 10.1080/00221686.2016.1168881.
Hibberd, S. and D. H. Peregrine (1979). "Surf and run-up on a beach: a uniform bore." *J. Fluid Mech. 95(2)*: 323-345 DOI: 10.1017/S002211207900149X.
Holthuijsen, L. H. (2007). Waves in Oceanic and Coastal Waters, Cambridge University Press.
Hu, K., C. G. Mingham and D. M. Causon (2000). "Numerical simulation of wave overtopping of coastal structures using the non-linear shallow water equations." *Coastal Engineering 41(4)*: 433-465 DOI: 10.1016/S0378-3839(00)00040-5.
Hughes, W. F. and J. A. Brighton (1999). Fluid Dynamics, Mc Graw-Hill.
Jafari, S., M. Salmanzadeh, M. Rahnama and G. Ahmadi (2010). "Investigation of particle dispersion and deposition in a channel with a square cylinder obstruction using the lattice Boltzmann method." *Journal of Aerosol Science 41(2)*: 198-206 DOI: DOI: 10.1016/j.jaerosci.2009.10.005.
Jenssen, C. B., T. Kvamdal, H. I. Andersson, B. Pettersen, P. Fox, N. Satofuka, et al. (2001). Parallel Computational Fluid Dynamics 2000: Trends and Applications, Elsevier Science.
Klar, A., M. Seaïd and G. Thömmes (2008). "Lattice Boltzmann simulation of depth-averaged models in flow hydraulics." *International Journal of Computational Fluid Dynamics 22(7)*: 507 - 522, http://www.informaworld.com/10.1080/10618560802243838.
Krüger, T., H. Kusumaatmaja, A. Kuzmin, O. Shardt, G. Silva and E. M. Viggen (2017). The Lattice Boltzmann Method Principles and Practice / by Timm Krüger, Halim Kusumaatmaja, Alexandr Kuzmin, Orest Shardt, Goncalo Silva, Erlend Magnus Viggen. Cham, Cham : Springer International Publishing : Imprint: Springer.
Kuzmin, D. (2007). Introduction to Computational Fluid Dynamics, Institute of Applied Mathematics, University of Dortmund.
La Rocca, M., C. Adduce, V. Lombardi, G. Sciortino and R. Hinkelmann (2012). "Development of a lattice Boltzmann method for two-layered shallow-water flow." *International Journal for Numerical Methods in Fluids 70(8)*: 1048-1072 DOI: 10.1002/fld.2742.
Latt, J. (2008) "Choice of units in lattice Boltzmann simulations."
Lattanzio, J. C., J. J. Monaghan, H. Pongracic and M. P. Schwarz (1985). "Interstellar cloud collisions." *Monthly Notices of the Royal Astronomical Society 215(2)*: 125-147 DOI: 10.1093/mnras/215.2.125.
Leveque, R. J. and D. L. George (2008). HIGH-RESOLUTION FINITE VOLUME METHODS FOR THE SHALLOW WATER EQUATIONS WITH BATHYMETRY AND DRY STATES, World Scientific Publishing Co. Pte. Ltd.
Liang, J., M. Ghidaoui and J. Liang (2006). BGK Boltzmann Model and Lattice Boltzmann Method for Shallow Water Flows. *XVI International Conference on Computational Methods in Water Resources (CMWR-XVI)*, Technical University of Denmark, Denmark.
Liu, H. and J. G. Zhou (2014). "Lattice Boltzmann approach to simulating a wetting–drying front in shallow flows." *743*: 32-59 DOI: 10.1017/jfm.2013.682.
Liu, H. and J. G. Zhou (2014). "Lattice Boltzmann approach to simulating a wetting–drying front in shallow flows." *743*: 32-59 DOI: 10.1017/jfm.2013.682.

Liu, H., J. G. Zhou and R. Burrows (2009). "Multi-block lattice Boltzmann simulations of subcritical flow in open channel junctions." *Computers & Fluids 38(6)*: 1108-1117 DOI: DOI: 10.1016/j.compfluid.2008.11.005.
Liu, H., J. G. Zhou, R. Burrows and Y. Peng (2009). A Lattice Boltzmann Model for Dam Break Flows. *World Environmental and Water Resources Congress 2009: Great Rivers*, American Society of Civil Engineers.
Lynett, P. and P. L. F. Liu (2002). "A Numerical Study of Submarine-Landslide-Generated Waves and Run-Up." *Proceedings: Mathematical, Physical and Engineering Sciences 458(2028)*: 2885-2910, http://www.jstor.org/stable/3560090.
Lynett, P. J., T.-R. Wu and P. L. F. Liu (2002). "Modeling wave runup with depth-integrated equations." *Coastal Engineering 46(2)*: 89-107 DOI: 10.1016/S0378-3839(02)00043-1.
Madsen, P. A., O. R. Sørensen and H. A. Schäffer (1997). "Surf zone dynamics simulated by a Boussinesq type model. Part I. Model description and cross-shore motion of regular waves." *Coastal Engineering 32(4)*: 255-287 DOI: 10.1016/S0378-3839(97)00028-8.
Mahdavi, A. and N. Talebbeydokhti (2009). "Modeling of non-breaking and breaking solitary wave run-up using FORCE-MUSCL scheme." *Journal of Hydraulic Research 47(4)*: 476-485 DOI: 10.1080/00221686.2009.9522023.
Maier, R. S. and R. S. Bernard (2010). "Lattice-Boltzmann accuracy in pore-scale flow simulation." *Journal of Computational Physics 229(2)*: 233-255 DOI: DOI: 10.1016/j.jcp.2009.09.013.
Mason, R. (2002). "A Multi-Speed Compressible Lattice-Boltzmann Model." *Journal of Statistical Physics 107(1)*: 385-400 DOI: 10.1023/A:1014535310153.
Maxwell, J. C. (1890). The scientific papers. Cambrdige, Cambridge University Press. 2: 681.
McNamara, G. and G. Zanetti (1988). "Use of Boltzmann Equation to Simulate Lattice-Gas Automata." *Physical Review Letters 61*: 2332-2335.
Mohamad, A. A. and A. Kuzmin (2010). "A critical evaluation of force term in lattice Boltzmann method, natural convection problem." *International Journal of Heat and Mass Transfer 53(5-6)*: 990-996 DOI: 10.1016/j.ijheatmasstransfer.2009.11.014.
Monaghan, J. J. (1992). "Smoothed Particle Hydrodynamics." *Annual review of astronomy and astrophysics 30*: 31.
Monaghan, J. J. (2012). "Smoothed Particle Hydrodynamics and Its Diverse Applications." *Annu. Rev. Fluid Mech. 44*: 323-346 DOI: 10.1146/annurev-fluid-120710-101220.
Nielsen, O., S. Roberts, D. Gray, A. McPherson, A. Hitchman, I. Zerger, et al. (2005). Hydrodynamic modelling of coastal inundation. MODSIM 2005 International Congress on Modelling and Simulation. A. I. Zerger and R. M. Argent, Modelling and Simulation Society of Australia and New Zealand: pp. 518-523.
Oey, L.-Y. (2005). "A wetting and drying scheme for POM." *Ocean Modelling 9(2)*: 133-150 DOI: 10.1016/j.ocemod.2004.06.002.
Preissmann, A. and j. A. Cunge (1961). Calcul des intumescences sur machines électroniques [Computation of open channel unsteady flows using electronic computers]. *9th IAHR Congress*, Dubrovnik.
Qian, Y. H., D. D'Humières and P. Lallemand (1992). "Lattice BGK Models for Navier-Stokes Equation." *Europhysics Letters 17(6)*: 479-484 DOI: 10.1209/0295-5075/17/6/001.
Reddy, J. (2005). An Introduction to the Finite Element Method, Mc Graw Hill.
Rosswog, S. (2015). "Boosting the accuracy of SPH techniques: Newtonian and special-relativistic tests." *Monthly Notices of the Royal Astronomical Society 448(4)*: 3628-3664.
Rosswog, S. (2015). "SPH Methods in the Modelling of Compact Objects." *Living Reviews in Computational Astrophysics 1(1)*: 1 DOI: 10.1007/lrca-2015-1.
Rothman, D. H. and S. Zaleski (1997). Lattice-Gas Cellular Automata: Simple models of complex hydrodynamics. Cambridge, Cambrdige University Press.

Salmon, R. (1999). "The lattice Boltzmann method as a basis for ocean circulation modeling." *Journal of Marine Research 57(3)*: 503-535 DOI: 10.1357/002224099764805174.
Schoenberg, I. J. (1946). "CONTRIBUTIONS TO THE PROBLEM OF APPROXIMATION OF EQUIDISTANT DATA BY ANALYTIC FUNCTIONS: PART B—ON THE PROBLEM OF OSCULATORY INTERPOLATION. A SECOND CLASS OF ANALYTIC APPROXIMATION FORMULAE." *Quarterly of Applied Mathematics 4(2)*: 112-141.
Servan-Camas, B. and F. T. C. Tsai (2009). "Non-negativity and stability analyses of lattice Boltzmann method for advection-diffusion equation." *Journal of Computational Physics 228(1)*: 236-256 DOI: DOI: 10.1016/j.jcp.2008.09.005.
Sielecki, A. and M. G. Wurtele (1970). "The numerical integration of the nonlinear shallow-water equations with sloping boundaries." *Journal of Computational Physics 6(2)*: 219-236 DOI: 10.1016/0021-9991(70)90022-7.
Sobey, R. J. (2009). "Wetting and drying in coastal flows." *Coastal Engineering 56(5)*: 565-576 DOI: 10.1016/j.coastaleng.2008.12.001.
Šoln, J. Z. (1996). Finite Element, Finite Difference and Finite Volume Methods: Examples and Their Comparisons. U. S. A. R. Laboratory: 57.
Sorensen, R. M. (2006). Basic Coastal Engineering. Boston, Boston, MA, USA: Springer US.
Sterling, J. D. and S. Chen (1996). "Stability Analysis of Lattice Boltzmann Methods." *Journal of Computational Physics 123(1)*: 196-206 DOI: DOI: 10.1006/jcph.1996.0016.
Succi, S. (2001). The Lattice Boltzmann Equation for Fluid Dynamics and Beyond, Oxford University Press.
Sukop, M. and D. Thorne (2007). Lattice Boltzmann Modeling: An Introduction for Geoscientists and Engineers. New York, Springer Berlin Heidelberg.
Synolakis, C. E. (1987). "The runup of solitary waves." *J. Fluid. Mech. 185(-1)*: 523-545 DOI: 10.1017/S002211208700329X.
Thomée, V. (2001). "From finite differences to finite elements." *Journal of Computational and Applied Mathematics 128(1)*: 1-54 DOI: http://dx.doi.org/10.1016/S0377-0427(00)00507-0.
Thömmes, G., M. Seaïd and M. K. Banda (2007). "Lattice Boltzmann methods for shallow water flow applications." *International Journal for Numerical Methods in Fluids 55(7)*: 673-692 DOI: 10.1002/fld.1489.
Titov, V. V. and C. E. Synolakis (1995). "Modeling of breaking and nonbreaking long-wave evolution and runup using VTCS-2. (one-dimensional long waves)." *Journal of Waterway, Port, Coastal and Ocean Engineering 121(6)*: 308.
Tubbs, K. R. and F. T. C. Tsai (2009). Simulation of Multilayer Shallow Water Fluid Flow Using Lattice Boltzmann Modeling and High Performance COmputing. *World Environmental and Water Resources Congress 2009: Great Rivers*, American Society of Civil Engineers.
Uhlenbeck, G. E. and G. W. Ford (1963). Lectures in statistical mechanics *Lectures in Applied Mathematics*, American Mathematical Society. 1: 181.
Valcke, S., S. De Rijcke, E. Roediger and H. Dejonghe (2010). "Kelvin–Helmholtz instabilities in smoothed particle hydrodynamics." *Monthly Notices of the Royal Astronomical Society 408(1)*: 71-86.
van Thang, P., B. Chopard, L. Lefèvre, D. A. Ondo and E. Mendes (2010). "Study of the 1D lattice Boltzmann shallow water equation and its coupling to build a canal network." *Journal of Computational Physics 229(19)*: 7373-7400 DOI: 10.1016/j.jcp.2010.06.022.
Warburton, T. (2005). Numerical Methods for Partial Differential Equations Rice University, Department of Computational and Applied Mathematics.

Wei, Z., R. A. Dalrymple, M. Xu, R. Garnier and M. Derakhti (2017). "Short-crested waves in the surf zone." *Journal of Geophysical Research: Oceans 122(5)*: 4143-4162 DOI: 10.1002/2016JC012485.
Wendland, H. (1995). "Piecewise polynomial, positive definite and compactly supported radial functions of minimal degree." *Advances in Computational Mathematics 4(1)*: 389-396 DOI: 10.1007/bf02123482.
Wolfram, S. (1986). "Cellular automaton fluids 1: Basic theory." *Journal of Statistical Physics 45(3-4)*: 471-526 DOI: 10.1007/BF01021083.
Womersley, J. R. (1955). "Method for the calculation of velocity, rate of flow and viscous drag in arteries when the pressure gradient is known." *The Journal of Physiology 127(3)*: 553-563, http://www.ncbi.nlm.nih.gov/pmc/articles/PMC1365740/.
Yang, L. M., C. Shu and J. Wu (2012). "Development and Comparative Studies of Three Non-free Parameter Lattice Boltzmann Models for Simulation of Compressible Flows." *Advances in Applied Mathematics and Mechanics 4(04)*: 454-472 DOI: 10.4208/aamm.10-m11146.
Yojina, J., W. Ngamsaad, N. Nuttavut, D. Triampo, Y. Lenbury, P. Kanthang, et al. (2010). "Investigating flow patterns in a channel with complex obstacles using the lattice Boltzmann method." *Journal of Mechanical Science and Technology 24(10)*: 2025-2034 DOI: 10.1007/s12206-010-0712-x.
Zhang, J., G. Yan and Y. Dong (2009). "A higher-order accuracy lattice Boltzmann model for the wave equation." *International Journal for Numerical Methods in Fluids 61(6)*: 683-697 DOI: 10.1002/fld.1981.
Zhou, J. (2002). "A lattice Boltzmann model for the shallow water equations." *Computer Methods in Applied Mechanics and Engineering 191(32)*: 3527-3539 DOI: DOI: PII S0045-7825(02)00291-8.
Zhou, J. (2004). Lattice Boltzmann Methods for Shallow Water Flows. New York, Springer-Verlag Berlin Heidelberg.
Zhou, J. (2007). "Lattice Boltzmann Simulations of Discontinuous Flows." *International Journal of Modern Physics C 18(1)*: 1-14.
Zhou, J. G. (2011). "Axisymmetric lattice Boltzmann method revised." *Physical review. E, Statistical, nonlinear, and soft matter physics 84(3 Pt 2)*: 036704.
Zhou, J. G. (2012). "MRT RECTANGULAR LATTICE BOLTZMANN METHOD." *International Journal of Modern Physics C 23(05)*: 1250040-1250041-1250040-1250017 DOI: 10.1142/S0129183112500404.
Zhou, J. G. (2014). "Lattice Boltzmann morphodynamic model." *Journal of Computational Physics 270*: 255.
Zhou, J. G. and H. Liu (2013). "Determination of bed elevation in the enhanced lattice Boltzmann method for the shallow-water equations." *Physical Review E 88(2)* DOI: 10.1103/PhysRevE.88.023302.
Zou, Q. and X. He (1997). "On pressure and velocity boundary conditions for the lattice Boltzmann BGK model." *Physics of Fluids 9(6)*: 1591-1598 DOI: 10.1063/1.869307.

Appendix A- Derivation of the equilibrium functions for the standard D2Q9 Shallow Water LBM

We assume that the equilibrium functions for the standard Lattice Boltzmann scheme can be expressed as a power series in macroscopic velocity as proposed by Rothman & Zaleski (1997) for the two-dimensional flow:

$$f_\alpha^{eq} = A_\alpha + B_\alpha e_{\alpha i}\mathbf{u_i} + C_\alpha e_{\alpha i}e_{\alpha j}\mathbf{u_i u_j} + D_\alpha \mathbf{u_i u_i} \quad \text{(A-1)}$$

This will be applied to a two-dimensional scheme shown below.

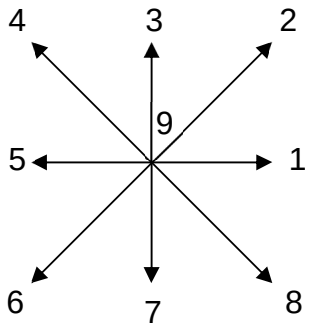

For the symmetry of the lattice, the coefficients A, B, C and D will have the same symmetric properties, so Equation A-1 may be written as:

$$f_0^{eq} = A_0 + D_0\mathbf{u_i u_i} \quad \text{(rest state)} \quad \text{(A-2)}$$

$$f_\alpha^{eq} = \bar{A} + \bar{B}e_{\alpha i}\mathbf{u_i} + \bar{C}e_{\alpha i}e_{\alpha j}\mathbf{u_i u_j} + \bar{D}\mathbf{u_i u_i} \quad (\text{odd } \alpha) \quad \text{(A-3)}$$

$$f_\alpha^{eq} = \tilde{A} + \tilde{B}e_{\alpha i}\mathbf{u_i} + \tilde{C}e_{\alpha i}e_{\alpha j}\mathbf{u_i u_j} + \tilde{D}\mathbf{u_i u_i} \quad (\text{even } \alpha) \quad \text{(A-4)}$$

where:

$$A_1 = A_3 = A_5 = A_7 = \bar{A} \text{ and } A_2 = A_4 = A_6 = A_8 = \tilde{A} \quad \text{(A-5)}$$

$$B_1 = B_3 = B_5 = B_7 = \bar{B} \text{ and } B_2 = B_4 = B_6 = B_8 = \tilde{B} \quad \text{(A-6)}$$

$$C_1 = C_3 = C_5 = C_7 = \bar{C} \text{ and } C_2 = C_4 = C_6 = C_8 = \tilde{C} \quad \text{(A-7)}$$

$$D_1 = D_3 = D_5 = D_7 = \bar{D} \text{ and } D_2 = D_4 = D_6 = D_8 = \tilde{D} \tag{A-8}$$

The equilibrium functions must preserve mass and momentum in the system. For shallow water flows these are expressed by the following equations:

$$\sum_{\alpha} f_{\alpha}^{eq}(x,t) = h(x,t) \tag{A-9}$$

$$\sum_{\alpha} e_{\alpha i} f_{\alpha}^{eq}(x,t) = h(x,t)u_i(x,t) \tag{A-10}$$

$$\sum_{\alpha} e_{\alpha i} e_{\alpha j} f_{\alpha}^{eq}(x,t) = \frac{1}{2} g h^2(x,t)\delta_{ij} + h(x,t)u_i(x,t)u_j(x,t). \tag{A-11}$$

Substituting Equations A-2 to A-4 into Eq. A-9 yields:

$$\begin{aligned}(A_0 + D_0 u_i u_i) + \left(4\bar{A} + \sum_{\alpha=1,3,5,7} \bar{B} e_{\alpha i} u_i + \sum_{\alpha=1,3,5,7} \bar{C} e_{\alpha i} e_{\alpha j} u_i u_j + 4\bar{D} u_i u_i\right) \\ + \left(4\tilde{A} + \sum_{\alpha=2,4,6,8} \tilde{B} e_{\alpha i} u_i + \sum_{\alpha=2,4,6,8} \tilde{C} e_{\alpha i} e_{\alpha j} u_i u_j + 4\tilde{D} u_i u_i\right) = h\end{aligned} \tag{A-12}$$

$\bar{B}$ coefficient:

$$i = 1: \sum_{\alpha=1,3,5,7} e_{\alpha i} u_i = (e_{11}u_1 + e_{31}u_1 + e_{51}u_1 + e_{71}u_1) = (e + 0 - e + 0)u_1 = 0$$

$$i = 2: \sum_{\alpha=1,3,5,7} e_{\alpha i} u_i = (e_{12}u_2 + e_{32}u_2 + e_{52}u_2 + e_{72}u_2) = (0 + e + 0 - e)u_2 = 0$$

$\bar{B}$ coefficient=0 u_i

$\bar{C}$ coefficient:

$$i = j = 1: \sum_{\alpha=1,3,5,7} e_{\alpha i} e_{\alpha j} u_i u_j = (e_{11}e_{11}u_1u_1 + e_{31}e_{31}u_1u_1 + e_{51}e_{51}u_1u_1 + e_{71}e_{71}u_1u_1)$$
$$= (e^2 + 0 + e^2 + 0)u_1u_1 = 2e^2u_1u_1$$

$$i = j = 2: \sum_{\alpha=1,3,5,7} e_{\alpha i} e_{\alpha j} u_i u_j = (e_{12}e_{12}u_2u_2 + e_{32}e_{32}u_2u_2 + e_{52}e_{52}u_2u_2 + e_{72}e_{72}u_2u_2)$$
$$= (0 + e^2 + 0 + e^2)u_2u_2 = 2e^2u_2u_2$$

$i = 1, j = 2$: $\sum_{\alpha=1,3,5,7} e_{\alpha i}e_{\alpha j}u_i u_j = (e_{11}e_{12}u_1u_2 + e_{31}e_{32}u_1u_2 + e_{51}e_{52}u_1u_2 + e_{71}e_{72}u_1u_2)$

$= (0 + +0 + 0 + 0)u_1u_2 = 0$

$\bar{C}$ coefficient = $2e^2u_iu_i$

$\tilde{B}$ coefficient:

$i = 1$: $\sum_{\alpha=2,4,6,8} e_{\alpha i}u_i = (e_{21}u_1 + e_{41}u_1 + e_{61}u_1 + e_{81}u_1) = (e - e - e + e)u_1 = 0$

$i = 2$: $\sum_{\alpha=2,4,6,8} e_{\alpha i}u_i = (e_{22}u_2 + e_{42}u_2 + e_{62}u_2 + e_{82}u_2) = (e + e - e - e)u_2 = 0$

$\tilde{B}$ coefficient=0 u

$\tilde{C}$ coefficient:

$i = j = 1$: $\sum_{\alpha=2,4,6,8} e_{\alpha i}e_{\alpha j}u_i u_j = (e_{21}e_{21}u_1u_1 + e_{41}e_{41}u_1u_1 + e_{61}e_{61}u_1u_1 + e_{81}e_{81}u_1u_1)$

$= (e^2 + e^2 + e^2 + e^2)u_1u_1 = 4e^2u_1u_1$

$i = j = 2$: $\sum_{\alpha=2,4,6,8} e_{\alpha i}e_{\alpha j}u_i u_j = (e_{22}e_{22}u_2u_2 + e_{42}e_{42}u_2u_2 + e_{62}e_{62}u_2u_2 + e_{82}e_{82}u_2u_2)$

$= (e^2 + e^2 + e^2 + e^2)u_2u_2 = 4e^2u_2u_2$

$i = 1, j = 2$: $\sum_{\alpha=2,4,6,8} e_{\alpha i}e_{\alpha j}u_i u_j = (e_{21}e_{22}u_1u_2 + e_{41}e_{42}u_1u_2 + e_{61}e_{62}u_1u_2 + e_{81}e_{82}u_1u_2)$

$= (0 + +0 + 0 + 0)u_1u_2 = 0$

$\tilde{C}$ coefficient= $4e^2u_iu_i$

Hence Eq. A-12 is simplified as:

$$(A_0 + D_0u_iu_i) + (4\bar{A} + 2e^2u_iu_i\bar{C} + 4\bar{D}u_iu_i) + \left(4\tilde{A} + 4e^2u_iu_i\tilde{C} + 4\tilde{D}u_iu_i\right) = h \qquad \text{(A-13)}$$

Or rearranged as:

$$\left(D_0 + 2e^2\bar{C} + 4e^2\tilde{C} + 4\bar{D} + 4\tilde{D}\right)u_iu_i + \left(A_0 + 4\bar{A} + 4\tilde{A} + A_0\right) = h \qquad \text{(A-14)}$$

Which yields two equations:

$$D_0 + 2e^2\bar{C} + 4e^2\tilde{C} + 4\bar{D} + 4\tilde{D} = 0 \tag{A-15}$$

$$A_0 + 4\bar{A} + 4\tilde{A} + A_0 \tag{A-16}$$

Substituting Equations A-2 to A-4 into Eq. A-10:

$$\begin{aligned}\left(A_0 e_{\alpha i} + D_0 e_{\alpha i} u_j u_j\right) + \sum_{\alpha=1,3,5,7} \left(\bar{A} e_{\alpha i} + \bar{B} e_{\alpha i} e_{\alpha j} u_j + \bar{C} e_{\alpha i} e_{\alpha j} e_{\alpha k} u_j u_k + \bar{D} e_{\alpha i} u_j u_j\right) \\ + \sum_{\alpha=2,4,6,8} \left(\tilde{A} e_{\alpha i} + \tilde{B} e_{\alpha i} e_{\alpha j} u_j + \tilde{C} e_{\alpha i} e_{\alpha j} e_{\alpha k} u_j u_k + \tilde{D} e_{\alpha i} u_j u_j\right) = h u_i\end{aligned} \tag{A-17}$$

$\bar{A}$ coefficient:

$$i = 1: \sum_{\alpha=1,3,5,7} e_{\alpha i} = (e_{11} + e_{31} + e_{51} + e_{71}) = (e + 0 - e + 0) = 0$$

$$i = 2: \sum_{\alpha=1,3,5,7} e_{\alpha i} = (e_{12} + e_{32} + e_{52} + e_{72}) = (0 + e + 0 - e) = 0$$

$\bar{A}$ coefficient = 0

$\bar{B}$ coefficient:

$$i = j = 1: \sum_{\alpha=1,3,5,7} e_{\alpha i} e_{\alpha j} u_j = (e_{11}e_{11}u_1 + e_{31}e_{31}u_1 + e_{51}e_{51}u_1 + e_{71}e_{71}u_1)$$

$$= (e^2 + 0 + e^2 + 0)u_1 = 2e^2 u_1$$

$$i = j = 2: \sum_{\alpha=1,3,5,7} e_{\alpha i} e_{\alpha j} u_j = (e_{12}e_{12}u_2 + e_{32}e_{32}u_2 + e_{52}e_{52}u_2 + e_{72}e_{72}u_2)$$

$$= (0 + e^2 + 0 + e^2)u_2 = 2e^2 u_2$$

$$i = 1, j = 2: \sum_{\alpha=1,3,5,7} e_{\alpha i} e_{\alpha j} u_j = (e_{11}e_{12}u_2 + e_{31}e_{32}u_2 + e_{51}e_{52}u_2 + e_{71}e_{72}u_2)$$

$$= (0 + +0 + 0 + 0)u_2 = 0$$

$\bar{B}$ coefficient = $2e^2 u_i$

$\bar{C}$ coefficient:

$i = j = k = 1$: $\sum_{\alpha=1,3,5,7} e_{\alpha i} e_{\alpha j} e_{\alpha k} u_j u_k$

$= (e_{11}e_{11}e_{11}u_1u_1 + e_{31}e_{31}e_{31}u_1u_1 + e_{51}e_{51}e_{51}u_1u_1 + e_{71}e_{71}e_{71}u_1u_1)$

$= (e^3 + 0 - e^3 + 0)u_1u_1 = 0$

$i = j = k = 2$: $\sum_{\alpha=1,3,5,7} e_{\alpha i} e_{\alpha j} e_{\alpha k} u_j u_k$

$= (e_{12}e_{12}e_{12}u_2u_2 + e_{32}e_{32}e_{32}u_2u_2 + e_{52}e_{52}e_{52}u_2u_2 + e_{72}e_{72}e_{72}u_2u_2)$

$= (0 + e^3 + 0 - e^3)u_2u_2 = 0$

$i = j = 1, k = 2$: $\sum_{\alpha=1,3,5,7} e_{\alpha i} e_{\alpha j} e_{\alpha k} u_j u_k$

$= (e_{11}e_{11}e_{12}u_1u_2 + e_{31}e_{31}e_{32}u_1u_2 + e_{51}e_{51}e_{52}u_1u_2 + e_{71}e_{71}e_{72}u_1u_2)$

$= (0 + 0 + 0 + 0)u_1u_2 = 0$

$i = j = 2, k = 1$: $\sum_{\alpha=1,3,5,7} e_{\alpha i} e_{\alpha j} e_{\alpha k} u_j u_k$

$= (e_{12}e_{12}e_{11}u_2u_1 + e_{32}e_{32}e_{31}u_2u_1 + e_{52}e_{52}e_{51}u_2u_1 + e_{72}e_{72}e_{71}u_2u_1)$

$= (0 + 0 + 0 + 0)u_2u_1 = 0$

$\bar{C}$ coefficient = 0

$\bar{D}$ coefficient:

$i = 1$: $\sum_{\alpha=1,3,5,7} e_{\alpha i} u_i u_i = (e_{11}u_1u_1 + e_{31}u_1u_1 + e_{51}u_1u_1 + e_{71}u_1u_1) = (e + 0 - e + 0)u_1u_1 = 0$

$i = 2$: $\sum_{\alpha=1,3,5,7} e_{\alpha i} u_i u_i = (e_{12}u_2u_2 + e_{32}u_2u_2 + e_{52}u_2u_2 + e_{72}u_2u_2) = (0 + e + 0 - e)u_2u_2 = 0$

$\bar{D}$ coefficient = 0

$\tilde{A}$ coefficient:

$i = 1$: $\sum_{\alpha=2,4,6,8} e_{\alpha i} = (e_{21} + e_{41} + e_{61} + e_{81}) = (e - e - e + e) = 0$

$i = 2$: $\sum_{\alpha=2,4,6,8} e_{\alpha i} = (e_{22} + e_{42} + e_{62} + e_{82}) = (e + e - e - e) = 0$

$\tilde{A}$ coefficient = 0

$\tilde{B}$ coefficient:

$i = j = 1$: $\sum_{\alpha=2,4,6,8} e_{\alpha i} e_{\alpha j} u_j = (e_{21} e_{21} u_1 + e_{41} e_{41} u_1 + e_{61} e_{61} u_1 + e_{81} e_{81} u_1)$

$= (e^2 + e^2 + e^2 + e^2) u_1 = 4e^2 u_1$

$i = j = 2$: $\sum_{\alpha=2,4,6,8} e_{\alpha i} e_{\alpha j} u_j = (e_{22} e_{22} u_2 + e_{42} e_{42} u_2 + e_{62} e_{62} u_2 + e_{82} e_{82} u_2)$

$= (e^2 + e^2 + e^2 + e^2) u_2 = 4e^2 u_2$

$i = 1, j = 2$: $\sum_{\alpha=2,4,6,8} e_{\alpha i} e_{\alpha j} u_j = (e_{21} e_{22} u_2 + e_{41} e_{42} u_2 + e_{61} e_{62} u_2 + e_{81} e_{82} u_2)$

$= (e^2 - e^2 + e^2 - e^2) u_2 = 0$

$\tilde{B}$coefficient = $4e^2 u_i$

$\tilde{C}$ coefficient:

$i = j = k = 1$: $\sum_{\alpha=2,4,6,8} e_{\alpha i} e_{\alpha j} e_{\alpha k} u_j u_k$

$= (e_{21} e_{21} e_{21} u_1 u_1 + e_{41} e_{41} e_{41} u_1 u_1 + e_{61} e_{61} e_{61} u_1 u_1 + e_{81} e_{81} e_{81} u_1 u_1)$

$= (e^3 - e^3 - e^3 + e^3) u_1 u_1 = 0$

$i = j = k = 2$: $\sum_{\alpha=2,4,6,8} e_{\alpha i} e_{\alpha j} e_{\alpha k} u_j u_k$

$= (e_{22} e_{22} e_{22} u_2 u_2 + e_{42} e_{42} e_{42} u_2 u_2 + e_{62} e_{62} e_{62} u_2 u_2 + e_{82} e_{82} e_{82} u_2 u_2)$

$= (e^3 + e^3 - e^3 - e^3) u_2 u_2 = 0$

$i = j = 1, k = 2$: $\sum_{\alpha=2,4,6,8} e_{\alpha i} e_{\alpha j} e_{\alpha k} u_j u_k$

$= (e_{21} e_{21} e_{22} u_1 u_2 + e_{41} e_{41} e_{42} u_1 u_2 + e_{61} e_{61} e_{62} u_1 u_2 + e_{81} e_{81} e_{82} u_1 u_2)$

$= (e^3 + e^3 - e^3 - e^3) u_1 u_2 = 0$

$i = j = 2, k = 1$: $\sum_{\alpha=2,4,6,8} e_{\alpha i} e_{\alpha j} e_{\alpha k} u_j u_k$

$= (e_{22} e_{22} e_{21} u_2 u_1 + e_{42} e_{42} e_{41} u_2 u_1 + e_{62} e_{62} e_{61} u_2 u_1 + e_{82} e_{82} e_{81} u_2 u_1)$

$= (e^3 - e^3 - e^3 + e^3) u_2 u_1 = 0$

$\tilde{C}$ coefficient = 0

$\tilde{D}$ coefficient:

$i = 1$: $\sum_{\alpha=2,4,6,8} e_{\alpha i} u_i u_i = (e_{21} u_1 u_1 + e_{41} u_1 u_1 + e_{61} u_1 u_1 + e_{81} u_1 u_1) = (e - e - e + e) u_1 u_1 = 0$

$i = 2$: $\sum_{\alpha=2,4,6,8} e_{\alpha i}u_i u_i = (e_{22}u_2u_2 + e_{42}u_2u_2 + e_{62}u_2u_2 + e_{82}u_2u_2) = (e + e - e - e)u_2u_2 = 0$

$\tilde{D}$ coefficient = 0

So Eq. A-17 is reduced to:

$$(0 + 0) + (0 + 2e^2u_i\bar{B} + 0 + 0) + \left(0 + 4e^2u_i\tilde{B} + 0 + 0\right) = hu_i \tag{A-18}$$

Or

$$\left(2e^2\bar{B} + 4e^2\tilde{B}\right)u_i = hu_i \tag{A-19}$$

Which yields another equation:

$$\left(2e^2\bar{B} + 4e^2\tilde{B}\right)u_i = hu_i \tag{A-20}$$

Substituting Equations A-2 to A-4 into Eq. A-11:

$$\begin{aligned}\left(A_0e_{\alpha i}e_{\alpha j} + D_0e_{\alpha i}e_{\alpha j}u_ku_k\right) + \sum_{\alpha=1,3,5,7} &(\bar{A}e_{\alpha i}e_{\alpha j} + \bar{B}e_{\alpha i}e_{\alpha j}e_{\alpha k}u_k \\ &+ \bar{C}e_{\alpha i}e_{\alpha j}e_{\alpha k}e_{\alpha l}u_ku_l) + \bar{D}e_{\alpha i}e_{\alpha j}u_ku_k \\ &+ \sum_{\alpha=2,4,6,8} (\tilde{A}e_{\alpha i}e_{\alpha j} + \tilde{B}e_{\alpha i}e_{\alpha j}e_{\alpha k}u_k + \tilde{C}e_{\alpha i}e_{\alpha j}e_{\alpha k}e_{\alpha l}u_ku_l \\ &+ \tilde{D}e_{\alpha i}e_{\alpha j}u_ku_k) = \frac{1}{2}gh^2\delta_{ij} + hu_iu_j\end{aligned} \tag{A-21}$$

$\bar{A}$ coefficient:

$i = j = 1$: $\sum_{\alpha=1,3,5,7} e_{\alpha i}e_{\alpha j} = (e_{11}e_{11} + e_{31}e_{31} + e_{51}e_{51} + e_{71}e_{71}) = (e^2 + 0 + e^2 + 0) = 2e^2$

$i = j = 2$: $\sum_{\alpha=1,3,5,7} e_{\alpha i}e_{\alpha j} = (e_{12}e_{12} + e_{32}e_{32} + e_{52}e_{52} + e_{72}e_{72}) = (0 + e^2 + 0 + e^2) = 2e^2$

$i = 1, j = 2$: $\sum_{\alpha=1,3,5,7} e_{\alpha i}e_{\alpha j} = (e_{11}e_{12} + e_{31}e_{32} + e_{51}e_{52} + e_{71}e_{72}) = (0 + 0 + 0 + 0) = 0$

$\bar{A}$ coefficient = $2e^2\delta_{ij}$

$\bar{B}$ coefficient:

$$i = j = k = 1: \sum_{\alpha=1,3,5,7} e_{\alpha i} e_{\alpha j} e_{\alpha k} u_k$$
$$= (e_{11}e_{11}e_{11}u_1 + e_{31}e_{31}e_{31}u_1 + e_{51}e_{51}e_{51}u_1 + e_{71}e_{71}e_{71}u_1)$$
$$= (e^3 + 0 - e^3 + 0)u_1 = 0$$

$$i = j = k = 2: \sum_{\alpha=1,3,5,7} e_{\alpha i} e_{\alpha j} e_{\alpha k} u_k$$
$$= (e_{12}e_{12}e_{12}u_2 + e_{32}e_{32}e_{32}u_2 + e_{52}e_{52}e_{52}u_2 + e_{72}e_{72}e_{72}u_2)$$
$$= (0 + e^3 + 0 - e^3)u_2 = 0$$

$$i = j = 1, k = 2: \sum_{\alpha=1,3,5,7} e_{\alpha i} e_{\alpha j} e_{\alpha k} u_k$$
$$= (e_{11}e_{11}e_{12}u_2 + e_{31}e_{31}e_{32}u_2 + e_{51}e_{51}e_{52}u_2 + e_{71}e_{71}e_{72}u_2)$$
$$= (0 + 0 + 0 + 0)u_2 = 0$$

$$i = j = 2, k = 1: \sum_{\alpha=1,3,5,7} e_{\alpha i} e_{\alpha j} e_{\alpha k} u_k$$
$$= (e_{12}e_{12}e_{11}u_1 + e_{32}e_{32}e_{31}u_1 + e_{52}e_{52}e_{51}u_1 + e_{72}e_{72}e_{71}u_1)$$
$$= (0 + 0 + 0 + 0)u_1 = 0$$

$\bar{B}$ coefficient = 0

$\bar{C}$ coefficient:

$$i = j = k = l = 1: \sum_{\alpha=1,3,5,7} e_{\alpha i} e_{\alpha j} e_{\alpha k} e_{\alpha l} u_k u_l$$
$$= (e_{11}e_{11}e_{11}e_{11}u_1u_1 + e_{31}e_{31}e_{31}e_{31}u_1u_1 + e_{51}e_{51}e_{51}e_{51}u_1u_1$$
$$+ e_{71}e_{71}e_{71}e_{71}u_1u_1) = (e^4 + 0 + e^4 + 0)u_1u_1 = 2e^4u_1u_1$$

$$i = j = k = l = 2: e_{\alpha i} e_{\alpha j} e_{\alpha k} e_{\alpha l} u_k u_l$$
$$= (e_{12}e_{12}e_{12}e_{12}u_2u_2 + e_{32}e_{32}e_{32}e_{32}u_2u_2 + e_{52}e_{52}e_{52}e_{52}u_2u_2$$
$$+ e_{72}e_{72}e_{72}e_{72}u_2u_2) = (0 + e^4 + 0 + e^4)u_2u_2 = 2e^4u_2u_2$$

$$i = j = k = 1, l = 2: \sum_{\alpha=1,3,5,7} e_{\alpha i} e_{\alpha j} e_{\alpha k} e_{\alpha l} u_k u_l$$
$$= (e_{11}e_{11}e_{11}e_{12}u_1u_2 + e_{31}e_{31}e_{31}e_{32}u_1u_2 + e_{51}e_{51}e_{51}e_{52}u_1u_2$$
$$+ e_{71}e_{71}e_{71}e_{72}u_1u_2) = (0 + 0 + 0 + 0)u_1u_2 = 0$$

$i = j = 2, k = l = 1$: $\sum_{\alpha=1,3,5,7} e_{\alpha i}e_{\alpha j}e_{\alpha k}e_{\alpha l}u_k u_l$

$= (e_{11}e_{11}e_{12}e_{12}u_1u_1 + e_{31}e_{31}e_{32}e_{32}u_1u_1 + e_{51}e_{51}e_{52}e_{52}u_1u_1$

$+ e_{71}e_{71}e_{72}e_{72}u_1u_1) = (0 + 0 + 0 + 0)u_1u_1 = 0$

$i = j = k = 2, l = 1$: $\sum_{\alpha=1,3,5,7} e_{\alpha i}e_{\alpha j}e_{\alpha k}e_{\alpha l}u_k u_l$

$= (e_{12}e_{12}e_{12}e_{11}u_2u_1 + e_{32}e_{32}e_{32}e_{31}u_2u_1 + e_{52}e_{52}e_{52}e_{51}u_2u_1$

$+ e_{72}e_{72}e_{72}e_{71}u_2u_1) = (0 + 0 + 0 + 0)u_2u_1 = 0$

$\bar{C}$ coefficient = $2e^4u_k u_l\delta_{ijkl}$

$\bar{D}$ coefficient:

$i = j = 1$: $\sum_{\alpha=1,3,5,7} e_{\alpha i}e_{\alpha j}u_k u_k = (e_{11}e_{11} + e_{31}e_{31} + e_{51}e_{51} + e_{71}e_{71})u_k u_k$

$= (e^2 + 0 + e^2 + 0)u_k u_k = 2e^2u_k u_k$

$i = j = 2$: $\sum_{\alpha=1,3,5,7} e_{\alpha i}e_{\alpha j}u_k u_k = (e_{12}e_{12} + e_{32}e_{32} + e_{52}e_{52} + e_{72}e_{72})u_k u_k$

$= (0 + e^2 + 0 + e^2)u_k u_k = 2e^2u_k u_k$

$i = 1, j = 2$: $\sum_{\alpha=1,3,5,7} e_{\alpha i}e_{\alpha j}u_k u_k = (e_{11}e_{12} + e_{31}e_{32} + e_{51}e_{52} + e_{71}e_{72})u_k u_k$

$= (0 + 0 + 0 + 0)u_k u_k = 0$

$\bar{D}$ coefficient = $2e^2u_k u_k\delta_{ij}$

$\tilde{A}$ coefficient:

$i = j = 1$: $\sum_{\alpha=2,4,6,8} e_{\alpha i}e_{\alpha j} = (e_{21}e_{21} + e_{41}e_{41} + e_{61}e_{61} + e_{81}e_{81}) = (e^2 + e^2 + e^2 + e^2) = 4e^2$

$i = j = 2$: $\sum_{\alpha=2,4,6,8} e_{\alpha i}e_{\alpha j} = (e_{22}e_{22} + e_{42}e_{42} + e_{62}e_{62} + e_{82}e_{82}) = (e^2 + e^2 + e^2 + e^2) = 4e^2$

$i = 1, j = 2$: $\sum_{\alpha=2,4,6,8} e_{\alpha i}e_{\alpha j} = (e_{21}e_{22} + e_{41}e_{42} + e_{61}e_{62} + e_{81}e_{82}) = (e - e + e - e) = 0$

$\tilde{A}$ coefficient = $4e^2\delta_{ij}$

$\tilde{B}$ coefficient:

$i = j = k = 1$: $\sum_{\alpha=2,4,6,8} e_{\alpha i} e_{\alpha j} e_{\alpha k} u_k$

$= (e_{21} e_{21} e_{21} u_1 + e_{41} e_{41} e_{41} u_1 + e_{61} e_{61} e_{61} u_1 + e_{81} e_{81} e_{81} u_1)$

$= (e^3 - e^3 - e^3 + e^3) u_1 = 0$

$i = j = k = 2$: $\sum_{\alpha=2,4,6,8} e_{\alpha i} e_{\alpha j} e_{\alpha k} u_k$

$= (e_{22} e_{22} e_{22} u_2 + e_{42} e_{42} e_{42} u_2 + e_{62} e_{62} e_{62} u_2 + e_{82} e_{82} e_{82} u_2)$

$= (e^3 + e^3 - e^3 - e^3) u_2 = 0$

$i = j = 1, k = 2$: $\sum_{\alpha=2,4,6,8} e_{\alpha i} e_{\alpha j} e_{\alpha k} u_k$

$= (e_{21} e_{21} e_{22} u_2 + e_{41} e_{41} e_{42} u_2 + e_{61} e_{61} e_{62} u_2 + e_{81} e_{81} e_{82} u_2)$

$= (e^3 + e^3 - e^3 - e^3) u_2 = 0$

$i = j = 2, k = 1$: $\sum_{\alpha=2,4,6,8} e_{\alpha i} e_{\alpha j} e_{\alpha k} u_k$

$= (e_{22} e_{22} e_{21} u_1 + e_{42} e_{42} e_{41} u_1 + e_{62} e_{62} e_{61} u_1 + e_{82} e_{82} e_{81} u_1)$

$= (e^3 - e^3 - e^3 + e^3) u_1 = 0$

$\tilde{B}$ coefficient = 0

$\tilde{C}$ coefficient:

$i = j = k = l = 1$: $\sum_{\alpha=2,4,6,8} e_{\alpha i} e_{\alpha j} e_{\alpha k} e_{\alpha l} u_k u_l$

$= (e_{21} e_{21} e_{21} e_{21} u_1 + e_{41} e_{41} e_{41} e_{41} u_1 + e_{61} e_{61} e_{61} e_{61} u_1 + e_{81} e_{81} e_{81} e_{81} u_1)$

$= (e^4 + e^4 + e^4 + e^4) u_1 u_1 = 4e^4 u_1 u_1$

$i = j = k = l = 2$: $e_{\alpha i} e_{\alpha j} e_{\alpha k} e_{\alpha l} u_k u_l$

$= (e_{22} e_{22} e_{22} e_{22} u_2 + e_{42} e_{42} e_{42} e_{42} u_2 + e_{62} e_{62} e_{62} e_{62} u_2 + e_{82} e_{82} e_{82} e_{82} u_2)$

$= (e^4 + e^4 + e^4 + e^4) u_2 u_2 = 4e^4 u_2 u_2$

$i = j = k = 1, l = 2$: $\sum_{\alpha=2,4,6,8} e_{\alpha i} e_{\alpha j} e_{\alpha k} e_{\alpha l} u_k u_l$

$= (e_{21} e_{21} e_{21} e_{22} u_2 + e_{41} e_{41} e_{41} e_{42} u_2 + e_{61} e_{61} e_{61} e_{62} u_2 + e_{81} e_{81} e_{81} e_{82} u_2)$

$= (e^4 - e^4 + e^4 - e^4) u_2 u_2 = 0$

$$i = k = 2, j = l = 1: \sum_{\alpha=2,4,6,8} e_{\alpha i} e_{\alpha j} e_{\alpha k} e_{\alpha l} u_k u_l$$
$$= (e_{21}e_{21}e_{22}e_{22}u_2u_1 + e_{41}e_{41}e_{42}e_{42}u_2u_1 + e_{61}e_{61}e_{62}e_{62}u_2u_1$$
$$+ e_{81}e_{81}e_{82}e_{82}u_2u_1) = (e^4 + e^4 + e^4 + e^4)u_2u_1 = 4e^4u_2u_1$$

$$i = k = 1, j = l = 2: \sum_{\alpha=2,4,6,8} e_{\alpha i} e_{\alpha j} e_{\alpha k} e_{\alpha l} u_k u_l$$
$$= (e_{21}e_{21}e_{22}e_{22}u_1u_2 + e_{41}e_{41}e_{42}e_{42}u_1u_2 + e_{61}e_{61}e_{62}e_{62}u_1u_2$$
$$+ e_{81}e_{81}e_{82}e_{82}u_1u_2) = (e^4 + e^4 + e^4 + e^4)u_1u_2 = 4e^4u_1u_2$$

$$i = j = k = 2, l = 1: \sum_{\alpha=2,4,6,8} e_{\alpha i} e_{\alpha j} e_{\alpha k} e_{\alpha l} u_k u_l$$
$$= (e_{22}e_{22}e_{22}e_{21}u_2u_1 + e_{42}e_{42}e_{42}e_{41}u_2u_1 + e_{62}e_{62}e_{62}e_{61}u_2u_1$$
$$+ e_{82}e_{82}e_{82}e_{81}u_2u_1) = (e^4 - e^4 + e^4 - e^4)u_2u_1 = 0$$

$\tilde{C}$ coefficient = $4e^4u_ku_l\delta_{kl} + 8e^4u_ku_l\delta_{ij}$

$\widetilde{D}$ coefficient:

$$i = j = 1: \sum_{\alpha=2,4,6,8} e_{\alpha i} e_{\alpha j} u_k u_k = (e_{21}e_{21} + e_{41}e_{41} + e_{61}e_{61} + e_{81}e_{81})u_ku_k$$
$$= (e^2 + e^2 + e^2 + e^2)u_ku_k = 4e^2u_ku_k$$

$$i = j = 2: \sum_{\alpha=2,4,6,8} e_{\alpha i} e_{\alpha j} u_k u_k = (e_{22}e_{22} + e_{42}e_{42} + e_{62}e_{62} + e_{82}e_{82})u_ku_k$$
$$= (e^2 + e^2 + e^2 + e^2)u_ku_k = 4e^2u_ku_k$$

$$i = 1, j = 2: \sum_{\alpha=2,4,6,8} e_{\alpha i} e_{\alpha j} u_k u_k = (e_{21}e_{22} + e_{41}e_{42} + e_{61}e_{62} + e_{81}e_{82})u_ku_k$$
$$= (0 + 0 + 0 + 0)u_ku_k = 0$$

$\widetilde{D}$ coefficient = = $2e^2u_ku_k\delta_{ij}$

So Eq. A-21 will be simplified as:

$$(0 + 0) + \left(2e^2\delta_{ij}\bar{A} + 0 + 2e^4\bar{C}u_iu_i + 2e^2\bar{D}u_iu_i\right)$$
$$+ \left[4e^2\delta_{ij}\tilde{A} + 0 + \left(4e^4u_iu_i + 8e^4u_iu_j\right)\tilde{C} + 4e^2u_iu_i\widetilde{D}\right]$$
$$= \frac{1}{2}gh^2\delta_{ij} + hu_iu_j \qquad \text{(A-22)}$$

Which may be rearranged as:

$$\left(2e^2\bar{A} + 4e^2\tilde{A}\right)\delta_{ij} + \left(4e^4\tilde{C} + 2e^2\bar{D} + 4e^2\tilde{D}\right)u_i u_i + 2e^4\bar{C}u_k u_l + 8e^4\tilde{C}u_i u_j = \frac{1}{2}gh^2\delta_{ij} + hu_i u_j \quad \text{(A-23)}$$

And the following equations are obtained:

$$2e^2\bar{A} + 4e^2\tilde{A} = \frac{1}{2}gh^2 \quad \text{(A-24)}$$

$$2e^4\bar{C} = h \quad \text{(A-25)}$$

$$8e^4\tilde{C} = h \quad \text{(A-26)}$$

$$4e^4\tilde{C} + 2e^2\bar{D} + 4e^2\tilde{D} = 0 \quad \text{(A-27)}$$

Equations A-15, A-16, A-20 and A-24 to A-27 give us six independent equations to determine the ten unknown, so we can freely choose two extra equations. Equations A-25 and A-26 suggest that

$$\bar{C} = 4\tilde{C} \quad \text{(A-28)}$$

Considering the symmetry of the lattice we can reasonably assume that:

$$\bar{A} = 4\tilde{A} \quad \text{(A-29)}$$

$$\bar{B} = 4\tilde{B} \quad \text{(A-30)}$$

$$\bar{D} = 4\tilde{D} \quad \text{(A-31)}$$

Which will allow us determine the unknown coefficients:

$$A_0 = h - \frac{5gh^2}{6e^2} \qquad D_0 = -\frac{2h}{3e^2}$$

$$\bar{A} = \frac{gh^2}{6e^2} \qquad \bar{B} = \frac{h}{3e^2} \qquad \bar{C} = \frac{h}{2e^4} \qquad \bar{D} = -\frac{h}{6e^2}$$

$$\tilde{A} = \frac{gh^2}{24e^2} \qquad \tilde{B} = \frac{h}{12e^2} \qquad \tilde{C} = \frac{h}{8e^4} \qquad \tilde{D} = -\frac{h}{24e^2}$$

By substituting these coefficients in Eq. A-1 the equilibrium functions for the D2Q9 scheme are derived as:

$$h_0^{eq} = h - \frac{5gh^2}{6e^2} - \frac{2h}{3e^2}\mathbf{u_i}\mathbf{u_i}$$

$$h_i^{eq} = \frac{gh^2}{6e^2} + \frac{h}{3e^2}e_{\alpha i}\mathbf{u_i} + \frac{h}{2e^4}e_{\alpha i}e_{\alpha j}\mathbf{u_i}\mathbf{u_j} - \frac{h}{6e^2}\mathbf{u_i}\mathbf{u_i} \quad \text{(odd i)} \qquad \text{(A-32)}$$

$$h_i^{eq} = \frac{gh^2}{24e^2} + \frac{h}{12e^2}e_{\alpha i}\mathbf{u_i} + \frac{h}{8e^4}e_{\alpha i}e_{\alpha j}\mathbf{u_i}\mathbf{u_j} - \frac{h}{24e^2}\mathbf{u_i}\mathbf{u_i} \quad \text{(even i)}$$

Which match those stated in the literature but the derivation has not been presented elsewhere to this level of detail.

Appendix B- Specific transformation of D2Q9 LBM

The Galilean transformation may also be applied to the standard D2Q9 scheme to yield an asymmetric two-dimensional LBM. In this section derivation of the transformed model is presented in detail, if the lattice travels at speed $U = {}^{e}/_{3}$ in direction 1 of the lattice.

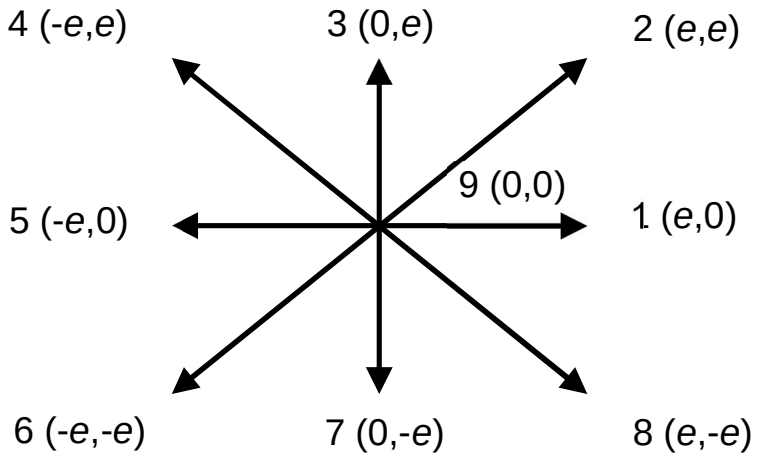

Figure B-1 standard D2Q9 LBM scheme

Substituting $(\mathbf{u_i} - {}^{e}/_{3})$ in the standard D2Q9 scheme:

$$f_0 = h - \frac{5gh^2}{6e^2} - \frac{2h}{3e^2}\left[(\mathbf{u_i} - \frac{e}{3})^2 + \mathbf{u_j}^2\right]$$

$$f_i = \frac{gh^2}{6e^2} + \frac{h}{3e^2}\left[e_{\alpha i}\left(\mathbf{u_i} - \frac{e}{3}\right) + e_{\alpha j}\mathbf{u_j}\right] + \frac{h}{2e^4}\left[{e_{\alpha i}}^2\left(\mathbf{u_i} - {}^{e}/_{3}\right)^2 + 2e_{\alpha i}\left(\mathbf{u_i} - \frac{e}{3}\right)e_{\alpha j}\mathbf{u_j} + {e_{\alpha j}}^2\mathbf{u_j}^2\right] - \frac{h}{6e^2}\left[(\mathbf{u_i} - \frac{e}{3})^2 + \mathbf{u_j}^2\right] \quad \text{(odd i)} \tag{B-1}$$

$$f_i = \frac{gh^2}{24e^2} + \frac{h}{12e^2}\left[e_{\alpha i}\left(\mathbf{u_i} - \frac{e}{3}\right) + e_{\alpha j}\mathbf{u_j}\right] + \frac{h}{8e^4}\left[{e_{\alpha i}}^2\left(\mathbf{u_i} - {}^{e}/_{3}\right)^2 + 2e_{\alpha i}\left(\mathbf{u_i} - \frac{e}{3}\right)e_{\alpha j}\mathbf{u_j} + {e_{\alpha j}}^2\mathbf{u_j}^2\right] - \frac{h}{24e^2}\left[(\mathbf{u_i} - \frac{e}{3})^2 + \mathbf{u_j}^2\right] \quad \text{(even i)}$$

After multiplication of the particle velocities by 3 (to avoid falling on non-integer positions) and further simplification, these reduce to:

$$f_0 = h - \frac{5gh^2}{54e^2} - \frac{2h}{27e^2}\left[(\mathbf{u_i} - e)^2 + \mathbf{u_j}^2\right]$$

$$f_i = \frac{gh^2}{54e^2} + \frac{h}{27e^2}\left[e_{\alpha i}(\mathbf{u_i} - e) + e_{\alpha j}\mathbf{u_j}\right] + \frac{h}{162e^4}\left[{e_{\alpha i}}^2(\mathbf{u_i} - e)^2 + 2e_{\alpha i}(\mathbf{u_i} - e)e_{\alpha j}\mathbf{u_j} + {e_{\alpha j}}^2\mathbf{u_j}^2\right] - \frac{h}{54e^2}\left[(\mathbf{u_i} - e)^2 + \mathbf{u_j}^2\right] \quad \text{(odd i)} \tag{B-2}$$

$$f_i = \frac{gh^2}{216e^2} + \frac{h}{108e^2}\left[e_{\alpha i}(\mathbf{u_i} - e) + e_{\alpha j}\mathbf{u_j}\right] + \frac{h}{64e^4}\left[{e_{\alpha i}}^2(\mathbf{u_i} - e)^2 + 2e_{\alpha i}(\mathbf{u_i} - e)e_{\alpha j}\mathbf{u_j} + {e_{\alpha j}}^2\mathbf{u_j}^2\right] - \frac{h}{216e^2}\left[(\mathbf{u_i} - e)^2 + \mathbf{u_j}^2\right] \quad \text{(even i)}$$

The new particle velocities are:

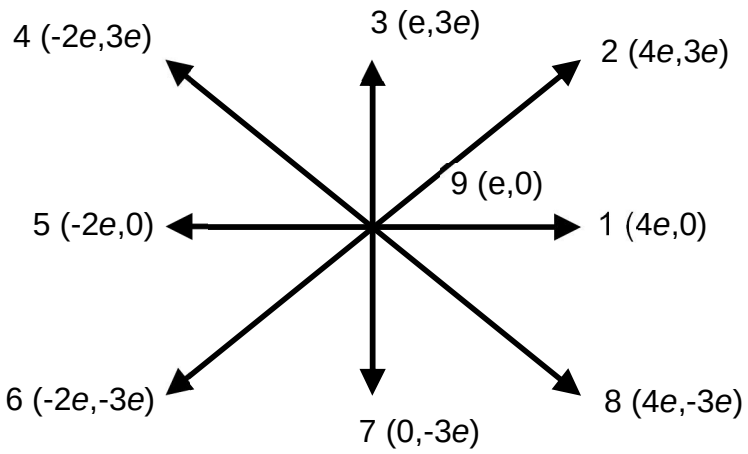

Figure B-2 transformed D2Q9 LBM scheme

The force term weight factors are derived through satisfying Equations (4.20) to (4.25), which would result in the following set of simultaneous equations:

$$w_1 + w_2 + w_3 + w_4 + w_5 + w_6 + w_7 + w_8 + w_9 = 1$$

$$4ew_1 + 4ew_2 + ew_3 - 2ew_4 - 2ew_5 - 2ew_6 + ew_7 + 4ew_8 + ew_9 = 0$$

$$3ew_2 + 3ew_3 + 3ew_4 - 3ew_6 - 3ew_7 - 3ew_8 = 0$$

$$16e^2w_1 + 16e^2w_2 + e^2w_3 + 4e^2w_4 + 4e^2w_5 + 4e^2w_6 + e^2w_7 + 16e^2w_8 + e^2w_9 = 0$$

$$9e^2w_2 + 9e^2w_3 + 9e^2w_4 + 9e^2w_6 + 9e^2w_7 + 9e^2w_8 = C_S^2$$

$$12e^2w_2 + 3e^2w_3 - 6e^2w_4 + 6e^2w_6 - 3e^2w_7 - 12e^2w_8 = 0$$

$$64e^3w_1 + 64e^3w_2 + e^3w_3 - 8e^3w_4 - 8e^3w_5 - 8e^3w_6 + e^3w_7 + 64e^3w_8 + e^3w_9 = 0 \quad \text{(B-3)}$$

$$48e^3w_2 + 3e^3w_3 + 12e^3w_4 - 12e^3w_6 - 3e^3w_7 - 48e^3w_8 = 0$$

$$36e^3w_2 + 9e^3w_3 - 18e^3w_4 - 18e^3w_6 - 9e^3w_7 + 36e^3w_8 = 0$$

$$256e^4w_1 + 256e^4w_2 + e^4w_3 + 16e^4w_4 + 16e^4w_5 + 16e^4w_6 + e^4w_7 + 256e^4w_8 + e^4w_9 = C_S^4$$

$$81e^4w_2 + 81e^4w_3 + 81e^4w_4 + 81e^4w_6 + 81e^4w_7 + 81e^4w_8 = C_S^4$$

$$144e^4w_2 + 9e^4w_3 + 36e^4w_4 + 36e^4w_6 + 9e^4w_7 + 144e^4w_8 = C_S^4$$

$$192e^4w_2 + 3e^4w_3 - 24e^4w_4 + 24e^4w_6 - 3e^4w_7 - 192e^4w_8 = 0$$

$$108e^4w_2 + 27e^4w_3 - 54e^4w_4 + 54e^4w_6 - 27e^4w_7 - 108e^4w_8 = 0$$

Because there are more unknowns than independent equations, the system of equations is underdetermined.

The inflow/outflow boundary conditions may be determined from the following equations:

$$f_1 + f_2 + f_3 + f_4 + f_5 + f_6 + f_7 + f_8 + f_9 = h$$

$$4ef_1 + 4ef_2 + 4ef_3 - 2ef_4 - 2ef_5 - 2ef_6 + ef_7 + ef_8 + ef_9 = Q \quad \text{(B-4)}$$

$$3ef_2 + 3ef_3 + 3ef_4 - 3ef_6 - 3ef_7 - 3ef_8 = 0$$

Applying bounce-back boundary condition on the non-equilibrium part:

$$f_1 - f_5 = f_1^{eq} + f_5^{eq} \quad \text{(B-5)}$$

At the inlet, the unknown EDFs will be determined from the following equations:

$$f_1 = f_5 + \frac{2h}{27e^2}(u - e)(u + 2e)$$

$$f_2 = \frac{3}{4}f_6 + \frac{3}{8}f_7 - \frac{5}{8}f_3 - \frac{1}{2}f_5 - \frac{h}{27e}(u - e)\left(2 + \frac{u}{e}\right) - \frac{1}{4}f_4 + \frac{1}{4}f_5 - \frac{1}{8}f_9 + \frac{Q}{8e} \quad \text{(B-6)}$$

$$f_8 = \frac{Q}{8e} - \frac{h}{27e}(u - e)\left(2 + \frac{u}{e}\right) - \frac{1}{4}f_6 + \frac{5}{8}f_7 + \frac{3}{8}f_3 - \frac{1}{2}f_5 + \frac{3}{4}f_4 + \frac{1}{4}f_5 - \frac{1}{8}f_9$$

Similarly, at the outlet:

$$f_5 = f_1 - \frac{2h}{27e^2}(u - e)(u + 2e)$$

$$f_4 = \frac{1}{2}f_1 + \frac{1}{2}f_2 - \frac{1}{4}f_3 + \frac{3}{4}f_7 + \frac{3}{2}f_8 + \frac{1}{4}f_9 + \frac{h}{27e}(u - e)\left(2 + \frac{u}{e}\right) - \frac{Q}{4e} \quad \text{(B-7)}$$

$$f_6 = \frac{1}{2}f_1 + \frac{3}{2}f_2 + \frac{3}{4}f_3 - \frac{1}{4}f_7 + \frac{1}{2}f_8 + \frac{1}{4}f_9 - \frac{Q}{4e} - \frac{h}{27e}(u - e)\left(2 + \frac{u}{e}\right)$$